The role of extracellular matrix laminin-10 in vascular inflammation, blood-brain barrier repair and angiogenesis after cerebrovascular disease.

A thesis submitted to The University of Manchester for the degree of Doctor of Philosophy in the Faculty of Biology, Medicine and Health

2020

Hannah Thurgur

School of Biological Sciences

Division of Neuroscience and Experimental Psychology

Contents

Word count: 42 920

List of Figures

List of Tables

Abbreviations

2D	Two-dimensional
3D	Three-dimensional
AP-1	Activator protein-1
ATP	Adenosine triphosphate
BBB	Blood–brain barrier
BCA	Bicinchoninic acid
BM	Basement membrane
BMI	Body mass index
BrdU	Bromodeoxyuridine
BSA	Bovine serum albumin
CBF	Cerebral blood flow
CNS	Central nervous system
Col IV	collagen IV
CRP	C-reactive protein
CSF	Cerebrospinal fluid
DAMP	Damage-associated molecular patterns
DMEM	Dulbecco's Modified Eagle Medium
DNA	Deoxyribonucleic acid
DNA	Deoxyribonucleic acid
EAE	Experimental autoimmune encephalomyelitis
ECGS	Endothelial cell growth supplement
ECM	Extracellular matrix
EGF	Epidermal growth factor
ELISA	Enzyme-linked immunosorbent assay
EPC	Endothelial progenitor cell
EPO	Erythropoietin
ERK	Extracellular signal-regulated kinase
FAK	Focal adhesion kinase
FBS	Fetal bovine serum
FGF-2	Fibroblast growth factor-2
GFAP	Glial fibrillary acidic protein
GPCR	G-protein-coupled receptor (GPCR)
HBSS	Hanks' Balanced Salt Solution
ICAM-1	Intercellular adhesion molecule-1
IFN	Interferons
IL	Interleukin
IL-1R1	Interleukin 1 receptor, type I
IL-1Ra	Interleukin-1 receptor antagonist
IL-1RAcP	Interleukin-1 receptor accessory protein
IRAK	Interleukin-1 receptor-associated kinases
JAMS	Junctional adhesion molecules
JNK	c-Jun N-terminal kinase

KO	Knockout
LG3	Laminin globular domain 3
LIF	Leukemia-inhibiting factor
LM	Laminin
LSCI	Laser speckle contrast imaging
MAPK	Mitogen-activated protein kinase
MBECs	Mouse brain endothelial cells
MCA	Middle cerebral artery
MCAO	Middle cerebral artery occlusion
MCP-1	Monocyte chemoattractant protein-1
MLC	Myosin light chain
MMPs	Metalloproteinases
MRI	Magentic resonance imaging
MyD88	Myeloid differentiation primary response gene 88
NF-κB	Nuclear Factor kappa-light-chain-enhancer of activated B cells
NMDA	N-methyl-D-aspartate receptor
NO	Nitric oxide
NPCs	Neural progenitor cells
NSCs	Neural stem cells
NVU	Neurovascular unit
OCT	Optimal cutting temperature compound
PBS	Phosphate-buffered saline
PBS^{+}	Phosphate-buffered saline with calcium and magnesium
PBST	PBS 0.1% (v/v) Tween 20
PDGF	Platelet-derived growth factor
PDS	Plasma dervived serum
PRRs	Pattern recognition receptors
PTX3	Pentraxin-3
PVDF	Polyvinylidene difluoride
qPCR	Quantitative polymerase chain reaction
REML	Mixed effects model
RNA	Ribonucleic acid
RNS	Reactive nitrogen species
ROCK	Rho-associated protein kinase
ROI	Region of interest
ROS	Reacitve oxygen species
RPMI	Roswell Park Memorial Institute
RT	Room temperature
RT-PCR	Reverse transcription polymerase chain reaction
SBP	Systolic blood pressure
SDS	Sodium dodecyl sulfate
SEM	Standard error of the mean

SGZ	Subgranular zone
SVC	Subventricular zone
TAZ	PDZ-binding motif
TEER	Transendothelial electrical resistance
TGF-β	Transforming growth factor beta
TJ	Tight junction
TLCK	Tosyl-L-lysine chloromethyl ketone hydrochloride
TNF	Tumour necrosis factor
TOAST	The Trial of Org 10172 in Acute Stroke Treatment
t-PA	Tissue plasminogen activator
TRAF6	TNF receptor–associated factor 6
Tregs	Regulatory T lymphocytes
VCAM-1	Vascular cell adhesion molecule 1
VEGF	Vascular endothelial growth factor
YAP	Yes-associated protein
ZO	Zonula occludens

Abstract

Stroke remains a devastating health issue worldwide with limited treatment available. Interleukin-1 (IL-1) is a major cytokine implicated in the pathogenesis of stroke, and the blood-brain barrier (BBB) is a major target of IL-1-induced neuroinflammation. The extracellular matrix (ECM) plays a dynamic role in the brain and recent evidence has identified laminin (LM)-10 as a mediator of BBB repair. The aim of this thesis was to determine the role of LM-10 as a modulator of endothelial inflammation and angiogenesis, as well as the role of cerebrovasculature IL-1R1 signalling on laminin expression after stroke.

First, I sought to establish a suitable *in vitro* model to investigate the role of LM-10 as a modulator of IL-1β-induced endothelial activation and the angiogenic response of cerebral endothelial cells. I determined a novel role of LM-10 as a modulator of IL-1β-induced intercellular adhesion molecule-1 (ICAM-1) and vascular cell adhesion molecule-1 (VCAM-1) expression in hCMEC/D3 cells and demonstrated that LM-10 increases endothelial proliferation and migration. I elucidated a novel relationship between IL-1β and Hippo signalling, and demonstrated altered Hippo signalling on LM-10.

In order to investigate the role of cerebrovasculature IL-1R1 signalling on laminin expression after cerebral ischaemia, I induced conditional deletion of IL-1R1 in brain endothelial cells and performed experimental stroke by occlusion of the middle cerebral artery (MCA). I found that laminin α4 (expressed in LM-8) is more dynamically regulated than laminin α5 (expressed in LM-10) across several time points post-stroke and that laminin α4 expression is regulated by endothelial IL-1R1 signalling.

To assess the role of laminin α5 after stroke *in vivo*, I generated a conditional deletion brain endothelial cell-specific laminin α5 mouse strain and successfully confirmed laminin α5 deletion. I induced experimental stroke by occlusion of the MCA but did not observe an effect of laminin α5 on infarct volume, neurological outcome or cerebral blood flow recovery after stroke.

Our results support evidence that the ECM plays a dynamic role in inflammatory conditions in the brain and I have identified a novel crosstalk between IL-1β and the Hippo pathway. Although I did not observe an effect of laminin α5 in ischaemic stroke, I believe that further investigation of the isoform specific roles of laminins in cerebrovascular diseases will provide new insights in the role of the ECM during the pathophysiology of stroke that could lead to new therapeutic treatments.

Declaration

I declare that no other portion of the work referred to in the thesis has been submitted in support of an application for another degree or qualification of this or any other university or other institute of learning.

Hannah Thurgur

Date 30/07/20

Copyright Statement

Experimental contributions

All experiments were designed and analysed by myself with the input of Dr Emmanuel Pinteaux. All experiments were performed by me with the input of others as stated below. In Chapter 4, Dr Nikolett Lénárt, working alongside Dr Adam Denés, performed the stroke surgeries, neurological scoring and tissue collection in regard to the strokes. Professor Jeffrey Miner provided the Lama5 floxed mice. In Chapter 5, Dr Raymond Wong performed the stroke surgeries with assistance from me, and Dr Raymond Wong performed the neurological scoring. In Chapter 5, Dr Raymond Wong and I performed the magnetic resonance imaging (MRI) together. In Chapter 4 and Chapter 5, Sarah Ma assisted in the collection of fluorescent images for analysis and infarct analysis in Chapter 4. In Chapter 5, Dr Eloise Lemarchand assisted in the infarct analysis of MRI images and provided assistance in the training of qPCR in Chapter 3. Further clarification is provided on the title page of each results chapter.

Acknowledgements

The acknowledgements page is often a hot topic amongst PhD students, who will make the cut, what will you say, how to not make it not sound like an Oscar acceptance speech. It's the section of the thesis where you pause to reflect on the past three years past the data, on life inside and outside the lab. In the years to come, it will not be the tiny details of experiments that I will remember, but the kindness and warmth that so many people have showed me throughout.

First, I would like to thank my supervisory team Emmanuel and Jeff for their support and guidance throughout. A special thanks to Emmanuel for believing in me from the start (I never thought I would be starting a PhD at 21!) and the consistent reassurance that it will always work out. I have been fortunate to have a supervisor who is approachable and understanding, such important qualities. Jeff, thank your feedback even during lockdown. A big thank you to the British Heart Foundation for funding this project and providing such a fantastic opportunity. I would also like to acknowledge and thank the Histology and Bioimaging facilities, as well as the BSF team. Thank you Niki Lénárt and Adam Denés for collaborating on an *in vivo* study and of being great help.

I am incredibly grateful to have been a part of the Brain Inflame group, a genuinely lovely bunch of people. I would like to thank Ray for his help with *in vivo* work and for your patience with my poor hand eye coordination. Eloise, you were a very welcome and supportive addition to the Pinteaux lab. Tess, what a year it was in our palace, I will always remember our year living together, the PhD would've been very different without you and I'm so grateful to have met you. Claire, you've been so good to me, a big heartfelt thank you from one cancer to another. Ohud, what a woman, so lucky to have had you by my side from the beginning. Bali, you brought a lot fun. And of course a big thank you to all the members, old and new, I have shared a pint of scrumpy with: Siobhan, Victor, Conor, Sid, Chris, Lucy, Matt. A very deserving thank you to Pat, Kieron, Jack G and Jack B, you have all been of such help to me at times, you will all make wonderful PIs in the future. Cath, you're such a kind and calming influence on the lab. Jo Neill, you've become a mentor without realising and have inspired me to pursue what I'm passionate about, thank you.

I am incredibly lucky and grateful to be surrounded by the most incredible group of friends I could ever wish for, making life fulfilled and meaningful, supporting each other through this journey. Every single one you (including all the B'ham girls), you fill it full of love, laughter and a lot of espresso martinis! Anya, you make every day yellow day, a bond nothing can break. Hannah and Kate it was an absolute blessing to meet you both, our lives are so much richer for it.

Finally, my family: Mum, Dad, Jess and Faye. Thank you for all you do, for giving us that all important perspective and self-belief, showing us what truly matters in life, compassion and integrity. Living life as a family with good humour. My Nana and Nan, this comes with all my love.

Live, Laugh, Lab

Chapter 1. **Introduction**

1.1. **Overview**

1.1.1. Cerebrovascular disease

Cerebrovascular disease is an umbrella term for a number of conditions associated with the cerebral blood vessels and blood supply to the brain. The brain is the most metabolically demanding organ of the body, consuming over 20% of the body's total energy, and hence requires a consistent blood supply (Raichle and Gusnard, 2002). Cerebrovascular diseases that disrupt blood flow have physiological implications that can subsequently result in neurological deficits. Although stroke is considered the primary presentation of cerebrovascular disease, it is important to highlight the myriad of other conditions affecting cerebral blood vessels. These include carotid stenosis, aneurysms and vascular malformations, all of which will contribute to an ischaemic cerebral state and disrupted homeostasis (Sharma, 2016). Although this thesis focuses on ischaemic stroke, there is a clear role of the extracellular matrix (ECM) and inflammation underpinning the broad spectrum of cerebrovascular disease. Thus, basic scientific mechanisms discussed in this thesis may be relevant beyond ischaemic stroke.

1.1.2. Stroke

Stroke remains a major worldwide health issue with a devastating clinical and socioeconomic impact (Feigin, 2019). Stroke is categorised into two distinct subsets; ischaemic and haemorrhagic stroke. Ischaemic stroke is caused by an occlusion in cerebral blood vessels resulting in restricted cerebral blood flow (CBF) (Musuka et al., 2015). Haemorrhagic stroke is the rupture of a blood vessel resulting in intracerebral haemorrhage or subarachnoid haemorrhage, which is respectively named dependent upon the location of the bleed in the brain (Musuka et al., 2015). The more prevalent subset of stroke is ischaemic, accounting for approximately 70% of clinical stroke cases (Feigin et al., 2017). Stroke is the second leading cause of mortality globally and constitutes the third most common cause of disability (Feigin et al., 2017). In the UK, a stroke occurs every 5 minutes and there are 1.2 million stroke survivors, subsequently this is associated with a substantial economic burden estimated at £26 billion per year in the UK (Stroke Association, 2018). Although stroke mortality is declining due to improvements in healthcare and improved awareness of risk factors, there is an ageing population that increases prevalence and with a larger population of survivors there is the

pressing clinical need for the identification of therapeutic targets that aid recovery (Feigin et al., 2017).

1.1.3. Aetiology of ischaemic stroke

The aetiology of ischaemic stroke is due to a thrombotic or embolic event that disturbs cerebral blood flow. The Trial of Org 10172 in Acute Stroke Treatment (TOAST) devised a classification system of ischaemic stroke based on five subsets: large-artery atherosclerosis, cardioembolism, small-vessel occlusion, stroke of other determined aetiology, and stroke of undetermined aetiology, depicted in Figure 1.1 (Adams et al., 1993). A thrombotic event is associated with a disruption to CBF due to an obstruction within the blood vessel. Thrombotic events are typically associated with large artery atherosclerosis (23%), whilst small vessel occlusions are also key contributors to ischaemic stroke cases (22%) (Adams et al., 1993). In contrast, embolic events are the result of blockage to a blood vessel caused by debris (thrombi) that have travelled from a distal location in the body. Most commonly this is a cardioembolic stroke (22%) whereby thrombi form in the atrium due to arrhythmias (Adams et al., 1993), which can become dislodged and travel in the vascular supply to occlude a vessel in the brain. A small proportion of ischaemic strokes are a result of known rare causes (3%), whilst a large proportion (26%) the aetiology is unknown (Adams et al., 1993).

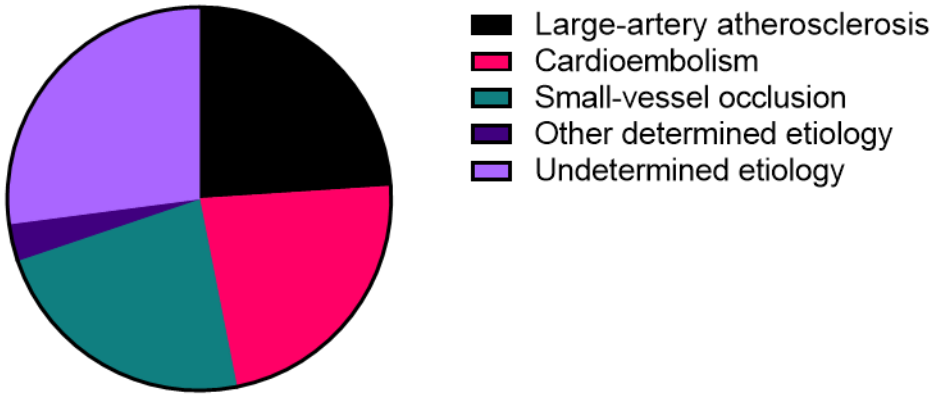

Figure 1.1 Aetiology of ischaemic stroke.
Relative proportion of each aetiology category from the TOAST trial. The five subsets are large-artery atherosclerosis, cardioembolism, small-vessel occlusion, stroke of other determined aetiology, and stroke of undetermined aetiology. Taken from Adams et al. 1993

Due to the varied aetiology of stroke there are a myriad of risk factors that have been identified that can be categorised as modifiable and non-modifiable. Indeed,

a global systematic study suggests that more than 90% of stroke burden is a result of modifiable risk factors (Feigin et al., 2016). Non-modifiable risk factors include age, sex, and genetic factors. Modifiable risk factors include behavioural factors such as diet, smoking, low physical activity, and metabolic factors such as high systolic blood pressure (SBP), high body mass index (BMI) and high total cholesterol. Interestingly, the study also identified environmental factors such as air pollution and lead exposure as major contributors to stroke burden.

1.1.4. Current treatments for ischaemic stroke

Currently treatment options for ischaemic stroke are the pharmacological break down (thrombolysis) or surgical removal of the clot in the blood vessel, both with the aim of restoring blood flow. Clinically, it is critical that ischaemic stroke is confirmed in patients using neuroimaging, this rules out haemorrhagic stroke and confirms the next stage of treatment (Bansal et al., 2013). The only licensed pharmacological intervention for ischaemic stroke is intravenous administration of tissue plasminogen activator (t-PA) (Bansal et al., 2013). A thrombus (the blood clot) is fibrin-rich and t-PA catalyses the transformation of plasminogen to plasmin, aiding the degradation of the thrombus and the restoration of blood flow. Administration of t-PA must occur within a therapeutic window of 4.5 h after stroke onset for safety and efficacy, which presents a major clinical limitation alongside strict suitability inclusion criteria for treatment that in practice has only resulted in 10% of stroke patients receiving the treatment in the UK (McMeekin et al., 2017). A recent advancement in the treatment of ischaemic stroke is the development of endovascular thrombectomy to surgically remove the thrombus. Meta analyses of five clinical trials confirmed the efficacy of endovascular thrombectomy as a treatment of ischaemic stroke, marking a pivotal turning point in stroke treatments available (Goyal et al., 2016). The analyses demonstrated an improved efficacy and a larger therapeutic time window. However, there are caveats associated with this approach as the procedure requires a highly skilled surgeon and thus clinical use of this surgery is limited to centres with trained surgeons.

1.2. **Pathogenesis of ischaemic stroke**

1.2.1. Ischaemic cascade

Cerebral ischaemia induced by an occlusion of a cerebral blood vessel initiates an ischaemic cascade. The obstruction to blood flow results in a reduction of oxygen

and glucose availability, which triggers a complex network of interconnected pathways resulting in energy failure, impairment of ionic homeostasis, oxidative stress, neuronal cell death and BBB dysfunction (Sandoval and Witt, 2008). Neuronal cell death can either occur by necrosis or apoptosis, and is dependent on the severity of injury and the brain region affected. Irreversible necrotic cell death occurs rapidly in the ischaemic core region in the minutes to hours after the initial ischaemic insult (Khoshnam et al., 2017). The area surrounding the ischaemic core, known as the ischaemic penumbra, is potentially salvageable as the cells in this region undergo delayed and controlled cell death by apoptosis. After the initial ischaemic insult, there is a period of reperfusion characterised by the reestablishment of CBF to the brain. Reperfusion induces further pathological damage to the brain and can result in haemorrhagic transformation known as reperfusion injury (Sandoval and Witt, 2008).

1.2.2. Impairment of ionic homeostasis and glutamate excitotoxicity

Cerebral ischaemia impairs the oxygen and glucose availability of the affected region and hence impairs adenosine triphosphate (ATP) production, ultimately leading to excitotoxicity. The reduction in ATP leads to failure of Na^+/K^+ ATPase pumps, resulting in the influx of Na^+ into the cell in exchange of K^+ entering the extracellular space (Woodruff et al., 2011). This excitotoxic response is further exacerbated by an influx of intracellular calcium, which activates several death-signalling enzymes including endonucleases, lipases, kinases and proteases (Khoshnam et al., 2017). A major consequence of the impairment to ionic homeostasis is the cytotoxic oedema that follows as a result of an influx of water into the brain due to changes in osmolality. Cytotoxic oedema occurs rapidly and causes swelling of endothelial cells, glia and neurones, contributing to necrotic cell death (Deb et al., 2010). During the hours and days after the initial ischaemic insult, cytotoxic oedema develops into vasogenic oedema which is characterised by an increased permeability of brain endothelial cells to serum proteins, resulting in an increased intracranial pressure (Deb et al., 2010). A further consequence of the energy failure and subsequent impairment of ionic homeostasis is glutamate excitotoxicity (Deb et al., 2010). There is reduced reuptake of the excitatory neurotransmitter glutamate leading to its excessive accumulation in the synaptic cleft (Woodruff et al., 2011). Glutamate can then further exacerbate cellular excitotoxicity through the activation of N-methyl-d-aspartate (NMDA) receptors,

resulting in a further influx of Ca^{2+} into neurones, and resulting in the activation of signalling pathways leading to neuronal damage and death (Khoshnam et al., 2017).

1.2.3. Oxidative stress and implications

Oxidative stress is a major consequence of the ischaemic cascade and has substantial cellular implications, resulting in tissue damage and cell death. Oxidative stress occurs when the brain is subjected to excess levels of free radicals such as reactive oxygen species (ROS) and reactive nitrogen species (RNS), which overwhelm the brain's endogenous antioxidant and free radical scavenging systems (Allen and Bayraktutan, 2009; Woodruff et al., 2011). Free radicals are highly reactive molecules with one or more unpaired electrons. They present a biphasic nature whereby under homeostatic conditions they play essential roles in immune defence, induction of mitogenic responses and cell signalling (Allen and Bayraktutan, 2009). However, during stroke the excess production of free radicals causes cellular damage and destruction by reacting with membranes, proteins, lipids and deoxyribonucleic acid (DNA) (Allen and Bayraktutan, 2009). The brain is particularly vulnerable to free radical-mediated damage due to limited antioxidant protective mechanisms and the high oxygen consumption of the brain (Allen and Bayraktutan, 2009; Li et al., 2012).

1.3. **The neurovascular unit**

1.3.1. Overview of the NVU

In order to understand the complexities associated with the pathophysiology of stroke and the impact it has on central nervous system (CNS) homeostasis, the blood-brain barrier (BBB) must be considered as part of an integrated and dynamic system of cells and ECM known as the neurovascular unit (NVU). The NVU is composed of astrocytes, perivascular microglia/macrophages, neurones, endothelial cells, pericytes and ECM molecules that form an intricate architecture which facilitates an integrated relationship between the components to maintain homeostasis of the CNS (Sandoval and Witt, 2008). It is the unique environment of the CNS and the dynamic crosstalk of signalling between the brain cells and ECM that produce the unique properties of the BBB.

1.3.2. Role of endothelial cells in the NVU

Endothelial cells of the cerebral vasculature form the foundations of the BBB providing the critical interface between the blood and CNS, and act as a highly selective barrier that maintains the fragile homeostasis of the brain required for neuronal health and function (Abbott et al., 2010). The unique barrier properties of the BBB are attributed to the formation of very close tight junctions (TJs) between cerebral endothelial cells that help control paracellular permeability across the BBB and provide asymmetric distribution of the apical and basolateral cell membranes of the endothelial cells (Sandoval and Witt, 2008). The integrity of TJs is maintained by three main transmembrane proteins; claudins, occludins and junctional adhesion molecules (JAMs). JAMs interact with intracellular scaffold proteins such as zonula occludens(ZO)-1, ZO-2 and ZO-3, which are anchored via cingulin dimers to actin and the cytoskeleton (Ballabh et al., 2004; Abbott et al., 2010). TJs proteins can be regulated at several levels including that of post-translational modification, via their cellular localisation or through cytoskeleton disruption (Luissint *et al*., 2012).

1.3.3. Role of astrocytes in the NVU

The anatomical position of astrocytes between neurones, endothelial cells and pericytes enables close communication and implicates them as a critical component of the NVU (Sandoval and Witt, 2008). Astrocytic endfeet are closely associated with the basal lamina of the endothelium and facilitate the maintenance of the BBB via astrocyte-endothelial interactions (Abbott et al., 2006). Glial cells produce several factors including transforming growth factor beta (TGF-β), basic fibroblast growth factor (FGF-2), angiopoetin-1 and glial derived neurotrophic factor, which mediate the induction and maintenance of the BBB (Abbott et al., 2006). There is also evidence that suggests the relationship between endothelial cells and astrocytes is bi-directional whereby endothelial cells induce astrocyte differentiation via the production of leukemia-inhibiting factor (LIF) (Mi et al., 2001). Co-culturing of endothelial cells and astrocytes enhances the antioxidative activity of both cell types after hypoxia, demonstrating the inductive role of astrocytes on the BBB (Schroeter et al., 1999).

1.3.4. Role of pericytes in the NVU

The CNS endothelium has a significantly higher pericyte coverage compared to peripheral tissues, which is reflective of their role as pivotal and multifunctional components of the NVU (Keaney and Campbell, 2015). Pericytes are encapsulated within the endothelial basal lamina and wrap around the endothelial cells, thus due to this unique distribution of pericytes around the endothelium they have contacts with astrocytes, neurones and perivascular microglia/macrophages (Rustenhoven et al., 2017). Increasing evidence has elucidated the versatile role of pericytes as coordinators of BBB and CNS homeostasis, regulators of CBF, providers of structural support and angioarchitecture and contributors to the secretion of ECM proteins (Winkler et al., 2011; Keaney and Campbell, 2015). There are several signalling pathways activated in pericyte-endothelial crosstalk including angiopoietin, platelet-derived growth factor (PDGF), Notch and TGF-β (Winkler et al., 2011). *In vitro* BBB models have demonstrated that secretion of multimeric angiopoietin-1 from pericytes activates the Tie-2 receptor to induce endothelial expression of the TJ protein occludin, suggesting that pericytes play a key role in maintenance of the BBB (Hori et al., 2004).

1.3.5. The extracellular matrix in the NVU

The full complexity and sophistication of the ECM as a dynamic component of the NVU has started to be elucidated as its diverse structural and signalling roles have been discovered. The ECM is an intricate network of extracellular glycoproteins and proteoglycans that surrounds cells and is adapted to the functional requirements of each organ. ECM molecules are mostly secreted by astrocytes, pericytes and endothelial cells in the CNS (Baeten and Akassoglou, 2011; Keaney and Campbell, 2015). Intricate signalling pathways are activated via interactions between ECM molecules and their receptors expressed on the cellular components to modulate cell survival, differentiation and activation (Lu et al., 2011). Similar to any protein, the ECM components are regulated at the level of transcription and translation. Further regulation of ECM turnover is through degradation by proteolytic enzymes, which can be of particular relevance during CNS diseases.

The ECM in the CNS can be categorised into 3 compartments; the basement membrane (BM), perineuronal nets and the neural interstitial matrix (ECM in the

parenchyma), each characterised by their distinct ECM molecule composition (Lau et al., 2013). The BM is the continuous sheet-like layer of ECM that ensheathes the parenchymal side of cerebral microvessels. It is typically composed of collagen IV, laminins, entactin, fibronectin, dystroglycan and perlecan. Perineuronal nets are formed of mesh-like ECM deposited in the space between neurones and astrocytic processes, and is mostly composed of proteoglycans and tenascin-C and –R (Kwok et al., 2011). The neural interstitial matrix is a dense network of ECM molecules dispersed in the parenchyma, which is not closely associated with perineuronal nets or the endothelial wall and is mostly composed of proteoglycans (Rauch, 2007). The neural interstitial matrix is composed of proteoglycans, hyaluronan, tenascins, as well as relatively small amounts of collagens, elastin, laminins and fibronectin.

ECM molecules self-assemble to form supramolecular assemblies that act as a functional three-dimensional (3D) scaffold matrix (Mouw et al., 2014). The self-assembly of ECM molecules into supramolecular structures is driven by innate intercompetent binding and polymerisation of ECM constituents (Yurchenco, 2011). The composition of the ECM confers the physical properties and hence structural role of the ECM in supporting tissue structure, cellular migration and cellular anchorage via interactions with ECM receptors (Lu et al., 2011). ECM molecules act as ligands for ECM receptors providing a complex adhesion surface for cell attachment (Mouw et al., 2014). Furthermore, the biochemical properties of the ECM confer the versatile and dynamic signalling mechanisms that can be elicited downstream of cellular binding to the ECM (Lu et al., 2011). Another function of the ECM is the ability of components to bind growth factors and chemokines and act as a reservoir, controlling their availability and creating concentration gradients (Lu et al., 2011; Mouw et al., 2014).

1.3.6. ECM receptors

Integrins and dystroglycan are the two main receptors that mediate cell-cell and cell-ECM interactions in the CNS. Integrins are a family of heterodimeric transmembrane glycoproteins composed of alpha and beta chains (Takada et al., 2007). They are expressed in all cells of the BBB including endothelial cells, astrocytes, pericytes, microglia and neurones, acting as receptors for several ECM ligands and eliciting a diverse range of signalling responses (Baeten and

Akassoglou, 2011; Wu and Reddy, 2012). Dystroglycan is expressed in endothelial cells, astrocytes and neurones (Baeten and Akassoglou, 2011). Dystroglycan consists of a highly glycosylated extracellular α-subunit that interacts with laminin G domain ligands, whilst the transmembrane β-subunit interacts with the actin filament network (Moore and Winder, 2010).

ECM receptors are essential mediators in eliciting the structural and functional roles of the ECM. They provide structural support by acting as a physical link between the cytoskeleton and the ECM. Cells express various ECM receptors and therefore interact with several ligands to elicit a diverse signalling response with multiple functional outcomes, which is adaptive to changes in the microenvironment (Baeten and Akassoglou, 2011). Integrins respond to changes in their microenvironment through three main signalling mechanisms: i) activation of integrins upon binding of ECM ligands, ii) via crosstalk between integrins and growth factors and iii) via transactivation of growth factor receptors (Baeten and Akassoglou, 2011). ECM ligands can bind to integrins and activate signalling pathways, modulating key cellular processes including gene regulation, cell proliferation, differentiation, survival and migration (Yurchenco, 2011). A myriad of signalling pathways can be activated including the focal adhesion kinase/c-Jun N-terminal kinase pathway (FAK/JNK), Ras/ERK (MAP kinase), and the small GTPases such as Rho (Miranti et al., 2015). Another mechanism of integrin signalling is via crosstalk between integrins and growth factors whereby integrins can activate latent growth factors such as TGF-β (Baeten and Akassoglou, 2011). Furthermore, integrins can also transactivate growth factors by co-clustering near growth factor receptors or can transactivate growth factor receptors in the absence of growth factor ligands (Baeten and Akassoglou, 2011).

1.4. **Laminin family**

1.4.1. Laminins general background

Laminins are a family of glycoproteins that are an integral component of the ECM throughout the body including the CNS. They are heterotrimeric proteins composed of α, β and γ chains, and are named according to their chain composition (Domogatskaya et al., 2012).The highly glycosylated α, β, and γ laminin chains assemble to form cross-shaped or T-shaped heterotrimers (Durbeej, 2010; Domogatskaya et al., 2012). The COOH-terminal ends of the

chains form a coiled coil structure and acts as the ‘long arm’ of the trimer, whilst the NH2-termini of the α, β, and γ chains act as the ‘short arms’ (Domogatskaya et al., 2012). Each chain has a specific set of globular domains (domains IV and VI), rod-like domains containing EGF-like repeats and domains (I and II) that form the α-helical coiled-coil (Hallmann, 2005). The composition of the chains determine the properties of the laminin isoform, which will subsequently influence BM self-assembly, surface receptor binding and ECM interaction (Hallmann, 2005; Domogatskaya et al., 2012). The α chains of laminins contain five LG domains at the COOH-terminal and are thought to contribute to cell binding, whilst domains IV and VI are involved in the self-assembly required for BM formation (Hallmann, 2005). Laminin is essential for BM assembly, organisation and BBB function (Baeten and Akassoglou, 2011). Mice knock outs of the subunit laminin γ1 are embryonic lethal due to the lack of laminin assembly and organisation, resulting in a lack of BM formation. Furthermore, mice lacking laminin α5 are embryonic lethal (Miner et al., 1998), whilst laminin α4 deletion results in vascular defects after birth in mice (Thyboll et al., 2002).

1.4.2. Laminin basement membrane formation in the CNS

Different isoforms of laminin are synthesised by different cell types of the NVU and therefore the composition of BMs can vary according to cellular proximity as illustrated in Figure 1.2. The four main laminin (LM) isoforms at the BBB are laminin411 (LM-8), laminin511 (LM-10), laminin111 (LM-1) and laminin211 (LM-2) (Sixt et al., 2001). LM-8 and LM-10 are expressed throughout the body and are major components of the endothelial basement membrane, whilst in contrast LM-1 and LM-2 are specifically expressed in the brain. In the CNS there are two distinct basement membranes associated with the vessels, an endothelial basement membrane composed of LM-10 and LM-8, and an outer parenchymal basement membrane composed of LM-1 and LM-2 (Sixt et al., 2001). This distinction is a result of differential laminin isoform synthesis by cells; astrocytes synthesise LM-2 (Jucker et al., 1996; Menezes et al., 2014; Hannocks et al., 2018), and LM-1 is secreted by pial cells (Hannocks et al., 2018) and leptomeningeal cells (Sixt et al., 2001). In contrast, cerebrovascular endothelial cells synthesise LM-8 and LM-10 (Sixt et al., 2001), and it has been demonstrated that mural cell also synthesise laminin α5 and laminin α4 containing isoforms (Gautam et al., 2016).

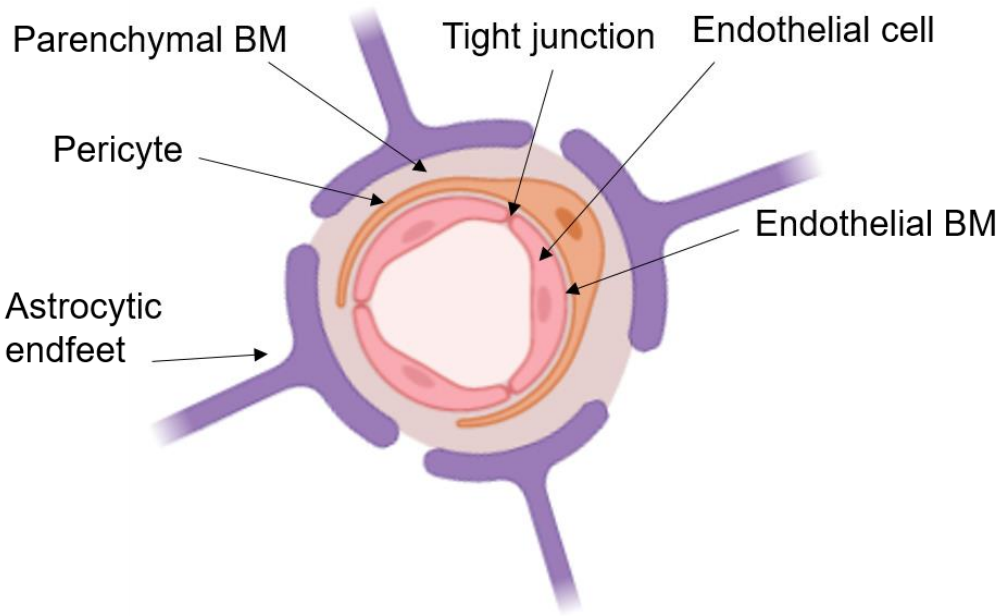

Figure 1.2. Schematic of the BM formation in the CNS.
The anatomical location of the endothelial BM and parenchymal BM, relative to endothelial cells, pericytes and astrocytic endfeet. The endothelial BM (composed of LM-8 and LM-10) is closely associated with the endothelial cells, whilst the parenchymal BM (composed of LM-1 and LM-2) is closely associated with the pericytes and astrocytic endfeet. Adapted from Xu et al., 2019.

1.4.3. Barrier function and protective properties of laminins

The dynamic and protective properties of laminins in the ECM of the CNS have been demonstrated in several studies. *In vitro* evidence have demonstrated that the composition of laminin isoforms in the BM influences the ability of transmigrating leukocytes across the BBB (Sixt et al., 2001; Wang et al., 2006). During experimental autoimmune encephalomyelitis (EAE), the CNS presents two biochemically distinct BMs, the endothelial (LM-8 and LM-10) and parenchyma BM (LM-1 and LM-2) (Sixt et al., 2001). The differential expression of laminin isoforms influences T cell infiltration, whereby inflammatory cuffs that permit infiltration occurred in regions of LM-8 expression, whilst there was no infiltration in regions of LM-10 expression (Sixt et al., 2001). LM-1 and LM-2 were shown to be non-adhesive for encephalitogenic T cell lines, and hence leukocyte penetration occurs after disruption to the BM (Sixt et al., 2001). Further evidence supporting the differential functions of ECM components on neutrophil transmigration has been demonstrated in a murine cremaster muscle model, which facilitates high resolution imaging, showing that regions of low BM protein expression (LM-10, collagen IV, and nidogen-2) is associated with neutrophil transmigration (Wang et al., 2006). These regions were found in gaps between pericytes and the evidence

suggested that neutrophils could remodel the BM to facilitate transmigration. A recent *in vitro* study using bEND.5 cells demonstrated that LM-10 reduces neutrophil transmigration, enhances transendothelial electrical resistance (TEER) and enhances junctional localisation of VE-cadherin, suggesting that LM-10 enhances endothelial barrier properties (Song et al., 2017). The protective properties of laminins on neuronal viability has been demonstrated whereby laminin degradation precedes neuronal loss and is associated with regions of neuronal loss, suggesting that neuronal interaction with laminins protects against neuronal death (Chen and Strickland, 1997). Further evidence supports the role of the laminin matrix in neuronal survival, whereby disruption of the hippocampal laminin matrix with soluble laminin makes the neurones susceptible to neuronal death after kainate injection (Indyk et al., 2003).

1.5. **Inflammatory response**

1.5.1. Inflammation

Inflammation is a physiological host defence response to infection that is critical in restoring homeostasis and promoting repair (Chen and Nuñez, 2010). Inflammation can be triggered in response to exogenous stimuli such as invading pathogens, or endogenous stimuli created as a result of injury such as during cerebral ischaemia. Inflammation triggered in the absence of a pathogen is referred to as sterile inflammation. Sterile inflammation is a key hallmark of several CNS diseases including stroke, Alzheimer's disease and Parkinson's disease.

1.5.2. Overview of the inflammatory response after ischaemic stroke

There is extensive experimental and clinical evidence that the inflammatory response activated post-ischaemia contributes to the pathogenesis of stroke. The energy failure, necrotic cell death and BBB disruption associated with the ischaemic cascade triggers a robust inflammatory response that forces the brain into a pro-inflammatory state characterised by the rapid activation of resident brain cells, the infiltration of peripheral immune cells and the upregulation of inflammatory mediators (Woodruff et al., 2011). Following the ischaemic cascade, there is the release of damage-associated molecular patterns (DAMPs) from stressed host cells, which can act on pattern recognition receptors (PRRs) expressed on neurones, glial cells and endothelial cells (Khoshnam et al., 2017). PRRs then activate intracellular signalling pathways resulting in the upregulation

of pro-inflammatory genes, leading to the expression of inflammatory mediators (Vidale et al., 2017). The inflammatory response activated is highly complex as cells and inflammatory mediators can present multiphasic natures of neurotoxic and neuroprotective properties, which can be influenced by their spatiotemporal context. Critical in understanding the CNS cellular response post-stroke is an appreciation of the inflammatory mediators produced, the cytokine/chemokine receptors expressed and the response elicited by each cell.

1.5.3. Role of microglia in the inflammatory response

Microglia are often described as the resident macrophages of the brain. During physiological conditions, microglia display a ramified morphology characterised by fine, outstretched processes that survey their environment. However, after ischaemia they become rapidly activated within hours and their morphology becomes amoeboid, characterised by the retracting of their processes. Their proliferation and activation peaks 2-3 days post-stroke (Denes et al., 2007). The degree of injury in different regions of the brain can influence microglial activation whereby the activation of microglia in the ischaemic core is triggered by excitotoxicity associated with the ischaemic cascade, whilst in the peri-infarct region, activation is governed by DAMPs (Guruswamy and Elali, 2017). The role of microglia in the pathogenesis of stroke is particularly complex as they present different phenotypes determined by their spatiotemporal context. It is thought that their pro-inflammatory phenotype is activated early after ischaemia and that microglia become protective at later time points (Y. K. Kim et al., 2016). Indeed, the early pro-inflammatory phenotype is attributed to the pro-inflammatory cytokines produced such as tumour necrosis factor (TNF)-α, interleukin (IL)-1β, IL-18 and IL-6 (Y. K. Kim et al., 2016; Vidale et al., 2017). In contrast, the neuroprotective phenotypic microglia are observed 24 h after the ischaemic insult and persists for a week before decreasing in number (Taylor and Sansing, 2013). The protective phenotype is thought to contribute to repair via the production of TGF-β, nerve growth factor, and IL-4 (Vidale et al., 2017). Indeed, it was demonstrated that depletion of microglia in mice exacerbates inflammation after ischaemia, specifically increasing pro-inflammatory mediators and leukocyte infiltration (Jin et al., 2017). Furthermore, in another study it has been demonstrated that microglia depletion resulted in a 60% increase in infarct size and dysregulated neuronal activity after cerebral ischaemia (Szalay et al., 2016).

1.5.4. Leukocyte infiltration

Disruption of the BBB further exacerbates post-ischaemic inflammation through facilitating the infiltration of peripheral immune cells. Peripheral immune cells including neutrophils, lymphocytes and blood-derived macrophages infiltrate the injured brain and further contribute to the pro-inflammatory state. After ischaemia, there is an upregulation of an array of cell adhesion molecules on the brain endothelium including selectins, integrins and immunoglobulins which mediate leukocyte infiltration. E- and P-selectins are upregulated on the vascular endothelium and mediate the recruitment and rolling of leukocytes via interactions with carbohydrate residues, and are known to influence outcome after stroke (Connolly et al., 1997; Huang et al., 2000). L-selectin is involved in leukocyte transmigration and inhibition studies of L-selectin in a rabbit model of transient focal cerebral ischaemia has shown that it does not influence outcome after stroke (Yenari et al., 2001). Expression of the intercellular cell adhesion molecule 1 (ICAM-1) and vascular cell adhesion molecule 1 (VCAM-1) on endothelial cells is also upregulated and act as ligands for integrins expressed on leukocytes, strengthening the attachment of leukocytes to the endothelial wall and facilitating diapedesis through the vessel (J. Y. Kim et al., 2016). Leukocyte recruitment to the site of injury is further mediated by the release of chemokines from the damaged tissues, which act as signalling ligands for chemokine receptors expressed on leukocyte plasma membranes (Ceulemans et al., 2010; Y. K. Kim et al., 2016).

1.5.5. Role of neutrophils in the inflammatory response

Neutrophils are the first subset of leukocytes to migrate and adhere to the brain endothelium (Y. K. Kim et al., 2016). They are thought to adhere to the brain endothelium within a few hours after the ischaemic insult, which is then followed by infiltration into the brain parenchyma at 24 h (Perez-de-Puig et al., 2015). After experimental stroke, levels of neutrophils peak 48-72 h after stroke and then start to decrease in number (Anrather and Iadecola, 2016). Neutrophils contribute to the post-ischaemic inflammation and damage through various mechanisms. Their attachment to the endothelium and production of vasoconstriction mediators further impairs already diminished blood flow to the damaged area (Kim et al., 2014). Furthermore, neutrophils release pro-inflammatory mediators such as ROS, proteases, collagenase and gelatinases, which contribute to BBB disruption and neuronal damage (Kim et al., 2014; Faraco et al., 2017).

1.5.6. Role of lymphocytes in the inflammatory response

The role of lymphocytes in the pathogenesis of stroke is less well characterised compared to other immune cells, and there is conflicting evidence concerning their properties in stroke. It is thought that there is a distinction between B cells and T cells, whereby it is specifically T lymphocytes that exert neurotoxic effects through the production of pro-inflammatory cytokines and cytotoxic substances (Kim et al., 2014). However, there is evidence that shows differential actions of T lymphocyte subsets showing that depletion of regulatory T lymphocytes (Tregs) increased infarct volume and deteriorated outcome, suggesting that Tregs act as cerebroprotective immunomodulators (Liesz et al., 2009). However, it is important to highlight that there is inconsistency in the evidence concerning the role of T lymphocytes in post-stroke pathogenesis and that their roles are still unclear (Y. K. Kim et al., 2016).

1.5.7. Role of inflammatory mediators

The robust inflammatory response activated after brain injury results in the upregulation of a vast array of cytokines and chemokines, which exhibit pro-inflammatory and anti-inflammatory properties. All resident brain cells and infiltrating immune cells produce and/or respond to a range of inflammatory mediators. Key inflammatory mediators known to be upregulated after stroke include IL-1, IL-6, IL-10, IL-17, IL-23, TNF-α, TGF-β and interferons (IFN)-γ (Lakhan et al., 2009).

1.6. **Interleukin-1**

1.6.1. The IL-1 family

The IL-1 family are critical mediators of the innate immune response and IL-1 is a major cytokine implicated in the inflammatory response activated after stroke. Although there have been 11 members of the IL-1 family identified (Dinarello, 2018), the two main agonists IL-1α and IL-1β, and the competitive antagonist, interleukin-1 receptor antagonist (IL-1Ra) are the most studied (Denes et al., 2011).

1.6.2. IL-1 expression, processing and secretion

IL-1 is constitutively expressed at low levels in the brain during physiological conditions and contributes to the maintenance of brain functions including sleep, memory formation and neuronal function (Murray et al., 2015). However, after cerebral ischaemia, IL-1 is rapidly upregulated by astrocytes, microglia and endothelial cells in the brain, which results in several downstream signalling cascades contributing to neuroinflammation (Basu et al., 2004). IL-1 gene expression is under the regulation of nuclear factor kappa-light-chain-enhancer of activated B cells (NF-κB), which is activated following TLR, a form of PRRs, activation (Dinarello, 2018).

IL-1α and IL-1β are products of different genes, but are both expressed as 31-kDa pro-forms that undergo proteolytic cleavage to produce bioactive 17-kDa forms (Murray et al., 2015; Sobowale et al., 2016). The pro-form of each isoform requires a different mechanism of activation. Proteolytic cleavage of pro-IL-1β is classically achieved via formation of the inflammasome, which recruits and activates the enzyme caspase-1 that cleaves pro-IL-1β (Brough and Denes, 2015; Sobowale et al., 2016). In contrast, the mechanism of pro-IL-1α activation is less well defined and there are several proposed mechanisms for the processing and release of IL-1α. Proposed mechanisms include cleavage of pro-IL-1α via the calpain family of calcium-dependent proteases and an inflammasome-dependent mechanism of processing and release from macrophages (Brough and Denes, 2015).

The subsequent secretion of IL-1α and IL-1β does not follow the conventional protein secretion pathway consisting of the endoplasmic reticulum and Golgi apparatus. Instead there are several proposed mechanisms of IL-1β secretion: i) rescue and redirect, ii) protected release and iii) terminal release (Lopez-Castejon and Brough, 2011). The ‘rescue and redirect’ mechanism is whereby IL-1β in the cytosol becomes enclosed in a double membrane structure called an autophagosome. Typically, autophagosomes are destined for degradation through fusion with lysosomes. However, when autophagy is inhibited the enclosed IL-1β may be ‘rescued’ from degradation and subsequently secreted (Harris et al., 2011). The ‘protected release’ mechanism is the release of IL-1β via the shedding of microvessels from the plasma membrane (MacKenzie et al., 2001). The ‘terminal release’ denotes IL-1β secretion as a result of pyroptosis, a form of pro-

inflammatory cell death that results in subsequent loss of plasma membrane integrity, for example through caspase-1 induced cell death in macrophages resulting in pyroptosis and release of IL-1β (Bergsbaken et al., 2009). Similarly to mechanisms of IL-1β secretion, several secretory mechanisms of IL-1α have been suggested yet it remains uncharacterised fully. This includes cell death pathway mechanisms such as necroptosis, as well as calcium-dependent and calpain-dependent mechanisms (Brough and Denes, 2015).

1.6.3. IL-1 signalling pathways

IL-1α and IL-1β exert their biological effects via the membrane bound interleukin 1 receptor, type I (IL-1R1) as illustrated in Figure 1.3. IL-1R1 is expressed on all brain cells with the exception of microglia (Pinteaux et al., 2002). IL-1α and IL-1β bind to IL-1R1, resulting in a conformational change to facilitate the recruitment of the IL-1 receptor accessory protein (IL-1RAcP), forming an IL-1R1/IL-1RAcP complex. The complex recruits myeloid differentiation primary response gene 88 (MyD88), which acts as a signalling adaptor molecule to recruit the serine-threonine kinase IL-1 receptor-associated kinase (IRAK)-4. This autophosphorylates and activates the two IL-1 receptor-associated kinases, IRAK-1 and IRAK-2, which act as adapter proteins and protein kinases for downstream signalling. This is subsequently followed by the recruitment and oligomerization of the ubiquitin E3 ligase TNF receptor–associated factor 6 (TRAF6) (Weber et al., 2010).

In order to induce IL-1-driven NF-κB signalling, an intracellular signalling cascade of combinatorial phosphorylation and ubiquitination events is triggered, ultimately resulting in phosphorylation and degradation of IκBα to facilitate the release of p50 and p65 NF-κB subunits and their nuclear translocation (Weber et al., 2010). There is also mitogen-activated protein kinases (MAPK) pathway activation including extracellular-signal-regulated kinase (ERK)1/2, c-Jun N-terminal kinases (JNK) and p38 mitogen-activated protein kinase pathways, which activate gene transcription through the activator protein 1 (AP-1) transcription factor. These downstream signalling pathways play a co-operative role in inducing inflammatory gene expression downstream of IL-1 (Weber et al., 2010). It is important to highlight that this is not an exhaustive list of signalling downstream of IL-1R1 and that there is network of dynamic pathways responsible for the vast biological effects of IL-1.

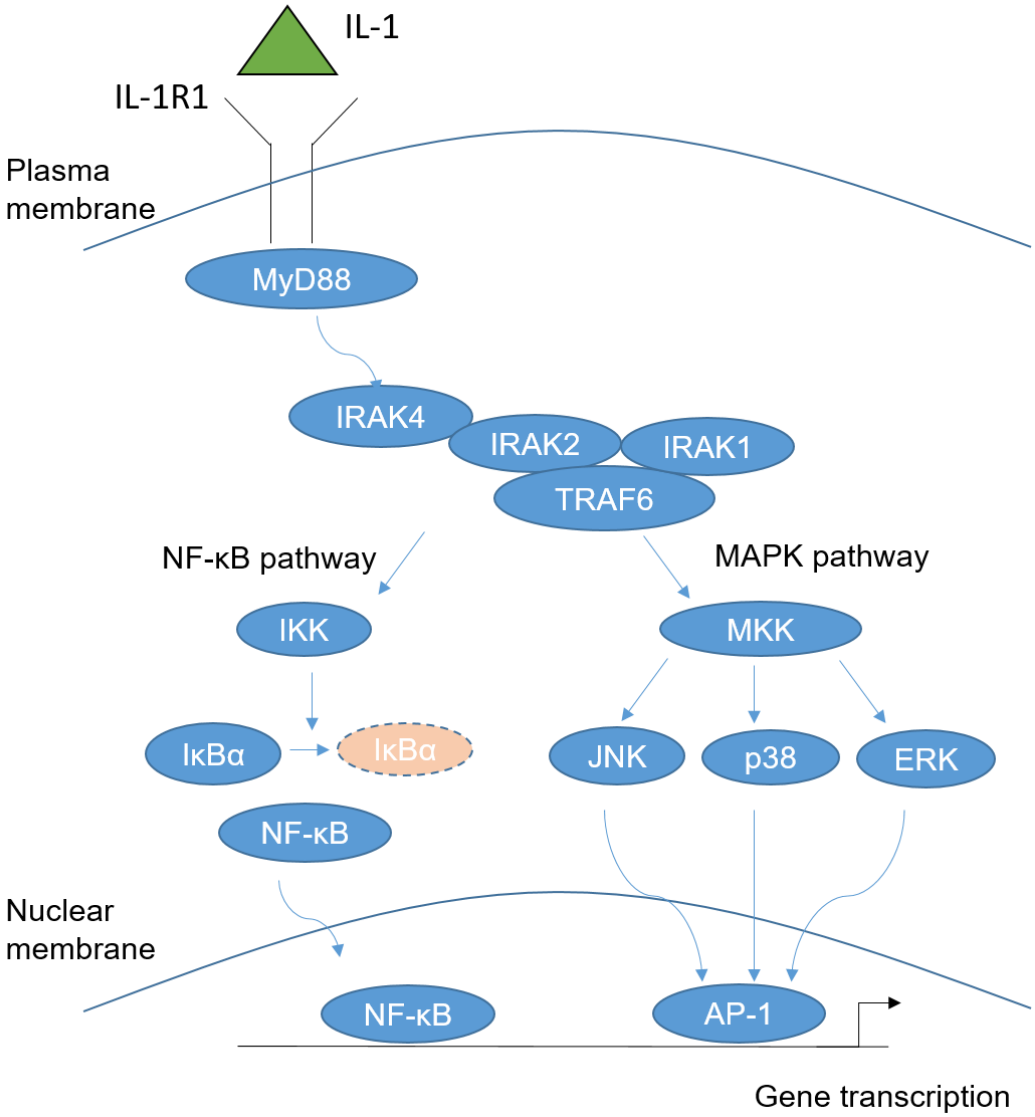

Figure 1.3. Schematic of IL-1R1 signalling.
Simplified illustration of the key components of the IL-1R1 signalling cascade. IL-1 binds to the IL-1R1, resulting in the recruitment of MyD88 and subsequent recruitment of IRAK4. This is followed by activation of IRAK1 and IRAK2, resulting in TRAF6 recruitment and oligomerization. Downstream of this is activation of the NF-κB and MAPK pathways, ultimately resulting in the activation of the transcription factors NF-κB and AP-1. In order for NF-κB to translocate into the nucleus, IKK phosphorylates IκBα resulting in the ubiquitination and subsequent degradation.

1.6.4. IL-1 in ischaemic stroke

Pre-clinical data has provided a strong evidence base for the role of IL-1 in ischaemic stroke (Sobowale et al., 2016). Early *in vivo* studies using a rat model of ischaemic stroke demonstrated that IL-1Ra was protective, identifying IL-1 as a mediator of ischaemic and excitotoxic brain damage (Relton and Rothwell, 1992).

The advancement in transgenic tools available in the early 2000's facilitated the deletion of IL-1α and IL-1β in mice, and subsequent use in a mouse model of ischaemic stroke reported 70% reductions in lesion volume after the simultaneous deletion of IL-1α and IL-1β (Boutin et al., 2001). Over the past 20 years, the neuroprotective effects of IL-1Ra after stroke have been demonstrated in a variety of animal species, models of ischaemia and via several different administration routes. Indeed, a meta-analysis of the efficacy of IL-1Ra in animal models of stroke determined that infarct volume was reduced by 38.2% (Banwell et al., 2009), and a more recent multi-centre study confirmed the protective properties of IL-1Ra (Maysami et al., 2016). Recent sophisticated studies have dissected the cell specific contribution of IL-1R1 signalling, which is of particular interest to fully understand the vast roles of IL-1 in ischaemic stroke (Liu et al., 2019; Wong et al., 2019). Wong and colleagues (2019) identified the cerebrovascular endothelium and cholinergic neurons as major targets for IL-1-mediated brain injury after cerebral ischemia in mice. Indeed, the study demonstrated that cerebrovascular endothelial IL-1R1 signalling contributed to vascular activation (ICAM-1 and VCAM-1) and neutrophil cerebrovascular migration (Wong et al., 2019). Liu and colleagues (2019) used a genetic knock-in reporter system that can track and reciprocally delete or express IL-1R1 in specific cell types to determine the cell-specific contribution of IL-1 signalling applicable in CNS disorders. The study provided further support for the role of cerebrovascular IL-1R1 signalling in the CNS demonstrating that endothelial IL-1R1 is a critical mediator of sickness behaviour, leukocyte recruitment, and neurogenesis (Liu et al., 2019).

1.6.5. Blocking IL-1 after ischaemic stroke

Due to the vast pre-clinical evidence implicating IL-1 in ischaemic stoke, there have been several clinical studies investigating the role of IL-1Ra as a therapeutic target in stroke. IL-1Ra as an inhibitor of IL-1 actions is an attractive therapeutic target due to its high specificity and human safety (Murray et al., 2015). The first randomised, double blinded, placebo controlled trial of IL-1Ra in acute stroke patients confirmed the safety and also demonstrated efficacy showing reduced blood levels of white blood cells, C-reactive protein (CRP) and IL-6 (Emsley et al., 2005). The study also demonstrated a trend towards an improved 3-month clinical outcome among patients with cortical infarcts treated with IL-1Ra. A further small phase II, double-blinded, randomised controlled study of IL-1Ra in subarachnoid

haemorrhage demonstrated safety and reduced levels of IL-6 in plasma and cerebrospinal fluid (CSF), but failed to show statistical significance due to a small sample size (Singh et al., 2014). In a recent phase II clinical trial, subcutaneous administration of IL-1Ra reduced plasma inflammatory markers CRP and IL-6, but was not associated with better outcome on direct analysis (Smith et al., 2018). It is critical to highlight the limitations in the current knowledge such as data on the therapeutic window of IL-1Ra administration, routes of administration in patients and interactions with pre-existing medications that patients may be taking or even thrombolytic drugs (Sobowale et al., 2016).

1.7. **Neurovascular damage after ischaemic stroke**

1.7.1. BBB damage after stroke

The integrity and function of the NVU depends upon the intricate interactions between the cellular and molecular components. However, during a diseased state the CNS endothelium and ECM undergoes profound changes including the breakdown of TJs, remodelling of the ECM and enzymatic degradation of ECM proteins by matrix metalloproteinases (MMPs) and ROS (Wang et al., 2007; Lu et al., 2011). The loss of BBB integrity and endothelial hyperpermeability exacerbates the damage post-ischaemia through facilitating the infiltration of macromolecular serum proteins, fluid and immune cells into the extracellular space, resulting in vasoactive oedema (Hu et al., 2017). The increased permeability of the TJs of endothelial cells to macromolecular serum proteins results in cerebral oedema, which accounts for much of the disability and death associated with stroke (Deb et al., 2010).

1.7.2. Evolution of BBB permeability

There are discrepancies in the studies regarding the evolution of BBB permeability. Several animal studies suggest that there is a biphasic profile of permeability characterised by an initial increase in permeability, followed by a refractory period of baseline BBB permeability then a delayed secondary increase in permeability (Belayev et al., 1996; Rosenberg et al., 1998; Sizemore et al., 1999). However, recent animal studies have disputed this and suggest that there is continuous leakage for days to weeks after the ischaemic insult (Lin et al., 2002; Strbian et al., 2008). A recent human study of ischaemic insult supports this profile of BBB

permeability and suggests that permeability remains elevated, but peaks 6-48 h after ischaemic insult (Merali et al., 2017).

Early BBB damage is characterised by increased paracellular permeability and weakening of endothelial TJ integrity. During normal physiology, TJ proteins and the actin cytoskeleton interact to maintain BBB integrity and function (Hu et al., 2017). A recent study has demonstrated that early BBB disruption within 1 h of ischaemia is caused by structural changes to endothelial cells and cytoskeletal rearrangement induced by activation of rho-associated protein kinase (ROCK)/ myosin light chain (MLC) signalling, disassembly of TJ proteins and actin polymerisation (Shi et al., 2016). The study suggests that these structural changes alter endothelial junctional sealing and facilitate infiltration of small macromolecules of ≤3 kDa. The early stage of damage is then thought to progress into late stage of BBB damage caused by MMP-9 occurring 3 h after ischaemia, facilitating the infiltration of larger macromolecules and immune cells (Shi et al., 2016). MMPs are a family of proteases that contribute to the degradation of TJ proteins and the BM after ischaemic stroke (Kim et al., 2013). MMP-2 and MMP-9 are known to be major BBB disruptors and are produced by endothelial cells, glial cells, and recruited immune cells (Hu et al., 2017). Indeed, genetic deletion of MMP-9 in mice or the pharmacological inhibition of MMPs reduced lesion volumes after cerebral ischaemia (Asahi et al., 2000).

1.7.3. Changes to the ECM after stroke

A dynamic ECM response is triggered after ischaemic stroke that involves the degradation, downregulation and upregulation of several ECM components (Kang and Yao, 2020). This will be determined spatially and temporally, varying across acute and chronic time points, as well as in proximity to the lesion. The changes to the ECM composition are related to the pathogenesis of ischaemic stroke, since the biological properties of the ECM having functional implications on BBB integrity, cellular transmigration across the BBB and repair mechanisms. There have been different approaches to investigate ECM changes, with earlier studies focusing on specific ECM components using histological techniques or reverse transcription polymerase chain reaction (RT-PCR), whilst more recent studies using ribonucleic acid (RNA) sequencing to determine vast gene expression. However, there remains a lack of consensus on the specific patterns of ECM

expression after cerebral ischaemia (Yao, 2019). It has been demonstrated after experimental stroke that BM degradation occurs as early as 10 min after reperfusion (Yepes et al., 2000). There is early upregulation of some ECM molecules as evidenced by the upregulation of fibronectin at 4 h in the stroke region of the brain post-MCAO, followed by downregulation at 24 h and 48 h (Summers et al., 2013). In contrast, collagen IV is upregulated at 48 h in the stroked region (Summers et al., 2013). However, in a different study fibronectin expression in the penumbra post-stroke was demonstrated at 7 d after surgery (Li et al., 2012). The differential regulation of laminin chains between 6 h and 24 h post-MCAO has been demonstrated and the role of COX-2 was observed, providing a link between inflammation and ECM remodelling (Ji and Tsirka, 2012). At the later time point of 7 d post-stroke, a study reported the observation that there is a decrease in endothelial laminin expression in the ischaemic core which is thought to be associated with the loss of vasculature, whilst no change of laminin in the penumbra was demonstrated (Li et al., 2012). A sophisticated study using a permanent model of MCAO and RNA sequencing at acute (24 h), sub-acute (72 h) and chronic (28 d) time points provides insight into the differential regulation of ECM components, including collagen, laminins, fibronectin, perlecan and syndecan, in the infarcted region (Munji et al., 2019). It is suggested that the early loss of BM is a result of protein degradation as a result of the early ischaemic cascade rather than decreased protein synthesis (Yao, 2019). At chronic time points, the ECM composition is modulated by the upregulation and downregulation of ECM protein expression. However, the mechanisms that regulate ECM expression are not fully known.

1.7.4. Changes to ECM receptors

As the NVU injury progresses the structural changes becomes more profound and the detachment of endothelial cells from the vessel wall occurs. This structural change alongside the effect of ischaemia and the altered ECM composition will have profound effects on ECM receptors. After cerebral ischaemia, the expression of ECM receptors can either be upregulated or downregulated and will in turn effect ECM-cell interactions (Baeten and Akassoglou, 2011; Edwards and Bix, 2019). After MCAO in baboons, there is a rapid loss of cerebral α1 or β1 integrin expression, showing a 30% reduction after 2 h and a higher 75% reduction after 24 h (Tagaya et al., 2001). A further study in baboons shows that after MCAO there

is the rapid loss of integrin α6β4 in the brain, resulting in a loss of astrocyte-ECM interaction leading to a loss of cell anchoring and integrin signalling (Wagner et al., 1997). Integrin expression is also modulated at later time points, including the upregulation of the fibronectin receptors, α5β1 and αvβ3 integrins at 7 d after stroke (Li et al., 2012).

1.8. **Repair process**

1.8.1. Repair process

After cerebral ischaemia, the brain mounts a complex and dynamic recovery process in an attempt to restore the diminished blood flow and aid neuronal replacement following cerebral damage. The response initiated involves several interconnected and coordinated processes of synaptic plasticity, gliogenesis, angiogenesis and neurogenesis (Gutiérrez et al., 2009). It is critical to appreciate that the remodelling of ischaemic tissue during the repair phase involves the coordinated response of all components of the NVU and the associated inflammatory cells, accompanied by endothelial progenitor cells (EPCs) and neural progenitor cells (NPCs) (Hermann et al., 2015). Although inflammation is considered detrimental during the acute phase of stroke, increasing evidence supports the protective role of inflammation during the repair phase and suggests a biphasic nature of many inflammatory mediators (Iadecola and Anrather, 2011).

1.8.2. Angiogenesis

Angiogenesis is the sprouting of new microvessels from pre-existing vasculature, and is known to be enhanced in the peri-infarct regions post-stroke (Hermann et al., 2015). There is experimental and clinical evidence showing a correlation of angiogenesis with improved tissue recovery and functional outcome (Krupinski et al., 1994; Hayashi et al., 2003; Arenillas et al., 2007; Liu et al., 2007). The process is tightly regulated through angiogenic growth factors and inhibitors to control the migration, proliferation and assembly of endothelial cells into tube-like structures which form networks to restore CBF (Seto et al., 2016). Angiogenesis is known to be induced by several growth factors such as vascular endothelial growth factor (VEGF), platelet-derived growth factor (PDGF), TGB-β and FGF-2 (Seto et al., 2016). Furthermore, evidence suggests that inflammatory mediators such as TNF-α and nitric oxide (NO), which are associated with early neurotoxicity, can mediate angiogenesis during the repair phase (Angels Font et al., 2010). Angiogenesis

contributes to repair in the post-ischaemic brain by restoring blood flow, through the stabilisation of brain hemodynamics and by providing a route for blood-derived macrophages to aid the removal of dead cells (Hermann et al., 2015). Furthermore, angiogenesis contributes to neurogenesis through the release of neurotrophic factors and the attraction of neural precursor cells that release growth factors (Hermann et al., 2015). Vasculogenesis is also induced after ischaemia and is thought to contribute to vascular remodelling via the *de novo* formation of blood vessels by bone marrow derived EPCs which are able to invade the ischaemic brain and differentiate (Arenillas et al., 2007). Clinically, higher levels of circulating EPCs is associated with improved patient outcome in acute ischaemic stroke patients (Sobrino et al., 2007).

1.8.3. Neurogenesis

The spatiotemporal dynamics of cerebral vascular remodelling and angiogenesis post-stroke is closely associated with stroke-induced neurogenesis. Neurogenesis is the formation of new neurones from neural stem cells (NSCs) and can occur endogenously post-stroke. NSCs can proliferate and differentiate into several neural cells including neurones, astrocytes, oligodendrocytes and ependymal cells, replacing damaged cells and contributing to the recovery process (Koh and Park, 2017). Stroke induces neurogenesis in several regions including the subventricular zone (SVC), subgranular zone (SGZ), striatum and cerebral cortex (Han et al., 2016; Koh and Park, 2017). Neurogenesis is controlled by several mediators including growth factors, cytokines and neurotransmitters. Co-coordinators of post-stroke neurogenesis include epidermal growth factor (EGF), FGF-2, erythropoietin (EPO), VEGF and NO (Wiltrout et al., 2007). Increasing evidence suggests an intimate relationship between post-ischaemic angiogenesis and neurogenesis (Merson and Bourne, 2014). Neurogenesis is closely associated with vascular remodelling and it is suggested that migrating neuroblasts use the vasculature to guide them to the damaged region (Angels Font et al., 2010). A study has demonstrated that the pro-angiogenic angiopoietin 2 is upregulated post-stoke and mediates the differentiation and migration of NPCs, contributing to neurogenesis post-stroke (Liu et al., 2009).

1.8.4. Glial scar

A key hallmark of CNS injury is reactive astrogliosis which is characterised by increased astrocyte proliferation and increased glial fibrillary acidic protein (GFAP) expression in the region surrounding the infarct, and contributes to the formation of the glial scar (Becerra-Calixto and Cardona-Gómez, 2017). The formation of the glial scar is a dynamic process involving reactive astrocytes, microglia, macrophages and ECM components (Rolls et al., 2009). It has been suggested that the glial scar presents a dual nature during the repair phase after stroke determined by its temporal context, exhibiting protective properties during the acute phase and acting as a barrier to repair during the late post-injury repair phase (Rolls et al., 2009; Cekanaviciute and Buckwalter, 2016). During the acute phase, the glial scar acts as a physical barrier that prevents the spread of toxicity from the damaged region and limits inflammation, which helps to limit tissue damage (Cekanaviciute and Buckwalter, 2016). However, during the chronic post-injury phase the glial scar is thought to impede recovery by preventing axonal regrowth via the production of CSPGs (Rolls et al., 2009; Cekanaviciute and Buckwalter, 2016).

1.8.5. Role of IL-1 and the ECM in the glial scar

There is *in vitro* and *in vivo* evidence that IL-1 is essential for the induction of reactive astrogliosis required for formation of the glial scar, demonstrating the role that inflammatory mediators can play during repair (Herx and Yong, 2001; John et al., 2004). Furthermore, a novel role of ECM molecules as critical regulators of IL-1β-induced signalling in astrocytes which results in cellular morphological changes and loss of focal adhesions associated with a reactive astrocyte phenotype has been demonstrated *in vitro* (Summers et al., 2010). The evidence suggests that vascular ECM molecules that become available to astrocytes after CNS injury may be critical regulators of IL-1β-induced astrogliosis. After experimental cerebral ischaemia there is an increase in key ECM molecules and increased expression and activation of the ECM receptor integrin β1 (Summers et al., 2013). This occurred concomitantly with increased IL-1 signalling in perivascular GFAP-positive astrocytes, providing further evidence that the ECM regulates IL-1-induced astrogliosis (Summers et al., 2013).

1.8.6. Role of IL-1 in repair

Although IL-1 is initially characterised as detrimental during the acute phase of stroke, increasing evidence suggests a biphasic nature that exhibits neuroprotective properties during the repair phase. After stroke, IL-1 is known to induce expression of the acute phase protein pentraxin-3 (PTX3) in the brain, contributing to BBB repair, angiogenesis and neurogenesis (Rodriguez-Grande et al., 2014, 2015). Further evidence that supports the protective properties of PTX3 has been demonstrated *in vivo*, showing that PTX3 promotes long-term angiogenesis and CBF recovery after cerebral ischaemia at chronic time points measured (Rajkovic et al., 2018). Differential actions of the isoforms of IL-1 have been demonstrated in several studies and attribute the neuroprotective properties to the IL-1α isoform. IL-1α has been shown to be a more potent inducer of laminin globular domain 3 (LG3) from perlecan, a component of the ECM of the NVU, which is thought to be neuroprotective and anti-apoptopic (Saini et al., 2011; Saini and Bix, 2012). Furthermore, a recent study has demonstrated that IL-1α induces endothelial activation and angiogenic markers, CXCL-1 and IL-6 *in vitro* (Salmeron et al., 2016).

1.8.7. Role of ECM in repair

The ECM provides a structural and functional environment for the cells of the NVU during physiological conditions. However, the ECM also plays a dynamic role in repair in the CNS. The importance of the ECM environment in the CNS after disease should be appreciated as supportive framework that can contribute to recovery (Burnside and Bradbury, 2014). ECM remodelling that occurs post-stroke creates ECM tracts that can be used by migrating endothelial cells to establish new capillary buds (Seto et al., 2016). Furthermore, integrin-laminin interactions have been identified as critical controllers of neurite outgrowth from adult dorsal root ganglion (DRG) neurones *in vitro*, contributing to neural regeneration (Plantman et al., 2008).

A novel function of the ECM as a regulator of IL-1-induced cerebral endothelial activation during acute brain injury has been demonstrated *in vitro*, whereby attachment of cells to ECM components enhances IL-1-induced activation of endothelial cells (Summers et al., 2013). ECM remodelling after CNS injury is associated with BBB repair, and therefore this has led to the hypothesis that BBB

repair driven by IL-1 could also be regulated by ECM remodelling. Kangwantas et al. (2016) have identified LM-10 as key ECM molecule involved in BBB repair after hypoxic injury and inflammation. The BBB dysfunction induced by oxygen glucose deprivation (OGD)/reperfusion and IL-1β treatment has been demonstrated *in vitro* using rat primary brain endothelial cells. The study showed changes to cell circulatory and the relocalisation of the TJ proteins occludin and ZO-1 from the plasma membrane to the cytoplasmic compartment (Kangwantas et al., 2016). The study distinguished LM-10 as the specific ECM molecule to reverse the key features of BBB dysfunction *in vitro*, including occludin cellular localisation and cellular morphology. Furthermore, LM-10 promoted endothelial cell attachment and spreading, with cell spreading an early marker of angiogenesis. This evidence suggests that ECM remodelling may be an essential step for restoring BBB integrity after CNS injury and implicates LM-10 as a potential mediator of BBB repair and recovery after stroke.

1.9. **The Hippo pathway**

1.9.1. Overview of the Hippo pathway

It is important to consider the potential signalling mechanisms that may regulate the repair response mediated by inflammation and the ECM after cerebral ischaemia. Indeed, the Hippo pathway is of particular interest. The Hippo pathway was originally identified in *Drosophila* and is highly conserved in mammals (Justice et al., 1995; Xu et al., 1995). Hippo signalling is often associated with development, controlling organ size, tissue homeostasis and during disease such as cancer (Meng et al., 2016). This signalling pathway plays key roles in cellular processes such as cell proliferation, differentiation, apoptosis, tissue homeostasis and organ morphogenesis. There are several upstream regulators of the Hippo cascade that have aptly depicted the pathway as sensors of the endothelium, specifically sensing the cells environment and physical nature, responding to different stimuli such as cell-cell contacts, cellular polarity, cellular metabolic stress, and of particular interest is the response to mechanical cues via the ECM and to secreted factors (Meng et al., 2016). Interestingly, pathways downstream of integrin-ECM signalling are known to regulate the Hippo pathway (Warren et al., 2018), implicating it as a critical pathway in understanding ECM function. More recently, crosstalk between the Hippo pathway and inflammation, specifically NF-κB, has been demonstrated which further highlights the complexities of the pathway (Wang

et al., 2020). Furthermore, Hippo signalling has been shown to have critical roles in vascular systems, contributing to vessel homeostasis, vascular development, angiogenesis (Park and Kwon, 2018).

1.9.2. The Hippo cascade

The Hippo pathway is a kinase cascade centred around the downstream effectors yes-associated protein (YAP) and transcriptional co-activator with PDZ-binding motif (TAZ) as illustrated in Figure 1.4 (Piccolo et al., 2014). The Hippo cascade is composed of a series of serine/threonine kinases MST1/2 and LATS1/2, the scaffolding protein WW45 and the downstream effectors of the pathway; the transcriptional co-activator YAP and its paralogue TAZ. The regulation of the pathway is focused around the cytoplasmic sequestration and nuclear shuffling of YAP/TAZ. The regulation of the pathway is dependent upon the phosphorylation of YAP by LATS1/2 at five serine/threonine residues (different sites on YAP), resulting in nuclear exclusion, and sequestration in the cytoplasm or proteasomal degradation. Hence, when the pathway is 'on' and the kinases are activated, YAP is subsequently phosphorylated and expelled from the nucleus and unable to activate genes. It has been well established that phosphorylation of YAP on S127 creates a binding consensus with 14-3-3 proteins, resulting in the sequestering of YAP in the cytoplasm (Zhao et al., 2007), whilst phosphorylation on S397 creates a phospho-degron motif for β-TrCP binding resulting in proteasomal degradation (Zhao, Li, Tumaneng, et al., 2010). When the pathway is switched 'off' and the kinases are inactivated, YAP is dephosphorylated and can translocate into the nucleus. Since YAP and TAZ are transcriptional coactivators they do not have DNA-binding domains, therefore they interact with the TEAD transcription factor family to mediate gene transcription (Zhao et al., 2008). It is important to appreciate that there are experimental circumstances that show contradictions to this and do not fully support this simple explanation of the model.

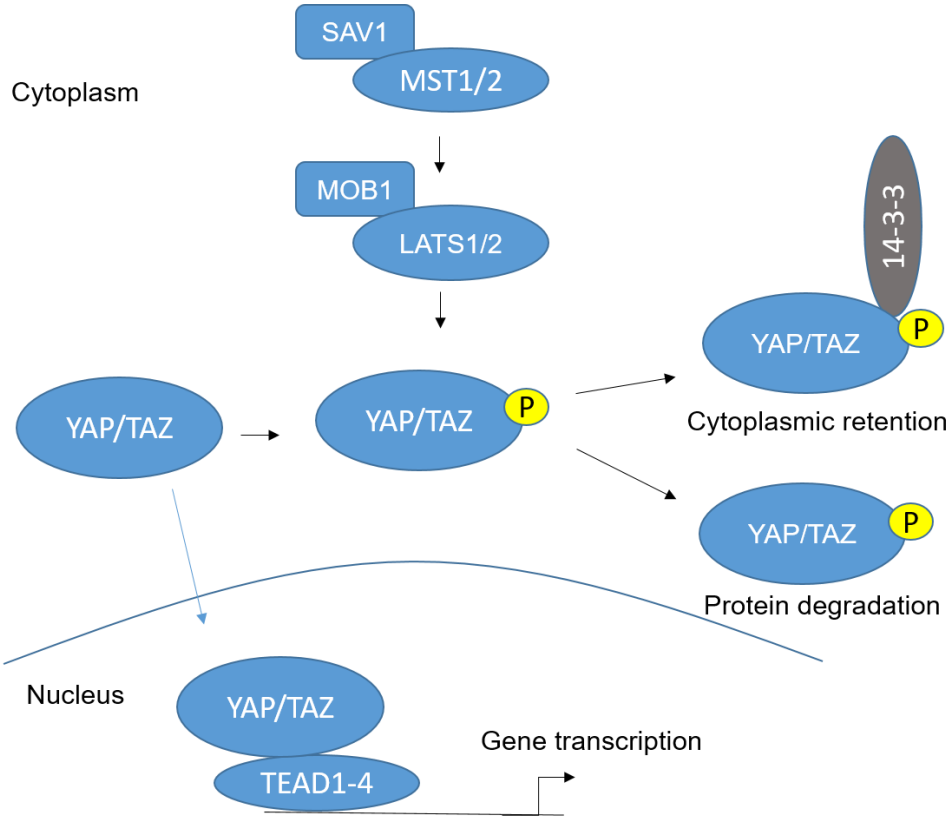

Figure 1.4. Schematic of the core Hippo kinase cascade.
When the Hippo pathway is on, upstream regulators regulate the phosphorylation of the core kinases, MST1/2 and LATS1/2. MST1/2 bind to their regulatory protein SAV1 to phosphorylate and activate the LATS1/2 kinases and the regulatory subunits MOB1. Resulting in subsequent YAP/TAZ phosphorylation and either cytoplasmic retention or degradation. When the Hippo pathway is off, YAP/TAZ is not phosphorylated and hence can translocate into the nucleus. Subsequently, YAP/TAZ can bind to TEAD transcription factors to induce gene transcription.

1.9.3. Upstream regulators of the Hippo pathway

The Hippo pathway is regulated in response to a myriad of extracellular and intracellular signals as previously mentioned. These include cell contact, cell polarity, mechanical signals, G-protein-coupled receptor (GPCR) signalling, cellular energy status. Typically these signals will modulate phosphorylation events of the core kinase cascade, resulting in altered MST1/2 and LATS1/2 activity and hence YAP phosphorylation status (Meng et al., 2016). However, it is important to appreciate that there are proteins that can directly regulate YAP localisation and activity, independent of the core kinase cascade. Furthermore, the Hippo pathway crosstalks with other signalling pathways such as Wingless/Ints (Wnt), TGF-β and bone morphogenetic proteins (BMPs), Notch, and Hedgehog (Hh), adding further complexity in understanding the regulation of the Hippo pathway (Zhao, Li and Guan, 2010).

Physical cues in the form of cell-cell contact and cellular attachment to the ECM are major regulators of YAP signalling. Cell-cell contact activates the kinase cascade and results in subsequent YAP phosphorylation and sequestration in the cytoplasm, hence proliferation associated genes are not activated providing an inhibitory mechanism to cell growth. It has been demonstrated in HUVECs that contact-inhibition is mediated by YAP/TAZ signalling through vascular endothelial cadherin (VE-cadherin)-mediated YAP phosphorylation (Choi et al., 2015). The attachment of cells to the ECM can regulate YAP signalling through pathways downstream of ECM-integrin signalling. This includes FAK-Src-PI3K signalling and Rho-GTPases that can directly affect the core kinase cascade or act independently to alter YAP activation (Meng et al., 2016).

1.9.4. Role of the Hippo pathway in inflammation, vessel biology and atherosclerosis

There is increasing evidence of crosstalk between the Hippo pathway and inflammation (Wang et al., 2020). Understanding the relationship between inflammation and Hippo signalling is a growing area and there is conflicting evidence demonstrating opposing effects of deletion of YAP (Lv et al., 2018) and knockdown of YAP/TAZ (K.-C. Wang et al., 2016) respectively. There is evidence that YAP/TAZ is involved in TNF-α-induced inflammatory responses in endothelial cells, whereby TNF-α induced YAP translocation into the nucleus and that nuclear YAP was required for optimal TNF-α induced ICAM-1 and VCAM-1 expression (Choi et al., 2018). The crosstalk between the Hippo pathway and other signalling pathways downstream of inflammatory stimuli has been observed at the level of p38 MAPK (Huang et al., 2016) and ERK1/2 (You et al., 2015) pathways, whereby kinases involved in these pathways may modulate kinases of the Hippo cascade.

Atherosclerosis is associated with endothelial dysregulation in the arterial wall (Libby et al., 2002). The haemodynamic forces acting on the vessel wall are determined by the flow patterns and direction of the blood in that region. In healthy vessels with straight forward flow, termed laminar sheer, the phenotype of the endothelial cell is described as athero-protective due to their anti-inflammatory and anti-proliferative properties (Chiu and Chien, 2011). However, atherosclerosis develops in arterial branches and the aortic arch when flow patterns in those areas

become disturbed, which results in an atheroprone phenotype characterised by pro-inflammatory state and pro-proliferation (Chiu and Chien, 2011). Considering that atherosclerosis is a mechanobiology-related disease and that YAP signalling is implicated in mechanotransduction, it is not surprising that there is evidence linking the Hippo pathway and atherosclerosis. Indeed, disturbed blood flow has been shown to activate YAP/TAZ signalling to induce an atheroprone phenotype and a reduced atheroprone phenotype was observed in atherosclerotic mice after YAP/TAZ inhibition (K.-C. Wang et al., 2016). Further support of YAP/TAZ in atherogenesis has been demonstrated whereby disturbed flow increases YAP/TAZ signalling, resulting in pro-inflammatory gene activation. The study investigated a mechanism whereby atherprotective unidirectional sheer stress triggers integrin signalling leading to integrin–Gα13 interaction, subsequent RhoA inhibition and YAP phosphorylation and sequestration in the cytoplasm (L. Wang et al., 2016).

There is increasing evidence implicating the Hippo pathway in angiogenesis (Boopathy and Hong, 2019). Indeed, YAP/TAZ has been implicated in endothelial cell proliferation, migration and survival. Furthermore, YAP/TAZ signalling has been critically implicated as regulator of vascular barrier formation, vascular sprouting and angiogenesis; further cementing the pathway in vessel physiology. VEGF is a key mediator of sprouting angiogenesis and blood vessel formation. It has been demonstrated that VEGF activates YAP/TAZ via its effects on the actin cytoskeleton to trigger a transcription programme required for a full angiogenic response (Wang et al., 2017). The multifaceted properties of YAP/TAZ in endothelial cell behaviour include actin cytoskeleton remodelling contributing to sprouting angiogenesis (Kim et al., 2017). Further dissection of the relationship between VEGF/VEGFR signalling was determined using a bioluminescence-based biosensor of LATS kinase activity that demonstrated VEGF triggers PI3K-AKT and MEK-ERK (MAPK) signalling which inhibits LATS kinase and thus enables YAP/TAZ activation and translocation into the nucleus (Azad et al., 2018). Angiopoietins are another family of growth factors that are known to bind to Tie receptors expressed on endothelial cells, contributing to angiogenesis and vascular remodelling. It has been demonstrated *in vitro* using endothelial cells that ANG-2 is a key transcriptional target of YAP which enhances angiogenesis sprouting (Choi et al., 2018).

1.10. **Mouse models of ischaemic stroke**

1.10.1. Overview of animal models

The ability to genetically manipulate mice has been a powerful tool for investigating gene function *in vivo* and genetic knockouts (KOs) can be used in experimental stroke models. A variety of animal stroke models have been developed to aid research into the underlying mechanisms and potential therapeutic targets associated with stroke. However, it is of paramount importance that the animal model used is carefully chosen to ensure that research is clinically translatable and ethically responsible. Animal models provide the benefit that they can be standardised and reproducible, whilst providing a tool that contains the vasculature needed to mimic the pathophysiology of stroke (Fluri et al., 2015). Animal models also enable direct access to brain tissue and provide tools that can be studied from the onset of ischaemia (Fluri et al., 2015). However, it is essential that the Animals (Scientific Procedures) Act 1986 (ASPA) is strictly followed and that the 3 R's of replacement, reduction, and refinement are achieved to the highest standard possible (Fenwick et al., 2009).

1.10.2. Occlusive middle cerebral artery stroke models

Occlusive middle cerebral artery (MCA) stroke models are thought to be the closest representation of human stroke as it is often the MCA and associated cerebral vessels that are affected in patients (Fluri et al., 2015). In order to induce an occlusion, an intraluminal filament is introduced into the carotid artery and advanced until it reaches the MCA. There are two approaches to this method; the Koizumi method whereby the filament is inserted directly through the common carotid artery and requires permanent ligation (Koizumi et al., 1986), or the Longa method whereby the filament is inserted into the external carotid artery and hence does not require ligation (Longa et al., 1989). The filament can be kept in place for the required time to induce an occlusion time of choice. The two approaches will trigger different reperfusion profiles, since the Longa method facilitates more reperfusion. These methods of occlusion produce striato-cortical lesions (Howells et al., 2010), malleable upon occlusion time. The model mimics the key hallmarks of ischaemic stroke in humans including neuronal cell death, neuroinflammation and BBB damage.

1.11. Summary and aims

The endogenous remodelling of the CNS associated with repair post-stroke is limited and therefore it would be of benefit for the development of therapeutic strategies that target the repair phase to aid recovery. The dynamic role of the ECM in the CNS has started to be appreciated as its ability to modulate cell survival, differentiation and activation has been discovered. Interestingly, there is growing evidence that laminins exert protective properties on the endothelium and neurones of the CNS. Furthermore, a novel role of the ECM as a regulator of IL-1-induced cerebral inflammation has been demonstrated and LM-10 has been identified as a mediator of BBB repair. This evidence suggests that targeting inflammation and components of the ECM, specifically LM-10, in order to create a cerebral environment that promotes BBB repair is an attractive therapeutic strategy post-stroke. However, the relationship between LM-10 and inflammation remains poorly understood.

The overarching aim of this thesis was to investigate the role of LM-10 on endothelial inflammation and repair mechanisms after cerebral ischemia using *in vitro* and *in vivo* approaches. This thesis will specifically aimed to:

1. Establish an *in vitro* model to investigate the effect of LM-10 on the IL-1β-induced activation, IL-1β-induced signalling and angiogenic response of cerebral endothelial cells.
2. Determine the role of IL-1R1 in the cerebrovasculature after cerebral ischaemia, specifically on laminin α4 and laminin α5 expression across several time points post-stroke.
3. Generate and characterise a brain endothelial laminin α5 conditional deletion genetic strain mouse, in order to investigate the role of brain endothelial laminin α5 in cerebral ischaemia.

Chapter 2. **Methods**

2.1. General cell culture and reagents

2.1.1. LM-10 and control wells plate coating

Tissue culture plates (Corning, UK) were pre-coated at 4°C overnight with human recombinant LM-10 (BioLamina, Sweden), diluted in phosphate-buffered saline with calcium and magnesium (PBS^+) at concentrations of 0.1, 1, 2.5, 5, 10 µg/ml. Control wells were incubated with filter sterilised (0.22 µm pore size filter, Starlab, UK) 0.1 % (w/v) low endotoxin bovine serum albumin (BSA) in PBS^+ or with 50 µg/ml mouse collagen IV (VWR, UK). After overnight incubation, LM-10 solutions were removed from the wells and stored at 4 °C. The collagen IV was stored at -20°C and the other control wells were aspirated into waste. PBS^+ was added to LM-10 coated wells and PBS without calcium and magnesium (PBS) to control wells to prevent drying out. Sterile gelatin 0.1 % (w/v) (BDH, UK) in distilled water was also added as a further control and incubated at 37°C and 5 % CO_2 for 1 h to allow the gelatin coating to set. Non-specific cell-binding sites were then blocked with filter sterilised (0.22 µm pore size filter) 0.1 % (w/v) low endotoxin BSA in PBS and plates were washed in PBS three times before cell seeding. The collagen IV and 0.1% gelatin wells were allowed to dry at room temperature 1 h prior to cell seeding, whilst extra care was taken with the LM-10 wells to ensure they never dried before seeding. For experiments using Matrigel (20 µg/ml), neat Matrigel (9.16 mg/ml, Corning) was diluted in Dulbecco's Modified Eagle's Medium to 20 µg/ml and stored at -20°C. Matrigel was thawed overnight on ice at 4°C. Tissue culture plates were pre-coated at 4°C overnight, alongside the LM-10 coating, and incubated at 37°C and 5 % CO_2 for 45 min. Plates were washed in PBS before cell seeding.

2.1.2. Bend.5 cell culture

The immortalised mouse brain endothelial cell line bEnd.5 was acquired from Public Health of England (UK). bEnd.5 cells were cultured and maintained in T 75cm^2 flasks (Corning) containing bEnd.5 maintenance media; Dulbecco's Modified Eagle's Medium (DMEM, high glucose with 4500 mg/L glucose, L-glutamine, and sodium bicarbonate) supplemented with 1 % L-glutamine solution, 10 % fetal bovine serum (FBS; Thermo Fisher Scientific, Hemel Hempstead, UK), 1 % penicillin-streptomycin and were kept at 37°C and 5 % CO^2. Cells were passaged at 80-90 % confluency using 10 % trypsin in PBS and counted using a haemocytometer.

2.1.3. Primary mouse brain endothelial cell culture

For experiments using primary mouse brain endothelial cells (MBECs), 8-12 week old adult male C57BL/6J (Charles River, UK) mice were used. Plates were coated as previously described in section 2.1.1. Primary MBEC starve media [(DMEM/F12, 1% penicillin streptomycin solution, 1 % L-glutamine] and primary MBEC maintenance media [(DMEM/F12, 5 % plasma derived serum (First link Ltd, UK), 5 % fetal calf serum, 1 % L-glutamine, 1 % penicillin streptomycin, heparin sodium salt (100 µg/ml) and endothelial cell growth supplement (100 µg/ml) (ECGS; VWR)] were prepared and stored in fridge.

For primary MBEC isolations, mice were euthanized using CO_2 gas and neck dislocation. Mice were decapitated, and brains were removed and kept in starve media on ice. The following recommended volumes are for 5 mice brains and the protocol should be performed under sterile conditions. The brains were dissected and the cerebellum, meninges and white matter were removed. The dissected brains were placed in starve media at a ratio of 1 brain:1 ml media and minced using a sterile scalpel, then homogenised using a dounce homogeniser. The homogenate was then centrifuged at 200 x g for 5 min at 4°C. The supernatant was removed and resuspended in 15 ml of 18 % (w/v) dextran (Affymetrix, Thermo-Fisher Scientific) in starve media and centrifuged at 3893 x g for 10 min at 4°C. The aqueous layer and white layer were removed and the dark red pellet was resuspended in 1 ml Hanks' balanced salt solution (HBSS) with sodium bicarbonate / without calcium chloride and magnesium sulphate. The suspension was passed through a 70 µm cell strainer (Falcon, Corning) and the microvessels were retained on the strainer. The cell strainer was inverted and rinsed nine times with 0.5 ml of HBSS to transfer microvessels into a glass dish and a further 0.5 ml of HBSS was added to the dish. The following three enzymes were added to the glass dish: 4.2 µl of DNase I (125.1 U/ml), 5 µl protease inhibitor Tosyl-L-lysine chloromethyl ketone hydrochloride (TLCK) (14.7 µg/ml) and 12.5 µl of collagenase/dispase (100 mg/ml). The glass dish was incubated at 37°C for 12 min or until the vessel walls take on the appearance of ‘pearls on a string’. The digested microvessel solution was collected and centrifuged at 800 x g for 5 min. The supernatant was removed and the pellet resuspended in the required volume of maintenance media containing puromycin at a 1:1000 ratio. MBECs were seeded

on plates. Media was replaced with maintenance media every two days and cells were grown until confluency (day 13-14).

2.1.4. hCMEC/D3 cell culture

The immortalised human cerebral microvascular endothelial cell line, hCMEC/D3, was purchased from Merck (UK). hCMEC/D3 cells were maintained in T75 cm^2 flasks pre-coated with rat tail collagen type I (Merck) diluted in phosphate buffered saline (PBS) 1:100 and incubated at 37°C for 30 min-1 h. hCMEC/D3 cells were maintained in EndoGRO-MV Complete Culture Media; 5 % FBS, L-glutamine (10 mM), EndoGRO-LS supplement (0.2 %), heparin sulphate (0.75 U/ml), ascorbic acid (50 µg/ml), hydrocortisone hemisuccinate (1 µg/ml), recombinant human epidermal growth factor (5 ng/ml), freshly added recombinant human fibroblast growth factor-basic (1 ng/ml; Merck) and 1 % penicillin-streptomycin maintained at 37°C in a humidified atmosphere containing 5 % CO_2. Cells were passaged at 80-90 % confluency using 0.25 % trypsin/ 1 mM EDTA solution.

2.2. **Cell attachment assays *in vitro***

2.2.1. bEnd.5 cell attachment assay (crystal violet assay)

96-well plates were coated with 0.1 % BSA in PBS^+, 50 µg/ml collagen IV, sterile 0.1 % gelatin and LM-10 (0.1, 1, 2.5, 5, 10 µg/ml) as previously described in section 2.1.1. bEND.5 cells were seeded at a density of 2 x 10^4 cells per well and incubated at 37°C and 5 % CO_2 for 1 h. To estimate 100 % cell attachment, the working concentration of 2 x 10^4 cells per well of bEnd.5 cells was diluted to 25 %, 50 % and 75 % using bEnd.5 maintenance media and 70 µl was added to uncoated, unblocked wells and was incubated for the same 1 h incubation as the sample wells.

Cells in the wells to be used for determining 0, 25 %, 50 %, 75 % and 100 % cell attachment were fixed by adding 20 µl of 25 % (w/v) glutaraldehyde directly to the well containing the media. Non-adherent and loosely attached cells were removed from all other wells by aspirating the solution, washing once with PBS and then fixing with 100 µl of 5 % (v/v) glutaraldehyde in PBS per well. The microtiter plates were incubated at room temperature for 30 min then washed three times with 200 µl of dH_2O. Cells were stained by adding 100 µl of vacuum filtered 0.1 % (w/v) crystal violet (Gurr Certistain, UK) in PBS to each well and incubating the microtiter

plates at room temperature for 1 h. Wells were then washed once with 200 µl of dH_2O, followed by 300 µl of dH_2O three times. The dye was solubilised in 100 µl of 10 % (v/v) acetic acid in dH2O and plates were shaken on a rocker at high speed for 5 min at room temperature. The absorbance at 570 nm measured using a Biotek plate reader (Synergy HT, BioTek, UK). Cell adhesion was measured by the absorbance at 570 nm, compared to the absorbance of the standard curve. The standard curve was fitted by a sigmoidal 4PL equation in GraphPad Prism 8.1.2 (GraphPad Software Inc). Number of cells attached was then calculated using the standard curve. Each condition was performed in triplicate and was repeated on 3 different cultures.

2.2.2. Primary MBEC cell attachment assay (crystal violet assay)

96-well plates were coated with 0.1 % BSA in PBS+, 50 µg/ml collagen IV, sterile 0.1% gelatin and LM-10 (0.1, 1, 2.5, 5, 10 µg/ml) as previously described in section 2.2. Primary MBEC were isolated as previously described in section 2.1.3, and grown to confluency (day 13-14). Cell attachment was measured as previously described using crystal violet staining in section 2.2.1. The absorbance at each coating is expressed as a percentage absorbance of each control. Each condition was performed in quintuple and was repeated on 4 different cultures.

2.2.3. Incucyte confluence measurement

24-well plates were pre-coated with Matrigel (20 µg/ml) or LM-10 (10 µg/ml) as previously described in section 2.1.1. hCMEC/D3 cells were seeded at several densities (5 x 10^4 cells/well, 1 x 10^5 cells/well, 2 x 10^5 cells/well) in EndoGRO-MV Complete Culture Media. Phase contrast images were acquired at 4 h and 24 h after seeding using an Incucyte Zoom Live Cell Analysis system (Essen BioScience, UK) with a 123 10x/1.22 Plan Apo OFN25 objective. The IncuCyte ZOOM's Confluence Processing analysis tool (Basic Analyzer) was used to calculate percentage confluence. Experiment was repeated on 3 different cultures.

2.3. **Endothelial IL-1β treatment *in vitro***

2.3.1. IL-1β treatment of bEnd.5 cells after a 24 h seeding time

48-well plates (Corning) were coated with 0.1 % BSA in PBS^+, 50 µg/ml collagen IV, sterile 0.1 % gelatin and 10 µg/ml LM-10 as previously described in section

2.1.1. The bEnd.5 cells were seeded at a density of 50,000 cells/ well on 48-well plates and were incubated for 24 h at 37°C and 5 % CO_2. Recombinant mouse IL-1β (R&D Systems, UK) was diluted in the bEnd.5 cell culture media; DMEM, supplemented with 1 % L-glutamine solution, 10 % FBS, 1 % penicillin-streptomycin. Cultures were treated with vehicle control (bEnd.5 media without IL-1β) or IL-1β (0.1, 1, 10, 100 ng/ml) and incubated for a further 24 h. Experiment was repeated on 3 different cultures.

2.3.2. IL-1β treatment of primary MBECs

96-well plates were coated with 0.1 % BSA in PBS+, 50 µg/ml collagen IV, sterile 0.1 % gelatin and 10 µg/ml LM-10 as previously described in section 2.1.1. Primary MBECs were isolated and grown to confluency (day 13-14) as previously described in section 2.1.3. Recombinant mouse IL-1β (R&D Systems) was diluted in the primary MBEC maintenance media. Cultures were treated with vehicle (MBEC maintenance media without IL-1β) or IL-1β (0.1, 1, 10, 100 ng/ml) and incubated for 24 h. Each condition was performed in quintuple and was repeated on 4 different cultures.

2.3.3. IL-1β treatment of bEnd.5 cells after a 4 h seeding time

24-well plates were pre-coated with Matrigel (20 µg/ml) or LM-10 (10 µg/ml) as previously described in section 2.1.1. bEnd.5 cells were seeded at a density of 200,000 cells/well for 4 h. Recombinant mouse IL-1β (R&D Systems) was diluted in the bEnd.5 cell culture media. Cells were treated with IL-1β (10 ng/ml) for 15, 30, 60,120 min. Cell supernatants and lysates were then collected. Experiment was repeated on 3 different cultures.

2.3.4. IL-1β treatment of hCMEC/D3 cells after a 4 h seeding time (log-concentration response)

24-well plates were pre-coated with Matrigel (20 µg/ml) or LM-10 (10 µg/ml) as previously described in section 2.1.1. hCMEC/D3 cells were seeded at a density of 200,000 cells/well for 4 h. Recombinant human IL-1β (R&D Systems) was diluted in the EndoGRO-MV Complete Culture Media. Cultures were treated with vehicle control (0 ng/ml of IL-1β in EndoGRO-MV Complete Culture Media) or IL-1β (0.1, 0.3, 1, 3, 10, 10, 100 ng/ml) and incubated for 24 h. Experiment was repeated on 4 different cultures.

2.3.5. IL-1β treatment of hCMEC/D3 cells for signalling pathway analysis, Western blots and qPCR

24-well plates were pre-coated with Matrigel (20 µg/ml) or LM-10 (10 µg/ml) as previously described in section 2.1.1. hCMEC/D3 cells were seeded at a density of 200,000 cells/well in EndoGRO-MV Complete Culture Media for 4 h. Recombinant human IL-1β (10 ng/ml) was added into wells for 5, 15, 30, 60,120 and 240 min as stated in figure legends. Experiment were repeated on 4 separate cultures.

2.4. **Neutrophil transmigration assay**

2.4.1. Neutrophil isolation

8-12 week mice were culled via CO_2 and cerebral dislocation as confirmation. The femur were then dissected out and maintained in Roswell Park Memorial Institute (RPMI) media (Thermo-Fisher Scientific) at room temperature (RT). The bone marrow was then extracted from the femur via a centrifuge flushing method consisting of a 0.5 ml eppendorf (with hole in the bottom created by a 21 gauge needle) placed inside a 2 ml eppendorf containing 200 µl sterile PBS. Femurs were cleaned with blue roll and a scalpel used to cut the femurs at the hip end, which were then placed cut end down into the flush tube. Centrifuge tubes were spun at maximum speed on micro centrifuge (10000 x g, 10 secs) and the bone marrow was flushed out of the femur. The supernatant (PBS) was removed to leave the red pellet. Pellet resuspended in 3 ml ACK lysis buffer (Thermo Fisher Scientific) for 3 min and reaction stopped with 7 ml DMEM. Suspensions were then passed through a 70 µM strainer and centrifuged at 1500 g, 4°C for 3 min. Supernatants were discarded and pellets were resuspended in 5 ml HBSS. 5 ml of 62 % isotonic percoll was added to suspensions and centrifuged at 1000 g, 30 min, 0 brake acceleration 3. Supernatant was then removed and pellets were resuspended in 10 ml HBSS. Suspensions were then centrifuged at 2000 x g, 4°C for 5 min. Finally, supernatants were discarded, pellets resuspended in 5 ml RPMI, and counted using a haemocytometer.

2.4.2. Neutrophil transmigration assay

The neutrophil transmigration assay was carried out as described previously with some modifications as detailed below (Allen et al., 2012). Transwell inserts (6.5 mm with 3.0 µm pore polycarbonate membrane) were coated with gelatin, collagen

IV and LM-10 as previously described in section 2.1.1. 1 x 10^5 cells/well of bEnd.5 cells in bEnd.5 maintenance media were seeded onto transwell inserts for 24 h. bEnd.5 cells were then pre-treated with mouse IL-1β (100 ng/ml) or vehicle for 4 h, in the presence or absence of IL-1Ra (100 µg/ml, Kineret, SOBI, Sweden) which was pre-treated in the well 15 min before IL-1β treatment. Inserts were then washed and transferred to a fresh 24-well plate. 5 x 10^5 neutrophils were added to the luminal compartment of the transwells inserts and allowed to transmigrate for 24 h into the abluminal compartment containing serum free RPMI. Cultures were collected from abluminal compartments and centrifuged at 2000 x g for 5 min and counted with a haemocytometer.

2.5. **Measurement of adhesion molecules and cytokines/chemokines**

2.5.1. Collection of supernatants and cell lysates for ELISAs

After treatment with IL-1β, the conditioned medium (supernatant) and cell lysates were collected. To collect the cell lysates, the wells were washed with PBS and 150 µl/well or 50µl/well of lysis buffer [0.1 % Triton X-100 in PBS + 1 % protease inhibitor cocktail (Merck)] was added to 48-well plates and 96-well plates respectively. Plates were kept on ice for 10 min and the cell layer was scratched mechanically using a 200 µl pipette tip. The lysed cells were collected and kept frozen at -20°C.

2.5.2. Analysis of cell number by total protein assay (bicinchoninic acid assay)

Total protein in the cell lysate of primary MBECs was assessed as an indirect measure of cell number. A Pierce™ bicinchoninic acid assay (BCA) Protein Assay Kit (Thermo-Fisher Scientific) was performed using a standard curve of BSA from 20 to 2000 µg/ml, according to manufacturer's instructions. Briefly, 10 µl of each sample or 10µl of BSA standard was added to a 96-well plate with 200 µl of working reagent, composed of 50 parts Reagent A (bicinchoninic acid solution) and 1 part Reagent B (4 % cupric sulphate). The plate was incubated at 37 °C in the dark for 30 min. The absorbance was measured at 570 nm and protein concentration in samples was calculated using the standard curve. Total protein was expressed as µg/ml of protein.

2.5.3. ELISAs

Human ICAM-1/VCAM-1, phospho-p38a and phospho-ERK1/2 in cell lysates, and IL-8 in supernatants were quantified by enzyme-linked immunosorbent assay (ELISA) (R&D Systems) according to manufacturer's instructions. Mouse ICAM-1/VCAM-1 and P/E-selectin in the cell lysate and mouse chemokine KC/CXCL1, VEGF, IL-6 and monocyte chemoattractant protein-1 (MCP-1) in the supernatant were quantified by ELISA (R&D Systems) according to manufacturer's instructions. Absorbance was measured at 450 nm and corrected at 570 nm with a plate reader (Synergy HT, BioTek, UK). The standard curve was fitted by a sigmoidal 4PL equation in GraphPad Prism. Concentrations of the samples were achieved by interpolating the values from the standard curve. Levels for all cytokines analysed were expressed as pg/ml. Levels of cytokines were corrected for cell number and expressed as pg/ml per µg/ml of total protein (pg/µg of protein), using total protein calculated in the BCA assay in section 2.5.2.

2.6. **Measurement of protein by Western blot**

2.6.1. Western blot

hCMEC/D3 cells were lysed in RIPA buffer (50 mM Tris-HCl, 150 mM NaCl, 1 % sodium deoxycholate, 0.1 % SDS, and 2 mM EDTA) supplemented with 1 % protease inhibitor cocktail and phosphatase inhibitors (1X). Lysates were scratched and titrated thoroughly before the addition of Laemmli buffer (2 % (w/v) SDS, 5 % (v/v) β-mercaptoethanol, 10 % (v/v) glycerol in 60mM Tris-HCl, pH 6.8). Samples were then boiled at 95°C for 5 min. Equal quantities of protein were loaded. Samples were run on 10 % SDS polyacrylamide gel at 70 V for 20 min then 120 V for 1 h. Proteins were transferred at 25 V (high MW setting) onto polyvinylidene difluoride (PVDF) (Bio-Rad) using a Trans-Blot Turbo Transfer System (Bio-Rad) before blocking with 5 % w/v BSA in PBS 0.1 % (v/v) Tween 20 (PBST) for 1 h at RT. Membranes were incubated (4°C) overnight in primary antibody in PBST 5 % BSA. Following this, membranes were washed in PBST (3 x 5 min wash) and incubated with secondary antibody in PBST % BSA for 1 h at RT. Details of all antibodies used are presented in Table 2.1. Membranes were washed in PBST (3 x 5 min wash) and then incubated in ECL Prime Western Blotting Detection Reagent (GE Life Sciences) before exposure with G:BOX (Syngene) and Genesys software. β-Actin (Abcam) was used as a loading control.

Densitometry was determined using ImageJ software and detected intensities were normalised against β-Actin. Ratios of pYAP/YAP were calculated.

Table 2.1. Primary and secondary antibodies for use in Western blots.
Antibody description and the correct dilution to use.

Antibody	Primary or Secondary	Company	Dilution
IκBα	Primary	Cell Signalling	1:1000
Phospho-p65 (Ser536)	Primary	Cell Signalling	1:1000
p-YAP127	Primary	Cell Signalling	1:1000
p-YAP397	Primary	Cell Signalling	1:1000
Rabbit anti-IgG (rabbit polyclonal)	Secondary	Agilent	1:1000
YAP	Primary	Cell Signalling	1:1000

2.7. **Measurement of gene expression by qPCR**

RNA was extracted using Purelink RNA minikit (Thermo Fisher Scientific) according to the manufacture's protocol, with the use of PureLink™ DNase Set (Thermo Fisher Scientific) for the DNase treatment as stated in the protocol. Extracted RNA was checked for yield and purity using the Nanodrop 1000. RNA (1 µg) was converted to cDNA using SuperScript™ III Reverse Transcriptase (Thermo Fisher Scientific), according to the manufacturer's protocol. Quantitative polymerase chain reaction (qPCR) was performed using Power SYBR Green PCR Master Mix (Thermo Fisher Scientific) in 384-well format using a 7900HT Fast Real-Time PCR System (Applied Biosystems). Three microliters of 1:20 diluted cDNA was loaded with 200 mmol/l of primers in triplicate, primers in Table 2.2. Data were normalized to the expression of the housekeeping gene *GAPDH*. Expression levels of genes of interest were calculated as follows: relative mRNA expression=E−(Ct of gene of interest)/ E−(Ct of housekeeping gene), where Ct is the threshold cycle value and E is efficiency.

Table 2.2. Primer sequences for genes of interest after IL-1β treatment in hCMEC/D3 cells.
Forward (FWD) and reverse (REV) primers for each gene target.

Gene Target	Primer sequence
Ctgf	FWD: CAGCATGGACGTTCGTCTG REV: AACCACGGTTTGGTCCTTGG
Serpine 1	FWD: ACCGCAACGTGGTTTTCTCA REV: TTGAATCCCATAGCTGCTTGAAT
GAPDH	FWD: GCACCGTCAAGGCTGAGAAC REV: AGGGATCTCGCTCCTGGAA

2.8. **Angiogenic assays**

2.8.1. Scratch assay

hCMEC/D3 cells were seeded at 40,000 cells/well in 96-well ImageLock plate (Essen BioScience) and left to adhere for 4 h. Wells were scratched using a 96-pin IncuCyte WoundMaker Tool (Essen BioScience), cells were then washed twice with PBS and replaced with fresh media. Phase contrast images were acquired at 2 h intervals for a period of 24 h on an Incucyte Zoom Live Cell Analysis system using a 4x/3.05 Plan Apo OFN25 objective. The 96-well Cell Migration Software Application Module (Essen BioScience) was used to quantify relative wound density. Relative wound density is a measure (%) of the density of the wound region relative to the density of the cell region:

$$\%RWD(t) = (w(t)-w(0)) / (c(t)-w(0)) \times 100$$

w(t)=Density of wound region at time, (t)

c(t)=Density of cell region at time, (t)

2.8.2. Tube formation assay

50 µl of undiluted Matrigel (9.16 mg/ml) was added to an ice-cold 96-Well plate and incubated at 37 °C for 45 min to gel. 70 µl of LM-10 (10 µg/ml) was added to any LM-10-supplemented wells, whilst PBS was added to control wells and the plate was incubated for a further 2 h at 37°C. The PBS and LM-10 aqueous layers on top of the Matrigel were aspirated. hCMEC/D3 cells were resuspended in media supplemented with 3 µg/ml bFGF at a density of 10,000 cells/well and seeded on the Matrigel layer. Phase contrast images were acquired at 0 and 6.5 h on an

Incucyte Zoom Live Cell Analysis system using a 4x/3.05 Plan Apo OFN25 objective. The angiogenesis analyser macro in ImageJ was used to quantify total number of branches and total branching length.

2.9. **Animals**

2.9.1. Animal housekeeping

All scientific animal procedures were carried out in accordance with the Animal Scientific Procedures Act (1986) and the European Council Directive 2010/63/EU, and procedures were approved by the Animal Welfare and Ethical Review Body, University of Manchester (UK), and the Animal Care and Use Committee of the Institute of Experimental Medicine, Budapest (Hungary). Experiments adhered to ARRIVE (Kilkenny et al., 2010) and IMPROVE guidelines (Percie du Sert et al., 2017). All animals were group housed in individually ventilated cages in standard housing conditions (temperature 21 ± 1°C; humidity 55% ± 10%; 12-hour light-dark cycle). Animals had free access to standard rodent diet (SDS, UK) and water. All C57BL/6J throughout studies were purchased from Charles River (UK).

2.9.2. Brain endothelial IL-1R1 KO mice

Brain endothelial-specific IL-1R1 knockout (KO) mice were generated and characterised as previously described (Wong et al., 2019). Mice were maintained at the Institute of Experimental Medicine, Budapest. Mice were previously generated by crossing mice in which exon 5 of the *Il1r1* gene is flanked with loxP sites (IL-1R1$^{fl/fl}$) (Abdulaal et al., 2016) with mice expressing Cre recombinase under the promoter of the thyroxine transporter (Slco1c1) that is specifically expressed in brain endothelial cells (Ridder et al., 2011). These mice are named throughout the studies as IL-1R1$^{fl/fl\ \Delta\ Slco1c1}$. Successful ablation of brain endothelial IL-1R1 deletion was achieved by a tamoxifen regimen consisting of 2 mg/100 µl tamoxifen in corn oil for five consecutive days in 6 week old male mice, followed by a period of 21 d (from the start of treatment) to ensure sufficient time for successful deletion. Controls were IL-1R1$^{fl/fl}$ mice treated with tamoxifen for the same regimen. Mice designated for experimental stroke underwent surgery at least 21 d after the start of tamoxifen regimen.

2.9.3. Brain endothelial laminin α5 KO mice

Brain endothelial-specific laminin α5 KO mice were generated at the University of Manchester, UK. Laminin alpha 5 (lamα5) floxed mice ($Lamα5^{fl/fl}$) mice were obtained from Miner and colleagues at Washington University, USA (Nguyen et al., 2005). Briefly, $Lamα5^{fl/fl}$ mice were generated by inserting a loxP site into intron 21 of Lamα5, and a second loxP site was inserted into intron 14 (Nguyen et al., 2005). Slco1c1 mice were previously generated (Ridder et al., 2011) and maintained at the University of Manchester. I generated a brain endothelium-specific laminin α5 KO ($Lamα5^{fl/fl\ \Delta\ Slco1c1}$) by crossing $Lamα5^{fl/fl}$ mice with mice expressing the Slco1c1. After Cre-mediated recombination, splicing from exon 14 to 22 occurs and removes exons 15-21. The 7 exons that are removed encode 40% of domain V, which consists of laminin EGF-like repeats (Nguyen et al., 2005).

$Lamα5^{fl/fl\ \Delta\ Slco1c1}$ mice and $Lamα5^{fl/fl}$ allocated for characterisation underwent a tamoxifen regimen consisting of 2 mg/100 µl tamoxifen in corn oil (Sigma-Aldrich) for five consecutive days in 6 week old male mice. Animals were culled 0, 7, 14 and 21 d after tamoxifen administration to determine successful ablation of laminin α5. All mice allocated for experimental stroke underwent surgery at least 21 days after the start of tamoxifen or vehicle administration.

2.10. **Genotyping**

2.10.1. DNA extraction

Extract-N-Amp™ Tissue PCR Kit (XNAT2-1KT) was used to extract DNA from samples (ear punches) according to the manufacture's protocol, with some modifications to volumes used stated below. Briefly, 25 µl of extraction solution and 6.25 µl of tissue preparation solution were added per sample and incubated at RT for 10 min, then 95^0C for 3 min. 25 µl neutralisation buffer was added per sample. Extracted DNA was kept at 4^0C.

2.10.2. IL-1R1, Lamα5 and Slco1c1 PCR genotyping

1 µl of DNA was added to the PCR master mix (For 1 PCR reaction: 10 µl 5x One Taq standard reaction buffer, 1 µl 10mM dNTPs mix, 0.25 µl One Taq Hot Start DNA Polymerase, 1 µl reverse primer (Table 2.3), 1 µl forward primer (Table 2.3), 35.75 µl Nuclease free water. A blank sample (1 µl of nuclear free water in 49 µl of PCR master mix) was used as a negative control. Samples were then run in Prime

elite PCR thermal cycler (Bibby Scientific, UK) set to the required PCR programme (Table 2.4).

6 µl of ladder (1 kb) (Bioline, UK) and 14 µl of DNA samples was mixed with 4 µl of DNA Loading Buffer Blue (Bioline), and loaded into a 2.5 % agarose gel containing SYBR™ Safe DNA Gel Stain (Thermo Fisher Scientific) and run at 100 V for 45 min. Bands were imaged using G:BOX (Syngene) and Genesys software. Representative gel from *Slco1c1* genotyping in Fig. 2.1.

Table 2.3. PCR primer sequences required to genotype IL-1R1, Lamα5 and Slco1c1 genes in mice.
Mice are genotyped to determine whether the floxed allele (IL-1R1 and Lamα5) and Slco1c1 gene is present. Primers flank the loxP site.

Gene	Primer	Band size
IL-1R1	40: GGGGATGGAGGTAGAGGTATGG 39: GATAAAGCAGAGCTGGAGACAGG	WT: 215 bp Floxed allele: 364 bp
Lamα5	Lamα5-F17: GTG CCG CCC TAA CAC CCA AGG Lamα5-R17: GTT GAA GCC AAA GCG TAC AGC G	WT:296 bp Floxed allele:460 bp
Slco1c1	Rec 1: GCTATTCATGTCTTGGAAGCC Rec 2: CAGGTTCTTCCTGACTTCATC	WT: no band Cre: 521 bp

Table 2.4. PCR programmes required for each primer pair.
Required temperature and time cycles for genotyping using a Prime elite PCR thermal cycler.

Gene	PCR programme
IL-1R1	95°C 5 min, 35 cycles (95°C 30 min, 60°C 30 min, 72°C 1 min, 72°C 10 min), 4°C hold
Lamα5	95°C 5 min, 30 cycles (95°C 30 min, 56°C 30 min, 72°C 30 min, 72°C 10 min), 4°C hold
Slco1c1	94°C 5 min, 29 cycles (94°C 30 min, 60°C 30 min, 72°C 45 min, 72°C 10 min), 4°C hold

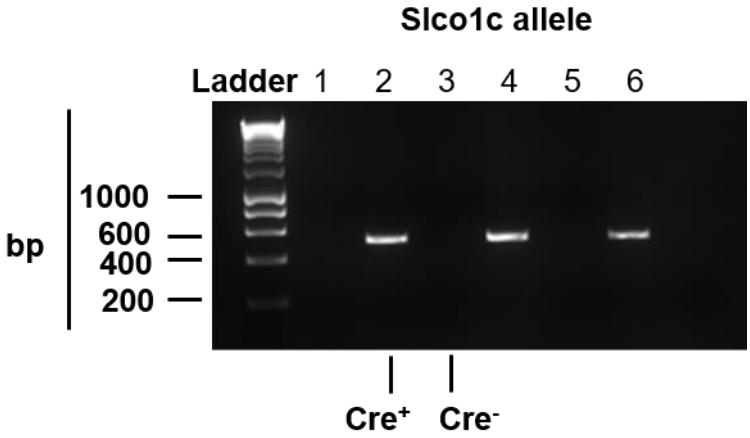

Figure 2.1. Representative PCR gel obtained from genotyping littermates for *Slco1c* gene.
Cre+ and Cre- bands are indicated on the gel. Band sizes are 521 bp (Cre+) and no band (Cre-).

2.11. Experimental design of studies and group sizes

2.11.1. Brain endothelial IL-1R1 MCAO study experimental design

There were two groups for the experimental study, IL-1R1$^{fl/fl}$+Tam mice and IL-1R1$^{fl/fl\ \Delta}$ Slco1c1+Tam mice. Mice recovered for 48 h, 14 d and 28 d post-stroke. Animals underwent surgery at least 21 d after the start of tamoxifen regimen (Section 2.9.2). Behavioural assessment (28-point neuroscore and Bederson's neuroscore) were determined at 24 h, 48 h, 7 d, 14 d and 28 d. Body weight was assessed at 24 h, 48 h, 7 d, 14 d, 21 d and 28 d. For mice recovering for 14 days, bromodeoxyuridine (BrdU) (50 mg/kg) was injected intraperitoneally once daily from days 10 to 14. Injecting BrdU at a later time window helps to ensure the optimum time point of proliferation close to the peak of angiogenesis is evaluated, and is important to ensure the strength of BrdU staining. Animals were then culled 2 d, 14 d or 28 d after surgery.

I allocated 6 animals per group (IL-1R1$^{fl/fl}$+Tam and IL-1R1$^{fl/fl\ \Delta\ Slco1c1}$+Tam) at each time point (48 h, 14 d, 28 d). A total of 36 animals were used. 1 animal (IL-1R1$^{fl/fl}$+Tam) died before the 28 d cull point. 1 animal (IL-1R1$^{fl/fl}$+Tam) at the 48 h time point clearly displayed a haemorrhage and was therefore excluded. The final animal numbers for histology are in Table 2.5. One animal from each group was not injected with BrdU due to technical limitations and the final BrdU stained animals are presented in Table 2.5.

Table 2.5. Final group sizes for brain endothelial IL-1R1 KO MCAO study.
Animal numbers for histology and BrdU analysis.

Group	Time point	Total animals used	Exclusions	Final animals for histology	BrdU injected animals
IL-1R1$^{fl/fl}$+Tam	48 h	6	1 (haemorrhage)	5	N/A
	14 d	6	0	6	4
	28 d	6	1 (died at 14 d)	5	N/A
IL-1R1$^{fl/fl\Delta Slco1c1}$+Tam	48 h	6	0	6	N/A
	14 d	6	0	6	5
	28 d	6	0	6	N/A

2.11.2. Brain endothelial laminin α5 characterisation study experimental design

There were two groups, Lamα5$^{fl/fl}$+Tam (n=12) and Lamα5$^{fl/fl\ \Delta\ Slco1c1}$+Tam (n=12). All animals underwent the tamoxifen regimen (Section 2.9.3). Animals were then culled at 0 d, 7 d, 14 d and 21 d after the start of the tamoxifen treatment. Animal numbers used in histological analysis for characterisation are shown in Table 2.6. Laser speckle contrast imaging (LSCI) was performed on animals at 21 d to measure baseline cerebral blood flow and animals used are shown in Table 2.7.

Table 2.6. Final group sizes for brain endothelial laminin α5 KO characterisation study.
Animal numbers for histology.

Group	Time point	Total animals used
Lamα5$^{fl/fl}$+Tam	0 d	4
	7 d	2
	14 d	2
	28 d	4
Lamα5$^{fl/fl\ \Delta\ Slco1c1}$+Tam	0 d	4
	7 d	2
	14 d	2
	28 d	4

Table 2.7. Final group sizes for brain endothelial laminin α5 KO characterisation study.
Animal numbers for LSCI.

Group	Total animals used in LSCI
Lamα5$^{fl/fl}$+Tam	3
Lamα5$^{fl/fl\ \Delta\ Slco1c1}$+Tam	3

2.11.3. Brain endothelial laminin α5 MCAO study experimental design

There were three groups, Lamα5$^{fl/fl\ \Delta\ Slco1c1}$+Veh, Lamα5$^{fl/fl}$+Tam and Lamα5$^{fl/fl\ \Delta\ Slco1c1}$+Tam. Animals underwent surgery at least 21 d after the start of tamoxifen/vehicle regimen (Section x). Infarct volume was assessed at 2 d post-stroke using MRI, and LSCI was performed at 3 d, 7 d and 14 d post-MCAO. Behavioural assessment (28-point neuroscore) was determined at 24 h, 48 h, 7 d and 14 d. Body weight was assessed at 24 h, 48 h, 3d, 4 d, 5 d, 6 d, 7 d, 14 d, 21 d and 28 d. BrdU (50 mg/kg) was injected intraperitoneally once daily from days 10 to 14. Animals were culled 14 d after surgery.

I allocated mice to each group Lamα5$^{fl/fl\ \Delta\ Slco1c1}$+Veh (n=8), Lamα5$^{fl/fl}$+Tam (n=8) and Lamα5$^{fl/fl\ \Delta\ Slco1c1}$+Tam (n=10) as shown in Table 2.8. During the 14 d post-MCAO, several animals reached humane endpoints for animal suffering (Percie du Sert et al., 2017) and therefore several were euthanised. A total of 6 animals were culled before MRI imaging [(Lamα5$^{fl/fl\ \Delta\ Slco1c1}$+Veh (n=1), Lamα5$^{fl/fl}$+Tam (n=3) and Lamα5$^{fl/fl\ \Delta\ Slco1c1}$+Tam (n=2)] .A further 3 animals (Lamα5$^{fl/fl\ \Delta\ Slco1c1}$+Tam) were

culled post-MRI but before 14 d. One animal each from Lamα5$^{fl/fl\ \Delta\ Slco1c1}$+Veh and Lamα5$^{fl/fl}$+Tam were excluded due to no stroke.

Table 2.8. Final group sizes for brain endothelial laminin α5 KO MCAO study.
Animal numbers for MRI, LSCI and histology are shown.

Group	Total animals used	Early culled animals due to humane end point	MRI animals	Excluded animals after MRI	Final animals in LSCI and histology
Lamα5$^{fl/fl\Delta\ Slco1c1}$+Veh	8	1	7	1 (no stroke)	6
Lamα5$^{fl/fl}$+Tam	8	3	5	1 (no stroke)	4
Lamα5$^{fl/fl\Delta\ Slco1c1}$+Tam	10	5	8	0	5

2.12. **MCAO surgery**

A code was allocated to each animal by a non-experimenter and animals were randomly assigned to different treatment groups and surgery days. During all surgical procedures and behaviour tests, the experimenter was blinded to genotype and treatment group. Induction of anaesthesia was achieved by inhalation of 4 % isoflurane (30 % oxygen and 70 % nitrous oxide gas mix, AbbVie Ltd, UK or Linde Ltd, Hungary) and was maintained at 1.75%. During surgery, core body temperature was monitored using a rectal probe and maintained at 37 ± 0.5°C with a homeothermic blanket (Harvard Apparatus, Edenbridge, Kent, UK). A laser Doppler monitor (Oxford Optronix, Abingdon, UK) was used to monitor CBF and confirm a drop in CBF in the MCA region following occlusion. Transient middle cerebral artery occlusion (MCAO) was used to induce focal cerebral ischaemia, based on a previously described protocol (Wong et al., 2019). Briefly, topical anaesthetic (EMLA, 5 % prilocaine and lidocaine, AstraZeneca, UK) was administered on to the areas of skin prior to incision. An incision was made into the temporalis muscle, located 6 mm lateral and 2 mm posterior from bregma, and the laser-Doppler probe was fixed on to the skull using tissue adhesive (Vetbond, UK). A midline incision was made into the middle front section of the neck, and the right

common carotid artery was exposed and ligated. The internal carotid artery was temporarily ligated. An incision in the common carotid artery was made for the insertion and advancement of a 6-0 monofilament (Doccol, Sharon, MA, USA) through into the internal carotid artery, advanced approximately 10 mm distal to the carotid bifurcation, beyond the origin of the middle cerebral artery. The Doppler monitor was used to ensure a reduction of CBF by at least 70% of pre-ischaemic values. After 30 min of occlusion (Chapter 4 - brain endothelial-specific IL-1R1 deletion study) or 25 min of occlusion (Chapter 5 - brain endothelial-specific laminin α5 deletion study) the filament was removed to allow reperfusion. The neck wound was sutured, and mice were administered subcutaneously saline (500 µl) for hydration and buprenorphine (0.05 mg/kg, Vetergesic, UK). Animals were allowed to recover in an incubator at 26–28°C, and then transferred to ventilated cages suspended over a heating pad (24°C) with free access to mashed food and water, under standard housing conditions for 24 h. After 24 h, cages were returned their home rack and kept under normal housing conditions for the remaining duration of the study. Animals were excluded from the studies if occlusion was not successful (defined as <70% reduction in cerebral blood flow and/or if no infarct detected by MRI in Chapter 5) or exceeded humane end points in the IMPROVE guidelines (Percie du Sert et al., 2017). Excluded animals detailed in section 2.11.2 and 2.11.3.

2.13. Behavioural outcomes after experimental stroke. Behavioural assessment and body weight measurement after experimental stroke

2.13.1. 28-point neuroscore

The 28-point neuroscore was used to assess sensorimotor function in the brain endothelial-specific IL-1R1 KO MCAO study (Chapter 4) and the brain endothelial-specific laminin α5 KO MCAO study (Chapter 5), modified from methods previously described (Encarnacion et al., 2011). Briefly, 7 tests with a cumulative maximum score of 28 were used; body symmetry, gait, climbing, circling behaviour, front limb symmetry, compulsory circling and whisker responses. Scoring was determined out of 4, where 0 is normal and 4 is severe impairment.

2.13.2. Bederson's neuroscore

Bederson's neuroscore was used to assess further functional outcome in the brain endothelial-specific IL-1R1 KO MCAO study (Chapter 4), as previously described (Wong et al., 2019). In brief, 6 tests with a cumulative score of 28 were used (score range as indicated); hair (0–2), ears (0–2), eyes (0–4), posture (0–4), spontaneous activity (0–4), and epileptic behaviour (0–12). Scoring scales stated, whereby 0 is deemed normal.

2.14. **Perfusion and processing of tissues**

2.14.1. Perfusion

Induction of anaesthesia was achieved by inhalation of 4 % isoflurane, the animal's cardiac blood was removed and perfused transcardially with 0.9 % saline. Liver and spleens were removed and snap frozen on dry ice, later stored at -80°C. Brains were removed and kept in saline on ice at 4°C. Subsequently, brains were coated in Optimal cutting temperature compound (OCT) and frozen in -50°C to -60°C isopentane using dry ice. Brains were stored at -80°C. Prior to perfusion, cardiac blood was removed from the right ventricle and centrifuged at 2000 g, 4°C for 10 min, and the plasma collected and stored at -80°C.

2.14.2. Brain sectioning

In the brain endothelial-specific IL-1R1 KO MCAO study (Chapter 4) and the brain endothelial-specific laminin α5 KO MCAO study (Chapter 5) 20 µm coronal sections were taken every 500 µm using a Leica cryostat. In the brain endothelial-specific laminin α5 KO characterisation study (Chapter 5), 10 µm coronal sections were taken every 500 µm using a Leica cryostat. All brain sections were mounted onto superfrost slides (Thermo Fisher Scientific) and stored wrapped in foil in the -80°C.

2.15. **Histology and quantification**

2.15.1. Cresyl violet

For lesion volume analysis of the brain endothelial-specific IL-1R1 KO, cryostat-cut sections (20 µm) were stained with cresyl violet and coverslipped with DPX mounting medium MCAO study (Chapter 4). Images were collected using a 3D Histec Pannoramic 250 slide scanner (3D Histec, Hungary). Lesion volume was

analysed using CaseViewer (3D Histec) and calculated as the sum of every lesion area multiplied by the distance between each section (0.5 mm). Analyses of images were carried out by a blinded experimenter.

2.15.2. Immunofluorescence

Slides were allowed to acclimatise to RT. For BrdU immunostaining, sections were fixed with ice cold acetone for 10 min at RT and dried at RT for 20 min. Slides were rehydrated in PBS for 10 min. For BrdU immunostaining, sections were pre-treated with 2 M HCl for 30 min at 37°C. Antibodies were diluted in 1 % (wt/vol) BSA in PBS and incubated on sections for 2 h (laminin α5) or ON at 4°C (laminin α4, BrdU), using a section of parafilm to place over the slide to evenly spread the antibody. Primary antibodies used were rabbit anti-laminin α5 (1:800, provided by Miner et al., 1997), goat anti-laminin 4 (1:400; R&D) and sheep anti-BrdU (1:200, Abcam). Slides were washed with PBS (3 x 5 min). Secondary antibodies were applied for 2 h, using a section of parafilm to place over the slide to evenly spread the antibody. Secondary antibodies used were donkey anti-rabbit Alexa Fluor 594 (1:400, Thermo Fisher Scientific), donkey anti-goat Alexa Fluor 594 (1:400, Thermo Fisher Scientific) and donkey anti-sheep Alexa Fluor 594 (1:400, Thermo Fisher Scientific). Slides were washed with PBS (3 x 5 min). Slides were gently rinsed in distilled water, dried overnight in the dark at RT and then coverslipped in ProLong Diamond anti-fade mountant (Thermo Fisher Scientific). Images were collected using a 3D Histec Pannoramic 250 slide scanner. CaseViewer was used to collect images from the ROIs. For quantifications, three region of interest (ROI) in the striatum and cortex of each hemisphere, across 3-4 sections per animal were collected. The percentage area, integrated density and cell count of the staining were calculated in ImageJ using the macro function. All collection and analyses of images were carried out in a blinded manner.

2.16. **Magnetic resonance imaging**

Magnetic Resonance Imaging (MRI) was used to assess infarct volume at 48 h post-MCAO in the brain endothelial-specific laminin α5 KO MCAO study (Chapter 5). Animals were anaesthetised with isoflurane and T2-weighted TurboRARE high resolution scans were conducted on a Bruker Advance III console (Bruker Biospin Ltd, UK) using a 7T horizontal bore magnet (Agilent Technologies). A water bath connected to the MRI's bed was used to maintain the animal's body temperature

for the short time of the scan. Multi-scale gradient echo sequence was used to collect coronal pilot images to ensure correct positioning of the brain in the MRI scanner. A total of 17 serial slices with a thickness of 0.8 mm were acquired. Lesion volumes were analysed using ImageJ and calculated as the sum of every lesion area multiplied by the distance between each section (0.8 mm). Analyses of images were carried out by a blinded experimenter.

2.17. Laser speckle contrast imaging

Laser speckle contrast imaging (LSCI) performed by a moorFLPI2 Full-Field Perfusion Imager (Moor instruments, UK) was used to measure CBF at 3 d, 7 d and 14 d post-MCAO in the brain endothelial-specific laminin α5 KO MCAO study (Chapter 5). Anaesthesia was induced in the mice with inhalation of 4 % isoflurane, and animals were secured in a stereotaxic frame (World Precision Instruments, USA) positioned under a moorFLPI2 Full-Field Perfusion Imager. Anaesthesia was maintained at 1.75% isoflurane throughout imaging. During imaging, core body temperature was monitored using a rectal probe and maintained at 37 ± 0.5°C with a homeothermic blanket (Harvard Apparatus). Topical anaesthetic (EMLA, 5 % prilocaine and lidocaine) was administered on to the areas of head prior to incision. A clean midline incision on the skin on top of the skull was used to expose the skull. To facilitate a clear image, ultrasound gel was applied on top of the skull and a 16 mm cover slip was placed on top. Animals were imaged for 5 min at 31 frames. CBF was analysed by the moorFLPI2 Full-Field Laser Perfusion Imager Review V5.0 software (Moor instruments, UK) and shown with arbitrary units in a 256-color palette. A ROI was drawn around the infarct area on the ipsilateral hemisphere and a matched ROI was reciprocated on the contralateral hemisphere. ROIs across the 3 time points for the same animal were matched by eye. Flux values for both regions of interest were extracted and an average was calculated. Average flux values for both ROI were used to express the ipsilateral flux as a percentage of contralateral flux. All analysis was performed under blinded conditions.

2.18. Statistical analysis

All data were analysed with GraphPad Prism 8.1.2 (GraphPad Software Inc) using the appropriate tests (further details stated in the figure legends). Homoscedasticity of the standard deviations were evaluated with a Brown-Forsythe and Bartlett's test, alongside the use of homoscedasticity plots (predicted

vs residual) and QQ plots to assess equal variance and normality. Appropriate transformations were applied where necessary. All figures show untransformed data even if data were transformed. Data are presented as mean ± standard error of mean (SEM). For data with non-normal distributions (body weight, neuroscore), mixed effects model (REML) was used and data is represented with a line at the median (neuroscore) and mean (body weight). Details of replicates are recorded in the figure legend. Statistical significance was accepted at *$p < 0.05$, **$p < 0.01$, ***$p < 0.001$, and ****$p < 0.0001$.

Chapter 3. **The role of the extracellular matrix protein LM-10 in inflammation, repair and IL-1β-induced YAP signalling in brain endothelial cells *in vitro*.**

All experiments were designed and analysed by myself with the input of Dr Emmanuel Pinteaux. All experiments and analysis were performed by me with the input of others as stated below. Dr Eloise Lemarchand provided assistance in the training of qPCR.

3.1. **Introduction**

The ECM of the CNS provides a structural and functional environment for the cells of the NVU during physiological conditions that is essential for maintaining BBB integrity and brain homeostasis. After cerebral ischaemia the BBB undergoes profound changes associated with the breakdown of TJs, remodelling of the ECM and enzymatic degradation of ECM proteins. The early events of BBB breakdown are also associated with leukocyte infiltration, mediated by cell adhesion molecules and chemokines. IL-1 is an established mediator of the inflammation associated with BBB dysfunction and subsequent tissue damage (Denes et al., 2011). Although IL-1 is initially characterised as detrimental during the acute phase of stroke, increasing evidence suggests a biphasic action of IL-1 that exhibits neuroprotective properties during the repair phase (Rodriguez-Grande et al., 2015). Furthermore, there is increasing evidence that suggests the ECM plays a dynamic role throughout pathology and mediates repair in the CNS during later stages post-stroke. Interestingly, a novel function of the ECM as a regulator of IL-1β-induced signalling in astrocytes and cerebral endothelial activation has been demonstrated *in vitro* (Summers et al., 2010, 2013). ECM remodelling after CNS injury is associated with BBB repair and IL-1 has been shown to mediate repair mechanisms, and therefore this has led to the hypothesis that BBB repair driven by IL-1 could be regulated by ECM remodelling. Our colleagues previously identified LM-10 as a key ECM molecule involved in BBB repair after hypoxic injury and IL-1-induced inflammation *in vitro* (Kangwantas et al., 2016). However, the role of LM-10 as regulator of inflammation and angiogenesis had not yet been determined.

The mechanisms underlying the dynamic relationship between the ECM and inflammation is still poorly understood. Although it has been previously demonstrated that different components of the ECM alter IL-1 signalling pathways in astrocytes and endothelial cells *in vitro* (Summers et al., 2010, 2013), the crosstalk between signalling pathways downstream of the IL-1R1 and other key signalling pathways has not been fully characterised. The Hippo pathway has gained significant interest as an extremely dynamic pathway that is not just responsible for controlling organ size, but is implicated in cancer and inflammatory diseases (Warren et al., 2018; Wang et al., 2020). It is well established that ECM-integrin signalling is a regulator of the Hippo pathway. Critically, recent evidence

has demonstrated a key role of YAP in TNF-α-induced endothelial activation (Choi et al., 2018). However, the role of YAP in endothelial cells after IL-1β treatment had not yet been determined, and whether LM-10 could modulate the response was unknown. Using *in vitro* approaches, I demonstrate that LM-10 modulates the inflammatory response in endothelial cells after IL-1β treatment through the upregulation of key adhesion molecules. Furthermore, I show that LM-10 increases endothelial proliferation and migration, key *in vitro* hallmarks of angiogenesis. Crucially, I reveal a novel mechanism whereby YAP is involved in endothelial activation by IL-1β, and whereby LM-10 modulates the temporal pattern of YAP phosphorylation.

3.2. **Aims**

The initial aim of this study was to establish an *in vitro* model that was suitable to investigate the effect of LM-10 on the IL-1β-induced activation and angiogenic response of cerebral endothelial cells. Specific objectives for this part of the study were:

- To investigate the role of LM-10 as a regulator of IL-1β-induced endothelial activation in mouse brain endothelial cell line (bEnd.5 cells) and primary MBECs.
- To determine the appropriate experimental conditions including control ECM coating, seeding time and endothelial cell type most suitable for our readouts.

Our next aim of the study was to use the chosen experimental model to thoroughly characterise the IL-1β-induced activation, IL-1β-induced signalling and angiogenic response of cerebral endothelial cells seeded on LM-10. Specific objectives for this part of the study were:

- To establish the role of LM-10 as a regulator of IL-1β-induced endothelial activation and IL-1β-induced signalling pathways in hCMEC/D3 cells.
- To investigate the crosstalk between IL-1β signalling and YAP in hCMEC/D3 cells.
- To determine the role of LM-10 in mechanisms of angiogenesis *in vitro*.

3.3. **Results**

3.3.1. Preliminary experiments investigating the effect of LM-10 on endothelial adhesion and inflammatory activation

Conventional cell culture involves either the use of primary cells or cell lines. Primary cells are isolated directly from tissue and then cultured, hence present a limited lifespan and there is batch variation (Helms et al., 2016). Cell lines are immortalised and therefore have the ability to proliferate indefinitely, offering stability, high throughput, and ease of use. The use of these *in vitro* models presents differing benefits and disadvantages, and therefore should be adapted to address the objectives of the experiment, readouts and practical limitations of the study in question. Thus, in this study, preliminary experiments were critical in determining the *in vitro* set-up most suitable for investigating the mechanisms of IL-1β-driven endothelial activation and angiogenesis I aimed to investigate in cerebral endothelial cells. The initial experiments consisted of the use and characterisation of the established mouse brain endothelial cell line (bEnd.5) and primary mouse brain endothelial cells (primary MBECs). The mouse bEnd.5 cell line was used for early preliminary experiments to test the hypothesis that LM-10 can promote endothelial cell attachment, and that IL-1β responses can be potentiated in endothelial cells adhered to LM-10. The bEnd.5 cell line was used for these early optimisation steps as they are a suitable *in vitro* model for mouse brain endothelial cells and are fast growing. The bEnd.5 cells exhibit typical endothelial phenotypes including tight junction proteins ZO-1 and occludin, claudin-1 and several key BBB transporter proteins, whilst also demonstrating barrier function (Yang et al., 2007).

In order to determine the effect of LM-10 on endothelial adhesion, bEnd.5 cell attachment on increasing concentrations of LM-10 was investigated (Fig. 3.1A). 0.1% BSA and 0.1% gelatin were used as non-ECM controls, whilst collagen IV (50 µg/ml) was used as a positive ECM control. There was an increase in bEnd.5 cell attachment on LM-10 in a concentration-dependent manner, with an optimum concentration of LM-10 achieved at 10 µg/ml. There were a low basal number of bEnd.5 cells attached on 0.1% BSA, collagen IV and 0.1% gelatin. Adhesion of bEnd.5 cells progressively increased between 0.1 and 5 µg/ml of LM-10 and a significant increase in bEnd.5 cell attachment was observed on 10 µg/ml of LM-10 compared to 0.1% BSA, collagen IV or 0.1% gelatin.

Another key component of our initial objective was to establish the role of LM-10 as a regulator of inflammation *in vitro* by measuring the effect of LM-10 on IL-1β-induced expression of endothelial cell adhesion molecules, as well as key cytokines and chemokines (Fig. 3.1B,C). IL-1β treatment resulted in elevated levels of ICAM-1 and chemokine KC with higher concentrations of IL-1β inducing a stronger cytokine response ($p=0.0008$, Fig. 3.1B; $p<0.0001$, Fig. 3.1C, respectively). This response reached maximum levels at the highest concentrations and was relatively consistent across all coating treatments. Plate coating (ECM) had a significant effect on ICAM-1 expression ($p=0.0001$), specifically LM-10 caused significantly elevated ICAM-1 levels compared to 0.1% BSA, Collagen IV and gelatin controls ($p=0.006$, $p=0.005$ and $p<0.0001$, respectively) (Fig. 3.1B). No differences in ICAM-1 expression were observed between the control groups. Plate coating did not have a significant effect on chemokine KC expression ($p=0.2488$, Fig. 3.1C).

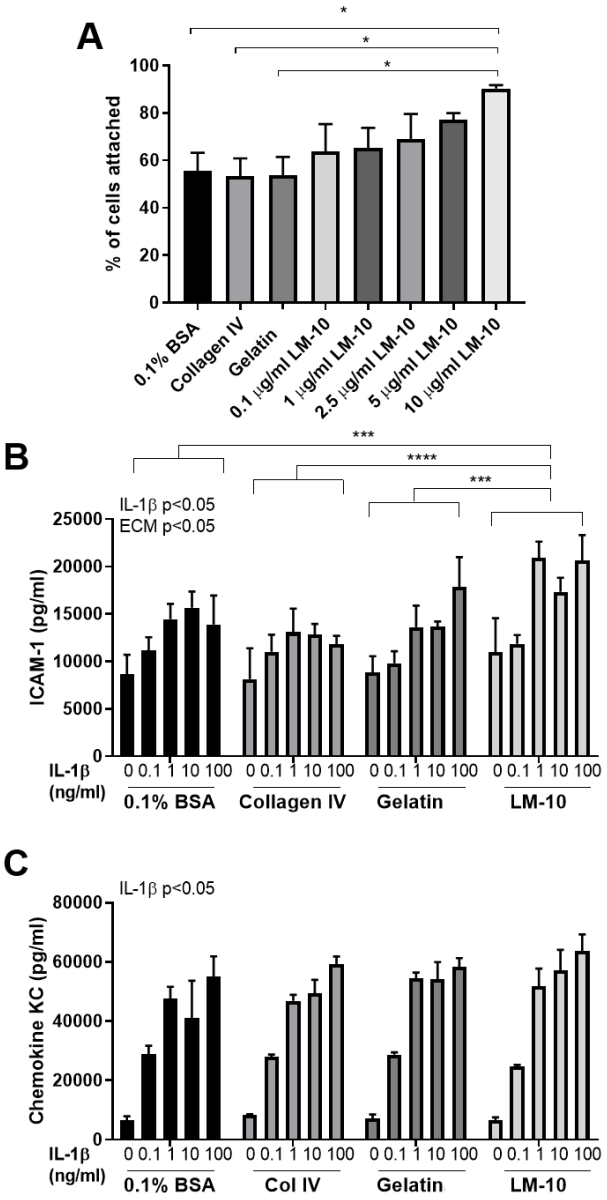

Figure 3.1. Effect of LM-10 on bEnd.5 cell attachment and IL-1β-induced endothelial cell activation.

(A) 96-well plates were coated with LM-10, 0.1% BSA, collagen IV or 0.1% gelatin prior to cell seeding. bEnd.5 cells were seeded at a density of 2 x 10^4 cells per well and cell attachment was measured by crystal violet staining after 1 h. Cell adhesion was measured by the absorbance at 570 nm, compared to the absorbance of the standard curve of bEnd.5 cells. (B-C) bEnd.5 cells were seeded at a density of 50,000 cells per well in a 48-well plate for 24 h. Cells were treated with IL-1β at various concentrations for 24 h. Cell supernatants and lysates were then collected. (B) Cell lysate was assayed for ICAM-1 by ELISA. (C) Cell supernatant was assayed for chemokine KC (CXCL1) by ELISA. Data are represented as mean ± SEM of 3 technical replicates and 3 biological replicates (n=3, A) and of 3 biological replicates (n=3, B-C). Data were assessed by a one-way ANOVA with Dunnett's multiple comparisons post-hoc, LM-10 concentrations versus controls (0.1% BSA, collagen IV and gelatin) (A); a two-way RM ANOVA with Tukey's multiple comparisons post-hoc comparing the means across each plate coating (B-C), significant main effects of IL-1β treatment and the ECM coating are indicated on the top left of the graphs, *p<0.05, **p<0.01, ***p<0.001, ****p<0.0001.

To validate our experiments in the mouse brain endothelial cell line, key experiments to determine the effect of LM-10 on cellular adhesion (Fig. 3.2A-B) and expression of key inflammatory markers (Fig. 3.2C-H) in primary MBECs were performed. The primary MBEC adhesion assay also acts as a measure of endothelial proliferation on each plate coating as the primary MBECs are grown over a 13/14 day period as opposed to the 1 h attachment period in the bEnd.5 cell attachment experiment. Gelatin was used as a non-ECM control and collagen IV was used as a positive ECM control. The controls were chosen as both have been used as effective plate coatings to support primary MBEC growth. Although not significant, there was a marked concentration-dependent effect of LM-10 on cell adhesion and proliferation, which was demonstrated when comparing the absorbance at each concentration of LM-10 to 0.1% gelatin (Fig. 3.2A) and collagen IV (Fig. 3.2B). The endothelial cell adhesion on LM-10 concentrations of 1, 2.5, 5 and 10 µg/ml was higher than the endothelial cell adhesion on 0.1% gelatin (Fig. 3.2A), whilst LM-10 concentrations of 2.5, 5, 10 µg/ml exceeded the endothelial cell adhesion on collagen IV (Fig. 3.2B), demonstrating that LM-10 enhances cell adhesion and proliferation. Notably, I observed a more apparent adhesion effect of LM-10 on primary MBECs compared to bEnd.5 cells.

I next investigated the effect of LM-10 on IL-1β-induced expression of key endothelial adhesion molecules and cytokines/chemokines in primary MBECs (Fig. 3.2C-H). I previously found no differences between the control groups (0.1% BSA, collagen IV and 0.1% gelatin) for ICAM-1 and chemokine KC expression in bEnd.5 cells (Fig. 3.1B,C), and therefore I decided to use gelatin as the control for IL-1β treatment experiments in primary MBECs. There was a significant effect of increasing IL-1β concentration on ICAM-1 ($p=0.0011$, Fig. 3.2C), VCAM-1 ($p=0.0355$, Fig. 3.2D), P-Selectin ($p=0.0016$, Fig. 3.2E), E-Selectin ($p=0.0009$, Fig. 3.2F), chemokine KC ($p<0.0001$, Fig. 3.2G) and IL-6 ($p=0.00199$, Fig. 3.2H) expression, showing that they were upregulated in response to IL-1β in a concentration-dependent manner. The ECM had a significant effect on the expression of ICAM-1 ($p=0.0368$, Fig. 3.2C) and P-selectin ($p=0.0133$, Fig. 3.2E), demonstrating an elevated expression of ICAM-1 and P-selectin in primary MBECs when grown on LM-10 compared to gelatin. Although not significant, a trend to increase in chemokine KC expression on LM-10 ($p=0.0567$, Fig. 3.2G) was detected. ECM did not have a significant effect on VCAM-1 ($p=0.4713$, Fig. 3.2D),

E-Selectin (p=0.1505, Fig. 3.2F) and IL-6 (p=0.1860, Fig. 3.2H) expression, suggesting that LM-10 does not influence their expression in primary MBECs. Furthermore, LM-10 induced a significantly higher expression of ICAM-1 in primary MBECs at 0.1 ng/ml (p=0.0426), 10 ng/ml (p=0.0015) and 100 ng/ml (6-fold increase, p=0.0204); P-selectin at 0.1 ng/ml (p=0.0316), 1 ng/ml (p=0.0149), 10 ng/ml (p=0.0029) and 100 ng/ml (5.3-fold increase, p=0.0008); and chemokine KC at 10 ng/ml (p=0.0022) and 100 ng/ml (2.5-fold increase, p=0.0224) of IL-1β treatment compared to corresponding IL-1β concentration treatments on gelatin. VEGF secretion was also measured in the supernatant but was not detected (data not shown).

Since I observed increased expression levels of inflammatory markers in endothelial cells on LM-10, I next sought to investigate the role of LM-10 as a regulator of neutrophil transmigration in an *in vitro* model of neutrophil transmigration across an IL-1β activated endothelial monolayer (Fig. 3.3). Due to experimental difficulty in culturing primary MBECs on Transwell inserts, I used the b.End5 cell line as the endothelial monolayer and isolated bone marrow derived neutrophils from wild type (WT) mice. Interestingly, the addition of the b.End5 monolayer increased transmigration compared to just ECM coating alone (no coating ($p<0.0001$), gelatin ($p<0.0001$), Col IV ($p<0.0001$) and LM-10 ($p<0.0001$), Fig. 3.3). I assessed the effects of IL-1β treatment within each matrix, compared to neutrophil transmigration across an untreated endothelial monolayer. IL-1β treatment induced a significant increase in neutrophil transmigration in no coating ($p<0.0001$), gelatin ($p<0.0001$), Col IV ($p<0.0001$) and LM-10 ($p<0.0001$) (Fig. 3.3). Interestingly, neutrophils transmigrated significantly less across an IL-1β activated endothelium seeded on LM-10 compared to all control groups (no coating, p=0.0016; gelatin, p=0.0005; Col IV, p=0.0128) (Fig. 3.3). IL-1Ra blocked the effect of IL-1β on all coatings apart from gelatin (Fig. 3.3).

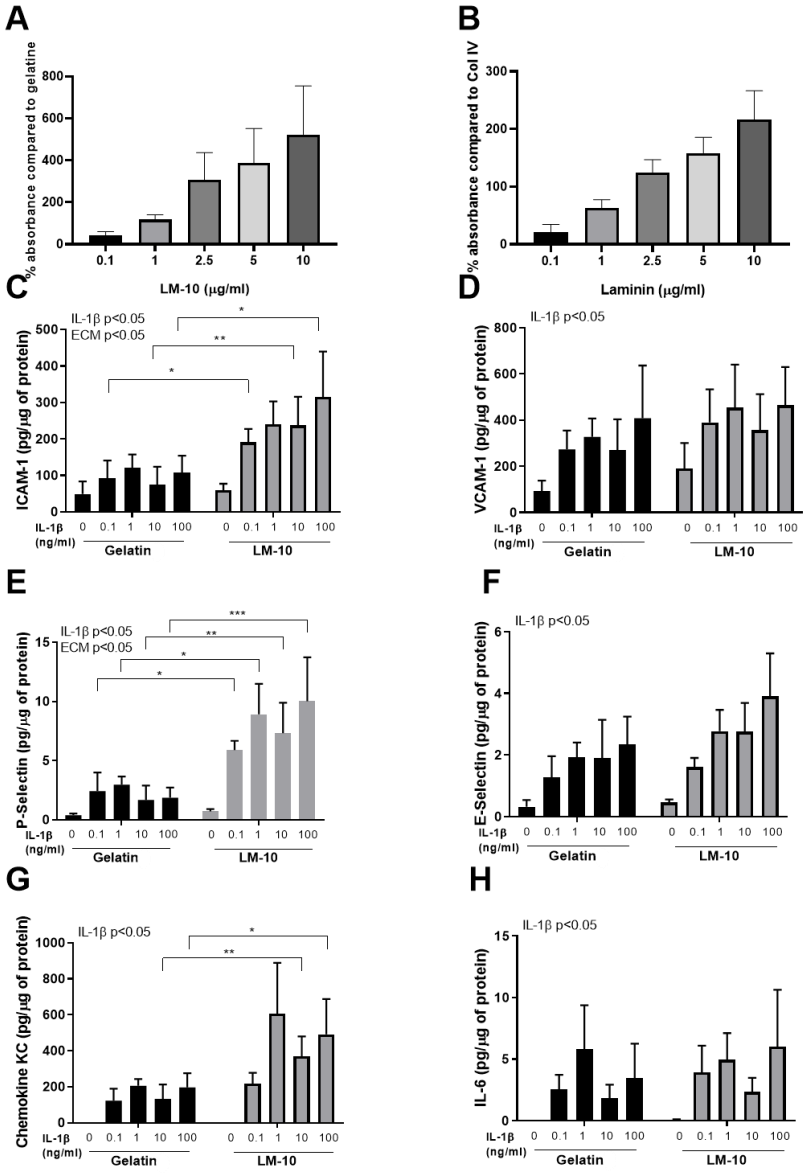

Figure 3.2. Effect of LM-10 on primary MBECs attachment and IL-1β-induced activation.

(A-B) Primary MBECs were seeded in pre-coated 96-well plates and grown to confluency (~day 13/14). Cell attachment was measured by crystal violet staining. The absorbance at 570 nm was measured and is proportional to cells attached. The absorbance at each concentration of LM-10 has been compared as a percentage of the absorbance of (A) gelatin and (B) collagen IV. Primary MBECs were seeded in pre-coated 96-well plates and grown to confluency (day 13/14). Cells were treated with IL-1β at various concentrations for 24 h. Cell supernatants and lysates were then collected. Cell lysates were assayed for ICAM-1 (C), VCAM-1 (D), P-Selectin (E), E-Selectin (F). Cell supernatants were assayed for chemokine KC (CXCL1) (G) and (F) IL-6. Data are represented as mean ± SEM of 5 technical replicates and 4 biological replicates (n=4, A-H). Data were assessed by one-sample t-test versus value of hypothetical value of 100% followed by Holm-Sidak corrections (A-B); a two-way RM ANOVA followed by Sidak's, post-hoc analysis comparing the means of expression of adhesion molecule/cytokine at corresponding concentrations of IL-1β treatment on gelatin vs LM-10 (C-H), significant main effects of IL-1β treatment and the ECM coating are indicated on the top left of the graphs *p<0.05, **p<0.01, ***p<0.001.

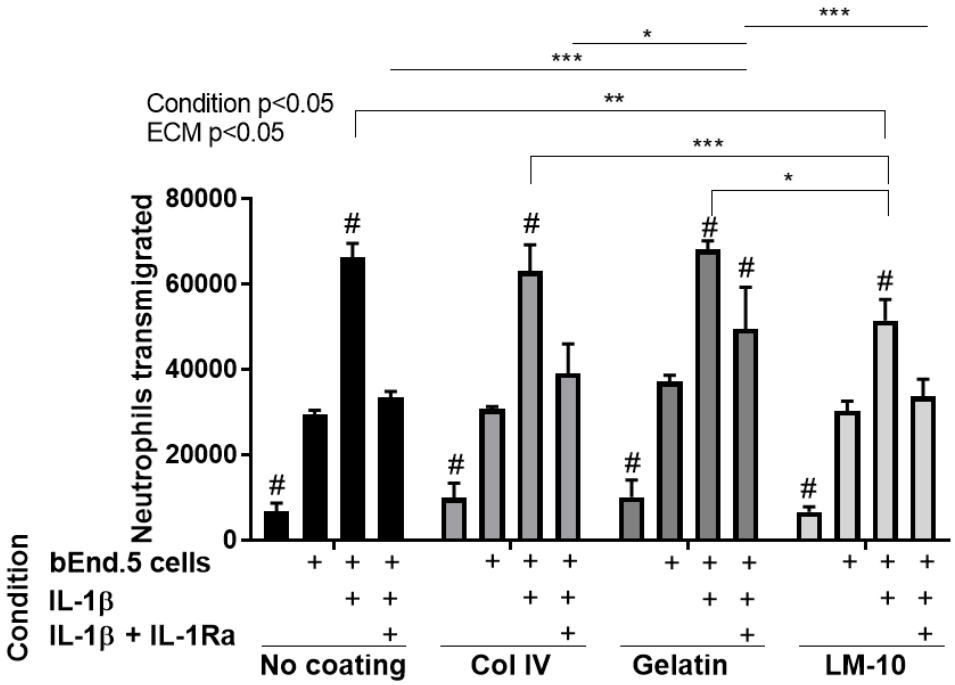

Figure 3.3. Effect of LM-10 on neutrophil transmigration across a bEnd.5 cell monolayer.

bEnd.5 cells (1 x 10^5 cells/well) were seeded onto pre-coated (0.1% gelatin, 0.1% BSA, collagen IV or LM-10) transwell inserts for 24 h. bEnd.5 cells were pre-treated with IL-1RA for 15 mins before IL-1B (100 ng/ml) treatment for 4 h. 5 x 10^5 neutrophils were added to the luminal compartment of the transwell and transmigrated neutrophils were counted after 24 h. Data are represented as mean ± SEM of 3 biological replicates (n=3). Data were assessed by a two-way RM ANOVA with Tukey's multiple comparisons post-hoc analysis, * denotes significance of transmigrated neutrophils across each ECM at corresponding treatment conditions, # denotes significance within ECM coating compared to untreated endothelial monolayer, significant main effects of treatment condition and the ECM coating are indicated on the top left of the graphs, *p<0.05, **p<0.01, ***p<0.001.

3.3.2. The effect of changing endothelial seeding time and control on outcome measures of IL-1β-driven endothelial activation

I decided to modulate experimental conditions to ensure that I were using the optimum experimental conditions for investigating the effect of the ECM on IL-1β-driven endothelial activation *in vitro*. Our two major alterations were the change of control condition, from cells seeded on gelatin to cells seeded on Matrigel, as well as the introduction of a 4 h seeding time as opposed to a 24 h seeding time. Matrigel is considered a more valid ECM control for *in vitro* experiments as it consists of key basement membrane proteins including laminin, collagen IV, heparan sulfate proteoglycans and entactin/nidogen. The Matrigel was used at a diluted concentration of 20 µg/ml to mimic similar 2D cell culture conditions between the LM-10 and Matrigel. The other key adjustment to experimental protocol was the reduction in seeding time from 24 h to 4 h, which is deemed to be critical in ensuring that the endothelial cells do not have sufficient time to secrete their own basement membrane and potentially mask the effect of the plate coating.

To validate our new experimental conditions, I used the bEnd.5 cell line to investigate the effect of shorter seeding time on chemokine KC (Fig 3.4.A) and MCP-1 (Fig. 3.4B) expression, with cells seeded on Matrigel as the control group. IL-1β treatment had a significant effect on MCP-1 ($p<0.0001$, Fig. 3.4A) and chemokine KC ($p=0.0010$, Fig. 3.4B) secretion in a time-dependent manner. ECM had a significant effect on MCP-1 ($p=0.0161$) and chemokine KC ($p=0.0027$) secretion, with an elevated expression of both markers when b.End5 cells were seeded on LM-10 compared to Matrigel. LM-10 triggered a higher expression of chemokine KC in bEnd.5 cells at 60 min ($p=0.0250$) and 120 min ($p=0.0028$) after IL-1β treatment, whilst a higher expression was observed at 240 min ($p<0.0001$) after IL-1β treatment for MCP-1 expression compared to corresponding time-points on Matrigel. A 1.3-fold and 1.2-fold increase in chemokine KC and MCP-1 expression, respectively, was observed 240 min after IL-1β treatment when cells were seeded on LM-10 compared to Matrigel.

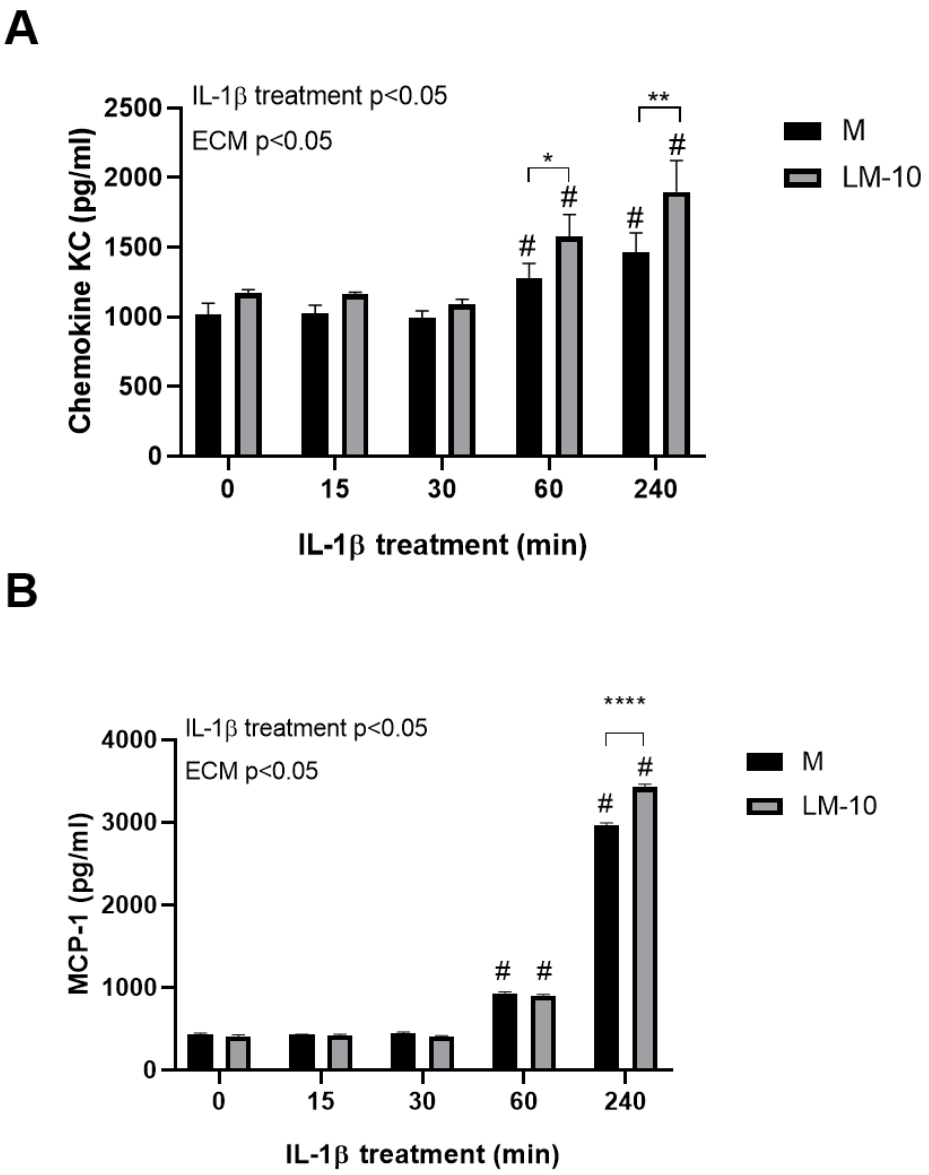

Figure 3.4. Effect of LM-10 on bEnd.5 IL-1β-induced activation after a reduced seeding time of 4 h.

(A-B) 24-well plates were pre-coated with Matrigel (20 µg/ml) or LM-10 (10 µg/ml). bEnd.5 cells were seeded at a density of 200,000 cells per well in a 24-well plate for 4 h. Cells were treated with IL-1β (10 ng/ml). Cell supernatants and lysates were then collected. (A-B) Cell supernatant was assayed for chemokine KC (CXCL1) and MCP-1 by ELISA. Data are represented as mean ± SEM of 3 biological replicates (n=3, A-B). Data were assessed by a two-way RM ANOVA with Sidak's post-hoc analysis, * represents significance comparing the means of cytokine expression at corresponding time points on Matrigel vs LM-10, # represents significance within ECM to untreated. Significant main effects of IL-1β treatment and the ECM coating are indicated on the top left of the graphs. *p<0.05, **p<0.01, ***p<0.001, ****p<0.0001.

Further optimisation of our experimental model involved the decision to acquire an endothelial cell line that would be suitable for future angiogenic assays and that resembled human cerebral endothelial cells better. The hCMEC/D3 cell line has been extensively characterised for brain endothelial phenotype and as a model of human BBB function (Weksler et al., 2013) and therefore I decided to use this cell line for future experiments. Subsequently, I sought to determine the effect of LM-10 on hCMEC/D3 cell adhesion at 4 h (Fig. 3.5B) and at 24 h (Fig. 3.5C) after seeding on Matrigel and LM-10 (Fig. 3.5A-C). I also assessed the effect of different seeding densities to determine the density at which the cells were sufficiently confluent for experimental assays (Fig. 3.5B,C). Throughout the study I were also open to alternative experimental techniques that could better answer our question. Therefore, I decided to use the Incucyte software to acquire images (Fig. 3.5A) of the hCMEC/D3 cells at 4 h and 24 h and subsequently measure confluence (Fig. 3.5B,C) as opposed to the crystal violet staining method for cellular adhesion. I observed no significant difference in confluency of hCMEC/D3 cells seeded on Matrigel compared to LM-10 at each seeding density assessed across the 4 h (Fig. 3.5B) and 24 h (Fig. 3.5C) time point after seeding.

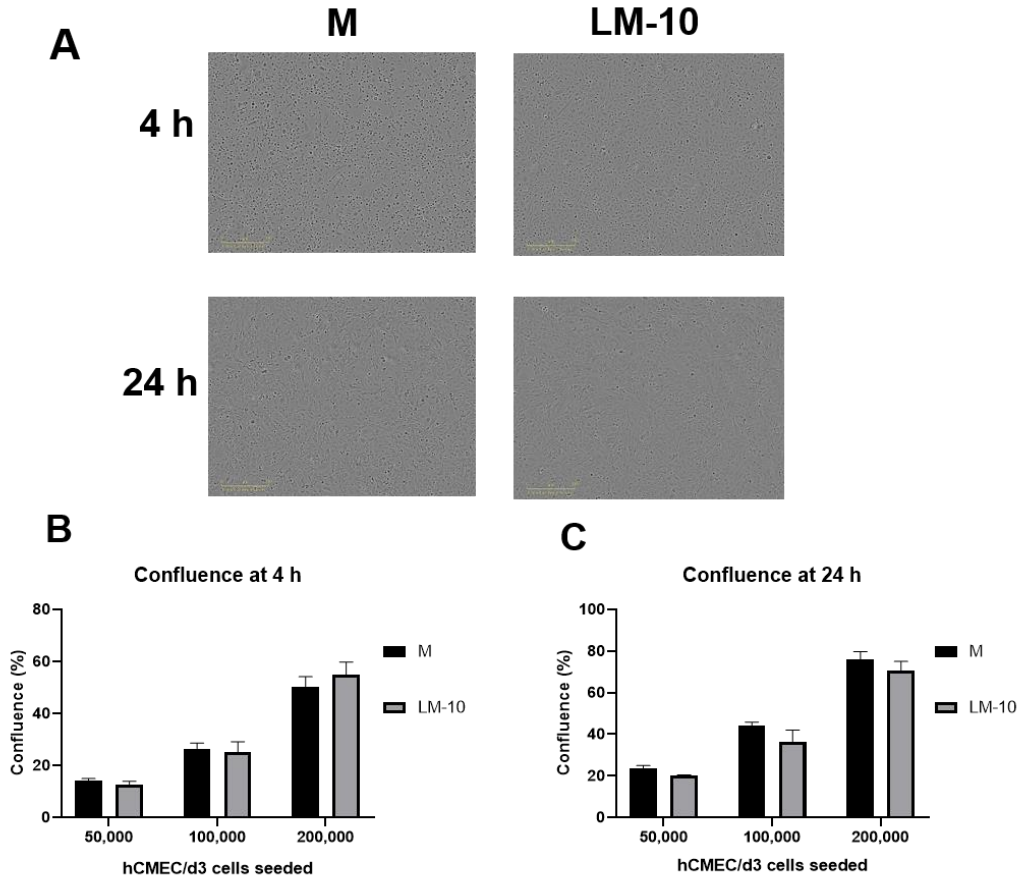

Figure 3.5. Effect of LM-10 on hCMEC/D3 cell adhesion.
(A) Representative images of hCMEC/D3 cells on different plate coatings and (B-C) quantification of confluence. 24-well plates were pre-coated with Matrigel (20 ug/ml) or LM-10 (10 ug/ml). Several densities of hCMEC/D3 cells were seeded. Phase contrast images were acquired at 4 h and 24 h on an Incucyte Zoom Live Cell Analysis system (Essen BioScience, UK) using a 123 10x/1.22 Plan Apo OFN25 objective. Scale bar 300 µm. (B-C) The IncuCyte ZOOM's Confluence Processing analysis tool (Basic Analyzer) was used to calculate percentage confluence at 4 h (B) and 24 h (C). Data are represented as mean ± SEM of 3 biological replicates (n=3). Data were assessed by a two-way ANOVA followed by Tukey's post-hoc analysis comparing the means of percentage confluence at each density of hCMEC/D3 cells across each plate coating.

3.3.3. The effect of LM-10 on expression of IL-1β-driven inflammatory markers in hCMEC/D3 cells

After our changes to the experimental model and choice of cell line, I next aimed to confirm that hCMEC/D3 cells replicated our previous findings that LM-10 modulates the inflammatory activation of endothelial cells. Therefore, I used the 4 h seeding time and a log-concentration response curve of IL-1β treatment to determine the inflammatory activation of hCMEC/D3 cells on LM-10 and Matrigel (Fig. 3.6A-C). IL-1β treatment had a significant effect on ICAM-1 ($p<0.0001$, Fig. 3.6A), VCAM-1 ($p<0.0001$, Fig. 3.6B) and IL-8 ($p<0.0001$, Fig. 3.6C) expression in a concentration-dependent manner. The ECM had a significant effect on expression of VCAM-1 ($p=0.0245$, Fig. 3.6B) demonstrating an elevated expression of VCAM-1 in hCMEC/D3 cells when grown on LM-10 compared to Matrigel, whilst a trend towards a statistically different effect of LM-10 on ICAM-1 ($p=0.0576$, Fig. 3.6A) expression was detected. Specifically, LM-10 induced a higher IL-1β-induced expression of ICAM-1 in hCMEC/D3 cells treated with IL-1β at 100 ng/ml (1.16 fold, $p=0.0089$) and VCAM-1 at 10 ng/ml (1.17 fold, $p=0.0058$), 30 ng/ml (1.16 fold, $p=0.0013$) and 100 ng/ml (1.22 fold, $p<0.0001$) compared to corresponding IL-1β concentrations on Matrigel. No significant effect of ECM coating on IL-8 ($p=0.6916$, Fig. 3.6C) expression was observed, suggesting that LM-10 does not influence IL-8 expression in hCMEC/D3.

Since I have demonstrated that LM-10 modulates the inflammatory activation of brain endothelial cells, I next investigated whether LM-10 alters IL-1β signalling pathways in those cells (Fig. 3.7A-B). The ERK1/2 signalling pathway mediates endothelial cell activation by IL-1β, and previous evidence has shown that different ECM components modulate this signalling pathway (Summers et al., 2013). Therefore, I hypothesised that LM-10 modulates the inflammatory activation of endothelial cells via the ERK1/2 pathway. Although IL-1β treatment ($p=0.0012$) affected phopsho-ERK1/2 levels in a time-dependent manner both on Matrigel and LM-10, no effect of ECM was determined (Fig. 3.7B). Therefore, I investigated alternative members of the MAPK family, specifically p38α. However, in a similar manner, IL-1β treatment ($p=0.0002$) significantly activated phospo-p38α levels in a time-dependent manner both on Matrigel and LM-10, whereas no effect of ECM was determined (Fig. 3.7A).

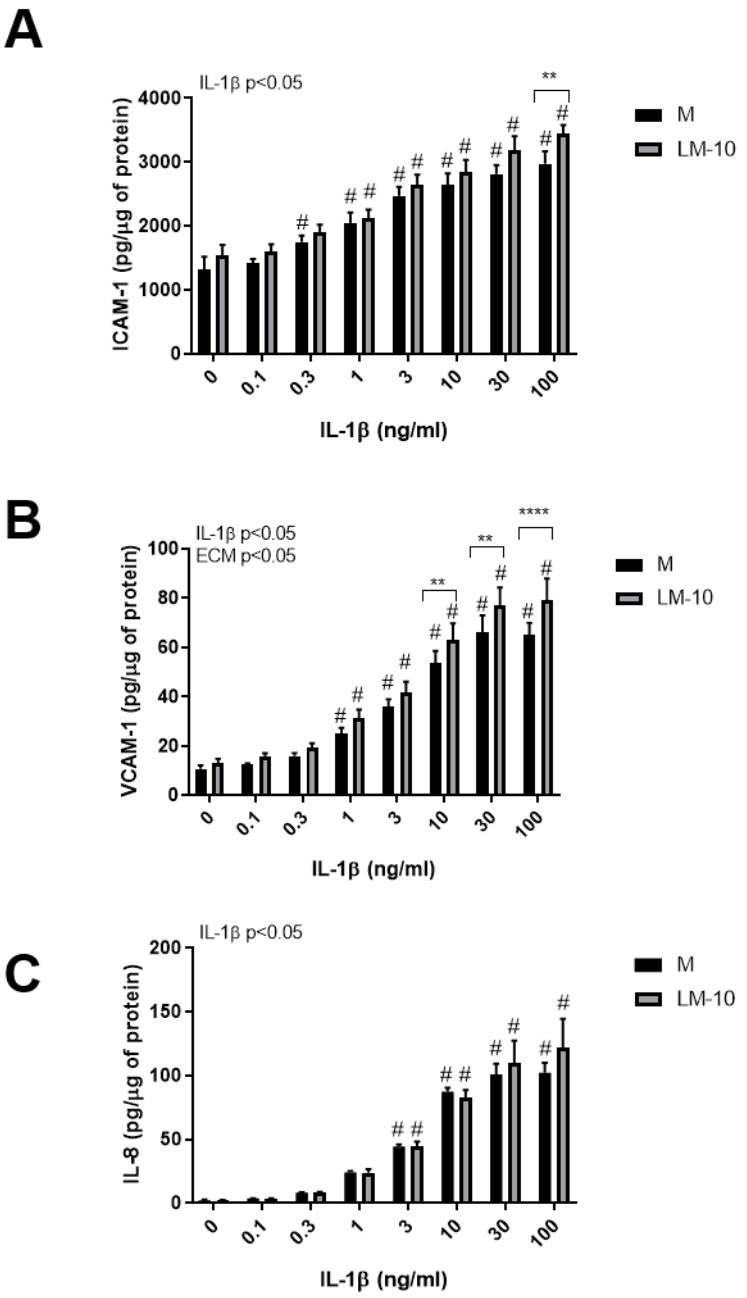

Figure 3.6. Effect of LM-10 on IL-1β-induced activation in hCMEC/D3 cells and IL-1β signalling pathways.
(A-C) hCMEC/D3 cells were seeded at a density of 200,000 cells/well per well in a 24-well plate for 4 h. Cells were treated with IL-1β at various concentrations for 24 h. Cell supernatants and lysates were then collected. Cell lysate was assayed for ICAM-1 (A) and VCAM-1 (B) by ELISA. Cell supernatant was assayed for chemokine IL-8 (C) by ELISA. Data are represented as mean ± SEM of 4 biological replicates (n=4, A-C). Data were assessed by a two-way RM ANOVA followed by Sidak's post-hoc analysis comparing the means of expression of adhesion molecule/cytokine at corresponding concentrations of IL-1β treatment on Matrigel vs LM-10 and comparing the means of signalling molecules at corresponding time points on Matrigel vs LM-10, # represents significance within ECM to untreated. Significant main effects of IL-1β treatment and the ECM coating are indicated on the top left of the graphs. *p<0.05, **p<0.01, ***p<0.001, ****p<0.0001.

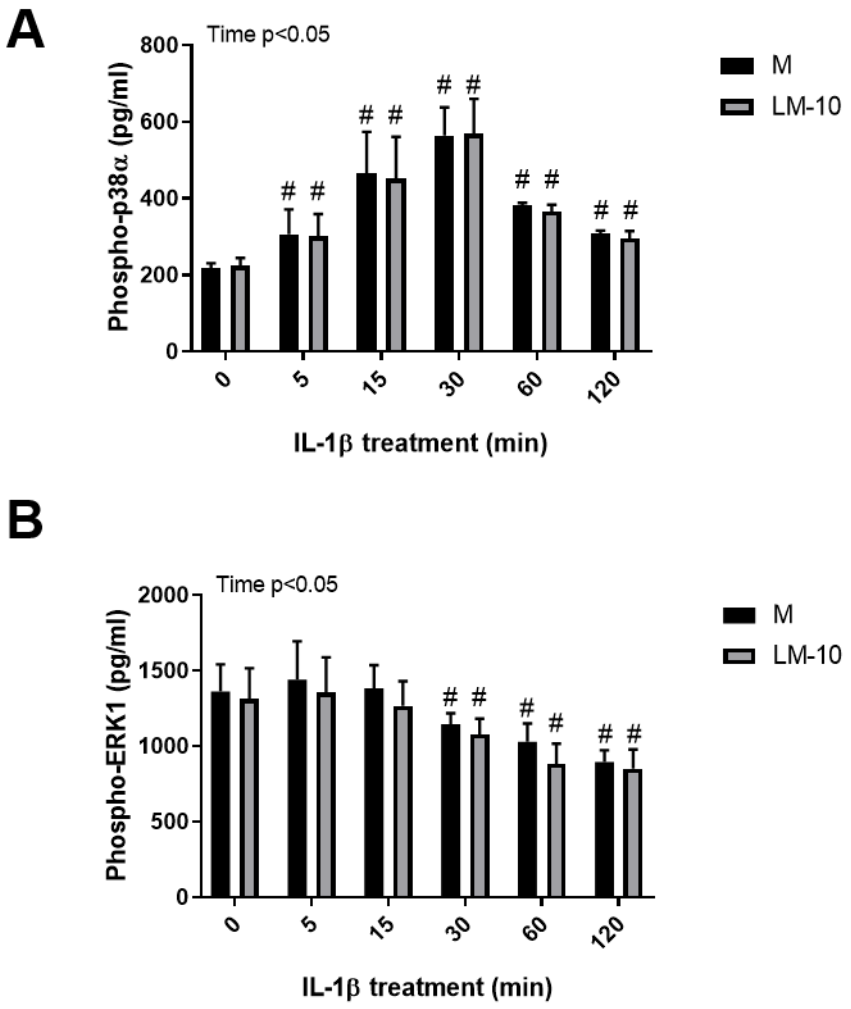

Figure 3.7. Effect of LM-10 on IL-1β signalling pathways in hCMEC/D3 cells.
(A-B) hCMEC/D3 cells were seeded at a density of 200,000/well in a 24-well plate for 4 h. Cells were treated with 10 ng/ml of IL-1β for various times. Cell lysate was assayed for phospho-p38α (A) and phospho-ERK1/2 (B) by ELISA. Data are represented as mean ± SEM of 4 biological replicates (n=4, A-B). Data were assessed by a two-way RM ANOVA followed by Sidak's post-hoc analysis comparing the means of signalling molecules at corresponding time points on Matrigel vs LM-10, # represents significance within ECM to untreated. Significant main effects of IL-1β treatment time and the ECM coating are indicated on the top left of the graphs

3.3.4. The effect of IL-1β treatment on YAP signalling and the modulation by LM-10

Having determined that ERK1/2 and p38α signalling were not affected by LM-10, I investigated alternative signalling pathways that may be modulated by LM-10 and may lead to the altered inflammatory activation I observed. The ECM has been implicated as a regulator of the Hippo pathway (Warren et al., 2018) and evidence suggests that inflammation can modulate Hippo signalling (Choi et al., 2018). Therefore, I hypothesised that IL-1 and/or LM-10 alters Hippo signalling in endothelial cells. To address this hypothesis, I initially measured the phosphorylation of YAP at S127 (Fig. 3.8) and S397 (Fig. 3.9) after IL-1β treatment. These phosphorylation sites play differential roles in YAP signalling whereby p-YAP(S127) induces cytoplasmic retention of YAP (Zhao et al., 2007, 2008), and p-YAP(S397) creates a phospho-degron motif for proteasomal degradation (Zhao, Li, Tumaneng, et al., 2010). The p-YAP(S127)/YAP and p-YAP(S397)/YAP ratios are an indicator of levels of dephosphorylated YAP in the cell that is able to translocate into the nucleus and activate associated genes.

IL-1β treatment ($p<0.0001$) affected p-YAP(S127) levels in a time-dependent manner both on Matrigel and LM-10 (Fig. 3.8). When hCMEC/D3 cells were seeded on Matrigel the phosphorylation of YAP(S127) decreased at 5 min (54%, $p=0.0.164$) and 15 min (54%, $p=0.0053$) compared to the respective baseline, then slowly returned to baseline levels at 120 min and 240 min. Similarly, a decrease in p-YAP(S127) was observed at 15 min (46%, $p=0.0038$) on LM-10, which then returned to baseline levels on LM-10 at 120 min and 240 min. No effect of ECM on p-YAP(S127) levels was observed, and no significant differences between Matrigel and LM-10 were observed at each time point after IL-1β treatment.

Similarly, I analysed the p-YAP(S397)/YAP ratio at the same time intervals after IL-1β treatment in hCMEC/D3 cells (Fig. 3.9). IL-1β treatment ($p=0.0002$) affected p-YAP(S397) levels in a time-dependent manner both on Matrigel and LM-10. When hCMEC/D3 cells were seeded on Matrigel, there was a small, not significant, initial reduction in p-YAP(397) levels at 5 min (35% $p=0.7288$) and 30 min (15%, $p=0.9978$) after IL-1β treatment compared to baseline. This was followed by a marked increase in p-YAP(397) levels between 30 min and 240 min after IL-1β treatment, and significant increases were observed at 120 min (2.7-fold increase,

p=0.0063) and 240 min (4.1-fold increase, p<0.0001) compared to baseline on Matrigel. In contrast, the signalling pattern of p-YAP(397) expression on hCMEC/D3 seeded on LM-10 did not resemble that on Matrigel. A consistent, significant reduction in p-YAP(397) levels in hCMEC/D3 cells on LM-10 were observed between 15 min and 120 min after IL-1β treatment compared to basal levels, with a significant reduction at 15 min (55%, p=0.0349), 30 min (72%, p=0.0089) and 60 min (69%, p=0.0073), with a small increase in levels observed at 240 min (36%, p=0.4310). Interestingly, the ECM (p=0.0112) had a significant effect on the levels of p-YAP(S397), demonstrating elevated levels of p-YAP(S397) on Matrigel compared to LM-10. On direct comparison between corresponding time points on Matrigel and LM-10, significantly higher levels of p-YAP(397) was observed at 30 min (4.2-fold increase, p=0.0219), 120 min (4.5-fold increase, p=0.0014), 240 min (3.63-fold increase, p<0.0001) after IL-1β treatment on Matrigel.

Alongside assessment of YAP activation, I also assessed the levels of phopsho-NF-κB p65 (Fig. 3.10) and IκBα (Fig. 3.11), well characterised components of NF-κB signalling, to confirm successful IL-1β activation at each time interval. IL-1β treatment (p=0.0002) affected the levels of phopsho-NF-κB p65 in a time-dependent manner both on Matrigel and LM-10 (Fig. 3.10). Similar patterns of phopsho- NF-κB p65 signalling were observed when cells are seeded on Matrigel or LM-10, whereby there was a rapid increase of phopsho-NF-κB p65 at 5 min after IL-1β treatment. In hCMEC/D3 cells seeded on Matrigel, there was a significant increase in phopsho-NF-κB p65 expression at 5 min (15.5-fold increase, p=0.0002) after IL-1β treatment compared to baseline, which slightly dropped but remained elevated at 15 min (11-fold increase, p=0.0081), 30 min (13-fold increase, p=0.0011), 60 min (11-fold increase, p=0.0063) before more markedly reducing at 120 min and 240 min after IL-1β treatment. A significant increase in phopsho-NF-κB p65 expression in hCMEC/D3 cells on LM-10 was observed at 5 min (12.8-fold increase, p<0.0001) after IL-1β treatment compared to baseline, which slightly dropped but remained elevated at 15 min (8.9-fold increase, p=0.0002) and 30 min (7-fold increase, p=0.0046), before markedly reducing at 60 min after IL-1β treatment. Interestingly the ECM (p=0.0161) had a significant effect on phopsho-NF-κB p65 levels, with significantly higher levels of phopsho-NF-κB p65 observed at 5 min (1.5-fold increase, p=0.0425) on LM-10 compared to 5 min on Matrigel.

I next assessed IκBα expression after IL-1β treatment in hCMEC/D3 cells (Fig. 3.11). Although IL-1β treatment ($p<0.0001$) affected IκBα in a time-dependent manner both on Matrigel and LM-10, no effect of ECM was determined. There was a marked, significant reduction in IκBα levels in hCMEC/D3 cells seeded on Matrigel after 5 min (84%, $p= 0.0021$), 30 min (95%, $p=0.0001$) and 60 min (87%, $p=0.0016$) of IL-1β treatment. A marked and significant reduction in IκBα at 5 min (82%, $p=0.0013$), 30 min (92%, $p=0.0001$) and 60 min (88%, $p=0.0005$) after IL-1β treatment was observed in hCMEC/D3 cells seeded on LM-10. Direct comparison between corresponding time-points on Matrigel and LM-10 showed no significant differences in IκBα levels were detected.

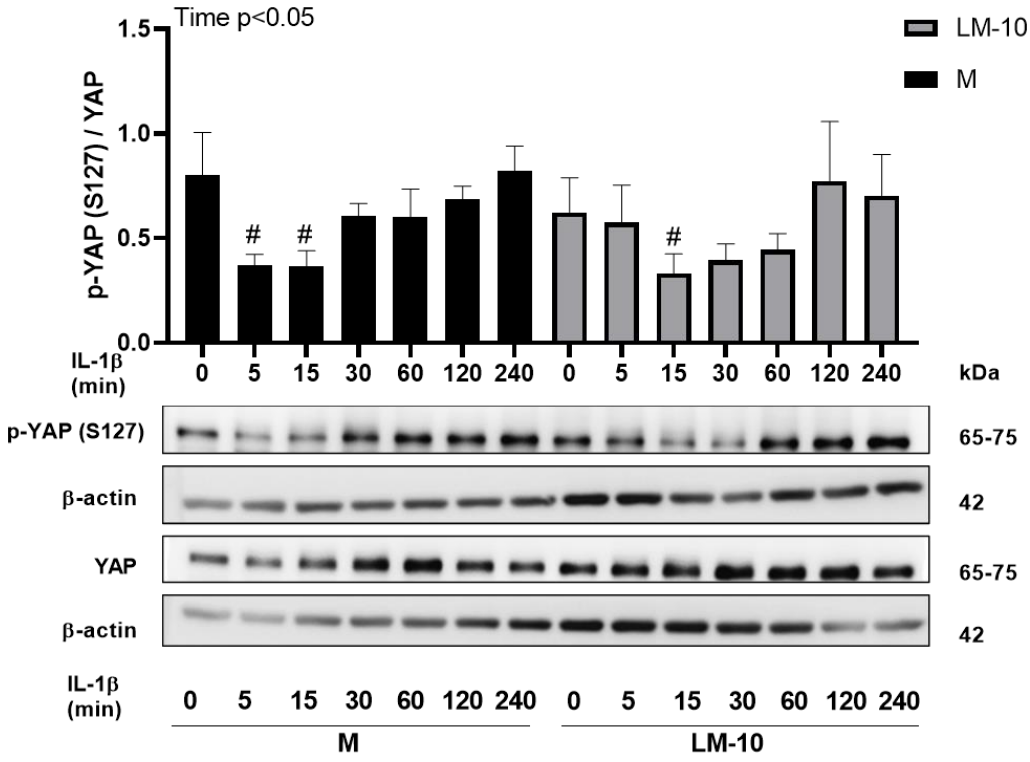

Figure 3.8. Effect of LM-10 on p-YAP(S127) signalling after IL-1β-induced activation in hCMEC/D3 cells.

hCMEC/D3 cells were seeded at a density of 200,000 cells/well in a 24-well plate for 4 h. Cells were treated with IL-1β (10 ng/ml) for various length of time (from 5 min to 240 min). Cell lysates were then collected and assayed for p-YAP(S127) and total YAP by Western blot. p-YAP(S127), YAP and β-actin were quantified using densitometry on ImageJ. p-YAP(S127) and YAP were normalised to β-actin, and the ratio of normalised p-YAP (S127)/total YAP was calculated. Data are represented as mean ± SEM of 4 biological replicates (n=4). The blot is a representative image. Data were assessed by a two-way RM ANOVA followed by Sidak's post-hoc analysis. * represents significance comparing the mean ratio of p-YAP(S127)/total YAP at corresponding time points on Matrigel vs LM-10 and # represents significance within ECM to baseline. Significant main effects of IL-1β treatment time and the ECM coating are indicated on the top left of the graphs. *p<0.05.

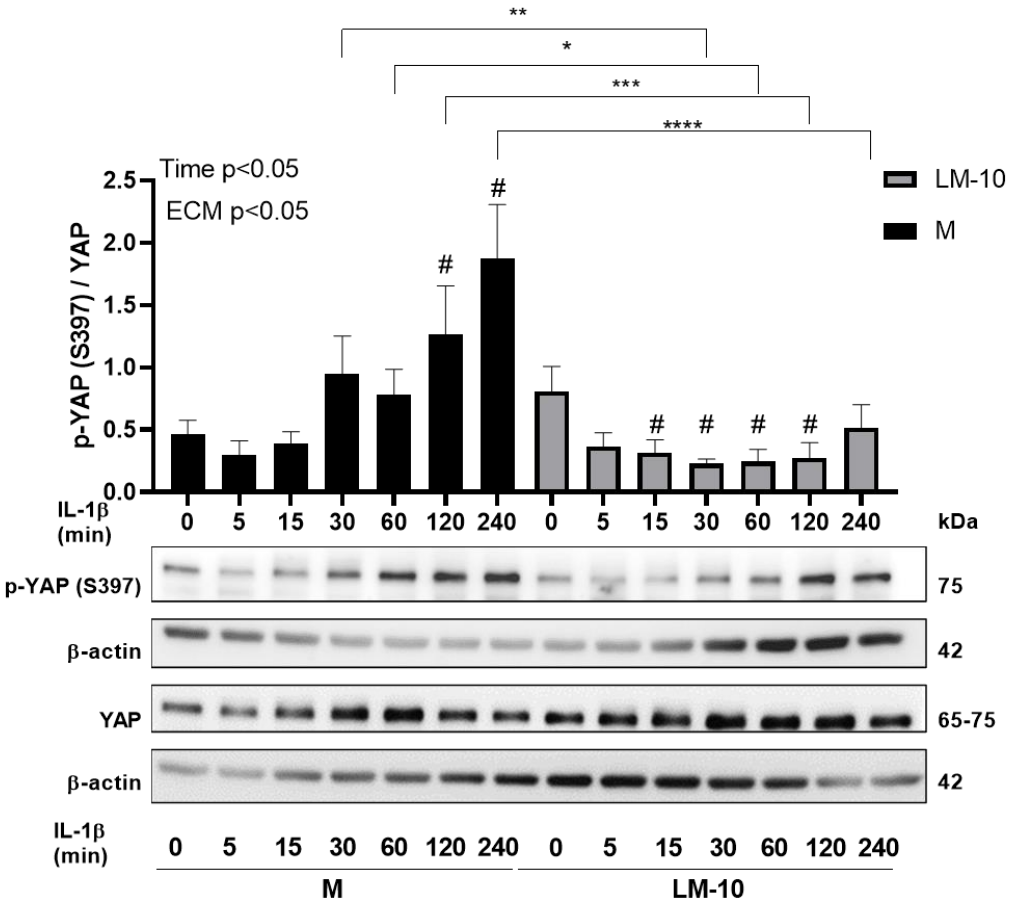

Figure 3.9. Effect of LM-10 on p-YAP(S397) signalling after IL-1β-induced activation in hCMEC/D3 cells.

hCMEC/D3 cells were seeded at a density of 200,000 cells/well per well in a 24-well plate for 4 h. Cells were treated with IL-1β (10 ng/ml) for various length of time (from 5 min to 240 min). Cell lysates were then collected and assayed for p-YAP(S397) and total YAP by Western blot. p-YAP(S397), YAP and β-actin were quantified using densitometry on ImageJ. p-YAP(S397) and YAP were normalised to β-actin, and the ratio of normalised p-YAP(S397)/total YAP was calculated. Data are represented as mean ± SEM of 4 biological replicates (n=4). The blot is a representative image. Data were assessed by a two-way RM ANOVA followed by Sidak's post-hoc analysis. * represents significance comparing the mean ratio of p-YAP(S397)/total YAP at corresponding time points on Matrigel vs LM-10 and # represents significance within ECM to baseline. Significant main effects of IL-1β treatment time and the ECM coating are indicated on the top left of the graphs. *p<0.05, **p<0.01, ***p<0.001, ****p<0.0001.

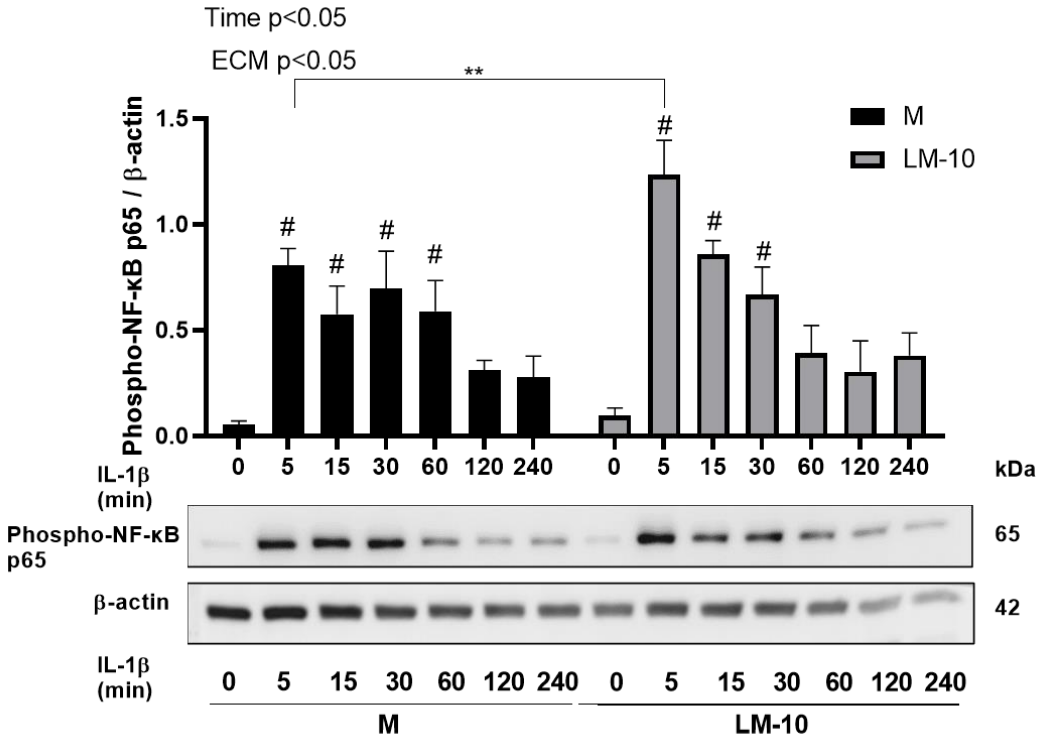

Figure 3.10. Effect of LM-10 on phospho-NF-κB p65 signalling after IL-1β-induced activation in hCMEC/D3 cells.
hCMEC/D3 cells were seeded at a density of 200,000 cells/well per well in a 24-well plate for 4 h. Cells were treated with IL-1β (10 ng/ml) for various length of time (from 5 min to 240 min). Cell lysates were then collected and assayed for phospho-NF-κB p65 by western blot. Phospho-NF-κB p65 and β-actin were quantified using densitometry on ImageJ. Phospho-NF-κB p65 was normalised to β-actin and the ratio is presented. Data are represented as mean ± SEM of 4 biological replicates (n=4). The blot is a representative image. Data were assessed by a two-way RM ANOVA followed by Sidak's post-hoc analysis * represents significance comparing phospho-NF-κB p65 at corresponding time points on Matrigel vs LM-10 and # represents significance within ECM to baseline. Significant main effects of IL-1β treatment time and the ECM coating are indicated on the top left of the graphs. *p<0.05.

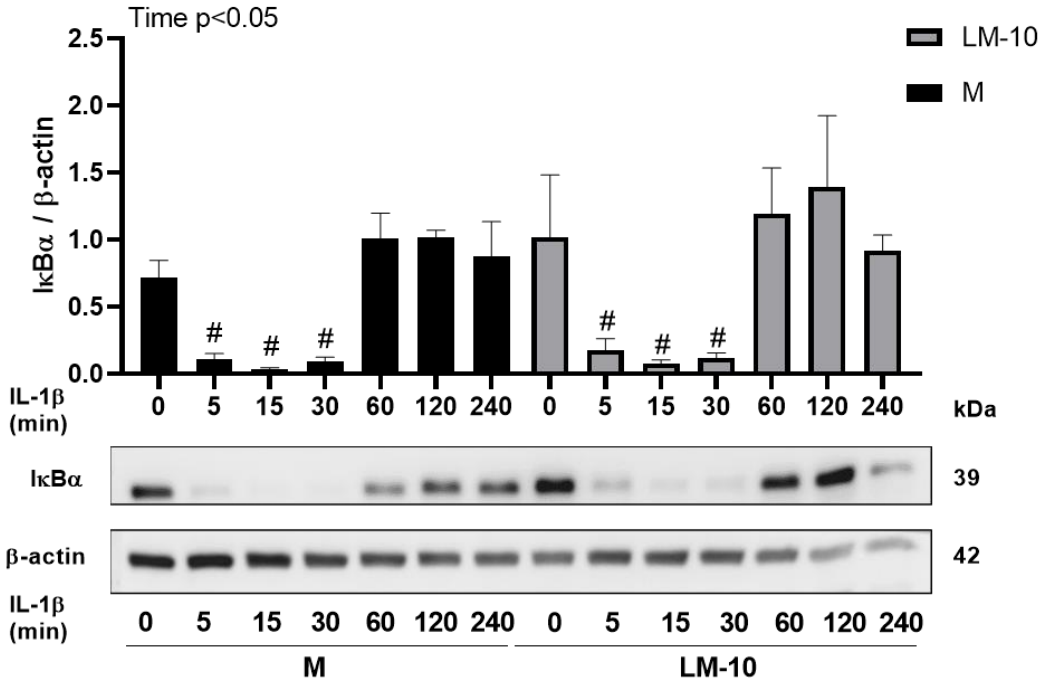

Figure 3.11. Effect of LM-10 on IκBα signalling after IL-1β-induced activation in hCMEC/D3 cells.

hCMEC/D3 cells were seeded at a density of 200,000 cells/well per well in a 24-well plate for 4 h. Cells were treated with IL-1β (10 ng/ml) for various length of time (from 5 min to 240 min). Cell lysates were then collected and assayed for IκBα by western blot. IκBα and β-actin were quantified using densitometry on ImageJ. IκBα was normalised to β-actin and the ratio is presented. Data are represented as mean ±SEM of 4 biological replicates (n=4). The blot is a representative image. Data were assessed by a two-way RM ANOVA followed by Sidak's post-hoc analysis * represents significance comparing IκBα at corresponding time points on Matrigel vs LM-10 and # represents significance within ECM to baseline. Significant main effects of IL-1β treatment time and the ECM coating are indicated on the top left of the graphs. *p<0.05.

To investigate the nuclear activity of YAP as a transcriptional co-activator, I analysed the mRNA levels of its target genes *Ctgf* (Fig. 3.12A) and *Serpine 1* (Fig. 3.12B). Interestingly, a main effect of IL-1β (p=0.0024) and a main effect of ECM (p=0.0026) on the mRNA levels of Ctgf was observed. There was a significant marked reduction (97%, p=0.0197) of Ctgf mRNA levels in hCMEC/D3 cells on Matrigel after IL-1β treatment, whilst the reduction on LM-10 was not significant (22%, p=0.6031). On direct comparison of baseline Ctgf mRNA levels between Matrigel and LM-10, there was notably elevated levels on LM-10 (1.6-fold increase, p=0.2515). After IL-1β treatment, there was a significant difference in levels of Ctgf mRNA levels between Matrigel and LM-10 (42-fold increase, p=0.0127). In contrast, I observed a different IL-1β effect on Serpine 1 mRNA levels whereby no overall effect of IL-1β was observed, whilst there was a trend towards significance effect of ECM (p=0.0667), suggesting potentially elevated levels of Serpine 1 mRNA on LM-10. On comparison within plate coating, although not significant, there was an increase (47%, p=0.6333) in Serpine 1 mRNA on Matrigel after IL-1β treatment compared to the untreated condition on Matrigel. However, this was not mirrored in cells seeded on LM-10 after IL-1β treatment. Similarly to basal levels of Ctgf, and although not significant, there was an increase of Serpine 1 mRNA levels at baseline in hCMEC/D3 cells seeded on LM-10 compared to Matrigel (1.7-fold increase, p=0.3836).

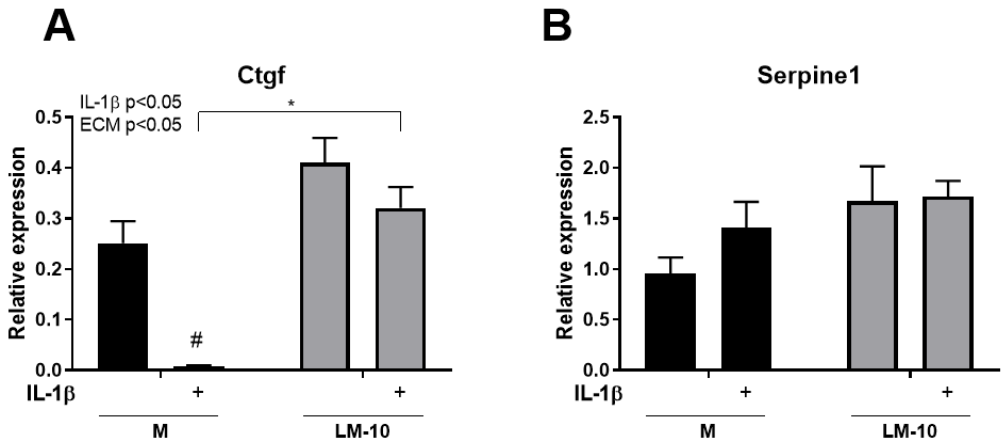

Figure 3.12. Effect of LM-10 on genes downstream of YAP after IL-1β-induced activation in hCMEC/D3 cells.
(A-B) hCMEC/D3 cells were seeded at a density of 200,000 cells/well per well in a 24-well plate for 4 h and cells were treated with IL-1β (10 ng/ml) for 2 h. Cell lysates were collected and mRNA levels (normalised to GAPDH housekeeping control) of Ctgf (A) and Serpine 1 (B) were assayed by qPCR. Data are represented as mean ± SEM of 4 biological replicates (n=4). Data were assessed by a two-way RM ANOVA followed by Sidak's post-hoc analysis, * represents significance between corresponding conditions on Matrigel vs LM-10 and # represents significance within ECM to baseline. Significant main effects of IL-1β treatment and the ECM coating are indicated on the top left of the graphs. *p<0.05.

3.3.5. The effect of LM-10 on hallmarks of angiogenesis in vitro

I have shown that LM-10 modulates the inflammatory activation of endothelial cells, and it has been well reported that inflammation plays a key role in angiogenesis (Ceulemans et al., 2010; Iadecola and Anrather, 2011). Despite evidence that laminins play protective roles in the CNS (Sixt et al., 2001; Indyk et al., 2003; Song et al., 2017; Zhang et al., 2017), the specific role of the LM-10 isoform in angiogenesis had not yet been determined. Therefore, I hypothesised that LM-10 is a key driver of angiogenesis, and I investigated this using the scratch assay (Fig. 3.13A,B) and the tube formation assay (Fig. 3.14A-C). The ECM affected the scratch essay in a time-dependent manner showing an increase in wound density over time, reflective of increased endothelial migration into the scratched region, and an elevated increase of wound density on LM-10 compared to Matrigel. LM-10 increased wound density in hCMEC/D3 cultures at every time-point (4 h (64%, p=0.0404), 8 h (60%, 0=0.0006), 12 h (52%, p=<0.0001), 16 h (39%, p=0.0001), 20 h (20.7%, p=0.0052) and 24 h (16%, p=0.0293)) measured across the 24 h period compared to corresponding time-points on Matrigel (Fig. 3.13B). Matrigel supplemented with LM-10 increased the number of branches (1.35-fold increase, p=0.0263, Fig. 3.14B) and total branching length (1.57-fold increase, p=0.0144, Fig. 3.14C) compared to Matrigel in the tube formation assay, showing that LM-10 increase tube-like structures and their length. These data suggest that LM-10 aids endothelial migration, a key hallmark in angiogenesis, and increases the ability of endothelial cells to form tube-like structures, a critical stage in angiogenesis.

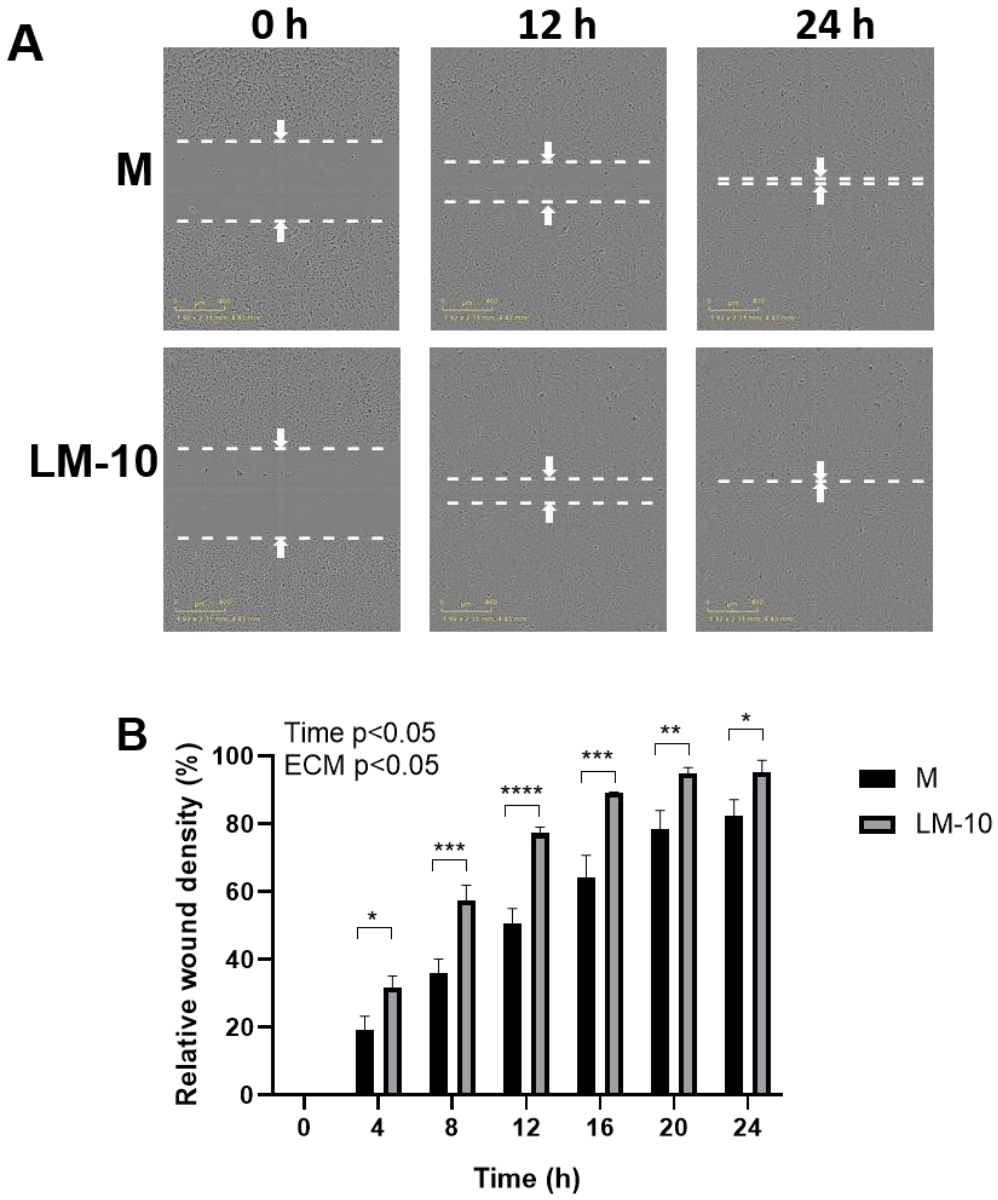

Figure 3.13. Effect of LM-10 on hCMEC/D3 cell migration.
(A) Representative images and (B) quantification of the scratch assay. 96-well Essen ImageLock plates were pre-coated with Matrigel (20 µg/ml) or LM-10 (10 µg/ml). 40,000 hCMEC/D3 cells were seeded for 4 h and the 96-pin IncuCyte WoundMaker Tool was used to create uniform cell-free zones. Phase contrast images were acquired every 4 h on an Incucyte Zoom Live Cell Analysis system using a 123 4x/3.05 Plan Apo OFN25 objective. Arrows indicate boundaries of the scratched regions. Scale bar 400 µm. The Incucyte scratch wound assay analysis software as used to calculate relative wound confluence (B). Data are represented as mean ± SEM of 3 technical replicates and 3 biological replicates (n=3). Data were assessed by a two-way RM ANOVA followed by Sidak's post-hoc analysis comparing the means of wound confluence at corresponding time points on Matrigel vs LM-10. Significant main effects of time and the ECM coating are indicated on the top left of the graphs *p<0.05, **p<0.01, ***p<0.001, ****p<0.0001.

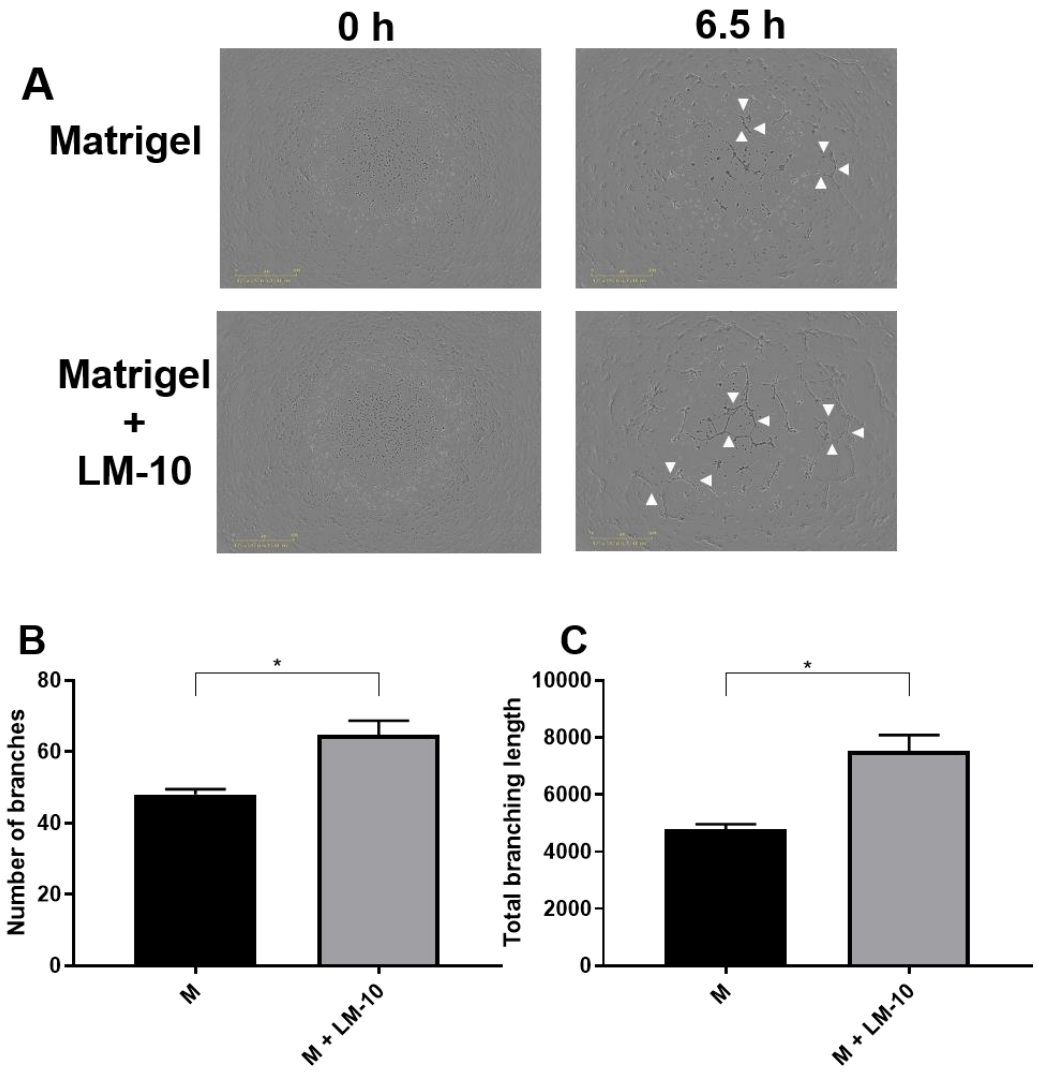

Figure 3.14. Effect of LM-10 on hCMEC/D3 cell tube formation.
(A) Representative images and quantification (B-C) of the tube formation assay. 96-well plates were pre-coated with Matrigel (9.16 mg/ml) or Matrigel (9.16 mg/ml) supplemented with LM-10 (10 µg/ml). 10,000 hCMEC/D3 cells were seeded on top of the Matrigel layer. Phase contrast images were acquired at 0 and 6.5 h on an Incucyte Zoom Live Cell Analysis system (Essen BioScience, UK) using a 123 4x/3.05 Plan Apo OFN25 objective. Scale bar 800 um. The angiogenesis analyser macro in ImageJ was used to quantify number of branches (B) and total branching length (C). Data are represented as mean ± SEM of 2 technical replicates and 4 biological replicates (n=4). Data were assessed by paired t-test to compare coatings. *p<0.05, **p<0.01, ***p<0.001, ****p<0.0001.

3.4. **Discussion**

Recent research has demonstrated a novel role of the ECM as a regulator of IL-1-induced endothelial inflammation *in vitro* (Summers et al., 2013) and LM-10 has been identified as a potential mediator of BBB repair *in vitro* (Kangwantas et al., 2016). However, the specific role of LM-10 as a regulator of IL-1-driven endothelial inflammation and angiogenesis *in vitro* remained unknown. Furthermore, the signalling crosstalk between IL-1 and Hippo signalling in endothelial cells has not been investigated. In this study, I have:

- Established an in vitro model using hCMEC/D3 cells, a short seeding time of 4 h and the plate coating control of Matrigel.
- Established a novel role of LM-10 as a modulator of IL-1β-induced ICAM-1 and VCAM-1 expression in hCMEC/D3 cells.
- Demonstrated that LM-10 increases endothelial proliferation and migration of hCMEC/D3 cells.
- Elucidated a novel crosstalk between IL-1β and Hippo signalling and demonstrated altered YAP signalling and YAP associated gene expression in hCMEC/D3 cells seeded on LM-10.

A focus point of discussion from this study is the development of the experimental model in order to address our first key aim. Our preliminary experiments used b.End5 cells and primary MBECs to initially establish the role of LM-10 on cellular adhesion and endothelial inflammation. I first showed that LM-10 increases bEnd.5 cell attachment in a concentration-dependent manner, whilst a stronger concentration-dependent effect of LM-10 on cellular adhesion was observed in primary MBECs compared to bEnd.5 cells. Our preliminary experiments investigating IL-1β treatment on bEnd.5 cells and primary MBECs showed the upregulation of several key adhesion molecules and cytokines/chemokines when endothelial cells were seeded on LM-10, supporting our hypothesis that LM-10 is a modulator of inflammation. I observed interesting results suggesting a protective barrier function role of LM-10 in the context of neutrophil transmigration, whereby LM-10 reduced neutrophil transmigration despite the enhanced inflammatory response observed, suggesting that LM-10 may increase barrier properties that attenuate the transmigratory effects of the upregulation of adhesion molecules.

This observed barrier properties is in agreement with other studies showing that LM-10 reduces neutrophil transmigration across an endothelium (Song et al., 2017) and the protective function of LM-10 in T cell transmigration in EAE (Sixt et al., 2001). A striking observation during the preliminary stages was the pronounced effect that a shorter seeding time of bEnd.5 cells had on the LM-10 effect as a modulator of inflammation, with marked increases in chemokine KC expression and MCP-1 observed. I speculate this is likely due to endothelial cells secreting their own basement membrane once seeded (Davis and Senger, 2005; Thomsen et al., 2017), and therefore over longer seeding periods the secreted basement membrane could potentially mask the effect of the ECM plate coating. Hence, this led us to decide on the use of a 4 h seeding time for future experiments, similar to that used in other studies (Yun et al., 2016). This resulted in the experimental reality that primary MBECs would not be viable for a shorter seeding time, and since I had technical difficulties using bEnd.5 cells in angiogenic assays I pursued other cell lines for future studies. Subsequently, our next pivotal decision was to use hCMEC/D3 cells, the human BBB endothelial cell line, since this is a better model of human cerebral endothelial cells and was suitable for future assays (Weksler et al., 2013). Furthermore, I decided that Matrigel was a more suitable ECM control to take forward for future experiments as it better mimicked the basement membrane of the CNS.

Consequently, this led onto our second key aim to thoroughly characterise the inflammatory, signalling and angiogenic response in hCMEC/D3 cells. I did not observe an increase in confluency of hCMEC/D3 cells on LM-10 and hence suggest this in indicative of no enhanced adhesion effect of LM-10 in this cell line. Although previous evidence has demonstrated a novel function of the ECM as a regulator of IL-1-induced cerebral endothelial activation *in vitro* whereby attachment of cells to ECM components enhances IL-1-induced activation of endothelial cells (Summers et al., 2013), the specific role of LM-10 had not yet been determined. Here, I demonstrated that novel function of LM-10 whereby endothelial attachment to LM-10 increased ICAM-1 and VCAM-1 expression in hCMEC/D3 cells after IL-1β treatment, further confirming that the LM-10 inflammatory modulatory effect is conserved between several endothelial cell lines. Indeed, after cerebral ischaemia there is the upregulation of several vascular adhesion molecules, including ICAM-1 and VCAM-1, which aid leukocyte

infiltration into the brain and contribute to subsequent tissue injury (Denes et al., 2011). However, it is critical that the potential role of adhesion molecules during angiogenesis is also considered (Liao et al., 2017). The dual nature of adhesion molecules adds complexity in understanding their overall contribution post-stroke, therefore their detrimental effects should be considered alongside their contribution to endothelial progenitor cell homing and angiogenesis. It has been demonstrated *in vitro* that VEGF upregulates ICAM-1 brain microvascular endothelial cells (Radisavljevic et al., 2000), mediating their migration, a key hallmark in angiogenesis, whilst *in vivo* data shows that ICAM-1 knockout mice show attenuated VEGF-mediated angiogenesis (Kasselman et al., 2007), suggesting that ICAM-1 plays a key role in pathological angiogenesis. There is similar evidence demonstrating conflicting roles of VCAM-1 with the potential angiogenic role evidenced in several studies (Gao et al., 2008; Kang et al., 2014). Interestingly, I saw a strongly potentiated response of VCAM-1 expression compared to ICAM-1 expression in hCMEC/D3 cells, therefore I speculate that they may be under different regulatory mechanisms. In line with this speculation, I did not observe a potentiation of IL-8 on hCMEC/D3 cells seeded on LM-10, which would suggest that it is not just an overall increased inflammatory profile when cells are seeded on LM-10, but a specific response dictated by the differential upregulation of adhesion molecules and cytokines. I appreciate that this is not an exhaustive list of adhesion molecules and cytokines/chemokines upregulated post-stroke and suggest that future work using LEGENDplex assays or RNA sequencing would be of benefit.

I next sought to determine the mechanisms by which LM-10 may modulate the inflammatory activation of endothelial cells and turned our focus to classical IL-1β signalling pathways. Previous studies had shown a novel regulatory mechanism by which the ECM modulates ERK1/2 signalling after IL-1β treatment in rat astrocytes and rat brain endothelial cells *in vitro* (Summers et al., 2010, 2013) and therefore this was our first avenue of investigation. However, I did not observe a modulatory effect of the ECM on phospho-ERK1/2 signalling. Furthermore, I did not observe the phospho-ERK1/2 signalling response previously observed after IL-1β treatment in hCMEC/D3 cells, whereby a transient increase in phospho-ERK1/2 would be expected around 15-30 min (Ni et al., 2017). Although, in other studies using primary mouse brain endothelial cells and a rat brain endothelial cell line

phospho-ERK1/2 activation in response to IL-1β treatment has not been observed (Thornton et al., 2010). This led to further investigation of the IL-1β signalling p38 MAPK pathway in which I did observe the signalling response expected of an increase in phospho-p38α around 15-30 min (Ni et al., 2017). However, I did not determine an altered signalling response in hCMEC/D3 cells on LM-10. Together, these findings suggest that the altered inflammatory activation of hCMEC/D3 cells on LM-10 was not dictated by these signalling mechanisms.

Although the Hippo pathway is typically associated with controlling cell size, increasing evidence has demonstrated a cross talk between the Hippo pathway and inflammation (Wang et al., 2020). Of particular interest is the involvement of YAP/TAZ in TNF-α-induced inflammatory responses in endothelial cells, whereby TNF-α induced YAP translocation into the nucleus and that nuclear YAP was required for optimal TNF-α-induced ICAM-1 and VCAM-1 expression (Choi et al., 2018). However, the interaction between IL-1β signalling and YAP/TAZ activation had not yet been investigated and this led to our overarching hypothesis that IL-1β signalling would modulate YAP/TAZ activation through downstream effectors. The understanding in the relationship between inflammation and Hippo signalling is a growing area and there is conflicting evidence demonstrating conflicting effects of deletion of YAP (Lv et al., 2018) and knockdown of YAP/TAZ (K.-C. Wang et al., 2016) respectively. Furthermore, Hippo signalling has been shown to have critical roles in vascular systems, contributing to vessel homeostasis, vascular development, angiogenesis (Park and Kwon, 2018). Another complexity in the Hippo pathway is the relationship with integrin-ECM signalling, whereby there is extensive evidence that integrin signalling leads to YAP/TAZ activation (Warren et al., 2018). Of particular interest are the downstream mechanisms in which integrins modulate YAP/TAZ, hence the cross-talk between other signalling pathways feeding into the Hippo cascade. There is extensive evidence implicating Src kinases, FAK, PAK proteins and Rho as potential effectors acting as bridge between integrin signalling and YAP/TAZ (Warren et al., 2018). This led to a further hypothesis centred on the differential integrin signalling pathways activated in hCMEC/D3 cells seeded on different ECM matrix, and whether these pathways can activate or inhibit kinases of the Hippo cascade and alter YAP/TAZ signalling, which in turn could then alter the inflammatory activation. There is evidence that signalling pathways triggered in response to inflammatory stimulus, such as p38

MAPK (Huang et al., 2016) and ERK1/2 (You et al., 2015), may modulate kinases of the Hippo cascade. A third hypothesis was also formed as to whether LM-10 triggers altered pathways downstream of IL-1R1 and whether these crosstalk with the Hippo pathway. It has been recently demonstrated that YAP can act as a transcriptional repressor of COX-2 transcription downstream of IL-1β signalling (Zhang et al., 2018). Thus, this led to speculation as to whether YAP could act as a transcription repressor or activator of other genes downstream of IL-1β/NF-κB.

To our knowledge this is the first study to show a YAP response after IL-1β treatment in hCMEC/D3 cells seeded on Matrigel and LM-10, specifically demonstrating a novel temporal pattern of YAP phosphorylation at S127 and S397. The subcellular distribution of YAP is controlled by the reversible phosphorylation of S127, resulting in 14-3-3 binding and cytoplasmic retention, hence unable to bind to TEADs (Zhao et al., 2007, 2008). Whilst, the phosphorylation of S397 creates a phospho-degron motif for β-TrCP binding resulting in proteasomal degradation, providing an irreversible longer-term mechanism of YAP inhibition (Zhao, Li, Tumaneng, et al., 2010). This is a coordinated response in the regulation of YAP activation and therefore understanding the patterns of both is critical to better reflect the status of the cell. After IL-1β treatment in hCMEC/D3 cells, a similar decrease in S127 was observed at 5-15 min on Matrigel and 15-60 min on LM-10, followed by an increase back to respective basal levels at 240 min. However, the temporal pattern of S397 phosphorylation was modulated on each ECM. I suggest that the rapid reductions in pYAP(127) and pYAP(397) on Matrigel at 5-15 min after IL-1β treatment are indicative of transient dephosphorylation of YAP, and hence translocation into the nucleus. This is then followed by a sustained sequestering of YAP in the cytoplasm between 30-240 min, maintained through sustained phosphorylation at S127, in which time YAP also becomes phosphorylated at S397, thus priming YAP for degradation. These findings suggest that the phosphorylation of YAP at S127 and S397 is coupled when cells are seeded on Matrigel and treated with IL-1β. In contrast, I suggest that the transient reductions in pYAP(127) and pYAP(397) on LM-10 at 15-60 min are indicative of slightly longer but still transient dephosphorylation of YAP, and hence translocation into the nucleus. This is then followed by a sustained sequestering of YAP in the cytoplasm through phosphorylation at S127 between 120-240 min in hCMEC/D3 cells on LM-10. Interestingly, the increase in YAP phosphorylation at S127 is not

mirrored at S397 in hCMEC/D3 cells on LM-10, instead a sustained decrease in phosphorylation at S397 is maintained from 5-120 min, until a slight increase at 240 min. This would suggest that when cells are seeded on LM-10, the phosphorylation of S127 and S397 is not coupled. Although, I should state that this is not categorically conclusive as a longer time course may be needed to determine whether there is a delayed upregulation of S397 on LM-10.

To further investigate the YAP response, the mRNA levels of key genes downstream of YAP were determined. Ctgf is a direct gene downstream of YAP that is important for cell growth (Zhao et al., 2008). In support of the increased, sustained phosphorylation of S127 and S397 observed on Matrigel, I show heavily decreased levels of Ctgf mRNA 2 h after IL-1β treatment, reflective of decreased activation of genes downstream of YAP-TEAD. In comparison, no significant change in Ctgf mRNA was observed 2 h after IL-1β treatment in hCMEC/D3 cells on LM-10, supporting our previous findings that YAP was not sequestered and degraded to the same degree as on Matrigel. However, I did not detect any significant change in Serpine1 mRNA levels. I speculate that since Serpine1 is typically associated with mechano-signalling (Liu et al., 2015), that there is the potential the gene is not regulated via YAP in hCMEC/D3 cells after IL-1β treatment. However, it is important to discuss the limitations of this experiment, by which I only measured the mRNA levels 2 h after IL-1β treatment and a limited number of genes. A more thorough approach in the future would be needed, critically including earlier time points that would measure any rapid upregulation of genes after the transient translocation of YAP into the nucleus. A time course would better reflect the upregulation and downregulation of genes associated with YAP, and enable the response to be mapped to the temporal phosphorylation of YAP and thus nuclear-cytoplasmic shuttling of YAP.

The NF-κB pathway is a critical mediator of the inflammatory response (Liu et al., 2017). It has a pivotal role in the expression of pro-inflammatory genes including chemokines, cytokines, chemokines such as TNF-α and IL-1. Whilst it is also implicated as a pivotal transcription factor in the downstream signalling response to activation by pro-inflammatory cytokines, including TNF-α and IL-1. Indeed, NF-κB induced by IL-1β is known to upregulate ICAM-1 and VCAM-1 expression (Collins et al., 1995). Alongside the YAP experiments, I determined the phopsho-

NF-κB p65 and IκBα temporal expression after IL-1β treatment to ensure I were stimulating sufficient IL-1β activation in the hCMEC/D3 cells. I observed phopsho-NF-κB p65 and IκBα signalling patterns in response to IL-1β treatment that were congruent with the well characterised NF-κB signalling (Oeckinghaus and Ghosh, 2009), demonstrating a rapid degradation in the inhibitory subunit IκBα coupled with rapid phosphorylation of phopsho-NF-κB p65 after IL-1β treatment. Furthermore, I observed a marked increase in phopsho-NF-κB p65 on LM-10 compared to Matrigel at 5 min after IL-1β treatment, suggesting higher levels of NF-κB activation. This result should be interpreted with some caution since I could not determine total p65 levels at the same time due to limited sample quantity. However, the phopsho-NF-κB p65 have been normalised using β-actin. Previous studies do demonstrate modulated NF-κB responses on different ECM coating (Summers et al., 2010, 2013), and therefore it is plausible speculation that the effect I observed are reflective of the true NF-κB signalling. In order to categorically confirm this finding it would be critical to perform further Western blotting to determine phopsho-NF-κB p65 to total p65 ratios, or to investigate NF-κB signalling through an alternative method such as a luciferase assay.

Our findings from the temporal phosphorylation pattern of YAP and the signalling pathways activated after IL-1β treatment can be drawn together and interpreted in the context our previously discussed YAP hypotheses. Although our findings support the hypothesis that IL-1β signalling modulates YAP phosphorylation and downstream YAP gene transcription, the mechanism behind the altered YAP signalling has not been fully determined. Despite no modulation of p38α and ERK1/2 pathways, I do observe altered NF-κB activation on LM-10. Hence, I can speculate that when cells are seeded on LM-10 and treated with IL-1β, there is an altered signalling cascade that leads to increased NF-κB activation, resulting in the upregulation of ICAM-1 and VCAM-1 I have observed. It has been clearly demonstrated that the Hippo kinase cascade can be dynamically regulated at several stages (Piccolo et al., 2014), and therefore I further speculate that the signalling cascade downstream of IL-1R1 responsible for the increased NF-κB activation observed on LM-10 may crosstalk with kinases of the Hippo pathway and act as a regulator of YAP signalling. However, there is another hypothesis that would need further exploring, which is whether YAP can act as a transcription repressor or activator of genes downstream of NF-κB, as previously demonstrated

(Zhang et al., 2018). Thus, whether the different YAP signalling on LM-10 is directly responsible for the modulated inflammatory response observed on ICAM-1 and VCAM-1. However, it is important to highlight that the increased expression of ICAM-1 and VCAM-1 could be NF-κB independent, similar to TNF-α endothelial activation, whereby YAP/TAZ plays critical roles in regulating endothelial cell adhesive properties independently of the NF-κB pathway (Choi et al., 2018). This could be further investigated by silencing YAP/TAZ in hCMEC/D3 cells or using YAP/TAZ inhibitors to determine the effect on NF-κB, and to confirm that YAP/TAZ is required for the upregulation of ICAM-1 and VCAM-1. The relationship between IL-1 and Hippo signalling is worthy of further investigation and its potential role as a regulator of the inflammatory responses on different ECM components should be further dissected.

Thus far I have explored the role of LM-10 on the inflammatory activation of endothelial cells and I next turned our focus to the role of LM-10 in *in vitro* pro-angiogenic assays. Extensive evidence suggests that the ECM plays a dynamic role in CNS repair, providing a supportive framework and contributing to recovery (Burnside and Bradbury, 2014). Indeed, laminin has been shown to be protective against neuronal loss and contributes to neuronal survival (Indyk et al., 2003). Furthermore, LM-10 has been shown to be protective *in vitro* and reverse key hallmarks of BBB dysfunction after inflammation in endothelial cells (Kangwantas et al., 2016). Endothelial cell proliferation and migration are key hallmarks of angiogenesis (Radisavljevic et al., 2000; Ucuzian et al., 2011). Here, I provide evidence that LM-10 increased endothelial proliferation and migration of hCMEC/D3 cells as demonstrated by the scratch assay. The tube formation assay indicated increased tube-like structures in hCMEC/D3 on LM-10, indicative of angiogenesis (DeCicco-Skinner et al., 2014). However, a caveat of the experimental design is that these were measured under normoxic conditions and for future investigations it would be important to also measure angiogenic assays under inflammatory (IL-1β treatment) and hypoxic conditions. Although, I speculate that since I observed increased ICAM-1 and VCAM-1 expression in hCMEC/D3 cells on LM-10 after IL-1B treatment, I would observe increased migration of endothelial cells under inflammatory conditions as evidence suggests that both are mediators of endothelial migration (Radisavljevic et al., 2000; Gao et al., 2008).

In summary, I provide further compelling evidence that there is a dynamic relationship between inflammation and the ECM. I have established a novel role of LM-10 as a modulator of IL-1β-induced ICAM-1 and VCAM-1 expression in hCMEC/D3 cells and that LM-10 increases endothelial proliferation and migration, which I suggest is indicative of an angiogenic role of LM-10 in BBB repair. I have elucidated a novel relationship between IL-1β and Hippo signalling, demonstrating altered YAP signalling and gene expression on LM-10. Further dissection of the cross-talk between IL-1 signalling and the Hippo pathway would be of particular interest due to the vast biological processes these signalling pathways underlie in homeostasis and disease.

Chapter 4. **The role of brain endothelial IL-1R1 deletion on laminin α5 and laminin α4 expression after cerebral ischaemia.**

All experiments were designed and analysed by myself with the input of Dr Emmanuel Pinteaux. All experiments were performed by me with the input of others as stated below. Dr Nikolett Lénárt and Dr Adam Denés maintained the IL-1R1$^{fl/fl\ +Tam}$ mice and IL-1R1$^{fl/fl\ \Delta\ Slco1c1+Tam}$ mice colony in Budapest, Hungary. Dr Nikolett Lénárt, working alongside Dr Adam Denés, performed the stroke surgeries, neurological scoring and tissue collection. I performed the tissue processing and histology. Sarah Ma assisted in the collection of fluorescent images for analysis and infarct analysis. I performed all other analysis and statistical analysis.

4.1. **Introduction**

A robust inflammatory response is initiated after ischaemic stroke and IL-1 is considered a key mediator of inflammation (Denes et al., 2011). IL-1, expressed as two key isoforms IL-1α and IL-1β, is rapidly upregulated in the brain after cerebral ischaemia (Luheshi et al., 2011). IL-1 is known to exert its effects via IL-1R1 and since brain endothelial cells express the IL-1R1 (Konsman et al., 2004), the cerebrovasculature is considered a major target of IL-1-induced inflammation. Several *in vitro* studies have demonstrated the effects of IL-1 on endothelial cells including the direct activation of brain endothelial cells in response to IL-1β treatment (Thornton et al., 2010; Summers et al., 2013) and neutrophil transmigration across an activated endothelial monolayer through the upregulation of chemokines (Allen et al., 2012). Through recent advancement in the genetic tools available, the conditional deletion of the IL-1R1 in specific cell types *in vivo* has become available (Abdulaal et al., 2016) and has been pivotal in our understanding in the role of IL-1 signalling in specific cell types after ischaemic stroke (Wong et al., 2019).

The inflammatory response post-stroke is accompanied by a dynamic ECM remodelling response. The ECM of the CNS plays a critical role in brain homeostasis and function. The laminin family of glycoproteins are a major component of the basement membrane (Baeten and Akassoglou, 2011). Laminins are heterotrimers formed of a α, β, and γ chain (Domogatskaya et al., 2012). In the CNS there are two distinct basement membranes associated with the vessels, an endothelial basement membrane composed of laminin α5 and laminin α4 (present in LM-10 and LM-8 respectively), and an outer parenchymal basement membrane composed of laminin α1 and laminin α2 (present in LM-1 and LM-2 respectively) (Sixt et al., 2001). The vascular laminins, laminin α5 and lamnin α4, were of interest in this study due to their close interaction with the endothelium. It has been demonstrated *in vitro* that laminin α5 and laminin α4 are regulated in response to IL-1 and TNF-α (Sixt et al., 2001). However, the *in vivo* contribution of endothelial IL-1 signalling on laminin α5 and laminin α4 expression in the context of stroke had not yet been determined. Using conditional deletion of IL-1R1 in brain endothelial cells and the MCAO model of experimental stroke, I investigated the contribution of IL-1 signalling in brain endothelial cells on infarct volume and laminin expression post-stroke. I show that in this present study endothelial IL-1R1 signalling does not

influence infarct volume or neurological outcome. Furthermore, I show that brain endothelial IL-1R1 dynamically regulates laminin α4 expression but not laminin α5 expression at 2 d and 28 d post-MCAO. I also assessed the effect of brain endothelial IL-1R1 on proliferation using BrdU staining and detected no effect after endothelial IL-1R1 deletion.

4.2. **Aims**

The aim of this study was to establish the role of the IL-1R1 in the cerebrovasculature after cerebral ischemia. Specific objectives were:

- To assess the role of the IL-1R1 on brain injury and neurological function after stroke.
- To determine the role of IL-1R1 on laminin α4 and laminin α5 expression across several time points post-stroke.
- To determine the role of IL-1R1 on angiogenesis post-stroke.

4.3. **Results**

4.3.1. Brain endothelial IL-1R1 deletion does not reduce infarct volume and does not improve neurological function

This study first aimed to replicate previous findings that deletion of IL-1R1 from the cerebrovasculature reduced infarct volume after cerebral ischaemia (Wong et al., 2019). IL-1R1$^{fl/fl\ +Tam}$ mice and IL-1R1$^{fl/fl\ \Delta\ Slco1c1+Tam}$ mice underwent a 30 min MCA occlusion. Assessment of infarct volume using cresyl violet revealed no significant difference in lesion volumes in IL-1R1$^{fl/fl\ \Delta\ Slco1c1+Tam}$ mice compared to IL-1R1$^{fl/fl\ +Tam}$ mice 48 h after MCAO (Fig. 4.1A-B). Although an improved neuroscore in IL-1R1$^{fl/fl\ \Delta\ Slco1c1+Tam}$ mice at 24 h after cerebral ischemia has been previously demonstrated (Wong et al., 2019), the effect of deletion of IL-1R1 on the cerebrovasculature on body weight and neurological scores at chronic time points post-cerebral ischemia had not been determined. I assessed the body weight and neurological scores of IL-1R1$^{fl/fl\ +Tam}$ mice and IL-1R1$^{fl/fl\ \Delta\ Slco1c1+Tam}$ mice across a 28 d period after MCAO. I observed no effect of deletion of IL-1R1 in brain endothelial cells on body weight (Fig. 4.2A) or neurological function assessed by 28-point neuroscore (Fig. 4.2B) and Bederson's neuroscore (Fig. 4.2C) across the 28 d period post-MCAO.

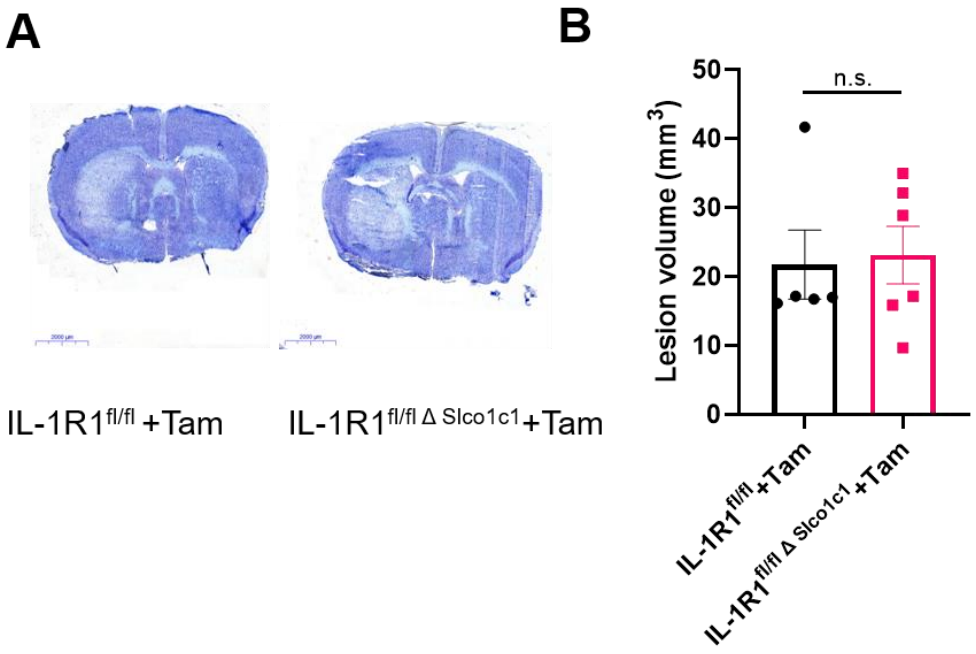

Figure 4.1. Brain endothelial IL-1R1 deletion does not influence infarct volume after stroke.
(A) Infarct volume at 48 h post-stroke was assessed on cresyl violet stained brain sections. Representative cresyl violet images are shown, scale bar 2000 µm. (B) Lesion volume analysis calculated using CaseViewer. Data are represented as mean ± SEM, IL-1R1$^{fl/fl+Tam}$; n=5, IL-1R1$^{fl/fl\ \Delta\ Slco1c1}$; n=6. Data were assessed by an unpaired t-test to compare genotypes (B), n.s.=not significant.

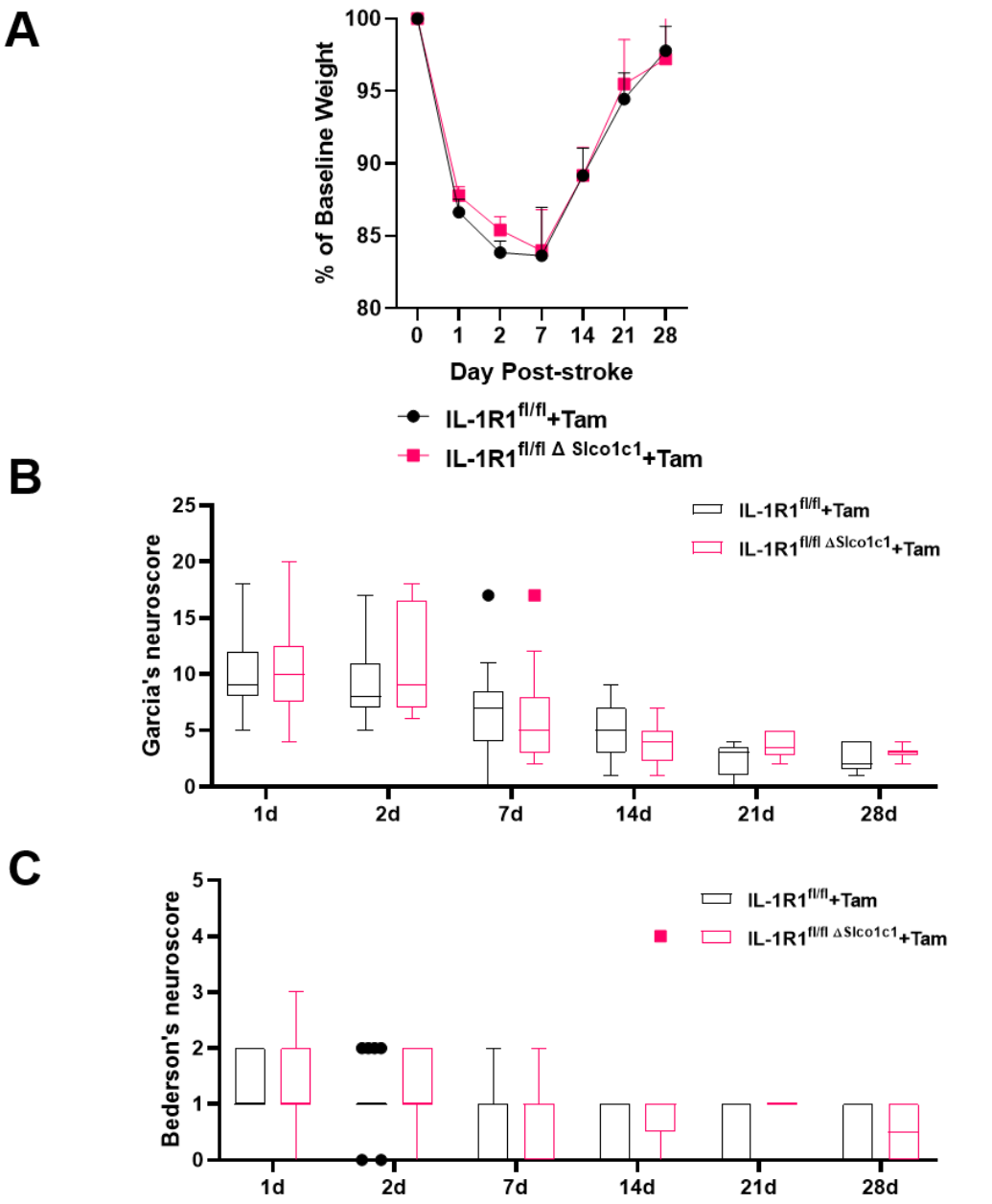

Figure 4.2. Brain endothelial IL-1R1 deletion does not influence body weight or neurological function after stroke.
(A) Weight of animals expressed as percentage (%) of baseline weight across the 28 d post-stroke. Neurological deficits were assessed using the Garcia's (28-point neuroscore) (B) and Bederson's neuroscore (C). Data are represented as mean ± SEM, IL-1R1$^{fl/fl+Tam}$; n=5-6, IL-1R1$^{fl/fl\ \Delta\ Slco1c1}$; n=5-6 at each time point. Data were assessed by mixed-effects model (REML) with Sidak's post-hoc analysis comparing weights/neuroscores at corresponding time points between genotypes (A-C).

4.3.2. Brain endothelial IL-1R1 deletion on laminin α5 across at 2 d, 14 d, 28 d post-MCAO

Although several studies have demonstrated a dynamic ECM response after cerebral ischemia, the role of brain endothelial IL-1R1 signalling on the expression of laminin α4 and laminin α5 had not yet been investigated. Therefore, I assessed the expression of laminin α5 at 2 d, 14 d and 28 d post-MCAO in IL-1R1$^{fl/fl\ +Tam}$ mice and IL-1R1$^{fl/fl\ \Delta\ Slco1c1+Tam}$ mice. Our findings revealed no significant effect of endothelial IL-1R1 deletion ($p=0.1433$) or stroke ($p=0.2468$) on laminin α5 expression in the cortex 2 d after MCAO (Fig. 4.3A,C), demonstrating that IL-1R1 deletion did not influence laminin α5 expression, and that laminin α5 expression was not differentially regulated on the ipsilateral side of the brain compared to the contralateral side after cerebral ischemia. Similarly, our findings revealed no significant effect of endothelial IL-1R1 deletion ($p=0.6589$) or stroke ($p=0.0753$) on laminin α5 expression in the striatum 2 d after MCAO (Fig. 4.3B,D), demonstrating that IL-1R1 deletion did not influence laminin α5 expression. I did not detect any significant differences upon direct comparison of the contralateral and ipsilateral hemispheres within genotypes and between genotypes at 2 d in the cortex and the striatum.

Since 14 d post-cerebral ischaemia is typically associated with BBB repair, I next assessed the effect of brain endothelial IL-1R1 deletion on laminin α5 expression post-MCAO to test our hypothesis that LM-10 expression is increased during the repair phase. Our findings revealed no significant effect of endothelial IL-1R1 deletion ($p=0.7452$) or stroke ($p=0.5975$) on laminin α5 expression in the cortex 14 d after MCAO (Fig. 4.4A,C), demonstrating that IL-1R1 deletion did not influence laminin α5 expression, and that laminin α5 expression was not differentially regulated on the ipsilateral side of the brain compared to the contralateral side after cerebral ischemia. Similarly, our findings revealed no significant effect of endothelial IL-1R1 deletion ($p=0.3781$) or stroke ($p=0.4701$) on laminin α5 expression in the striatum 14 d after MCAO (Fig. 4.4B,D). Furthermore, I did not detect any significant differences upon direct comparison of the contralateral and ipsilateral hemispheres within genotypes and between genotypes at 14 d in the cortex and the striatum.

As relatively little is known about the chronic repair mechanisms in mice after cerebral ischaemia, I next assessed the effect of brain endothelial IL-1R1 deletion on laminin α5 expression 28 d post-cerebral ischemia. Our findings revealed no significant effect of endothelial IL-1R1 deletion ($p=0.9153$) or stroke ($p=0.0791$) on laminin α5 expression in the cortex 28 d after MCAO (Fig. 4.5A,C), demonstrating that IL-1R1 deletion did not influence laminin α5 expression. Similarly, our findings revealed no significant effect of endothelial IL-1R1 deletion ($p=0.9066$) or stroke ($p=0.3058$) on laminin α5 expression in the striatum 14 d after MCAO (Fig. 4.5B,D), demonstrating that IL-1R1 deletion did not influence laminin α5 expression, and that laminin α5 expression was not differentially regulated on the ipsilateral side of the brain compared to the contralateral side after cerebral ischemia. Furthermore, I did not detect any significant differences upon direct comparison of the contralateral and ipsilateral hemispheres within genotypes and between genotypes at 28 d in the cortex and the striatum.

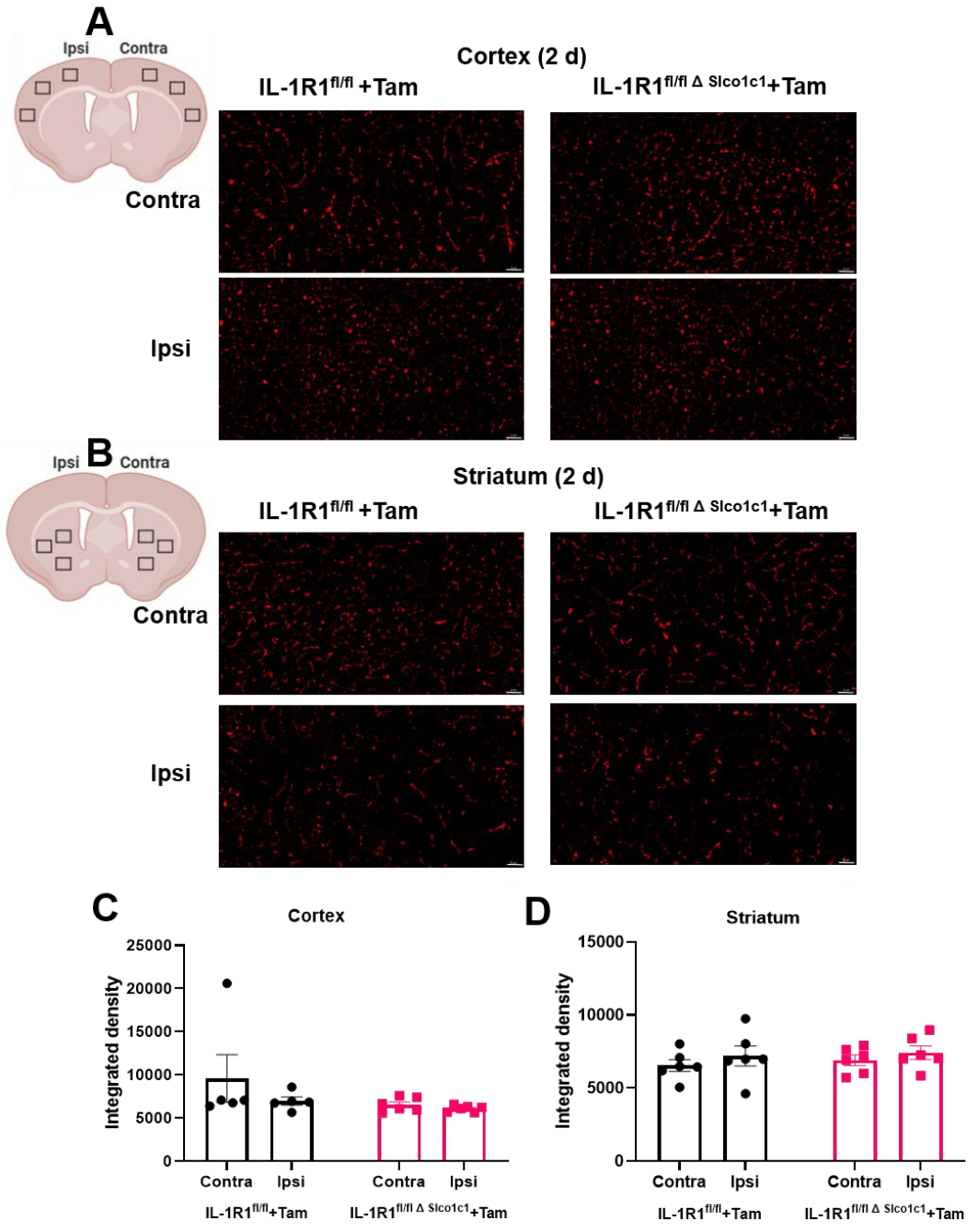

Figure 4.3. Brain endothelial IL-1R1 deletion does not influence cortical or striatal laminin α5 expression 2 d post-stroke.
(A-B) Laminin α5 (red) immunohistochemistry in ipsilateral or contralateral hemispheres of cortical (A) and striatal (B) regions 2 d post-stroke. Scale bar 50 µm. (C-D) Integrated density (percentage area x mean fluorescence intensity) of laminin α5 staining in ipsilateral or contralateral hemispheres of cortical and striatal regions was quantified with ImageJ software. Data are represented as mean ± SEM, IL-1R1$^{fl/fl+Tam}$; n=5, IL-1R1$^{fl/fl\ \Delta\ Slco1c1}$; n=6. Data were assessed by a RM two-way ANOVA followed by Sidak's post-hoc analysis comparing the expression of laminin α5 between genotypes (C,D).

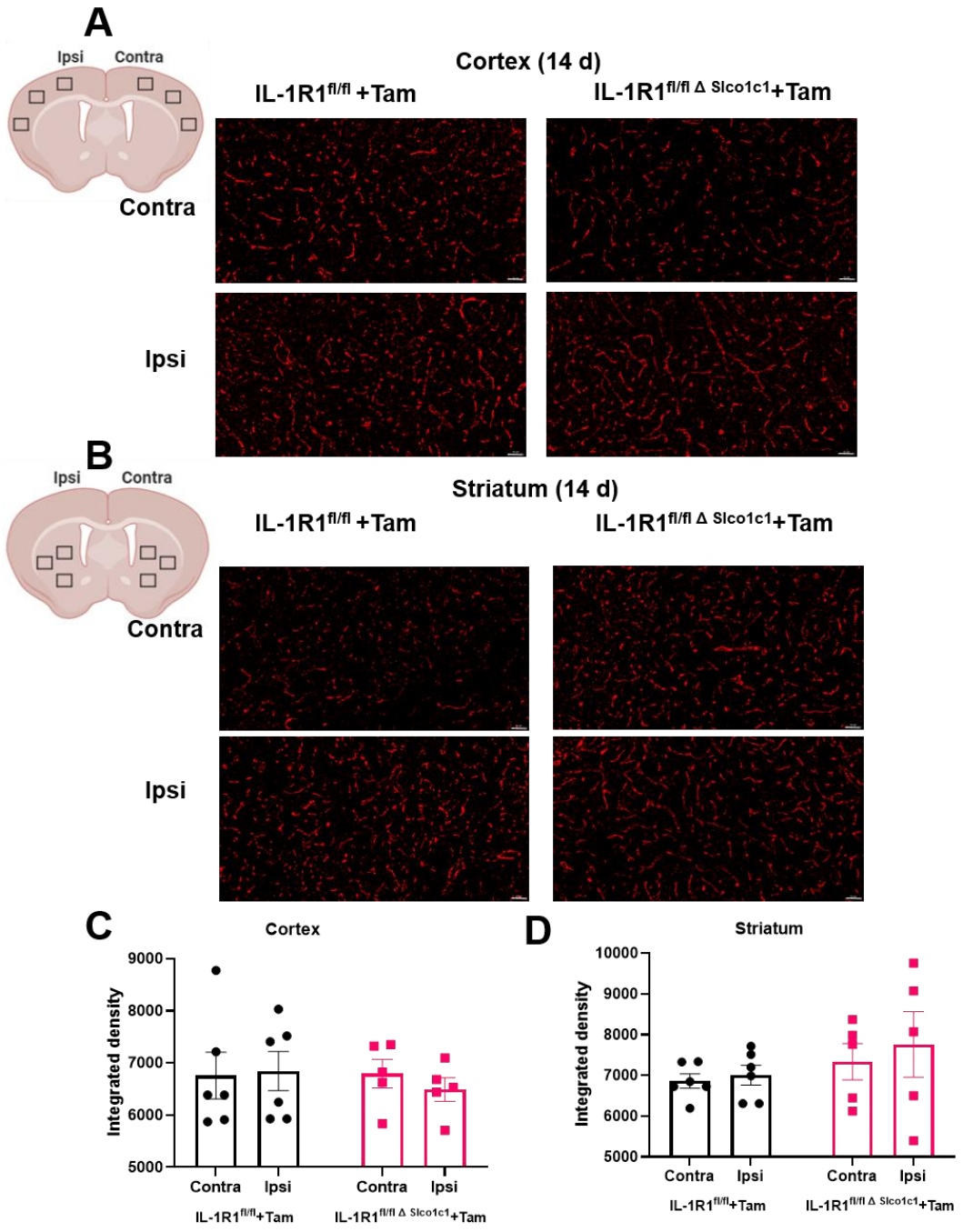

Figure 4.4. Brain endothelial IL-1R1 deletion does not influence cortical or striatal laminin α5 expression 14 d post-stroke.
(A-B) Laminin α5 (red) immunohistochemistry in ipsilateral or contralateral hemispheres of cortical (A) and striatal (B) regions 14 d post-stroke. Scale bar 50 µm. (C-D) Integrated density (percentage area x mean fluorescence intensity) of laminin α5 staining in ipsilateral or contralateral hemispheres of cortical and striatal regions was quantified with ImageJ software. Data are represented as mean ± SEM, IL-1R1$^{fl/fl+Tam}$; n=6, IL-1R1$^{fl/fl\ \Delta\ Slco1c1}$; n=5. Data were assessed by a RM two-way ANOVA followed by Sidak's post-hoc analysis comparing the expression of laminin α5 between genotypes (C,D).

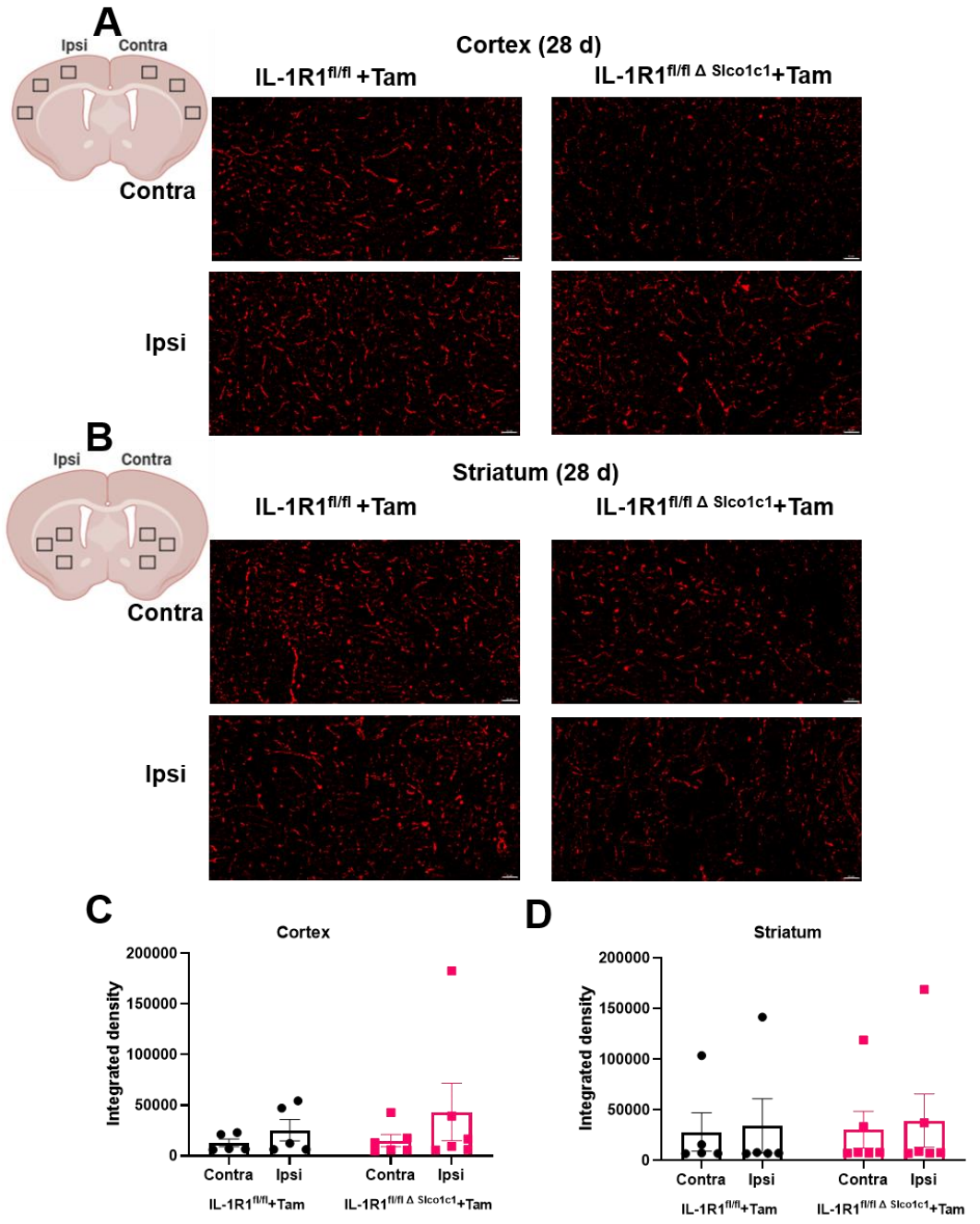

Figure 4.5. Brain endothelial IL-1R1 deletion does not influence cortical or striatal laminin α5 expression 28 d post-stroke.
(A-B) Laminin α5 (red) immunohistochemistry in ipsilateral or contralateral hemispheres of cortical (A) and striatal (B) regions 28 d post-stroke. Scale bar 50 µm. (C-D) Integrated density (percentage area x mean fluorescence intensity) of laminin α5 staining in ipsilateral or contralateral hemispheres of cortical and striatal regions was quantified with ImageJ software. Data are represented as mean ± SEM, IL-1R1$^{fl/fl+Tam}$; n=5, IL-1R1$^{fl/fl\ \Delta\ Slco1c1}$; n=6. Data were assessed by a RM two-way ANOVA followed by Sidak's post-hoc analysis comparing the expression of laminin α5 between genotypes (C,D).

4.3.3. Brain endothelial IL-1R1 deletion on laminin α4 at 2 d, 14 d and 28 d post-MCAO

Since laminin α4 is the other major laminin isoform associated with the vasculature in the CNS, I next investigated the effect of endothelial IL-1R1 deletion on the expression of the laminin α4 after cerebral ischemia. Our findings revealed a significant effect of stroke (p=0.0146) on laminin α4 expression in the cortex 2 d after MCAO (Fig. 4.6A, C), demonstrating that laminin α4 expression was differentially regulated on the ipsilateral and contralateral sides of the brain. Although not significant, there was a trend towards a significant reduction in laminin α4 in the ipsilateral side of the cortex compared to the contralateral in IL-1R1$^{fl/fl\ +Tam}$ mice (14% reduction, p=0.0582, Fig. 4.6C). In contrast, no change in laminin α4 expression in the cortex 2 d post-stroke was observed in IL-1R1$^{fl/fl\ \Delta\ Slco1c1+Tam}$ mice (Fig. 4.6C). A significant effect of endothelial IL-1R1 deletion (p=0.0210) on laminin α4 expression in the cortex 2 d after MCAO was observed (Fig. 4.6A, C). Specifically, IL-1R1$^{fl/fl\ +Tam}$ mice show elevated expression of laminin α4 in the contralateral side of the brain compared to the contralateral of IL-1R1$^{fl/fl\ \Delta\ Slco1c1+Tam}$ mice in the cortex at 2 d (40% difference, p=0.0299, Fig. 4.6C). Although not significant, a marked reduction in laminin α4 was observed in IL-1R1$^{fl/fl\ \Delta\ Slco1c1+Tam}$ mice in the ipsilateral side of the cortex at 2 d compared to IL-1R1$^{fl/fl\ +Tam}$ mice (37% difference, p=0.0611, Fig. 4.6C).

No significant effect of stroke on laminin α4 expression in the striatum at 2 d post-MCAO was observed (p=0.1811); however despite not being significant, there was a marked reduction in laminin α4 expression in IL-1R1$^{fl/fl\ +Tam}$ mice in the ipsilateral side compared to the contralateral side (60% reduction, p=0.1052, Fig. 4.6D), suggesting that laminin α4 may be downregulated in the striatum after MCAO in mice with endothelial IL-1R1 deletion. No significant difference was observed between the contralateral and ipsilateral striatal regions of IL-1R1$^{fl/fl\ +Tam}$ mice at 2 d (Fig. 4.6D). Although not significant, a trend towards a significant effect of endothelial IL-1R1 deletion on laminin α4 expression in the striatum at 2 d post-MCAO was detected (p=0.1017, Fig. 4.6B,D), demonstrating that IL-1R1 deletion may influence laminin α4 expression in this region at this time point. Interestingly, upon direct comparisons of the contralateral striatal regions between IL-1R1$^{fl/fl\ +Tam}$ mice and IL-1R1$^{fl/fl\ \Delta\ Slco1c1+Tam}$ mice, there was a significant reduction in laminin α4 expression in IL-1R1$^{fl/fl\ \Delta\ Slco1c1+Tam}$ mice (62% reduction, p=0.0475, Fig. 4.6D). No

significant difference was observed between the ipsilateral striatal regions of IL-1R1$^{fl/fl\ +Tam}$ mice and IL-1R1$^{fl/fl\ \Delta\ Slco1c1+Tam}$ mice at 2 d (Fig. 4.6D).

I also measured laminin α4 expression at 14 d after MCAO in the cortex and striatum. Our findings revealed no significant effect of stroke (p=0.8475) or endothelial IL-1R1 deletion (p=0.5661) on laminin α4 expression in the cortex 14 d after MCAO (Fig. 4.7A,C). Upon direct comparison between the cortical contralateral and ipsilateral regions within each genotype, although not significant, a trend toward a significant increase in the ipsilateral region in IL-1R1$^{fl/fl\ +Tam}$ mice (33% increase, p=0.2763, Fig. 4.7C) and decrease in the ipsilateral region of IL-1R1$^{fl/fl\ \Delta\ Slco1c1+Tam}$ mice (28% decrease, p=0.1817, Fig. 4.7C) compared to their respective contralateral regions were detected. Interestingly, upon direct comparisons of the contralateral cortical regions between IL-1R1$^{fl/fl\ +Tam}$ mice and IL-1R1$^{fl/fl\ \Delta\ Slco1c1+Tam}$ mice, there was a trend towards a significant increase in laminin α4 expression in IL-1R1$^{fl/fl\ \Delta\ Slco1c1+Tam}$ mice (58% increase, p=0.1546, Fig. 4.7C). Whereas, no significant difference between the ipsilateral cortical regions of IL-1R1$^{fl/fl\ +Tam}$ mice and IL-1R1$^{fl/fl\ \Delta\ Slco1c1+Tam}$ mice was detected (p=0.6413, Fig. 4.7C). Our findings revealed no significant effect of stroke (p=0.2761) or endothelial IL-1R1 deletion (p=0.5365) on laminin α4 expression in the striatum 14 d after MCAO (Fig. 4.7B,D). Although not significant, there is a trend towards a significant increase in laminin α4 in the ipsilateral side of the striatum compared to the contralateral in IL-1R1$^{fl/fl\ +Tam}$ mice (increase, p=0.1435, Fig. 4.7D). In contrast, no change in laminin α4 expression in the ipsilateral region of the striatum compared to the contralateral regions 14 d post-stroke was observed in IL-1R1$^{fl/fl\ \Delta\ Slco1c1+Tam}$ mice (p=0.9246, Fig. 4.7D). I did not detect any significant differences upon direct comparison of the contralateral and ipsilateral hemispheres between genotypes in the striatum at 14 d (Fig. 4.7D).

I also measured laminin α4 expression 28 d post-MCAO. Our findings revealed no significant effect of stroke (p=0.5020) or endothelial IL-1R1 deletion (p=0.1721) on laminin α4 expression in the cortex 28 d after MCAO (Fig. 4.8A,C). Direct comparison between the cortical contralateral and ipsilateral regions within each genotype revealed no significant differences (IL-1R1$^{fl/fl\ +Tam}$ mice, p=0.4307 and IL-1R1$^{fl/fl\ \Delta\ Slco1c1+Tam}$ mice, p=0.9392, Fig.8C). Upon direct comparisons of the contralateral (p=0.8575) and ipsilateral (p=0.1500) cortical regions between IL-

1R1$^{fl/fl\ +Tam}$ mice and IL-1R1$^{fl/fl\ \Delta\ Slco1c1+Tam}$ mice, no significant differences were detected (Fig. 4.8C). Our findings revealed no significant effect of stroke ($p=0.6840$) or endothelial IL-1R1 deletion ($p=0.1577$) on laminin α4 expression in the striatum 28 d after MCAO (Fig. 4.8B,D). Direct comparison between the striatal contralateral and ipsilateral regions within each genotype revealed no significant differences (IL-1R1$^{fl/fl\ +Tam}$ mice, $p=0.7973$ and IL-1R1$^{fl/fl\ \Delta\ Slco1c1+Tam}$ mice, $p=0.9980$, Fig. 4.8D). Upon direct comparisons of the contralateral ($p=0.4396$) and ipsilateral ($p=0.2353$) striatal regions between IL-1R1$^{fl/fl\ +Tam}$ mice and IL-1R1$^{fl/fl\ \Delta\ Slco1c1+Tam}$ mice, no significant differences were detected (Fig. 4.8D).

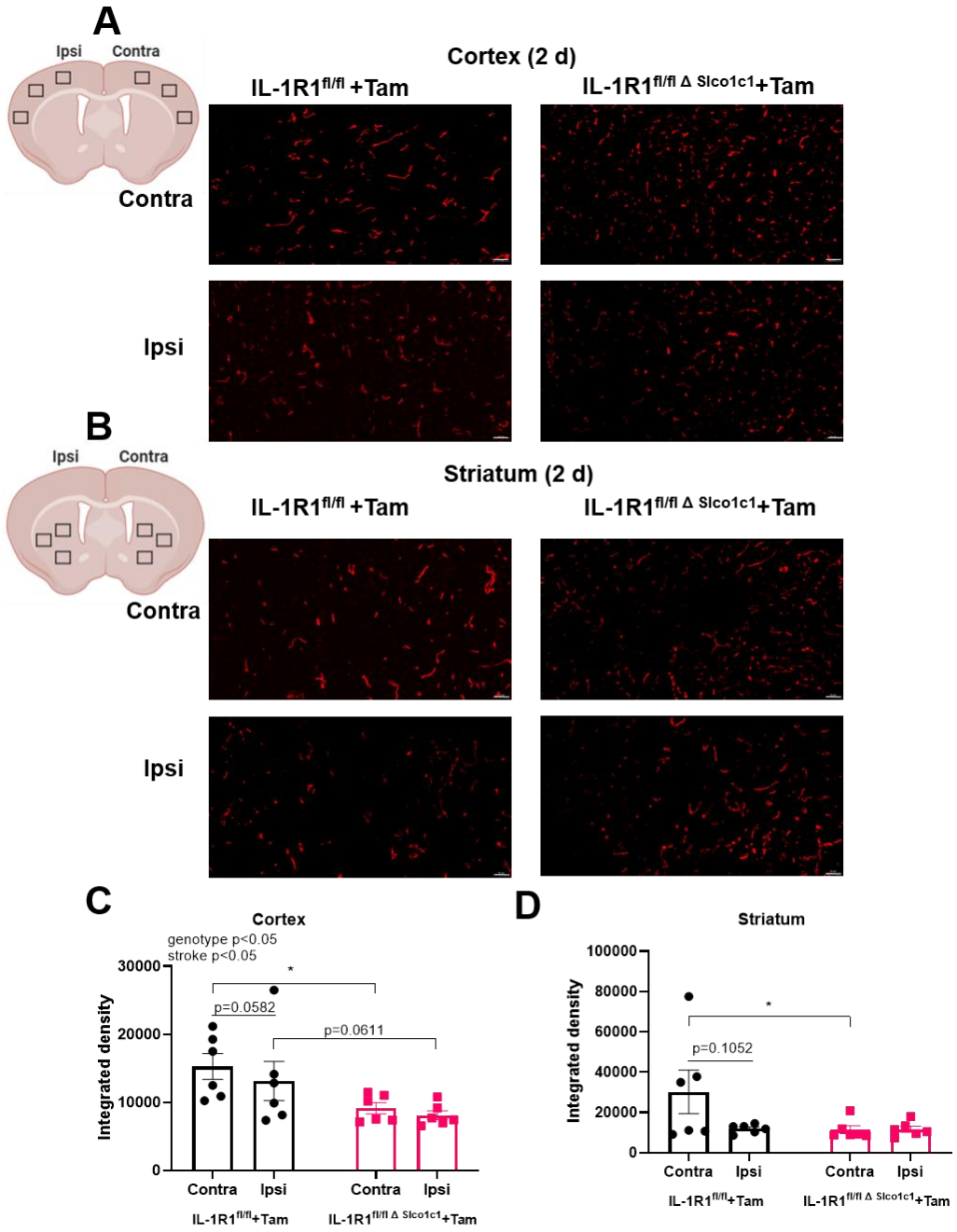

Figure 4.6. Brain endothelial IL-1R1 deletion influences cortical and striatal laminin α4 expression 2 d post-stroke.
(A-B) Laminin α4 (red) immunohistochemistry in ipsilateral or contralateral hemispheres of cortical (A) and striatal (B) regions 2 d post-stroke. Scale bar 50 µm. (C-D) Integrated density (percentage area x mean fluorescence intensity) of laminin α4 staining in ipsilateral or contralateral hemispheres of cortical and striatal regions was quantified with ImageJ software. Data are represented as mean ± SEM, IL-1R1$^{fl/fl+Tam}$; n=6, IL-1R1$^{fl/fl\ \Delta\ Slco1c1}$; n=6. Data were assessed by a RM two-way ANOVA followed by Sidak's post-hoc analysis comparing the expression of laminin α4 between genotypes (C,D).

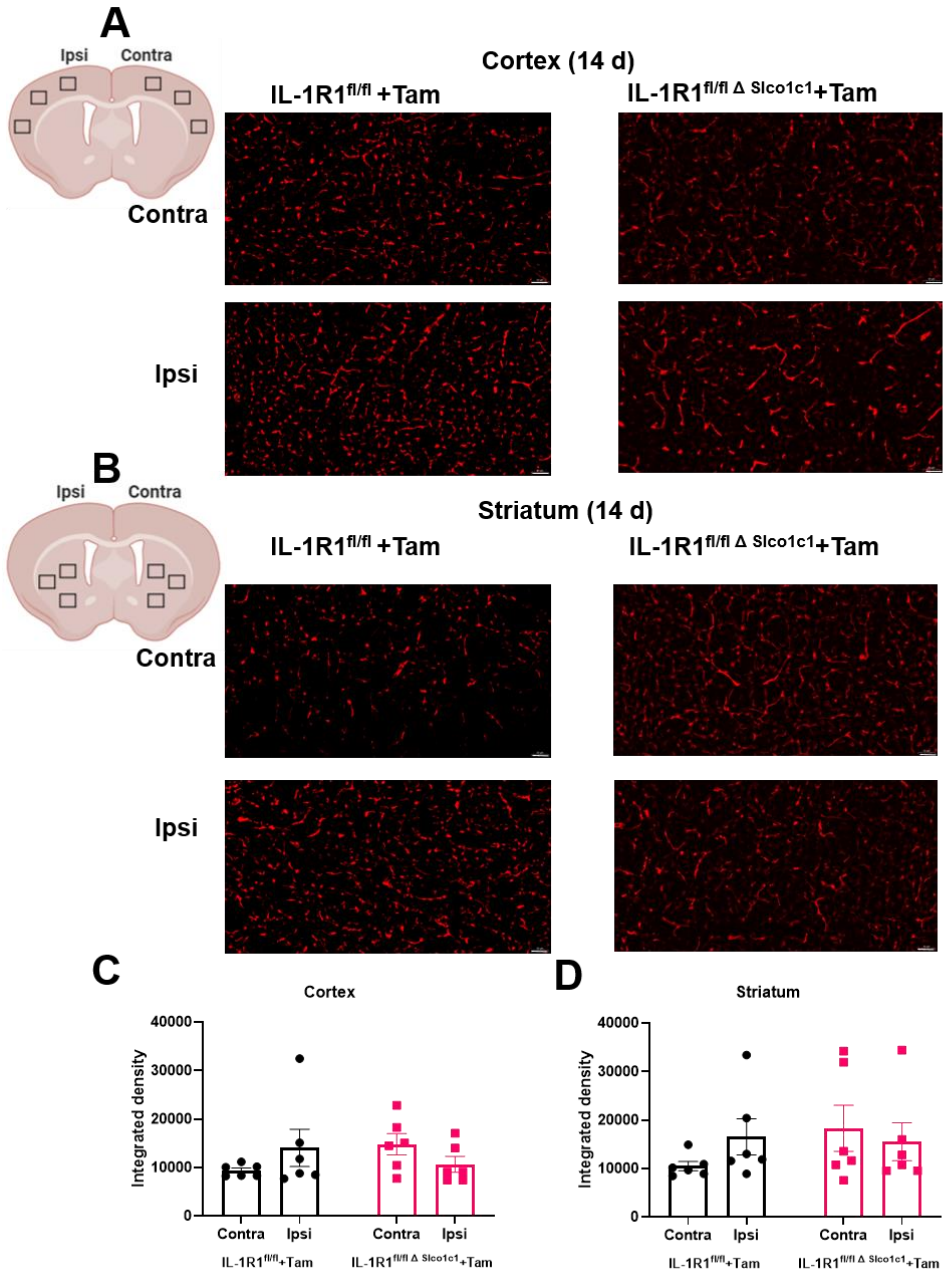

Figure 4.7. Brain endothelial IL-1R1 deletion does not significantly influence cortical and striatal laminin α4 expression 14 d post-stroke.
(A-B) Laminin α4 (red) immunohistochemistry in ipsilateral or contralateral hemispheres of cortical (A) and striatal (B) regions 14 d post-stroke. Scale bar 50 µm. (C-D) Integrated density (percentage area x mean fluorescence intensity) of laminin α4 staining in ipsilateral or contralateral hemispheres of cortical and striatal regions was quantified with ImageJ software. Data are represented as mean ± SEM, IL-1R1$^{fl/fl+Tam}$; n=6, IL-1R1$^{fl/fl\ \Delta\ Slco1c1}$; n=6. Data were assessed by a RM two-way ANOVA followed by Sidak's post-hoc analysis comparing the expression of laminin α4 between genotypes (C,D).

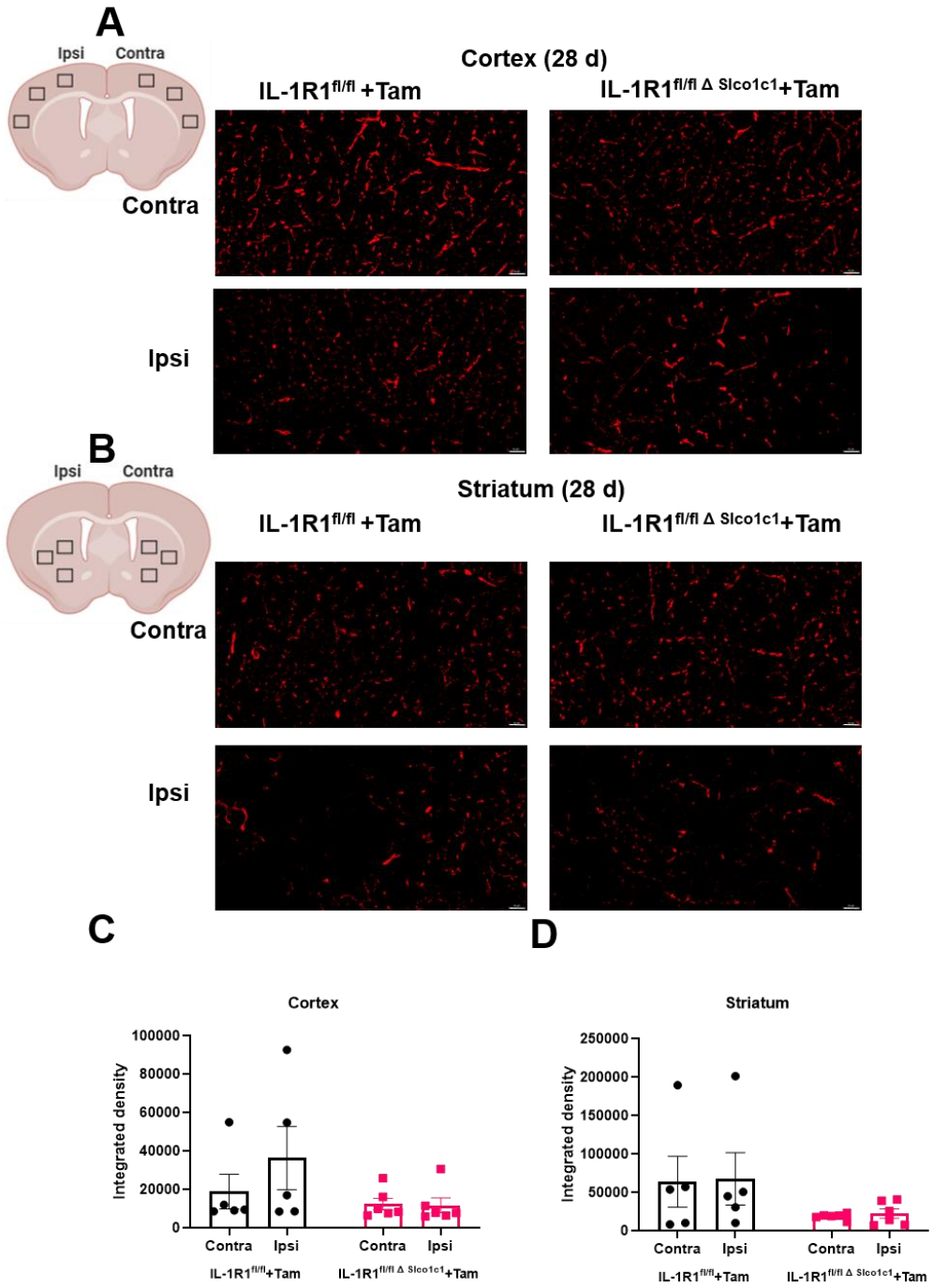

Figure 4.8. Brain endothelial IL-1R1 deletion does not significantly influence cortical and striatal laminin α4 expression 28 d post-stroke.
(A-B) Laminin α4 (red) immunohistochemistry in ipsilateral or contralateral hemispheres of cortical (A) and striatal (B) regions 28 d post-stroke. Scale bar 50 µm. (C-D) Integrated density (percentage area x mean fluorescence intensity) of laminin α4 staining in ipsilateral or contralateral hemispheres of cortical and striatal regions was quantified with ImageJ software. Data are represented as mean ± SEM, IL-1R1$^{fl/fl+Tam}$; n=5, IL-1R1$^{fl/fl\ \Delta\ Slco1c1}$; n=6. Data were assessed by a RM two-way ANOVA followed by Sidak's post-hoc analysis comparing the expression of laminin α4 between genotypes (C,D).

4.3.4. Brain endothelial IL-1R1 deletion on laminin α5 and laminin α4 expression across a 28 d period post-MCAO

In order to determine the temporal profile of laminin expression post-stroke, I presented the data across the 28 d period for the cortex and striatum. Our findings revealed a significant effect of time on laminin α5 expression in the cortex ($p=0.0002$, Fig. 4.9A) and striatum ($p=0.0002$, Fig. 4.9B) after MCAO. No significant changes in laminin α5 expression was observed at 14 d in both IL-1R1$^{fl/fl\ +Tam}$ mice and IL-1R1$^{fl/fl\ \Delta\ Slco1c1+Tam}$ mice when compared to respective regions at 2 d. There was no significant increase in laminin α5 expression in the contralateral cortical regions of IL-1R1$^{fl/fl\ +Tam}$ mice and IL-1R1$^{fl/fl\ \Delta\ Slco1c1+Tam}$ mice at 28 d post-MCAO compared to their respective contralateral cortical regions at 2 d post-stroke (Fig. 4.9A). Laminin α5 expression significantly increased in the ipsilateral cortical regions of IL-1R1$^{fl/fl\ +Tam}$ mice ($p=0.0454$) and IL-1R1$^{fl/fl\ \Delta\ Slco1c1+Tam}$ mice ($p=0.0045$) at 28 d post-MCAO compared to their respective ipsilateral cortical regions at 2 d post-stroke (Fig. 4.9A). Laminin α5 expression increased in the contralateral striatal regions of IL-1R1$^{fl/fl\ +Tam}$ ($p=0.0492$) mice and IL-1R1$^{fl/fl\ \Delta\ Slco1c1+Tam}$ mice ($p=0.0384$) at 28 d post-MCAO compared to their respective contralateral striatal regions at 2 d post-stroke (Fig. 4.9B). Although not significant, there was a trend towards an increase in the ipsilateral striatal regions of IL-1R1$^{fl/fl\ +Tam}$ mice ($p=0.2418$) and IL-1R1$^{fl/fl\ \Delta\ Slco1c1+Tam}$ mice ($p=0.0756$) at 28 d post-MCAO compared to their respective contralateral ipsilateral striatal at 2 d post-stroke (Fig. 4.9B). No significant effect of genotype/hemisphere of the brain was observed in the cortex ($p=0.8696$, Fig. 4.9A) or striatum ($p=0.7745$, Fig. 4.9B) across the 28 d.

Our findings revealed a trend toward significant effect of time on laminin α4 expression in the cortex ($p=0.1106$, Fig. 4.9C) after MCAO. No significant changes in laminin α4 expression was observed at 14 d in both IL-1R1$^{fl/fl\ +Tam}$ mice and IL-1R1$^{fl/fl\ \Delta\ Slco1c1+Tam}$ mice when compared to respective regions at 2 d. There was no significant change in laminin α4 expression in the contralateral cortical regions in IL-1R1$^{fl/fl\ +Tam}$ mice and IL-1R1$^{fl/fl\ \Delta\ Slco1c1+Tam}$ mice at 28 d compared to their respective contralateral cortical regions at 2 d post-stroke (Fig. 4.9C). Laminin α4 increased in the ipsilateral cortical regions of IL-1R1$^{fl/fl\ +Tam}$ mice at 28 d post-MCAO compared to their respective ipsilateral cortical regions at 2 d post-stroke ($p=0.0206$, Fig. 4.9C). However, no significant change in laminin α4 expression in the ipsilateral cortical regions of IL-1R1$^{fl/fl\ +Tam}$ mice at 28 d post-MCAO compared

to their respective ipsilateral cortical regions at 2 d post-stroke (0.7819, Fig. 4.9C). Although not significant, a trend towards a significant effect of genotype/hemisphere of the cortex (p=0.0578) was observed. Specifically, IL-1R1$^{fl/fl\ +Tam}$ mice demonstrated elevated levels of laminin α4 in the ipsilateral cortical regions at 28 d post-MCAO compared to the contralateral (p=0.0326) and ipsilateral (p=0.0181) regions of IL-1R1$^{fl/fl\ \Delta\ Slco1c1+Tam}$ mice at 28 d (Fig. 4.9C). Our findings revealed a significant effect of time on laminin α4 expression in the striatum (p=0.0009, Fig. 4.9D) after MCAO. Although there was a trend toward an increase in laminin α4 in the contralateral striatal region of IL-1R1$^{fl/fl\ +Tam}$ mice at 28 d compared to 2 d (p= 0.1971, Fig. 4.9D), there was a significant increase in the ipsilateral striatal region of IL-1R1$^{fl/fl\ +Tam}$ mice at 28 d compared to 2 d (p=0.0026, Fig. 4.9D). However, no significant changes were observed in the contralateral (p= 0.6015) and ipsilateral (p= 0.5140) regions of IL-1R1$^{fl/fl\ \Delta\ Slco1c1+Tam}$ mice at 28 d compared to 2 d post-MCAO (Fig. 4.9D). A trend towards a significant effect of genotype/hemisphere of the striatum (p=0.1286) was observed. Specifically, IL-1R1$^{fl/fl\ +Tam}$ mice demonstrated elevated levels of laminin α4 in the ipsilateral striatal regions at 28 d post-MCAO compared to the contralateral (p=0.0476) and ipsilateral (p= 0.0724) regions of IL-1R1$^{fl/fl\ \Delta\ Slco1c1+Tam}$ mice at 28 d (Fig. 4.9D).

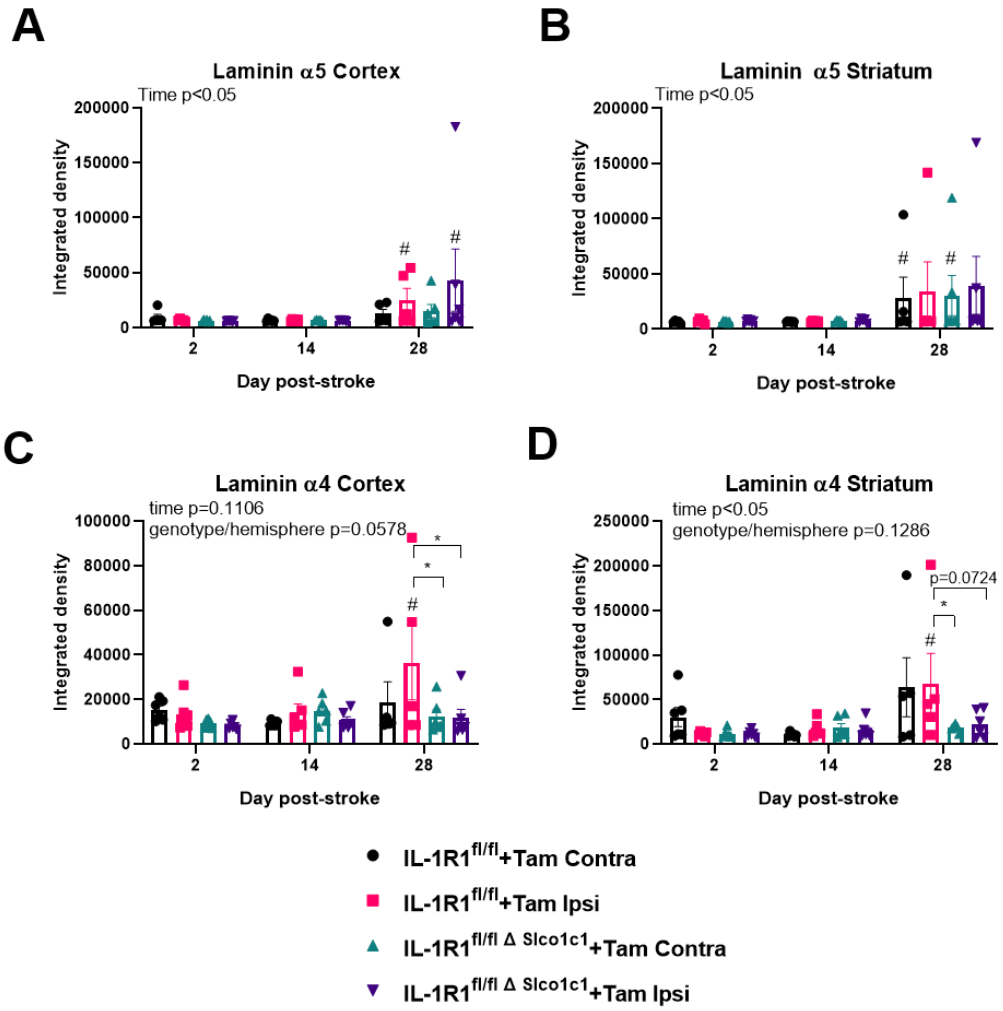

Figure 4.9. Overview of laminin α5 and laminin α4 expression in the cortex and striatum across each time point.
(A-D) Summary of the integrated density (percentage area x mean fluorescence intensity) of laminin α5 (A-B) and laminin α4 (C-D) staining in the cortex and striatum. Data are represented as mean ± SEM, IL-1R1$^{fl/fl+Tam}$; n=5-6, IL-1R1$^{fl/fl\ \Delta\ Slco1c1}$; n=5-6 at each time point. Data were assessed by a two-way ANOVA followed by Tukey's post-hoc analysis, * denotes significance comparing the expression of laminin α5/laminin α4 in each region of interest and # denotes significance comparing back to the respective regions at 2 d post-stroke (A-D).

4.3.5. Brain endothelial IL-1R1 deletion does not modulate proliferation of cells at 14 d post-MCAO

Since I hypothesised that the cerebral vascular IL-1R1 would play a critical role in repair post-stroke, I next measured BrdU staining as an indication of cellular proliferation and angiogenesis. IL-1R1$^{fl/fl\ +Tam}$ mice and IL-1R1$^{fl/fl\ \Delta\ Slco1c1+Tam}$ mice to be culled at 14 d had injections of BrdU daily beginning at 10 d after MCAO until the day of sacrifice. The ipsilateral hemisphere was assessed in the cortex (Fig. 4.10A,C) and striatum (Fig. 4.10B,C) for BrdU positive cells. Although not significant, there was trend toward an increase in BrdU positive cells in the ipsilateral striatal regions of IL-1R1$^{fl/fl\ +Tam}$ mice ($p=0.1663$) and IL-1R1$^{fl/fl\ \Delta\ Slco1c1+Tam}$ mice ($p=0.2555$) compared to their respective ipsilateral cortical regions (Fig. 4.10C). However, on direct comparison of the ipsilateral cortex ($p=0.8305$) and ipsilateral striatum ($p=0.7183$) between genotypes, no significant differences were detected suggesting that endothelial IL-1R1 deletion does not affect cellular proliferation at 14 d (Fig. 4.10C).

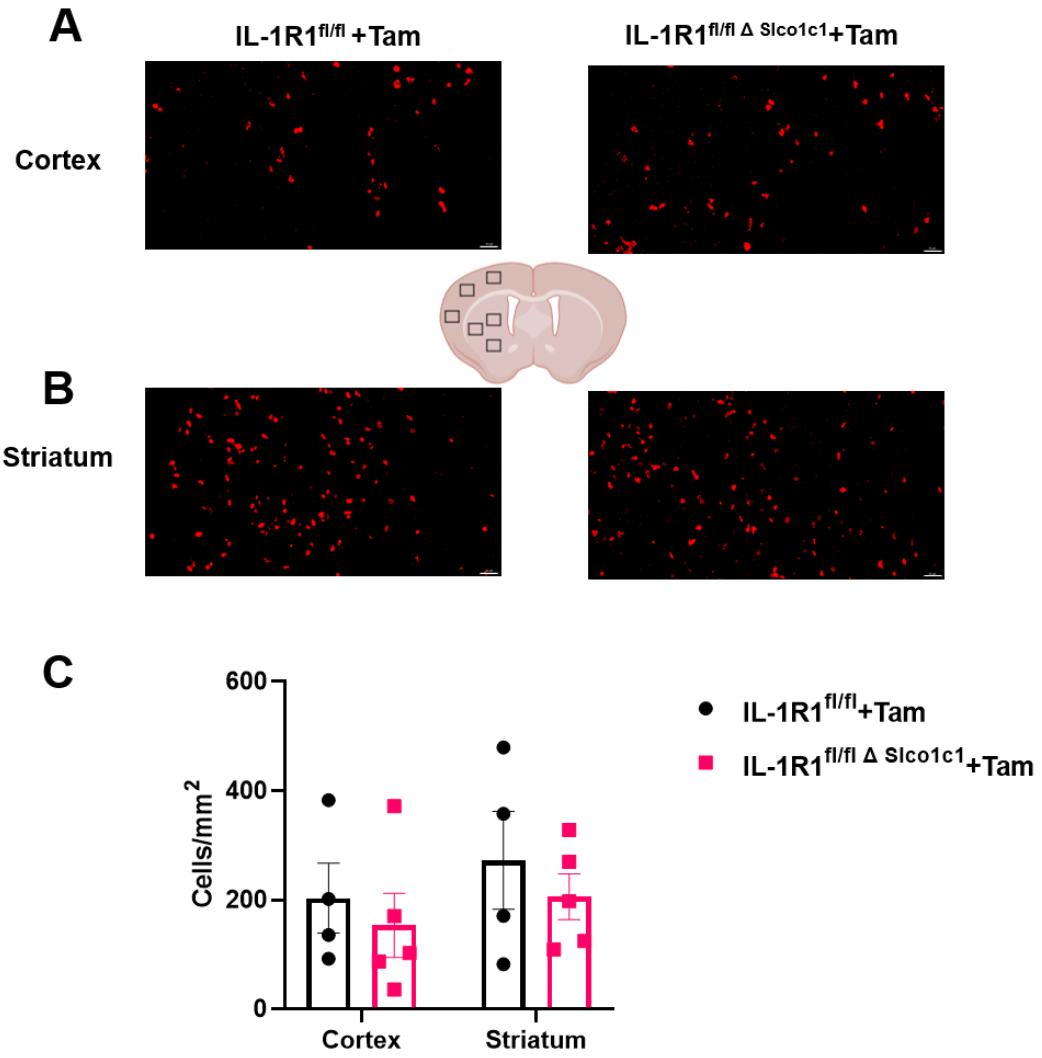

Figure 4.10. Brain endothelial IL-1R1 deletion does not influence ipsilateral cortical and striatal cellular proliferation 14 d post-stroke.
(A-B) Animals to be culled at 14 d had injections of BrdU daily beginning at 10 d after MCAO until the day of sacrifice. BrdU (red) immunohistochemistry in the ipsilateral hemisphere of cortical (A) and striatal (B) regions 14 d post-stroke. Scale bar 50 µm. (C) Proliferation was quantified by counting the number of bromodeoxyuridine (BrdU)-positive cells in a defined region using ImageJ. Data are represented as mean +/- SEM, IL-1R1$^{fl/fl+Tam}$; n=4, IL-1R1$^{fl/fl\ \Delta\ Slco1c1+Tam}$; n=5. Data were assessed by a two-way RM ANOVA followed by Sidak's post-hoc analysis comparing within genotypes and between genotypes.

4.4. **Discussion**

There is a dynamic ECM remodelling response post-stroke that occurs alongside a potent inflammatory response driven by IL-1 signalling. The endothelium is a known target of IL-1 signalling (Allen et al., 2012) and endothelial cells have been demonstrated to increase laminin expression in response to IL-1 *in vitro* (Sixt et al., 2001). However, the exact contribution of endothelial IL-1R1 signalling on laminin α5 and laminin α4 expression post-stroke at acute and chronic time points had not yet been investigated. Our data demonstrates that laminin α4 is more dynamically regulated than laminin α5 post-stroke and that laminin α4 expression is regulated by endothelial IL-1R1 signalling. In this study, I have:

- Demonstrated that endothelial IL-1R1 signalling does not influence infarct volume or neurological outcome after MCAO.
- Demonstrated that brain endothelial IL-1R1 dynamically regulates laminin α4 expression but not laminin α5 expression at 2 d and 28 d post-MCAO.
- Demonstrated that endothelial IL-1R1 signalling does not influence cellular proliferation at 14 d after MCAO.

The sophisticated transgenic capacity to knockout the IL-1R1 in specific cell types prior to experimental stroke has been a valuable tool to determine the cell specific contribution of IL-1 signalling to brain injury. A recent study by Wong and colleagues (2019) induced conditional IL-1R1 deletion in brain endothelial cells, cholinergic neurons and blood cells, identifying the cerebrovascular endothelium and cholinergic neurons as the major targets for IL-1-mediated brain injury after cerebral ischemia in mice. Specifically, a 29% reduction in infarct size and reduced neurological deficits after IL-1R1 deletion in brain endothelial cells was observed at 24 h post stroke (Wong et al., 2019). However, despite the same occlusion time of 30 min and the use of the same brain endothelial IL-1R1 deletion mouse strain, I did not replicate the reduction in infarct size or improved neurological function at 48 h in our study. The stroke surgery in this study was performed by our collaborators in Hungary and it was of importance that the strokes induced in the animals did not result in a high mortality rate since I were interested in chronic time points post-stroke. I were concerned that if I had produced the same size cortical lesions produced by Wong and collaborators (2019) then this would have induced

high animal mortality after 24-48 h. Therefore, our collaborators and the surgeon adjusted the occlusion time to induce striatal strokes in their hands and hence when taking this into consideration the stroke sizes observed were expected.

A dynamic ECM response after stroke involving the upregulation and downregulation of several ECM components has been demonstrated in *in vivo* models of stroke (Summers et al., 2013). Indeed, transient laminin remodelling after MCAO has been demonstrated at the acute phase post-stroke (Ji and Tsirka, 2012) and laminin expression has been demonstrated to be dynamically regulated after chronic mild hypoxia (Halder et al., 2018). In a recent study using a permanent model of MCAO and RNA sequencing, laminin α5 and laminin α4 gene expression was dynamically regulated at 24 h, 72 h and 28 d post-stroke (Munji et al., 2019). It has been demonstrated that there is a distinct endothelial basement membrane consisting of LM-8 and LM-10, the vascular laminins, and a parenchymal membrane of LM-1 and LM-2 (Sixt et al., 2001). The vascular laminins were of particular interest in this study and I aimed to determine the specific patterns of laminin α4 and laminin α5 expression post-stroke. Furthermore, OGD and IL-1 *in vitro* has been demonstrated to regulate the expression of ECM components, including the laminin α4 and α5 isoforms (Kangwantas et al., 2016). Similarly, the role of inflammatory cytokines IL-1β and TNF-α on laminin expression in endothelial cells has also been demonstrated *in vitro* (Sixt et al., 2001). This led to our hypothesis that endothelial IL-1 could regulate laminin expression post-stroke. I first assessed the levels of laminin α5 at 2 d, 14 d and 28 d post-MCAO. At 2 d and 14 d post-MCAO I observed no increase in laminin α5 expression in the ipsilateral hemispheres of both genotypes, demonstrating no clear effect of stroke on laminin α5 expression at these time points. However, at 28 d I observed an increase in laminin α5 expression in both hemispheres (contralateral and ipsilateral) of both genotypes, suggesting a widespread effect on laminin α5 expression post-stroke at chronic time points. I observed no effect of genotype on laminin α5 expression at each time point measured, suggesting that endothelial IL-1 signalling does not regulate laminin α5 expression. In contrast, laminin α4 expression appeared to be more dynamically regulated post-stroke. At 2 d post-stroke, laminin α4 expression reduced in the ipsilateral hemispheres in IL-1R1$^{fl/fl}$ $^{+Tam}$ mice, whilst no change in laminin α4 expression was observed in IL-1R1$^{fl/fl\ \Delta}$ $^{Slco1c1+Tam}$ mice, demonstrating that endothelial IL-1R1 signalling regulates the

acute reduction in laminin α4 expression. Although I did not detect any significant effect of stroke or genotype on laminin α4 expression at 14 d post-stroke, there are some trends towards significant differences in IL-1R1$^{fl/fl\ +Tam}$ mice, providing some potential evidence to support the hypothesis that laminin α4 is more dynamically regulated. Interestingly, at 28 d post-stroke I observed an increase in laminin α4 expression in both hemispheres of IL-1R1$^{fl/fl\ +Tam}$ mice compared to 2 d, which was not reciprocated in the IL-1R1$^{fl/fl\ \Delta\ Slco1c1+Tam}$ mice. This further demonstrated that laminin α4 expression was more dynamically regulated than laminin α5 and that endothelial IL-1R1 is likely to play a key role in laminin α4 expression.

To summarise our findings on laminin expression post-stroke, our data suggest that laminin α4 is more dynamically regulated than laminin α5 and that laminin α4 expression is regulated by endothelial IL-1R1 signalling. Although our colleagues had previously demonstrated in primary rat brain endothelial cells that laminin α5 was regulated in response to IL-1 and OGD *in vitro* (Kangwantas et al., 2016), there are several other studies that support the concept that laminin α4 is more dynamically regulated. The *in vitro* investigation of laminin α4 and α5 expression after IL-1 treatment in endothelial cells demonstrated that laminin α4 mRNA was upregulated to a higher degree than laminin α5 (Sixt et al., 2001). This concept has been further supported in a model of chronic mild hypoxia in mice, which is associated with vascular remodelling response, has demonstrated a strong upregulation of the laminin α4 but not laminin α5 over a 14 d period (Halder et al., 2018).

In order to speculate the physiological relevance of our findings, they can be interpreted with other relevant studies. Of particular interest is our observation that at 2 d the IL-1R1$^{fl/fl\ \Delta\ Slco1c1+Tam}$ mice demonstrate reduced expression of laminin α4 in the contralateral and ipsilateral hemispheres of the cortex compared to IL-1R1$^{fl/fl\ +Tam}$ mice. Wong and collaborators (2019) have previously demonstrated that at 24 h IL-1R1$^{fl/fl\ \Delta\ Slco1c1+Tam}$ mice demonstrate dramatically reduced neutrophil transmigration. Laminin α4 has been demonstrated as permissive to infiltrating T cells in EAE, highlighting laminin α4 permissive barrier properties (Sixt et al., 2001). Furthermore, increased neutrophil transmigration across a bEND.5 cell monolayer seeded on LM-8 after TNF-α treatment compared to LM-10 had been demonstrated *in vitro* (Song et al., 2017). Therefore, I speculate that if the reduced

levels of laminin α4 expression I observed at 2 d in IL-1R1$^{fl/fl\ \Delta\ Slco1c1+Tam}$ mice is also present at 24 h post-MCAO, that this could impact neutrophil transmigration and be a contributing factor to the reduced neutrophil transmigration observed by Wong and colleagues (2019).

Previous studies have identified 14 d post-stroke as a critical time point for angiogenesis (Rodriguez-Grande et al., 2015; Rajkovic et al., 2018) and therefore I assessed angiogenesis at this time point. Furthermore, *in vitro* studies have demonstrated that IL-1α has proangiogenic properties (Salmeron et al., 2016), which led to our hypothesis that IL-1 regulates repair at chronic time points after stroke. BrdU staining can be a useful tool to identify proliferating cells, however a limitation of it use in histology is the requirement of pre-treatment of the tissue with acid to expose the BrdU epitope (Ligasová et al., 2017). This presented us with the technical challenge of optimising an endothelial marker that survived this stringent processing. Unfortunately, I did not determine a suitable endothelial marker to stain alongside BrdU in fresh frozen tissue and therefore I only have single BrdU staining, hence it does not indicate which cell type is proliferating. However, since I injected with BrdU from day 10 post-stroke, I speculate that I have avoided early staining of mass glial proliferation, and that the staining is indicative of endothelial proliferation during the peak of angiogenesis. Although our data do suggest that proliferation increases in the striatum compared to the cortex for both genotypes, no difference between the genotypes was observed, suggesting that at 14 d endothelial IL-1R1 signalling does not regulate cellular proliferation. However, further investigation of angiogenesis through different methods including EdU staining (Salic and Mitchison, 2008), which does not require HCl pre-treatment, alongside endothelial staining would be more suitable to categorically determine endothelial proliferation and angiogenesis. Furthermore, LSCI could be used to measure CBF recovery after stroke as a direct functional measure.

Although I did not detect any differences in cellular proliferation between genotypes at 14 d, it is important to highlight that this was a time point when I did not observe upregulation of either isoforms of laminin. However, I did observe differences in laminin expression at 28 d. I observed a widespread increase in laminin α5 expression in both hemispheres in IL-1R1$^{fl/fl\ +Tam}$ mice and IL-1R1$^{fl/fl\ \Delta\ Slco1c1+Tam}$ mice at 28 d, and increased laminin α4 expression observed in IL-1R1$^{fl/fl\ +Tam}$ mice

compared to IL-1R1$^{fl/fl\ \Delta\ Slco1c1+Tam}$ mice at 28 d. Therefore I suggest that it would be interesting to determine the physiological implications of the altered laminin α4 expression observed between genotypes at 28 d post-stroke. I had previously hypothesised that LM-10 could confer protective and reparative properties due to several studies suggesting that LM-10 exerts vasculorepair (Kangwantas et al., 2016) and increases endothelial barrier function (Song et al., 2017). Sorokin and collaborators have demonstrated that LM-10 increases endothelial barrier function by stabilizing the tight junction protein VE-cadherin and through downregulation of CD99L2, and that LM-10 increases TEER and reduces neutrophil transmigration rather than LM-8 (Song et al., 2017) . However, Milner and collaborators (2018) suggested that in the model of chronic mild hypoxia, the increased laminin α4 and laminin α1 expression observed is associated with increased tight junction proteins claudin-5 and ZO-1 and hence increases barrier integrity. It is clear that there is conflicting evidence surrounding the differing roles of laminin isoforms in the brain under different inflammatory and ischaemic conditions. Therefore, it would be interesting to investigate the physiological consequences of the altered laminin α4 expression in IL-1R1$^{fl/fl\ \Delta\ Slco1c1+Tam}$ mice I observed to further determine the role of endothelial IL-1R1 signalling.

It is important to consider the methodological limitations associated with this study. The genetic strain used in this study incorporates a tamoxifen-inducible Cre system and spontaneous activation *in vivo* has been demonstrated (Kristianto et al., 2017), therefore it is important that potential limitations in the models used is highlighted. There are other advanced models such as the genetic knockin reporter system that can track and reciprocally delete or express IL-1R1 in specific cell types (Liu et al., 2019). It is also important to critique the experimental techniques of this study and discuss other valid approaches. This study implemented a histological approach to the detection of laminin expression post-stroke, however there are other methods including proteomics and RNA sequencing that would offer alternative readouts. It would also be of benefit to have control brains for both genotypes to measure laminin expression prior to stroke and determine whether there any basal differences.

In summary, I provide novel evidence that endothelial IL-1R1 regulates laminin α4 expression but not laminin α5 expression post-stroke. In particular, endothelial IL-

1R1 signalling dynamically regulates laminin α4 expression at 2 d post-stroke which could have interesting implications on physiological processes such as neutrophil transmigration during the acute phase of stroke. Furthermore, our study identified 28 d post-MCAO as a critical time point for laminin α5 and α4 expression, demonstrating that there are dynamic changes during the chronic phase after stroke. Although I demonstrate that endothelial IL-1R1 signalling regulated laminin α4 expression at 28 d, I do not provide evidence on whether this is detrimental or protective. Understanding the role of endothelial IL-1R1 signalling at acute and chronic phases post-stroke is of importance to fully elucidate the scope of detrimental and protective properties of IL-1 signalling, whilst helping to shape the approach to treatments such as IL-1RA aimed at blocking IL-1 signalling. Furthermore, understanding the cell-specific contribution of IL-1R1 signalling, in this study endothelial IL-1R1 signalling, is of importance as this would inform potential therapeutic approaches such as the cell-specific targeting of IL-1R1 in the brain after stroke to ensure they reap the most benefit.

Chapter 5. **The generation of a brain endothelial laminin α5 conditional deletion genetic mouse strain and the role of laminin α5 in cerebral ischaemia.**

All experiments were designed and analysed by myself with the input of Dr Emmanuel Pinteaux. All experiments were performed by me with the input of others as stated below for further clarification. Professor Jeffrey Miner provided the $Lama5^{fl/fl}$ mice. I generated the brain endothelial laminin α5 conditional deletion mouse strain and performed all characterisation experiments and analysis, including LSCI. Dr Raymond Wong performed the stroke surgeries with assistance from me, and Dr Raymond Wong performed the neurological scoring. Dr Raymond Wong and I performed the MRI together. I performed all LSCI after strokes. I performed all perfusions, tissue processing and histology. Sarah Ma assisted in the collection of fluorescent images for analysis. Dr Eloise Lemarchand assisted in the infarct analysis of MRI images. I performed all other image analysis and statistical analysis.

5.1. **Introduction**

The BBB is part of an integrated and dynamic system of cells and ECM known as the NVU. The cellular constituents of the NVU include endothelial cells, pericytes, astrocytes, perivascular microglia/macrophages and neurones (Sandoval and Witt, 2008). The critical role of the ECM as a component of the NVU has started to be elucidated as the diverse structural and signalling roles are discovered. The BM is located at the abluminal side of endothelial cells in the brain and is composed of several ECM components, of which the family of glycoproteins laminin are a major component. In the CNS there are two distinct basement membranes associated with the vessels, an endothelial basement membrane composed of laminin α5 and laminin α4 (present in LM-10 and LM-8 respectively), and an outer parenchymal basement membrane composed of laminin α1 and laminin α2 (present in LM-1 and LM-2 respectively) (Sixt et al., 2001). Different cells of the NVU typically synthesise the different isoforms of laminins; namely astrocytes synthesise LM-2 (Jucker et al., 1996; Menezes et al., 2014; Hannocks et al., 2018), and LM-1 is secreted by pial cells (Hannocks et al., 2018) and leptomeningeal cells (Sixt et al., 2001). In contrast, brain endothelial cells synthesise LM-8 and LM-10 (Sixt et al., 2001). However, it is also important to note that mural cell (pericytes and smooth muscle cells) also synthesise laminin α5 and laminin α4 containing isoforms (Gautam et al., 2016).

Understanding the specific contributions of the isoforms of laminin during homeostasis and different disease conditions has gained much interest. There are several studies demonstrating the diverse roles of laminins in the brain as regulators of BBB integrity and neuronal survival. Indeed, in an intracerebral haemorrhage stroke model using endothelial laminin α5 conditional knockout mice, laminin α5 KO mice demonstrated an increased injury volume, reduced BBB integrity and increased neuronal death (Gautam et al., 2019). In contrast, in an ischaemic model of stroke, mural derived laminin α5 has been shown to be detrimental since KO mice displayed reduced infarct volume, neuronal damage and vascular damage (Nirwane et al., 2019). However, the role of brain endothelial derived laminin α5 after ischaemic stroke on brain injury and repair mechanisms had not yet been determined. Here, I have generated a brain endothelial specific laminin α5 conditional deletion genetic strain mouse. I confirmed that laminin α5 expression is successfully ablated in brain blood vessels, and that laminin α4

expression and CBF during homeostasis remain unaffected after laminin α5 deletion. Using the conditional deletion of brain endothelial laminin α5 in mice and the MCAO model of ischaemic stroke, I show that endothelial laminin α5 does not regulate infarct volume, neurological outcome or CBF recovery post-stroke.

5.2. **Aims**

The first aim of this study was to generate a brain endothelial laminin α5 conditional deletion genetic strain mouse. Specific objectives were:

- To successfully generate a brain endothelial laminin α5 conditional deletion mouse strain by crossing Lamα5$^{fl/fl}$ mice with mice expressing Cre recombinase under the promoter of the thyroxine transporter (Slco1c1-CreERT^{T2}).
- To characterise successful and specific deletion of laminin α5 expression.

The second aim of this study was to investigate the role of brain endothelial laminin α5 in cerebral ischaemia. Specific objectives were:

- To assess the role of laminin α5 on infarct volume and neurological outcome after stroke.
- To determine the role of laminin α5 on repair mechanisms after stroke.

5.3. **Results**

5.3.1. The generation and characterisation of a brain endothelial laminin α5 conditional deletion in mice

I obtained lamα5 floxed mice (Lamα5$^{fl/fl}$) mice from Miner and colleagues (Nguyen et al., 2005), and Slco1c1-CreERT^{T2} mice were previously generated (Ridder et al., 2011) and maintained at the University of Manchester. Mice were genotyped for *Lamα5fl* (Fig. 5.1B) and *Slco1c1* (Fig. 5.1C). I generated a brain endothelium-specific laminin α5 KO (Lamα5$^{fl/fl\ \Delta\ Slco1c1}$) by crossing Lamα5$^{fl/fl}$ mice with mice expressing Cre recombinase under the promoter of the thyroxine transporter (Slco1c1-CreERT^{T2}) (Fig. 5.1A). After Cre-mediated recombination induced by tamoxifen, splicing from exon 14 to 22 occurs and removes exons 15-21 (Fig. 5.1A). The 7 exons that are removed encode 40% of domain V, which consists of laminin EGF-like repeats (Nguyen et al., 2005).

To confirm deletion of lamα5, I performed immunohistochemical analysis for laminin α5 (Fig. 5.2A-B). Lamα5$^{fl/fl}$ and Lamα5$^{fl/fl\ \Delta\ Slco1c1}$ were treated with tamoxifen for 5 consecutive days and culled after 7 d, 14 d or 21 d from first day of tamoxifen treatment. I observed a steady decrease in laminin α5 expression from 7 d to 21 d after tamoxifen treatment in Lamα5$^{fl/fl\ \Delta\ Slco1c1}$ mice but not in Lamα5$^{fl/fl}$ mice. In Lamα5$^{fl/fl\ \Delta\ Slco1c1}$ mice at 21 d post-tamoxifen treatment a 58% reduction in laminin α5 expression was observed compared to the respective baseline ($p=0.0163$, Fig. 5.2B), this reduction was not reciprocated in Lamα5$^{fl/fl}$ mice. Genotype had a significant effect on laminin α5 expression ($p<0.0001$), specifically I observed a significant reduction in laminin α5 expression in Lamα5$^{fl/fl\ \Delta\ Slco1c1}$ mice compared to Lamα5$^{fl/fl}$ mice at 21 d (72%, $p<0.0001$, Fig. 5.2B).

To validate for specificity of the laminin α5 deletion, I also assessed laminin α4 expression in Lamα5$^{fl/fl}$ and Lamα5$^{fl/fl\ \Delta\ Slco1c1}$ mice 21 d after tamoxifen treatment (Fig. 5.3). I observed no difference in laminin α4 expression in Lamα5$^{fl/fl\ \Delta\ Slco1c1}$ mice compared to Lamα5$^{fl/fl}$ mice ($p=0.6864$, Fig. 5.3). To determine if loss of laminin α5 affected CBF during homeostasis, I assessed overall CBF 21 d after tamoxifen treatment (Fig. 5.4). CBF was unaffected in Lamα5$^{fl/fl\ \Delta\ Slco1c1}$ mice as no difference between Lamα5$^{fl/fl}$ mice was detected ($p=0.8498$, Fig. 5.4).

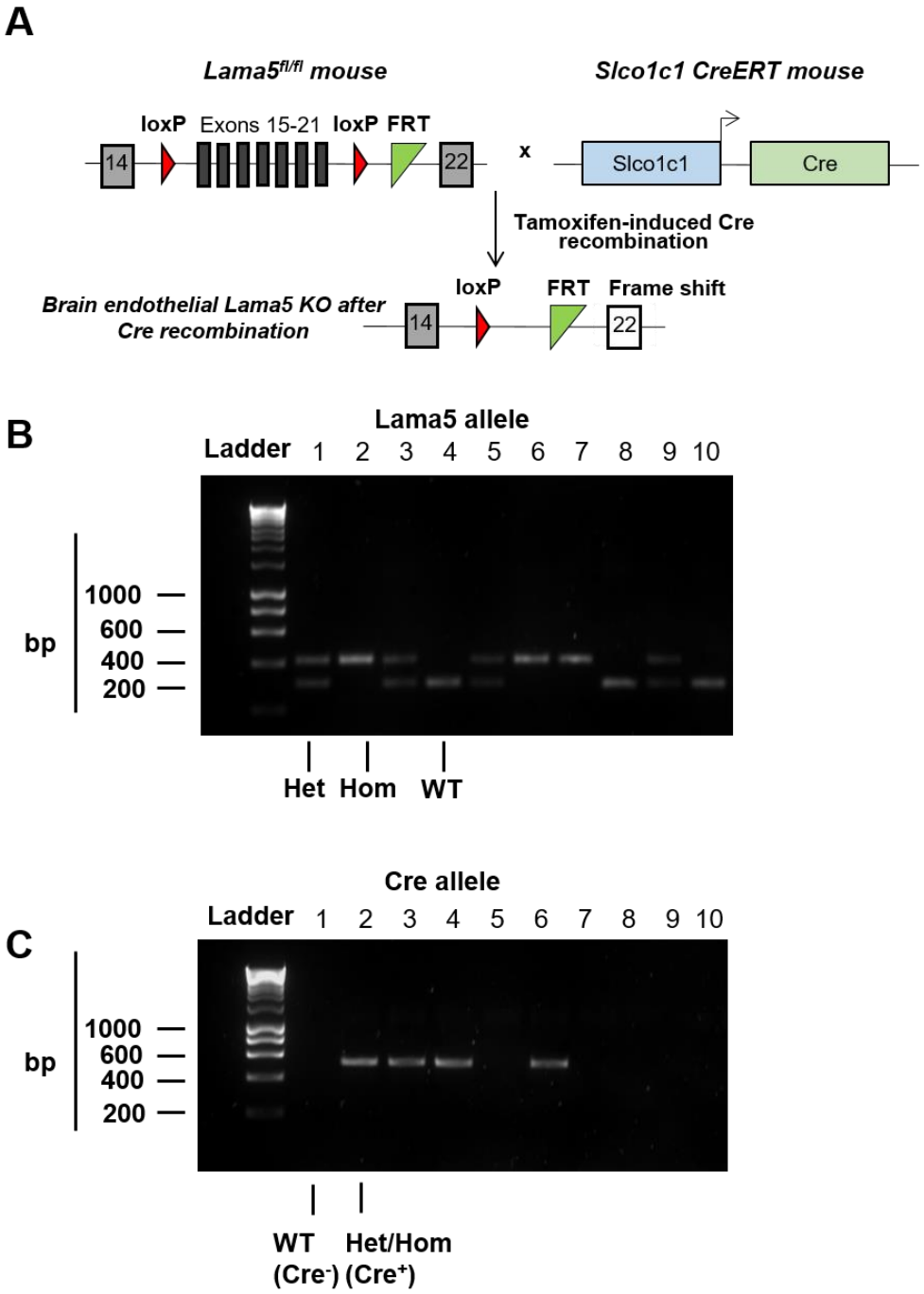

Figure 5.1. Generation of Lamα5$^{fl/fl\ \Delta\ Slco1c1}$ mice and representative PCR gel obtained from genotyping littermates.
(A) Lamα5$^{fl/fl\ \Delta\ Slco1c1}$ (Brain endothelial-specific laminin α5) mice were generated by crossing Lamα5$^{fl/fl}$ mice (exon 15-21 of the *Lamα5* gene flanked with loxP sites) with Slco1c1-CreER^{T2} mice (expressing Cre recombinase under the promoter of the thyroxine transporter). Representative PCR gel obtained from genotyping animals for the Lamα5 allele (B) and the Slco1c1-CreER^{T2} allele (C). (B) WT (296 bp), Hom (460 bp), Het (296 bp and 460 bp) bands are indicated on the gel. (C) Cre^{+} (521 bp) and Cre^{-} (no band) bands are indicated on the gel.

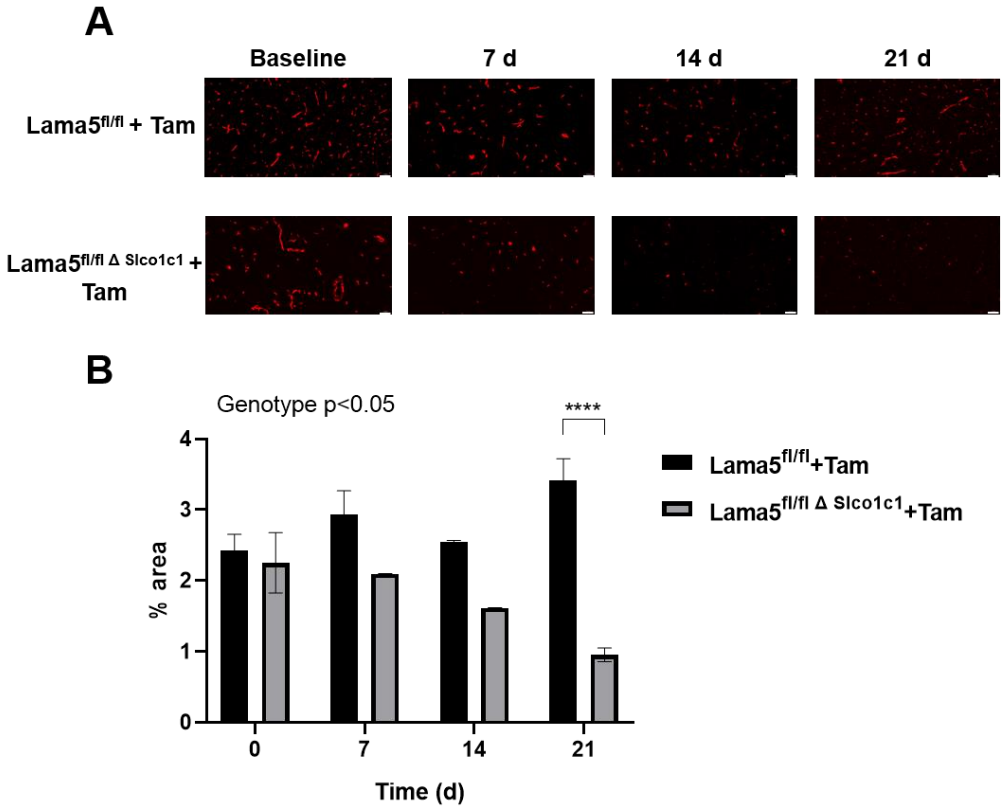

Figure 5.2. Brain endothelial laminin α5 expression reduces over time after tamoxifen treatment in Lamα5$^{fl/fl\ \Delta\ Slco1c1}$ animals.
(A-B) Lamα5$^{fl/fl}$ and Lamα5$^{fl/fl\ \Delta\ Slco1c1}$ were treated with tamoxifen (2 mg/100 µl) for 5 consecutive days and culled after 7 d, 14 d or 21d from first day of treatment. Laminin α5 expression was identified by laminin α5 immunostaining. (A) Representative images of laminin α5 staining is shown, scale bar 50 µm. (B) Percentage (%) area of laminin α5 was quantified with ImageJ software and significant deletion was detected in Lamα5$^{fl/fl\ \Delta\ Slco1c1}$ animals by day 21. Data are represented as mean ± SEM, Baseline, 7 d, 14 d; Lamα5$^{fl/fl}$ and Lamα5$^{fl/fl\ \Delta\ Slco1c1}$ n=2, 21 d; Lamα5$^{fl/fl}$ and Lamα5$^{fl/fl\ \Delta\ Slco1c1}$ n=4. Data were assessed by a two-way ANOVA followed by Sidak's post-hoc analysis comparing the means of expression of laminin α5 at each time point.

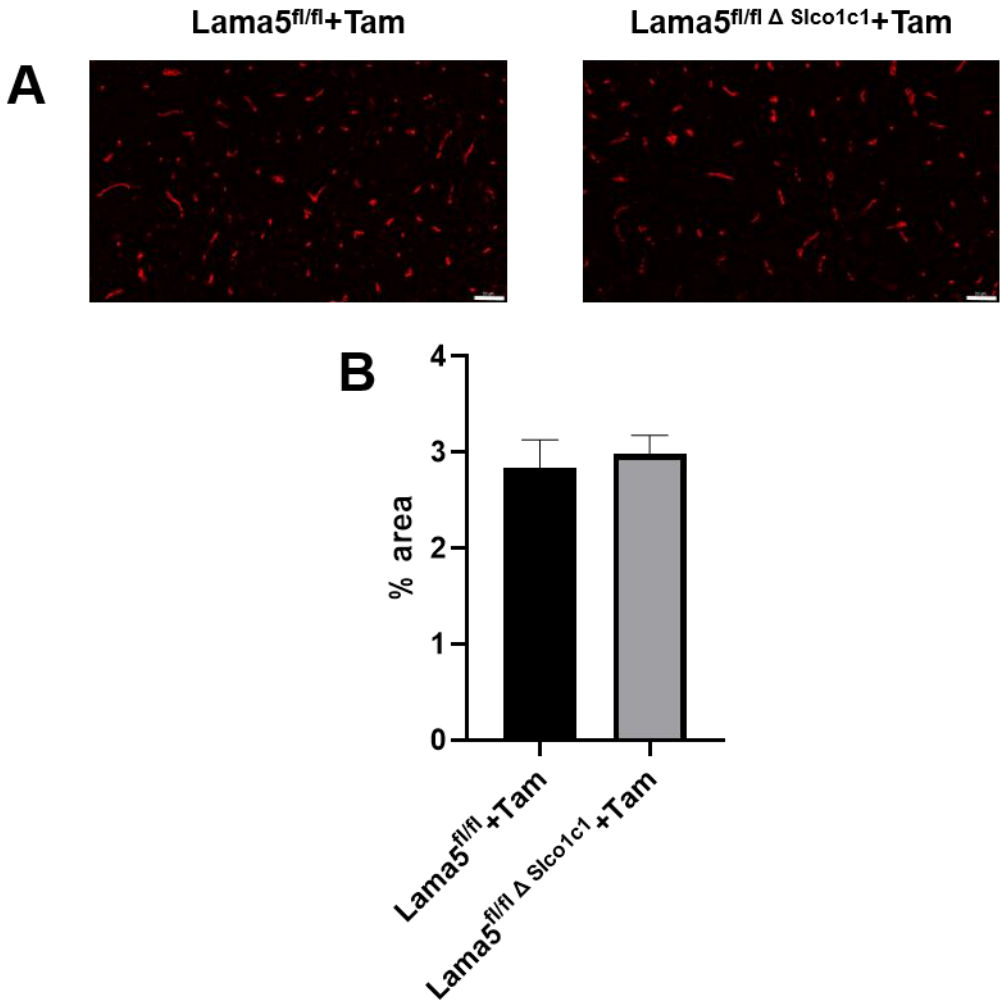

Figure 5.3. Laminin α4 expression in the brain is unaffected after brain endothelial laminin α5 deletion.
Lamα5$^{fl/fl}$ and Lamα5$^{fl/fl\ \Delta\ Slco1c1}$ mice were treated with tamoxifen (2 mg/100 ul) for 5 consecutive days and culled after 21 d from first day of treatment. Laminin α4 expression was identified by laminin α4 immunostaining. (A) Representative images of laminin α4 staining are shown, scale bar 50 µm. (B) Percentage (%) area of laminin α4 was quantified with ImageJ software. Data are represented as mean ± SEM, Lamα5$^{fl/fl}$+Tam; n=4, Lamα5$^{fl/fl\ \Delta\ Slco1c1}$+Tam; n=4. Data were assessed by an unpaired t-test to compare genotypes (B).

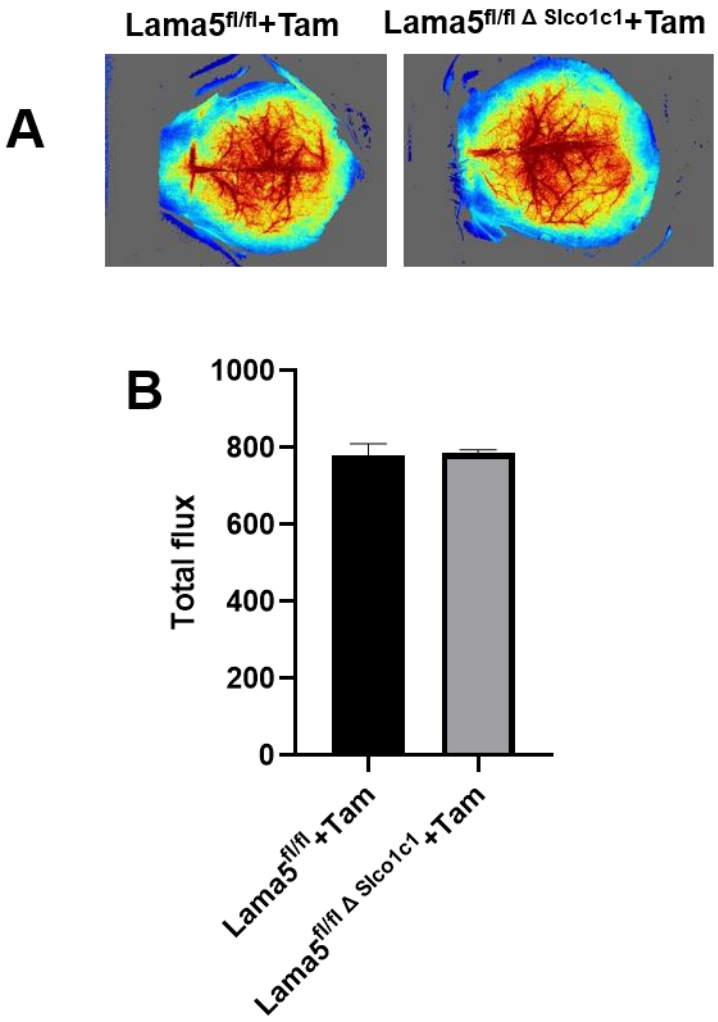

Figure 5.4. Overall cerebral blood flow in the brain under homeostatic conditions is unaffected after brain endothelial laminin α5 deletion.
(A-B) Lamα5$^{fl/fl}$ and Lamα5$^{fl/fl\ \Delta\ Slco1c1}$ mice were treated with tamoxifen (2 mg/100 µl) for 5 consecutive days and culled after 21 d from first day of treatment. CBF was quantified using LSCI. (A) Representative images are shown and (B) analysis of cerebral blood flow across the whole brain was calculated. Total flux is the average of raw flux values measured across the whole brain during the imaging period. Data are represented as mean ± SEM, Lamα5$^{fl/fl}$+Tam; n=3, Lamα5$^{fl/fl\ \Delta\ Slco1c1}$+Tam; n=3. Data was assessed by an unpaired t-test to compare genotypes (B).

5.3.2. Brain endothelial laminin α5 deletion does not affect infarct volume and does not influence neurological function

Since I had previously confirmed that 21 d after tamoxifen treatment was sufficient for laminin α5 deletion, I devised an experimental design that consisted of a tamoxifen or vehicle treatment regimen followed by MCAO surgery 21 d after the regimen (Fig. 5.5A). All mice underwent a 25 min MCA occlusion. In order to determine the role of brain endothelial laminin α5 post-stroke, I assessed infarct volume at 2 d and used LSCI to measure CBF at 3 d, 7 d and 14 d post-MCAO. I observed some animal mortality throughout the 14 d post-MCAO across all genotypes (Fig. 5.5B). However, higher mortality rates were observed in Lamα5$^{fl/fl}$+Tam and Lamα5$^{fl/fl\ \Delta\ Slco1c1}$+Tam compared to Lamα5$^{fl/fl\ \Delta\ Slco1c1}$+Veh (Fig. 5.5B)

To assess the role of brain endothelial laminin α5 on brain injury post-stroke, I measured infarct volume using MRI at 2 d post-MCAO surgery (Fig. 5.6). I observed no significant difference in infarct volume across the three groups, demonstrating that brain endothelial laminin α5 deletion does not modify infarct volume at 2 d post-MCAO (Fig. 5.6). I assessed bodyweight and neurological scores of all mice across a 14 d period after MCAO. I observed a significant effect of time on bodyweight ($p<0.0001$, Fig. 5.7A) and neuroscore ($p<0.0001$, Fig. 5.7B), demonstrating an improvement in both outcomes across the 14 d period. I observed no significant effect of laminin α5 deletion of body weight (Fig. 5.7A) or neurological score as assessed by 28-point neuroscore (Fig. 5.7B).

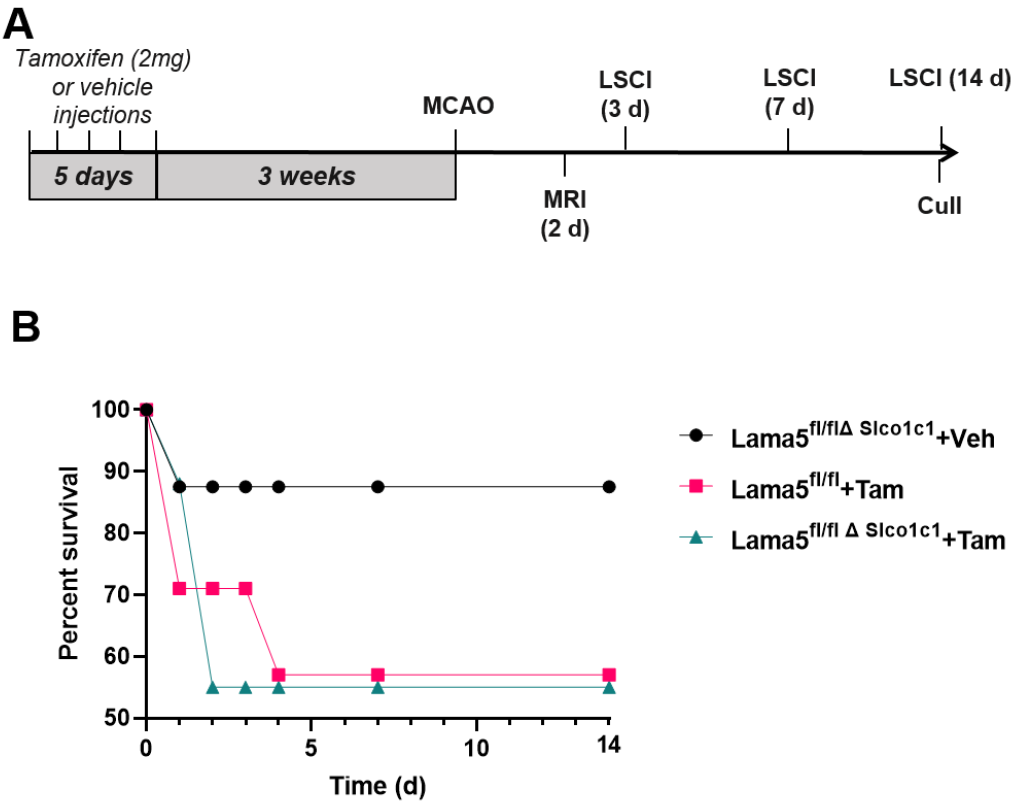

Figure 5.5. Experimental design of brain endothelial laminin α5 deletion MCAO study and survival graph from the study.
(A) Experimental design consisted of 5 day tamoxifen (2 mg/100 µl) or vehicle treatment regimen followed by MCAO surgery (25 min occlusion) 21 d after the start of the tamoxifen/vehicle treatment. MRI was performed at 2 d post-stroke. LSCI was performed at 3 d, 7 d and 14 d post-stroke. Animals culled at 14 d. (B) Survival graph of the three experimental groups across the 14 d period. Results are shown as percentage (%) survival of total animals (Lamα5$^{fl/fl\ \Delta\ Slco1c1}$+Veh; n=8, Lamα5$^{fl/fl}$+Tam; n=8, Lamα5$^{fl/fl\ \Delta\ Slco1c1}$+Tam; n=10) used in each group.

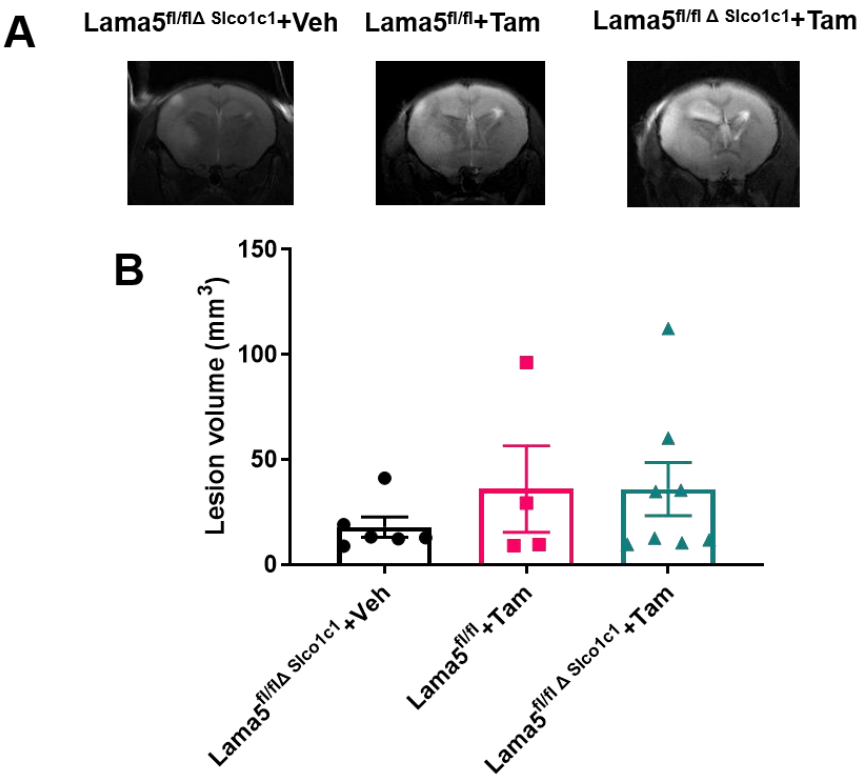

Figure 5.6. Brain endothelial laminin α5 deletion does not influence infarct volume after stroke.
(A) Representative T2-weighted MRI scans conducted at day 2 post-stroke. (B) Quantification of lesion volume using ImageJ software. Data are represented as mean ± SEM, Lamα5$^{fl/fl\ \Delta\ Slco1c1}$+Veh; n=6, Lamα5$^{fl/fl}$+Tam; n=4, Lamα5$^{fl/fl\ \Delta\ Slco1c1}$+Tam; n=8. Data were assessed by a one-way ANOVA followed by Tukey's post-hoc analysis comparing each treatment group.

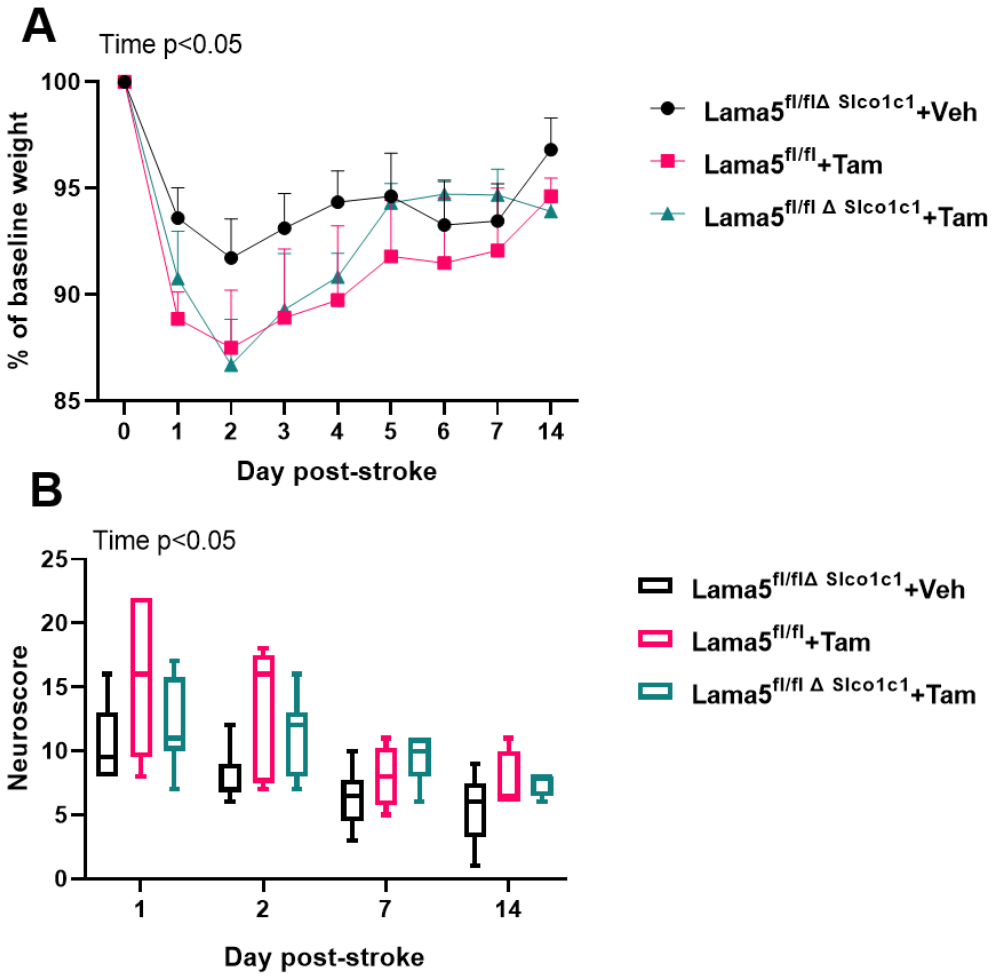

Figure 5.7. Brain endothelial laminin α5 deletion does not influence body weight or neurological function after stroke.
(A) Weight of animals expressed as percentage (%) of baseline weight across the 14 d post-stroke. (B) Neurological deficits were assessed using the 28 point neuroscore. Data are represented as mean ± SEM, Lamα5$^{fl/fl\ \Delta\ Slco1c1}$+Veh; n=6, Lamα5$^{fl/fl}$ +Tam; n=6, Lamα5$^{fl/fl\ \Delta\ Slco1c1}$+Tam; n=8. Data were assessed by mixed-effects model (REML) with Tukey's post-hoc analysis comparing weights/neuroscores at corresponding time points (A,B).

5.3.3. Brain endothelial laminin α5 deletion does not regulate CBF recovery or increase cellular proliferation after MCAO

In Chapter 3, I demonstrated that LM-10 (isoform containing laminin α5) regulated endothelial proliferation and tube formation *in vitro*. In order to test our hypothesis that LM-10 regulated repair *in vivo*, I aimed to determine whether brain endothelial laminin α5 deletion regulated recovery of CBF after cerebral ischemia. I measured CBF 3 d, 7 d and 14 d after MCAO surgery using LSCI (Fig. 5.8A,B). There was a significant effect of time on CBF (p=<0.0001, Fig. 5.8B), demonstrating an improvement of CBF over time across the three groups. However, no effect of laminin α5 deletion was observed (p=0.4750). I observed no significant difference in CBF at 3 d (Fig. 5.8B). Although, not significant, at 7 d there was a marked CBF improvement in Lamα5$^{fl/fl}$+Tam mice compared to Lamα5$^{fl/fl\ \Delta\ Slco1c1}$+Tam (55%, p=0.1163) and Lamα5$^{fl/fl\ \Delta\ Slco1c1}$+Veh (51%,p= 0.2232) (Fig. 5.8B). However, at 14 d I observed no significant differences in CBF between the three groups.

I also assessed BrdU staining at 14 d post-stroke as an indication of cellular proliferation. All mice had injections of BrdU daily beginning at 10 d after MCAO until the day of sacrifice. The ipsilateral hemisphere was assessed in the cortex and striatum for BrdU positive cells (Fig. 5.9A,B). Although not significant, there was a slight trend towards an increase in BrdU positive cells in the ipsilateral striatal regions of Lamα5$^{fl/fl\ \Delta}$+Tam (41%,p=0.2393) and Lamα5$^{fl/fl\ \Delta\ Slco1c1}$+Tam (48%, p=0.2181) compared to their respective ipsilateral cortical regions (Fig. 5.9B). However, no significant increase in BrdU positive cells in the ipsilateral striatum compared to the ipsilateral cortex was observed in Lamα5$^{fl/fl}$+Tam mice (p=0.9889, Fig. 5.9B). On direct comparison of the ipsilateral cortex and ipsilateral striatum between genotypes, no significant differences were detected suggesting that endothelial laminin α5 deletion does not affect cellular proliferation at 14 d (Fig. 5.9B).

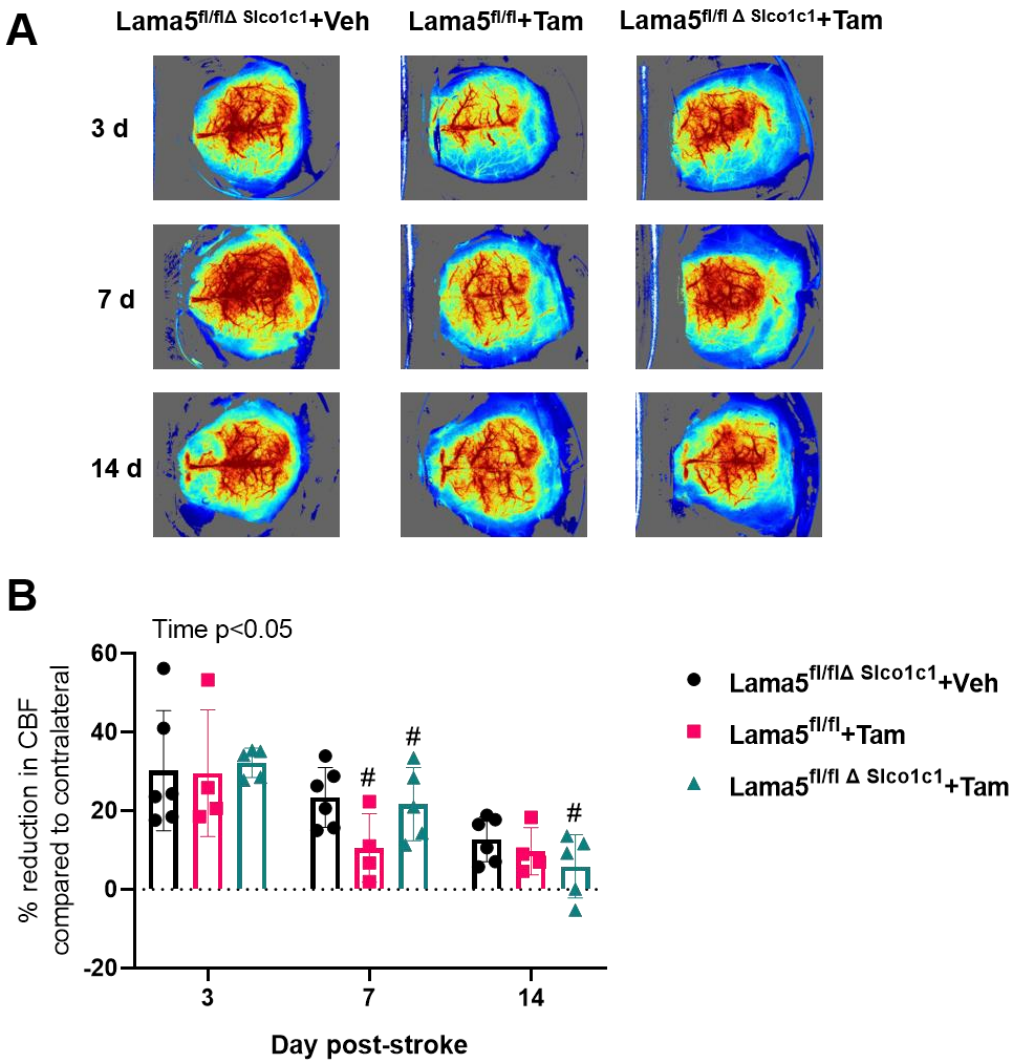

Figure 5.8. Brain endothelial laminin α5 deletion does not influence long term CBF recovery after stroke.
(A) CBF was measured using LSCI. Representative images are shown. (B) The region of interest was determined according to the site of occlusion and the respective area on the contralateral hemisphere. CBF quantified with moorFLPI2 Full-Field Laser Perfusion Imager Review V5.0 software and expressed as reduction in CBF in the ipsilateral hemisphere compared to the contralateral hemisphere. Data are represented as mean ± SEM, Lamα5$^{fl/fl\ \Delta\ Slco1c1}$+Veh; n=5, Lamα5$^{fl/fl}$ +Tam; n= 4, Lamα5$^{fl/fl\ \Delta\ Slco1c1}$+Tam; n=5. Data were assessed by a two-way RM ANOVA followed by Dunnet post-hoc analysis comparing groups at each time point and # denotes significance comparing back to the respective regions at 3 d post-stroke (B).

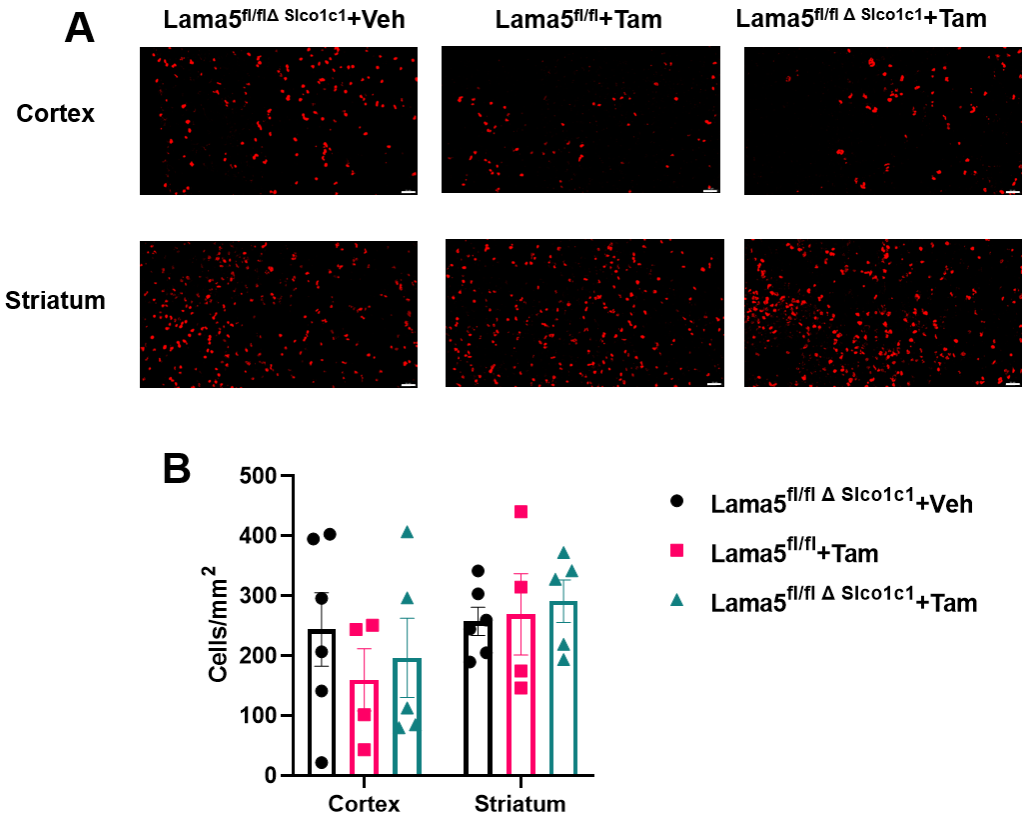

Figure 5.9. Brain endothelial laminin α5 deletion does not influence ipsilateral cortical and striatal cellular proliferation 14 d post-stroke.
(A-B) Animals had injections of BrdU daily beginning at 10 d after MCAO until the day of sacrifice at 14 d. BrdU (red) immunohistochemistry in the ipsilateral hemisphere of cortical and striatal regions 14 d post-stroke. Scale bar 50 um. (B) Proliferation was quantified by counting the number of BrdU-positive cells in a defined region using ImageJ. Data are represented as mean ± SEM, Lamα5$^{fl/fl\ \Delta\ Slco1c1}$+Veh; n=5, Lamα5$^{fl/fl}$ +Tam; n= 4, Lamα5$^{fl/fl\ \Delta\ Slco1c1}$+Tam; n=5. Data were assessed by a two-way RM ANOVA followed by Tukey's post-hoc analysis comparing within genotypes and between genotypes (B).

5.4. **Discussion**

Laminins are a major component of the BM in the CNS. Understanding the specific roles of the different laminin isoforms during homeostasis and disease conditions are of particular interest. In particular, the role of endothelial laminin α5 in ischaemic stroke had not yet been determined. In this study, I have:

- Generated a brain endothelial specific laminin α5 conditional deletion genetic strain mouse and confirmed that laminin α5 expression is ablated in brain blood vessels, without affecting laminin α4 expression or CBF during homeostasis.
- Demonstrated that endothelial laminin α5 does not regulate infarct volume, neurological outcome or CBF recovery after MCAO.

The endothelial BM, also called the vascular BM, is composed of LM-8 (containing laminin α4) and LM-10 (containing laminin α5) (Sixt et al., 2001). In the CNS, brain endothelial cells are major contributors to the synthesis of laminin α5 (Sixt et al., 2001; Hannocks et al., 2018). However an important consideration is that mural cells, including smooth muscle cells and pericytes, also synthesise laminin α5 (Gautam et al., 2016). Since I were interested in the laminin α5 that composes the endothelial BM, I decided to create a brain endothelial-specific laminin α5 KO in order to investigate the role of LM-10 on BBB repair. Although the Tie2-Cre line has been previously used to induce endothelial-specific laminin α5 deletion (Gautam et al., 2019), I used the Slco1c1-CreER^{T2} line as this was more specific to the brain vasculature than Tie2-Cre that is known to cause widespread endothelial deletion (Assmann et al., 2016). At 21 d after tamoxifen treatment, which was used to induce Cre recombination, our genetic cross successfully ablated laminin α5 expression by 72% compared to control animals. Furthermore, I show that laminin α4 expression and CBF is unaffected in the Lamα5$^{fl/fl\ \Delta\ Slco1c1}$+Tam mice during homeostatic conditions. This finding is consistent with other Lamα5$^{fl/fl}$ lines that demonstrate laminin α4 expression, BBB integrity and brain angioarchitecture remain unaffected in laminin α5 KO animals (Gautam et al., 2019). An important consideration with the use of cell-specific laminin KO models, is the possibility of compensation mechanisms whereby there is an increase in the other endothelial laminin isoform, LM-8, or whether mural cells

increase their expression of LM-10 to compensate for the lack of endothelial expression. Considering that mural cells are closely associated with the vasculature, it is a plausible suggestion that mural cells could increase laminin α5 expression to contribute to the endothelial BM. However, I did not observe any compensatory increase in laminin α4, and I were satisfied with the knockdown of laminin α5 expression I achieved which did not cause concern of compensatory mechanisms by other cell types.

Previous studies have demonstrated diverse properties of LM-10 during several disease conditions. Sorokin and colleagues have consistently demonstrated the endothelial barrier properties of LM-10 compared to LM-8 (Sixt et al., 2001; Wu et al., 2009; Song et al., 2017). Specifically, a study using laminin α4 KO mice, which show compensatory ubiquitous expression of laminin α5 along the vasculature, demonstrated reduced T lymphocyte infiltration in an experimental model of multiple sclerosis, EAE (Wu et al., 2009). A further study by Sorokin and colleagues have demonstrated that in the cremaster muscle model whereby TNF-α is used to induce leukocyte infiltration, increased leukocyte infiltration is observed in regions of low laminin α5 expression (Song et al., 2017). Yao and colleagues have demonstrated that endothelial-derived laminin α5 is protective in an intracerebral haemorrhage stroke model (Gautam et al., 2019). The extensive evidence demonstrating endothelial barrier properties in several contexts and the protective role of endothelial laminin α5 in haemorrhagic stroke led to our hypothesis that endothelial laminin α5 would regulate brain injury and neurological outcome after ischaemic stroke. However, I observed no effect of brain endothelial laminin α5 deletion on infarct volume at 48 h, or body weight and neurological scores across a 14 d period.

Although I did not detect an effect of laminin α5 on brain injury at acute time points post-stroke, our next key objective was to determine the role of laminin α5 in repair mechanisms at chronic time points after stroke. There is evidence that CBF after ischaemic stroke is associated with neurological outcome and functional recovery in clinical patients (Arkuszewski et al., 2009). The protective properties of laminin α5 containing isoforms on neuronal health and function have been demonstrated in several studies, including the promotion of survival and differentiation of midbrain dopaminergic neurones (Zhang et al., 2017) and protection of neurones

by the laminin matrix during excitotoxic damage (Indyk et al., 2003). Kangwantas and colleagues (2016) identified LM-10 as a key ECM molecule that reversed hallmarks of BBB dysfunction after OGD and IL-1 *in vitro*, specifically occludin cellular localisation and cellular morphology, demonstrating the protective properties of LM-10 on endothelial cells. Therefore, taking the literature and our results in Chapter 3 that demonstrated the pro-angiogenic properties of LM-10 *in vitro* into consideration, I hypothesised that LM-10 would be a regulator of repair post-stroke *in vivo*. Since previous *in vivo* stroke studies have identified 14 d post-stroke as a critical time point for angiogenesis (Rodriguez-Grande et al., 2015; Rajkovic et al., 2018), I assessed CBF recovery at 3 d, 7 d and 14 d post-stroke. Indeed, angiogenesis after ischaemia is also associated with improved tissue recovery and functional outcome (Krupinski et al., 1994; Slevin et al., 2006; Adamczak et al., 2014). Endothelial proliferation is a key stage of angiogenesis (Ucuzian et al., 2011) and therefore I assessed cellular proliferation at 14 d using BrdU staining. In this study, I did not detect any significant effect of brain endothelial laminin α5 deletion on CBF or cellular proliferation. However, a noteworthy observation is that at 7 d Lamα5$^{fl/fl}$+Tam mice show a marked improvement compared to Lamα5$^{fl/fl\ \Delta\ Slco1c1}$+Veh mice and Lamα5$^{fl/fl\ \Delta\ Slco1c1}$+Tam mice. At 14 d, the CBF across the three groups returned to similar levels. I speculate that the altered CBF response at 7 d may be an interesting finding, indicating different repair responses. However, this result should be approached with caution since the Lamα5$^{fl/fl\ \Delta\ Slco1c1}$+Veh mice should present a similar response to Lamα5$^{fl/fl}$+Tam mice as they both should not induce laminin α5 deletion. Spontaneous activation of the Cre system has been demonstrated *in vivo*, which is an important consideration when discussing the limitations of the methods as this could be a plausible explanation our findings (Kristianto et al., 2017). However, due to the small sample sizes involved in this study, it is reasonable to say that no categorically correct conclusions can be drawn.

It is important to discuss the limitations associated with this study. I experienced animal mortality throughout the MCAO study, which resulted in smaller group sizes than intended. Due to the low group sizes, it is hard to categorically rule out a potential effect of laminin α5 in ischaemic stroke. Although the literature highlighted 14 d as a critical time point for repair post-stroke, it is important to discuss that there could be potential interesting findings at more chronic time points such as 28

d post-stroke. A recent study using a permanent model of MCAO and RNA sequencing, demonstrated that laminin α5 gene expression was dynamically regulated at 24 h, 72 h and 28 d post-stroke, showing an increase in gene expression between 72 h and 28 d (Munji et al., 2019). Therefore, I can speculate that laminin α5 may contribute to chronic repair mechanisms, but unfortunately due to time constraints of the study I could not further investigate. A methodological limitation that has been previously discussed in chapter 4 is the technical challenges associated with BrdU staining. I faced similar challenges of co-staining the brain tissue with an endothelial marker and therefore suggest that similar studies in the future that use EdU staining are recommended (Salic and Mitchison, 2008).

An important limitation to discuss is the potential influence of the mouse genetic backgrounds on the results observed in this study. The genetic background of the Lama5$^{fl/fl}$ mice was not pure and instead consisted of a mixture of C57BL/6J and CBA/J strains of mice. In contrast, the genetic background of the Slco1c1-CreERT^{T2} line was pure C57BL/6J. Since this study was the first to generate a Lamα5$^{fl/fl}$ x Slco1c1-CreERT^{T2} genetic strain of mouse, the potential toxicity effects of tamoxifen on this strain of mouse had not been investigated before. It has been documented that the metabolism of tamoxifen can vary across different strains of mice and hence the effects of tamoxifen can also vary (Valny et al., 2016). Furthermore, there has been evidence that tamoxifen can affect glucose tolerance (Ceasrine et al., 2019), as well as reduce food intake and reduce bodyweight (Wade and Heller, 1993). In this study, the Lamα5$^{fl/fl}$+Tam group and the Lamα5$^{fl/fl}$ $^{\Delta\ Slco1c1}$+Tam group demonstrated similar weight loss and survival patterns after MCAO that were not reciprocated by the vehicle control group (Lamα5$^{fl/fl\ \Delta\ Slco1c1}$+Veh). I had expected the two control groups (Lamα5$^{fl/fl}$+Tam mice and Lamα5$^{fl/fl\ \Delta\ Slco1c1}$+Veh) to have the same effect on outcome measures, similar to the comparable tamoxifen and vehicle controls in the brain endothelial IL-1R1 conditional deletion MCAO study performed by Wong and colleagues (2019). A noteworthy difference is that the IL-1R1$^{fl/fl}$ mice used in Wong et al. (2019) are on a pure C57BL/6J genetic background. Therefore, the results I observed in this study may suggest a potential tamoxifen effect on the Lamα5$^{fl/fl}$ mice, which could be explained due to their mixed genetic background. This highlights the challenges that may be faced when creating a new genetic strain.

In summary, I have created a novel brain endothelial laminin α5 conditional deletion genetic strain of mouse. I confirmed successful and specific ablation of endothelial laminin α5 in the brain after tamoxifen-Cre induction. However, our study did not demonstrate a role of endothelial laminin α5 after ischaemic stroke on infarct volume, neurological outcome, CBF recovery or cellular proliferation. Understanding the diverse roles of laminin isoforms and the cell-specific contributions in different disease settings such as stroke and multiple sclerosis still remains worthy of investigation to identify therapeutic targets for potential intervention.

Chapter 6. **Discussion**

6.1. **Summary**

Stroke remains a major worldwide health issue and there are currently limited treatment options. Specifically, there are no therapies aimed at the repair phase to aid recovery after ischaemic stroke. There has been increasing evidence that inflammation presents a dual nature of detrimental and neuroprotective properties during the pathogenesis of stroke and it has been suggested that IL-1 could play a key role in repair mechanisms. Furthermore, the dynamic role of the ECM in cerebrovascular diseases has started to be elucidated. Here, I investigated the role of LM-10 on IL-1β-driven cerebral endothelial inflammation and repair mechanisms *in vitro* and generated a brain endothelial laminin α5 conditional deletion genetic strain mouse to investigate the role of LM-10 after cerebral ischaemia *in vivo*. Furthermore, I investigated the role of cerebral endothelial IL-1R1 signalling on laminin α4 and laminin α5 expression after stroke to determine the crosstalk between IL-1 and laminin expression.

The overarching aim of this thesis was to investigate the role of LM-10 on endothelial inflammation and repair mechanisms after cerebral ischemia using *in vitro* and *in vivo* approaches. The key findings from this thesis are presented in Figure 6.1. This thesis specifically aimed to:

1. Establish an *in vitro* model to investigate the effect of LM-10 on the IL-1β-induced activation, IL-1β-induced signalling and angiogenic response of cerebral endothelial cells. (Chapter 3)
2. Determine the role of IL-1R1 in the cerebrovasculature after cerebral ischemia, specifically on laminin α4 and laminin α5 expression across several time points post-stroke. (Chapter 4)
3. Generate and characterise a brain endothelial laminin α5 conditional deletion genetic strain mouse, in order to investigate the role of brain endothelial laminin α5 in cerebral ischaemia. (Chapter 5)

In Chapter 3, I aimed to establish a suitable *in vitro* model to investigate the effect of LM-10 on the IL-1β-induced activation, IL-1β-induced signalling pathways and angiogenic response of cerebral endothelial cells. In this study, I established an appropriate *in vitro* model using hCMEC/D3 cells, a short seeding time of 4 h and the plate coating control of Matrigel. I established a novel role of LM-10 as a

modulator of IL-1β-induced ICAM-1 and VCAM-1 expression in hCMEC/D3 cells and demonstrated that LM-10 increases endothelial proliferation and migration, which I hypothesise is indicative of an angiogenic role of LM-10 in BBB repair. I have elucidated a novel crosstalk between IL-1β and Hippo signalling. Furthermore, I demonstrated altered YAP signalling and YAP associated gene expression in hCMEC/D3 cells seeded on LM-10.

In Chapter 4, I aimed to determine the role of the IL-1R1 in the cerebrovasculature after cerebral ischemia, focusing on laminin α4 and laminin α5 expression across several time points post-stroke. I found that laminin α4 is more dynamically regulated than laminin α5 post-stroke and that laminin α4 expression is regulated by endothelial IL-1R1 signalling. Specifically, endothelial IL-1R1 signalling dynamically regulates laminin α4 expression at 2 d and 28 d post-stroke. Furthermore, our study identified 28 d post-MCAO as a critical time point for laminin α5 and α4 expression, demonstrating that there are dynamic changes during the chronic phase after stroke. Additionally, I also assessed the role of the IL-1R1 on brain injury and neurological function, as well as the role of IL-1R1 on cellular proliferation at 14 d. However, I found no effect of cerebrovascular endothelial IL-1R1 deletion on infarct volume at 2 d or neurological outcomes, as well as no significant difference in cellular proliferation at 14 d post-stroke.

In Chapter 5, I aimed to generate and characterise a brain endothelial specific laminin α5 conditional deletion genetic strain mouse, in order to use the strain to determine the role of laminin α5 after cerebral ischemia. Specifically, I aimed to determine the role of laminin α5 on outcome measures of infarct volume, neurological function and CBF recovery post-stroke. I successfully generated the new genetic line and confirmed that laminin α5 expression is ablated in brain blood vessels, without affecting laminin α4 expression or CBF during homeostasis. However, I found that cerebral endothelial laminin α5 does not regulate infarct volume, neurological outcome or CBF recovery post-stroke.

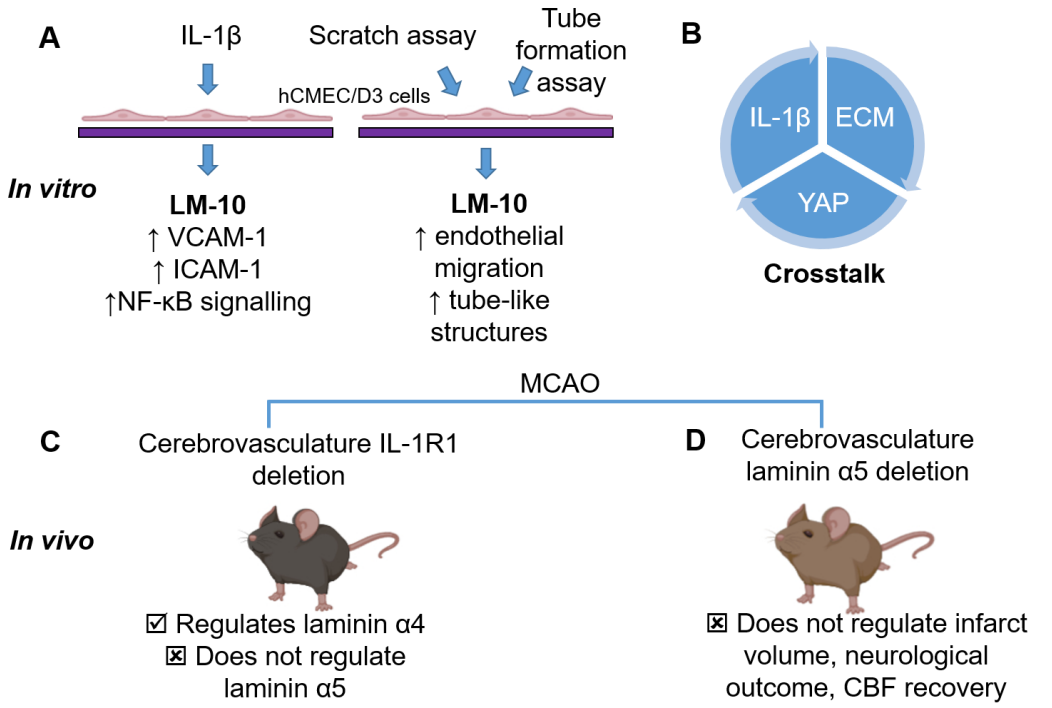

Figure 6.1. Key *in vitro* and *in vivo* findings of the thesis.
(A) The seeding of hCMEC/D3 cells on LM-10 (compared to Matrigel) increased VCAM-1 and ICAM-1 expression, as well as NF-κB signalling after IL-1β treatment. LM-10 increases endothelial migration and the formation of tube-like structures in the scratch assay and tube formation assay respectively. (B) Novel crosstalk between IL-1β, the ECM and the Hippo (YAP) pathway was demonstrated *in vitro*. (C) Cerebrovasculature IL-1R1 deletion regulated laminin α4 expression but not laminin α5 expression after experimental stroke (MCAO) across several time points measured. (D) Cerebrovasculature laminin α5 deletion did not regulate infarct volume, neurological outcome or CBF recovery after experimental stroke (MCAO).

6.2. Discussion

6.2.1. The role of LM-10 as a regulator of inflammation

There is some disparity in our *in vitro* and *in vivo* data concerning the role of LM-10 on inflammation, whereby I demonstrate an altered inflammatory activation *in vitro* but do not detect an effect of laminin α5 deletion on brain injury *in vivo.* However, it is important to highlight that infarct volume is not a direct measure of inflammation and hence although I observed increased VCAM-1 and ICAM-1 expression *in vitro,* this does not necessarily translate to increased brain injury *in vivo.* Thus, future experiments determining ICAM-1 and VCAM-1 expression and neutrophil transmigration *in vivo* after ischaemic stroke using the laminin α5 KOs would be of benefit to fully determine the role of laminin α5 on inflammatory mechanisms post-stroke. Another important consideration is that our *in vitro* model may not fully translate findings in our *in vivo* genetic KO model. Our *in vitro* model

consisted of hCMEC/D3 cells seeded on LM-10 in a two-dimensional (2D) environment without other cells of the NVU present, whilst our *in vivo* approach enables investigation of the 3D environment of the brain in the *in vivo* state. Thus, mimicking complex cell-ECM interactions *in vitro* is difficult and *in vivo* models facilitate the genetic deletion of genes of interest providing more physiological relevant insight. However, an important future consideration is the recent development of 3D *in vitro* cell culture, whereby immortalized cells or stem cells are placed within hydrogel matrices, which facilitates the creation of environments that enable complex cell-cell and cell-ECM interactions (Antoni et al., 2015). Indeed, tissue engineering and bioprinting presents the possibility of layered 3D NVU models that could be designed with the required properties, which would enable the investigation of different ECM compositions and the effect on outcome measures such as BBB function and endothelial integrity (Potjewyd et al., 2018).

A further consideration is that the genetic line I created to facilitate the conditional deletion of laminin α5 used the Slco1c1-CreERT^{T2} to induce the deletion in brain endothelial cells. There is evidence that mural cells, including smooth muscle cells and pericytes, also synthesise laminin α5 (Gautam et al., 2016) and thus there is the possibility of compensatory mechanisms whereby mural cells may increase LM-10 synthesis. However, I were satisfied with the 72% reduction in laminin α5 expression in Lamα5$^{fl/fl\ \Delta\ Slco1c1}$+Tam mice I observed after tamoxifen-induced laminin α5 deletion. There is also the potential that other ECM components may be upregulated as compensation. Although I did not observe any changes to laminin α4 expression after laminin α5 deletion, I did not measure changes to other ECM components and therefore it is important to consider there may be other altered expression of BM proteins. However, I speculate that this is unlikely as it has been reported that laminin α5 deletion under a Tie2-Cre (endothelial-specific Cre) does not result in BM or structural changes (Song et al., 2017). However this is a noteworthy contrast compared to mice lacking laminin α4, whereby there is compensatory mechanisms resulting in the ubiquitous expression of laminin α5 along the vessel tree (Wu et al., 2009). This highlights the importance of characterising new genetic lines and understanding the limitations of genetic manipulations used.

6.2.2. The crosstalk between IL-1β, the ECM and the Hippo pathway

In Chapter 3, I explored the Hippo (YAP) signalling pathway as a mechanism that may be altered after IL-1β treatment in hCMEC/D3 cells to induce an altered inflammatory response on LM-10. Consequently, the *in vitro* data provides novel evidence of a dynamic crosstalk between IL-1β and Hippo signalling. Furthermore, to our knowledge this is the first study to show a YAP response after IL-1β treatment in hCMEC/D3 cells seeded on Matrigel and LM-10, specifically demonstrating a novel temporal pattern of YAP phosphorylation at S127 and S397 on each ECM coating. I believe that these findings are of particular significance and highly consider the crosstalk between IL-1β, the ECM and Hippo signalling worthy of further investigation. Our evidence is novel at two levels; first the crosstalk between IL-1β and Hippo signalling (as indicated by the temporal patters of YAP phosphorylation after IL-1β treatment) and second the potential role of Hippo signalling as a regulator of the inflammatory responses on different ECM components (as indicated by the modulated temporal patters of YAP phosphorylation on different ECM components). It adds to evidence in the literature that YAP plays a key role in endothelial inflammation, previously demonstrated in the case of TNF-α, another key inflammatory cytokine (Choi et al., 2018).

It is important that the limitations of our experimental approach in Chapter 3 are appreciated and future experiments discussed. As previously suggested in Chapter 3, a more comprehensive time course of pYAP(127) and pYAP(397) levels, as well as a time course of YAP-related gene expression after IL-1β treatment would enable fully supported conclusions. Furthermore, I did not determine the direct mechanisms whereby the IL-1 signalling pathway and the Hippo pathway may crosstalk, specifically which kinases of the pathways may be critical in mediating the crosstalk. I speculate that NF-κB may act as a link between the pathways as the cross-talk has been discussed in the literature (Wang et al., 2020), and here I presented evidence that cells seeded on LM-10 induce a higher NF-κB response after IL-1β treatment, resulting in the upregulation of ICAM-1 and VCAM-1. I further speculate that the signalling cascade downstream of IL-1R1 responsible for the increased NF-κB activation observed on LM-10 may crosstalk with kinases of the Hippo pathway and act as a regulator of YAP signalling. However, another mechanism could be that YAP acts as a transcription repressor or activator of genes downstream of NF-κB (Zhang et al., 2018). It is evident that

the mechanisms behind the crosstalk between IL-1, the ECM and Hippo signalling require further investigations. Advanced *in vitro* approaches such as the silencing of YAP/TAZ in endothelial cells or YAP/TAZ inhibitors would elucidate whether YAP/TAZ is required for the modulated inflammatory response observed on LM-10. Furthermore, kinases of the IL-1R1 signalling cascade could also be silenced or inhibited to determine the effect on Hippo signalling. In future experiments, *in vivo* genetic tools to conditionally delete YAP in endothelial cells would enable the *in vivo* investigation of Hippo signalling in disease models such as ischaemic stroke.

6.2.3. The role of LM-10 as a regulator of repair mechanisms and angiogenesis

Data presented in Chapter 3 supported a pro-angiogenic role of LM-10 compared to Matrigel. Specifically, I presented evidence that LM-10 increased endothelial proliferation and migration of hCMEC/D3 cells, as well as increased tube-like structures in hCMEC/D3 cells on LM-10 as demonstrated by tube formation assay. In contrast, data presented in Chapter 5 provided some insight into the role of LM-10 on repair mechanisms after cerebral ischaemia *in vivo*. Specifically, I demonstrated that cerebral endothelial laminin α5 does not regulate infarct volume, neurological outcome or CBF recovery after ischaemic stroke. This would suggest that LM-10 does not regulate repair mechanisms *in vivo*.

Similar to the disparity between our *in vitro* and *in vivo* data concerning the role of LM-10 on inflammation, there is also discrepancies between our *in vitro* and *in vivo* data regarding the role of LM-10 on BBB repair mechanisms and angiogenesis. However, it is important to consider the methodological limitations in our approaches. Our *in vitro* experiments were performed under normoxic conditions, and hence I suggest that a better representation of ischaemic conditions would be for the scratch assay and tube formation assay to be performed under inflammatory and hypoxic conditions. This would enable more representative translation between *in vitro* conditions and the *in vivo* conditions observed after cerebral ischemia such as inflammation and hypoxia (Woodruff et al., 2011). However, it is also important to appreciate that even with those modifications, the *in vitro* approach will not fully resemble the complex *in vivo* environment of all cells of the NVU that contribute to repair. In Chapter 5, I used LSCI to measure CBF at 3 d, 7

d and 14 d after stroke. The benefit of measuring CBF is that it is a functional outcome measure of perfusion dynamics (Kazmi et al., 2015) and thus can indicate the recovery of CBF, providing some indication of angiogenesis. Although I attempted to measure BrdU staining alongside a vascular marker to provide a direct measure of new blood vessels, I failed to optimise the use of a vascular marker. I suggest that future experiments should utilise EdU staining that requires less stringent tissue processing (Salic and Mitchison, 2008), alongside a vessel stain to enable the measurement of new blood vessels. Studies that incorporate CBF measurements as a functional outcome of repair mechanisms, alongside staining techniques such as EdU staining to demonstrate proliferating vessels would provide a more comprehensive and robust measure of changes. I also suggest that further staining including measurements of vessel diameter and integrin staining, as performed in other studies (Rajkovic et al., 2018), would be good indicators of neurovascular repair post-stroke. Furthermore, there is evidence that LM-10 promotes midbrain dopaminergic neuron survival (Zhang et al., 2017) and therefore I suggest future *in vivo* experiments to measure neurogenesis in laminin α5 KOs after cerebral ischaemia to draw further conclusions regarding the repair role of LM-10.

In the case of the stroke study in Chapter 5, the major limitation that made data interpretation difficult was the low group sizes due to the high animal mortality I observed despite the adjustment of the occlusion time to 25 min. Mortality is associated with the MCAO model of stroke, especially during chronic time point studies. Although there was only one early cull in the Lamα5$^{fl/fl\ \Delta\ Slco1c1}$+Veh group (87.5% survival rate), I observed lower survival rates in the Lamα5$^{fl/fl}$+Tam (62.5% survival) and Lamα5$^{fl/fl\ \Delta\ Slco1c1}$+Tam (50% survival). I are unsure the potential explanations for this as I did not observe larger infarcts in any of the groups that would explain higher mortality. A potential explanation, previously discussed in Chapter 5, is that the mixed genetic background of the Lamα5$^{fl/fl}$ mice could result in a higher tamoxifen toxicity in this strain of mouse. A higher powered study would provide conclusive data regarding any significant differences, especially for the CBF recovery data. Unfortunately due to time constraints of this thesis, I were unable to use more animals in this study.

6.2.4. The role of endothelial IL-1R1 signalling on ECM expression and cellular proliferation

Understanding the cell-specific contribution of IL-1R1 signalling, as well as the temporal profile of protective and detrimental properties of IL-1 signalling is critical in understanding the pathology of ischaemic stroke and would inform cell-specific targeting of IL-1R1 or therapies aimed at blocking IL-1R1. Data presented in Chapter 3 provides *in vitro* insight into the signalling pathways activated in response to IL-1β. Indeed, I show altered phospho-p38α signalling and NF-κB signalling after IL-1β treatment in hCMEC/D3 cells. However, I did not demonstrate altered ERK1/2 signalling in hCMEC/D3 cells after IL-1β treatment. This illustrates that the signalling pathways elicited downstream of the IL-1R1 can depend upon cell type and can vary according to experimental study, highlighting the complexities in understanding signalling mechanisms.

The advancement of genetic tools have facilitated the genetic deletion of genes of interest in mice. Indeed, a brain endothelial specific IL-1R1 conditional KO had been previously generated (Wong et al., 2019). Although Wong and colleagues (2019) have demonstrated the role of cerebrovasculature IL-1R1 signalling during the acute phase after stroke, I aimed to determine the role of brain endothelial IL-1R1 signalling during the chronic phase of stroke, and in particular on laminin α4 and laminin α5 expression across several time points post-stroke in Chapter 4. It was of particular importance that I determined the patterns of expression of the specific isoforms of laminins as in other stroke studies a pan-laminin antibody that stains all isoforms is often used (Yao, 2019). This approach does not facilitate the detection in changes of specific isoforms which is of importance considering the different physiological properties of laminin isoforms in disease conditions. Data presented in Chapter 4 provided insight into the temporal profiles of laminin α4 and laminin α5 after stroke. Our data suggested that laminin α4 expression is more dynamically regulated as a result of MCAO than laminin α5 at each time point measured post-stroke and that laminin α4 expression is regulated by endothelial IL-1R1 signalling. I observed no effect of stroke on laminin α5 expression in both IL-1R1$^{fl/fl\ +Tam}$ mice and IL-1R1$^{fl/fl\ \Delta\ Slco1c1+Tam}$ mice at 2 d and 14 d post-stroke. However at 28 d I observed an increase in laminin α5 expression in the ipsilateral cortex and contralateral striatum in both IL-1R1$^{fl/fl\ +Tam}$ mice and IL-1R1$^{fl/fl\ \Delta\ Slco1c1+Tam}$ mice compared to the respective regions at 2 d, suggesting that laminin α5

expression may be regulated post-stroke at chronic time points. In contrast, at 2 d post-stroke, our data demonstrated that endothelial IL-1R1 signalling regulates the acute reduction in laminin α4 expression observed in the ipsilateral hemisphere. Interestingly, at 28 d post-stroke I observed an increase in laminin α4 expression in the ipsilateral cortex and striatum of control (IL-1R1$^{fl/fl\ +Tam}$) mice compared to their respective regions at 2 d. This was not reciprocated in mice with cerebrovasculature IL-1R1 deleted, demonstrating that cerebrovasculature IL-1R1 signalling regulates laminin α4 expression. However, our findings did not corroborate with previous *in vitro* evidence that demonstrated laminin α5 is regulated after IL-1 and OGD in rat brain endothelial cells (Kangwantas et al., 2016).Consequently, our findings in Chapter 4 support the hypothesis in the literature that it is laminin α4 that is more dynamically regulated than laminin α5 by inflammation *in vitro* (Sixt et al., 2001) and after hypoxia *in vivo* (Halder et al., 2018). The discrepancies between the studies investigating laminin expression can be explained by different experimental settings and thus suggest that laminin expression is under several regulatory inducers including inflammation and hypoxia, but that the exact mechanisms are unclear. There is evidence in the literature that IL-1 contributes to repair mechanisms (Salmeron et al., 2016) and therefore I hypothesised that cerebrovasculature IL-1R1 would regulate cellular proliferation. However, I did not observe an effect of cerebrovasculature IL-1R1 signalling on cellular proliferation at 14 d post-stroke.

There are several limitations associated with the *in vivo* stroke study in Chapter 4. As previously discussed regarding the BrdU staining in Chapter 5, I were also challenged with experimental difficulty in performing a dual stain of BrdU and an endothelial marker. Therefore, I would recommend the same approach of EdU staining instead (Salic and Mitchison, 2008). Critically, in Chapter 4 I observed that 28 d post-stroke was a key time-point for laminin expression and would therefore suggest further investigation at this time point. In future experiments, it would be interesting to determine the physiological implications of the altered laminin expression observed in the IL-1R1 KOs during the pathogenesis of stroke. Hence, at 2 d post-stroke it would be of interest to determine inflammatory cell infiltration of neutrophils and leukocytes, as well as markers of BBB breakdown and vascular inflammation. At 28 d, the investigation of neurogenesis and angiogenesis would provide insight into whether the altered laminin expression modulates repair mechanisms. Further approaches such as LSCI to measure CBF, would act as a

functional outcome measure alongside EdU staining of vessels to provide a more comprehensive investigation of angiogenesis. Considering the experimental approach to answer all the intended questions of the study is always of importance and there are other approaches such as RNA sequencing (Munji et al., 2019) that would facilitate a vast readout of genes, but do come at a financial cost.

6.3. **Future directions**

Although I have previously discussed future experiments regarding studies performed in this thesis, there are two broad further areas of research the data in this thesis supports. The two broad areas are the:

1. Further investigation of the differential expression of laminin isoforms and pathophysiological relevance of different laminin isoforms in stroke and other CNS diseases.
2. Investigation of the crosstalk between IL-1 signalling, the ECM and the Hippo pathway.

The data presented in this thesis add to evidence in the literature that laminin isoforms are differentially regulated and confer different physiological properties. Indeed, the differential roles of LM-8 and LM-10 have been demonstrated in an experimental model of multiple sclerosis (Sixt et al., 2001) and different laminin isoforms are differentially expressed after hypoxia (Halder et al., 2018). In Chapter 3 I demonstrated that different ECM coatings modulate the inflammatory response of cerebral endothelial cells *in vitro*, and in Chapter 4 I demonstrated that laminin α4 and laminin α5 are differentially regulated after stroke and are under different mechanisms as only laminin α4 is regulated by endothelial IL-1R1 signalling. Critically, the study in Chapter 4 identified 28 d post-stroke as a key time point for laminin expression. Thus, I suggest that this acts as evidence of the importance of research during the chronic phase post-stroke to understand repair mechanisms, since currently the majority of studies have focussed on the acute phase. Although I demonstrated a temporal profile of laminin α4 and laminin α5 expression, I only investigated BrdU analysis at 14 d and did not investigate other outcome measured of angiogenesis, neurogenesis or inflammation. Future experiments should determine the physiological relevance of altered laminin α4 expression after IL-1R1 deletion. In particular the effect of the altered laminin α4 expression at 2 d on

neutrophil transmigration and BBB integrity should be determined. Furthermore, the measurement of CBF in the cerebral endothelial IL-1R1 KO mice at chronic time points would be of particular interest as it has been previously demonstrated that deletion of endothelial IL-1R1 reduces early perfusion deficits 30 min after reperfusion in ischaemic stroke (Wong et al., 2019). Other techniques such as MRI to measure brain angiogenesis could also be employed (Seevinck et al., 2010). Although I did not observe an effect of laminin α5 deletion on infarct volume or CBF recovery after ischaemic stroke in Chapter 5, I still believe that the cell-specific deletion of laminin isoforms provide a valuable tool in order to determine the roles of laminin isoforms in disease. Considering that I observed an increase in laminin α5 expression at 28 d in Chapter 4, I suggest that future experiments using the brain endothelial laminin α5 KO should investigate repair mechanisms at 28 d as this may be the critical time point. The role of laminin α4 in ischaemic stroke should be investigated through conditional genetic deletion in cerebral endothelial cells. Although this thesis focused on ischaemic stroke, the literature demonstrates the role of laminin in different disease settings such as EAE and thus I suggest future experiments should also be aimed at dissecting basic mechanisms whereby laminin produces an altered physiological response. In particular these mechanisms may be focused on cellular transmigration, BBB integrity and endothelial activation under inflammatory and hypoxic stimulus.

A key finding from this thesis that should inform future studies is the relationship between IL-1β signalling pathways, the ECM and the Hippo pathway. Considering the contribution of IL-1 in the pathogenesis of stroke and the findings in Chapter 3 demonstrating novel crosstalk between IL-1β and YAP, the role of the Hippo pathway should be investigated further in stroke since research in the literature is currently limited. However, a recent study demonstrated that the YAP agonist dexamethasone reduced infarct volume and increased TJ proteins after cerebral ischaemia, suggesting that YAP may play a protective role (Gong et al., 2019). Future studies should use a combination of *in vitro* and *in vivo* approaches which would help to provide comprehensive insights and enable both the *in vitro* dissection of mechanisms and *in vivo* observations after genetic deletion of YAP in experimental stroke models. Furthermore, understanding the cell-specific contribution of IL-1 and YAP signalling would also help to shape cell-specific targeting therapies or therapy aimed at blocking IL-1R1. There has been increasing

evidence implicating the Hippo pathway in inflammation and vascular biology (Boopathy and Hong, 2019; Wang et al., 2020). Interestingly, YAP signalling has been implicated in atherosclerosis (K.-C. Wang et al., 2016; L. Wang et al., 2016), and ECM changes (Katsuda and Kaji, 2003; Chistiakov et al., 2013) and inflammation (Libby, 2009) are associated with the development of the disease. Thus, the investigation of Hippo signalling, IL-1 and ECM changes in atherosclerotic prone mice would also be of particular interest. The investigation of Hippo/YAP signalling could also be critical in other cerebrovascular diseases and Alzheimer's disease considering the inflammatory components often associated with them.

6.4. **Concluding remarks**

In summary, this thesis has contributed to advanced knowledge regarding the relationship between IL-1β and the ECM *in vitro*, specifically the role of LM-10, as well as the role of cerebrovasculature IL-1R1 signalling on laminin expression after cerebral ischaemia *in vivo*. I established LM-10 as a modulator of IL-1β-induced cerebral endothelial activation and of angiogenic mechanisms *in vitro*. I have elucidated a novel crosstalk between IL-1β and Hippo signalling. I provided novel evidence that endothelial IL-1R1 regulates laminin α4 expression but not laminin α5 expression post-stroke. Although I successfully created a new brain endothelial laminin α5 conditional deletion genetic strain of mouse, I did not demonstrate a role of laminin α5 deletion after ischaemic stroke. Despite not demonstrating a role of laminin α5 in ischaemic stroke, I still stress that further investigation of the isoform specific roles of laminins in CNS disorders is of importance. I strongly believe that further investigation of the crosstalk between IL-1, the ECM and the Hippo pathway could underpin several cerebrovascular diseases. Through the identification of signalling mechanisms, the potential of identifying therapeutic targets could become a reality and offer clinical relevance for a broad spectrum of diseases.

Bibliography

Abbott, N. J., Patabendige, A. A. K., Dolman, D. E. M., Yusof, S. R. and Begley, D. J. (2010). Structure and function of the blood-brain barrier. *Neurobiology of Disease*, 37(1), 13–25.

Abbott, N. J., Rönnbäck, L. and Hansson, E. (2006). Astrocyte-endothelial interactions at the blood-brain barrier. *Nature Reviews Neuroscience*, 7(1), 41–53.

Abdulaal, W. H., Walker, C. R., Costello, R., Redondo-Castro, E., Mufazalov, I. A., Papaemmanouil, A., Rothwell, N. J., Allan, S. M., Waisman, A., Pinteaux, E. and Müller, W. (2016). Characterization of a conditional interleukin-1 receptor 1 mouse mutant using the Cre/LoxP system. *European Journal of Immunology*, 46(4), 912–918.

Adamczak, J. M., Schneider, G., Nelles, M., Que, I., Suidgeest, E., van der Weerd, L., Löwik, C. and Hoehn, M. (2014). In vivo bioluminescence imaging of vascular remodeling after stroke. *Frontiers in cellular neuroscience*, 8(September), 274.

Adams, H. ., Bendixen, B. ., Kappelle, L. ., Biller, J., Love, B. ., Gordon, D. . and Marsh, E. . (1993). Classification of Subtype of Acute Ischemic Stroke. *Stroke*, 23(1), 35–41.

Allen, C. L. and Bayraktutan, U. (2009). Oxidative stress and its role in the pathogenesis of ischaemic stroke. *International Journal of Stroke*, 4(6), 461–470.

Allen, C., Thornton, P., Denes, A., McColl, B. W., Pierozynski, A., Monestier, M., Pinteaux, E., Rothwell, N. J. and Allan, S. M. (2012). Neutrophil Cerebrovascular Transmigration Triggers Rapid Neurotoxicity through Release of Proteases Associated with Decondensed DNA. *The Journal of Immunology*, 189(1), 381–392.

Angels Font, M., Arboix, A. and Krupinski, J. (2010). Angiogenesis, Neurogenesis and Neuroplasticity in Ischemic Stroke. *Current Cardiology Reviews*, 6(3), 238–244.

Anrather, J. and Iadecola, C. (2016). Inflammation and Stroke: An Overview. *Neurotherapeutics*, 13(4), 661–670.

Antoni, D., Burckel, H., Josset, E. and Noel, G. (2015). Three-dimensional cell culture: a breakthrough in vivo. *International journal of molecular sciences*, 16(3), 5517–27.

Arenillas, J. F., Sobrino, T., Castillo, J. and Dávalos, A. (2007). The role of angiogenesis in damage and recovery from ischemic stroke. *Current Treatment Options in Cardiovascular Medicine*, 9(3), 205–212.

Arkuszewski, M., Świat, M. and Opala, G. (2009). Perfusion computed tomography in prediction of functional outcome in patients with acute ischaemic stroke. *Nuclear Medicine Review*, 12(2), 89–94.

Asahi, M., Asahi, K., Jung, J. C., Del Zoppo, G. J., Fini, M. E. and Lo, E. H. (2000). Role for matrix metalloproteinase 9 after focal cerebral ischemia: Effects of gene knockout and enzyme inhibition with BB-94. *Journal of Cerebral Blood Flow and Metabolism*, 20(12), 1681–1689.

Assmann, J. C., Körbelin, J. and Schwaninger, M. (2016). Genetic manipulation of brain endothelial cells in vivo. *Biochimica et Biophysica Acta - Molecular Basis of Disease*, 1862(3), 381–394.

Azad, T., Janse Van Rensburg, H. J., Lightbody, E. D., Neveu, B., Champagne, A., Ghaffari, A., Kay, V. R., Hao, Y., Shen, H., Yeung, B., Croy, B. A., Guan, K. L., Pouliot, F., Zhang, J., Nicol, C. J. B. and Yang, X. (2018). A LATS biosensor screen identifies VEGFR as a regulator of the Hippo pathway in angiogenesis. *Nature Communications*, 9(1),.

Baeten, K. M. and Akassoglou, K. (2011). Extracellular matrix and matrix receptors in blood-brain barrier formation and stroke. *Developmental Neurobiology*, 71(11), 1018–1039.

Ballabh, P., Braun, A. and Nedergaard, M. (2004). The blood-brain barrier: An overview: Structure, regulation, and clinical implications. *Neurobiology of Disease*, 16(1), 1–13.

Bansal, S., Sangha, K. S. and Khatri, P. (2013). Drug Treatment of Acute Ischemic Stroke. *American Journal of Cardiovascular Drugs*, 13(1), 57–69.

Banwell, V., Sena, E. S. and Macleod, M. R. (2009). Systematic Review and Stratified Meta-analysis of the Efficacy of Interleukin-1 Receptor Antagonist in Animal Models of Stroke. *Journal of Stroke and Cerebrovascular Diseases*, 18(4), 269–276.

Basu, A., Krady, J. K. and Levison, S. W. (2004). Interleukin-1: A master regulator of neuroinflammation. *Journal of Neuroscience Research*, 78(2), 151–156.

Becerra-Calixto, A. and Cardona-Gómez, G. P. (2017). The role of astrocytes in neuroprotection after brain stroke: Potential in cell therapy. *Frontiers in Molecular Neuroscience*, 10(April), 1–12.

Belayev, L., Busto, R., Zhao, W. and Ginsberg, M. D. (1996). Quantitative evaluation of blood-brain barrier permeability following middle cerebral artery occlusion in rats. *Brain Research*, 739(1–2), 88–96.

Bergsbaken, T., Fink, S. L. and Cookson, B. T. (2009). Pyroptosis: Host cell death and inflammation. *Nature Reviews Microbiology*, 7(2), 99–109.

Boopathy, G. T. K. and Hong, W. (2019). Role of Hippo Pathway-YAP/TAZ signaling in angiogenesis. *Frontiers in Cell and Developmental Biology*, 7(APR), 1–12.

Boutin, H., LeFeuvre, R. A., Horai, R., Asano, M., Iwakura, Y. and Rothwell, N. J. (2001). Role of IL-1α and IL-1β in ischemic brain damage. *Journal of Neuroscience*, 21(15), 5528–5534.

Brough, D. and Denes, A. (2015). Interleukin-1α and brain inflammation. *IUBMB Life*, 67(5), 323–330.

Burnside, E. R. and Bradbury, E. J. (2014). Review: Manipulating the extracellular matrix and its role in brain and spinal cord plasticity and repair. *Neuropathology and Applied Neurobiology*, 40(1), 26–59.

Ceasrine, A. M., Ruiz-Otero, N., Lin, E. E., Lumelsky, D. N., Boehm, E. D. and Kuruvilla, R. (2019). Tamoxifen Improves Glucose Tolerance in a Delivery-, Sex-, and Strain-Dependent Manner in Mice. *Endocrinology*, 160(4), 782–790.

Cekanaviciute, E. and Buckwalter, M. S. (2016). Astrocytes: Integrative Regulators of Neuroinflammation in Stroke and Other Neurological Diseases. *Neurotherapeutics*, 13(4), 685–701.

Ceulemans, A. G., Zgavc, T., Kooijman, R., Hachimi-Idrissi, S., Sarre, S. and Michotte, Y. (2010). The dual role of the neuroinflammatory response after ischemic stroke: Modulatory effects of hypothermia. *Journal of Neuroinflammation*, 7(1), 74.

Chen, G. Y. and Nuñez, G. (2010). Sterile inflammation: Sensing and reacting to damage. *Nature Reviews Immunology*, 10(12), 826–837.

Chen, Z. L. and Strickland, S. (1997). Neuronal death in the hippocampus is promoted by plasmin-catalyzed degradation of laminin. *Cell*, 91(7), 917–925.

Chistiakov, D. A., Sobenin, I. A. and Orekhov, A. N. (2013). Vascular extracellular matrix in atherosclerosis. *Cardiology in Review*, 21(6), 270–288.

Chiu, J. J. and Chien, S. (2011). Effects of disturbed flow on vascular endothelium: Pathophysiological basis and clinical perspectives. *Physiological Reviews*, 91(1), 327–387.

Choi, H.-J., Kim, N.-E., Kim, B., Seo, M. and Heo, J. (2018). TNF-α-Induced YAP/TAZ Activity Mediates Leukocyte-Endothelial Adhesion by Regulating VCAM1 Expression in Endothelial Cells. *International Journal of Molecular Sciences*, 19(11), 3428.

Choi, H. J., Zhang, H., Park, H., Choi, K. S., Lee, H. W., Agrawal, V., Kim, Y. M. and Kwon, Y. G. (2015). Yes-associated protein regulates endothelial cell contact-mediated expression of angiopoietin-2. *Nature Communications*, 6(May), 1–14.

Collins, T., Read, M. A., Neish, A. S., Whitley, M. Z., Thanos, D. and Maniatis, T. (1995). Transcriptional regulation of endothelial cell adhesion molecules: NF-κB and cytokine-inducible enhancers. *The FASEB Journal*, 9(10), 899–909.

Connolly, E. S., Winfree, C. J., Prestigiacomo, C. J., Kim, S. C., Choudhri, T. F., Hoh, B. L., Naka, Y., Solomon, R. A. and Pinsky, D. J. (1997). Exacerbation of Cerebral Injury in Mice That Express the P-Selectin Gene. *Circulation Research*, 81(3), 304–310.

Davis, G. E. and Senger, D. R. (2005). Endothelial extracellular matrix: Biosynthesis, remodeling, and functions during vascular morphogenesis and neovessel stabilization. *Circulation Research*, 97(11), 1093–1107.

Deb, P., Sharma, S. and Hassan, K. M. (2010). Pathophysiologic mechanisms of acute ischemic stroke: An overview with emphasis on therapeutic significance beyond thrombolysis. *Pathophysiology*, 17(3), 197–218.

DeCicco-Skinner, K. L., Henry, G. H., Cataisson, C., Tabib, T., Curtis Gwilliam, J., Watson, N. J., Bullwinkle, E. M., Falkenburg, L., O'Neill, R. C., Morin, A. and Wiest, J. S. (2014). Endothelial cell tube formation assay for the in vitro study of angiogenesis. *Journal of Visualized Experiments*, 10(91), 1–8.

Denes, A., Pinteaux, E., Rothwell, N. J. and Allan, S. M. (2011). Interleukin-1 and stroke: Biomarker, harbinger of damage, and therapeutic target. *Cerebrovascular Diseases*, 32(6), 517–527.

Denes, A., Vidyasagar, R., Feng, J., Narvainen, J., McColl, B. W., Kauppinen, R. A. and Allan, S. M. (2007). Proliferating resident microglia after focal cerebral ischaemia in mice. *Journal of Cerebral Blood Flow and Metabolism*, 27(12), 1941–1953.

Dinarello, C. A. (2018). Overview of the IL-1 family in innate inflammation and acquired immunity. *Immunological Reviews*, 281(1), 8–27.

Domogatskaya, A., Rodin, S. and Tryggvason, K. (2012). Functional Diversity of Laminins. *Annual Review of Cell and Developmental Biology*, 28(1), 523–553.

Durbeej, M. (2010). Laminins. *Cell and Tissue Research*, 339(1), 259–268.

Edwards, D. N. and Bix, G. J. (2019). Roles of blood-brain barrier integrins and extracellular matrix in stroke. *American Journal of Physiology - Cell Physiology*, 316(2), C252–C263.

Emsley, H. C. A., Smith, C. J., Georgiou, R. F., Vail, A., Hopkins, S. J., Rothwell, N. J. and Tyrrell, P. J. (2005). A randomised phase II study of interleukin-1 receptor antagonist in acute stroke patients. *Journal of Neurology, Neurosurgery and Psychiatry*, 76(10), 1366–1372.

Encarnacion, A., Horie, N., Keren-Gill, H., Bliss, T. M., Steinberg, G. K. and Shamloo, M. (2011). Long-term behavioral assessment of function in an experimental model for ischemic stroke. *Journal of Neuroscience Methods*, 196(2), 247–257.

Faraco, G., Park, L., Anrather, J. and Iadecola, C. (2017). Brain perivascular macrophages: characterization and functional roles in health and disease. *Journal of Molecular Medicine*, 95(11), 1143–1152.

Feigin, V. L. (2019). Anthology of stroke epidemiology in the 20th and 21st centuries: Assessing the past, the present, and envisioning the future. *International Journal of Stroke*, 14(3), 223–237.

Feigin, V. L., Norrving, B. and Mensah, G. A. (2017). Global Burden of Stroke. *Circulation Research*, 120(3), 439–448.

Feigin, V. L., Roth, G. A., Naghavi, M., Parmar, P., Krishnamurthi, R., Chugh, S.,

Mensah, G. A., Norrving, B., Shiue, I., Ng, M., Estep, K., Cercy, K., Murray, C. J. L. and Forouzanfar, M. H. (2016). Global burden of stroke and risk factors in 188 countries, during 1990–2013: a systematic analysis for the Global Burden of Disease Study 2013. *The Lancet Neurology*, 15(9), 913–924.

Fenwick, N., Griffin, G. and Gauthier, C. (2009). The welfare of animals used in science: how the 'Three Rs' ethic guides improvements. *The Canadian veterinary journal = La revue veterinaire canadienne*, 50(5), 523–30.

Fluri, F., Schuhmann, M. K. and Kleinschnitz, C. (2015). Animal models of ischemic stroke and their application in clinical research. *Drug Design, Development and Therapy*, 9 3445–3454.

Gao, D., Nolan, D. J., Mellick, A. S., Bambino, K., McDonnell, K. and Mittal, V. (2008). Endothelial Progenitor Cells Control the Angiogenic Switch in Mouse Lung Metastasis. *Science*, 319(5860), 195–198.

Gautam, J., Miner, J. H. and Yao, Y. (2019). Loss of Endothelial Laminin α5 Exacerbates Hemorrhagic Brain Injury. *Translational Stroke Research*, 10(6), 705–718.

Gautam, J., Zhang, X. and Yao, Y. (2016). The role of pericytic laminin in blood brain barrier integrity maintenance. *Scientific Reports*, 6(October), 1–13.

Gong, P., Zhang, Z., Zou, C., Tian, Q., Chen, X., Hong, M., Liu, X., Chen, Q., Xu, Z., Li, M. and Wang, J. (2019). Hippo/YAP signaling pathway mitigates blood-brain barrier disruption after cerebral ischemia/reperfusion injury. *Behavioural Brain Research*, 356(July 2018), 8–17.

Goyal, M., Menon, B. K., Van Zwam, W. H., Dippel, D. W. J., Mitchell, P. J., Demchuk, A. M., Dávalos, A., Majoie, C. B. L. M., Van Der Lugt, A., De Miquel, M. A., Donnan, G. A., Roos, Y. B. W. E. M., Bonafe, A., Jahan, R., Diener, H. C., Van Den Berg, L. A., Levy, E. I., Berkhemer, O. A., Pereira, V. M., Rempel, J., Millán, M., Davis, S. M., Roy, D., Thornton, J., Román, L. S., Ribó, M., Beumer, D., Stouch, B., Brown, S., Campbell, B. C. V., Van Oostenbrugge, R. J., Saver, J. L., Hill, M. D. and Jovin, T. G. (2016). Endovascular thrombectomy after large-vessel ischaemic stroke: A meta-analysis of individual patient data from five randomised trials. *The Lancet*, 387(10029), 1723–1731.

Guruswamy, R. and Elali, A. (2017). Complex roles of microglial cells in ischemic stroke pathobiology: New insights and future directions. *International Journal of Molecular Sciences*, 18(3),.

Gutiérrez, M., Merino, J. J., Alonso de Leciñana, M. and Díez-Tejedor, E. (2009). Cerebral protection, brain repair, plasticity and cell therapy in ischemic stroke. *Cerebrovascular diseases (Basel, Switzerland)*, 27 Suppl 1(SUPPL. 1), 177–86.

Halder, Sebok K., Kant, R. and Milner, R. (2018). Chronic mild hypoxia increases expression of laminins 111 and 411 and the laminin receptor α6β1 integrin at the blood-brain barrier. *Brain Research*, 1700(12), 78–85.

Hallmann, R. (2005). Expression and Function of Laminins in the Embryonic and Mature Vasculature. *Physiological Reviews*, 85(3), 979–1000.

Han, M. H., Lee, E. H. and Koh, S. H. (2016). Current opinion on the role of neurogenesis in the therapeutic strategies for alzheimer disease, parkinson disease, and ischemic stroke; considering neuronal voiding function. *International Neurourology Journal*, 20(4), 276–287.

Hannocks, M. J., Pizzo, M. E., Huppert, J., Deshpande, T., Abbott, N. J., Thorne, R. G. and Sorokin, L. (2018). Molecular characterization of perivascular drainage pathways in the murine brain. *Journal of Cerebral Blood Flow and Metabolism*, 38(4), 669–686.

Harris, J., Hartman, M., Roche, C., Zeng, S. G., O'Shea, A., Sharp, F. A., Lambe, E. M., Creagh, E. M., Golenbock, D. T., Tschopp, J. and Kornfeld, H. (2011). Autophagy controls IL-1β secretion by targeting Pro-IL-1β for degradation. *Journal of Biological Chemistry*, 286(11), 9587–9597.

Hayashi, T., Noshita, N., Sugawara, T. and Chan, P. H. (2003). Temporal profile of angiogenesis and expression of related genes in the brain after ischemia. *Journal of Cerebral Blood Flow and Metabolism*, 23(2), 166–180.

Helms, H. C., Abbott, N. J., Burek, M., Cecchelli, R., Couraud, P.-O., Deli, M. A., Förster, C., Galla, H. J., Romero, I. A., Shusta, E. V, Stebbins, M. J., Vandenhaute, E., Weksler, B. and Brodin, B. (2016). In vitro models of the blood–brain barrier: An overview of commonly used brain endothelial cell culture models and guidelines for their use. *Journal of Cerebral Blood Flow & Metabolism*, 36(5), 862–890.

Hermann, D. M., Buga, A. M. and Popa-Wagner, A. (2015). Neurovascular remodeling in the aged ischemic brain. *Journal of Neural Transmission*, 122 25–33.

Herx, L. M. and Yong, V. W. (2001). Interleukin-1β is required for the early evolution of reactive astrogliosis following CNS lesion. *Journal of Neuropathology and Experimental Neurology*, 60(10), 961–971.

Hori, S., Ohtsuki, S., Hosoya, K. I., Nakashima, E. and Terasaki, T. (2004). A pericyte-derived angiopoietin-1 multimeric complex induces occludin gene expression in brain capillary endothelial cells through Tie-2 activation in vitro. *Journal of Neurochemistry*, 89(2), 503–513.

Howells, D. W., Porritt, M. J., Rewell, S. S. J., O'Collins, V., Sena, E. S., Van Der Worp, H. B., Traystman, R. J. and MacLeod, M. R. (2010). Different strokes for different folks: The rich diversity of animal models of focal cerebral ischemia. *Journal of Cerebral Blood Flow and Metabolism*, 30(8), 1412–1431.

Hu, X., Michael De Silva, T., Chen, J. and Faraci, F. M. (2017). Cerebral Vascular Disease and Neurovascular Injury in Ischemic Stroke. *Circulation Research*, 120(3), 449–471.

Huang, D., Li, X., Sun, L., Huang, P., Ying, H., Wang, H., Wu, J. and Song, H. (2016). Regulation of Hippo signalling by p38 signalling. *Journal of Molecular Cell Biology*, 8(4), 328–337.

Huang, J., Choudhri, T. F., Winfree, C. J., McTaggart, R. A., Kiss, S., Mocco, J., Kim, L. J., Protopsaltis, T. S., Zhang, Y., Pinsky, D. J. and Connolly, E. S. (2000). Postischemic Cerebrovascular E-Selectin Expression Mediates Tissue Injury in Murine Stroke. *Stroke*, 31(12), 3047–3053.

Iadecola, C. and Anrather, J. (2011). Stroke research at a crossroad: asking the brain for directions. *Nature neuroscience*, 14(11), 1363–8.

Indyk, J. A., Chen, Z. L., Tsirka, S. E. and Strickland, S. (2003). Laminin chain expression suggests that laminin-10 is a major isoform in the mouse hippocampus and is degraded by the tissue plasminogen activator/plasmin protease cascade during excitotoxic injury. *Neuroscience*, 116(2), 359–371.

Ji, K. and Tsirka, S. E. (2012). Inflammation modulates expression of laminin in the central nervous system following ischemic injury. *Journal of Neuroinflammation*, 9(1), 610.

Jin, W. N., Shi, S. X. Y., Li, Z., Li, M., Wood, K., Gonzales, R. J. and Liu, Q. (2017). Depletion of microglia exacerbates postischemic inflammation and brain injury. *Journal of Cerebral Blood Flow and Metabolism*, 37(6), 2224–2236.

John, G. R., Chen, L., Rivieccio, M. A., Melendez-Vasquez, C. V., Hartley, A. and Brosnan, C. F. (2004). Interleukin-1β Induces A Reactive Astroglial Phenotype Via Deactivation of the Rho GTPase-Rock Axis. *Journal of Neuroscience*, 24(11), 2837–2845.

Jucker, M., Tian, M., Norton, D. D., Sherman, C. and Kusiak, J. W. (1996). Laminin α2 is a component of brain capillary basement membrane: Reduced expression in dystrophic dy mice. *Neuroscience*, 71(4), 1153–1161.

Justice, R. W., Zilian, O., Woods, D. F., Noll, M. and Bryant, P. J. (1995). The Drosophila tumor suppressor gene warts encodes a homolog of human myotonic dystrophy kinase and is required for the control of cell shape and proliferation. *Genes and Development*, 9(5), 534–546.

Kang, M. and Yao, Y. (2020). Basement Membrane Changes in Ischemic Stroke. *Stroke* 1344–1352.

Kang, Z., Zhu, H., Luan, H., Han, F. and Jiang, W. (2014). Curculigoside A induces angiogenesis through VCAM-1/Egr-3/CREB/VEGF signaling pathway. *Neuroscience*, 267 232–240.

Kangwantas, K., Pinteaux, E. and Penny, J. (2016). The extracellular matrix protein laminin-10 promotes blood–brain barrier repair after hypoxia and inflammation in vitro. *Journal of Neuroinflammation*, 13(1), 25.

Kasselman, L. J., Kintner, J., Sideris, A., Pasnikowski, E., Krellman, J. W., Shah, S., Rudge, J. S., Yancopoulos, G. D., Wiegand, S. J. and Croll, S. D. (2007). Dexamethasone treatment and ICAM-1 deficiency impair VEGF-induced angiogenesis in adult brain. *Journal of Vascular Research*, 44(4), 283–291.

Katsuda, S. and Kaji, T. (2003). Atherosclerosis and extracellular matrix. *Journal of atherosclerosis and thrombosis*, 10(5), 267–274.

Kazmi, S. M. S., Richards, L. M., Schrandt, C. J., Davis, M. A. and Dunn, A. K. (2015). Expanding applications, accuracy, and interpretation of laser speckle contrast imaging of cerebral blood flow. *Journal of Cerebral Blood Flow and Metabolism*, 35(7), 1076–1084.

Keaney, J. and Campbell, M. (2015). The dynamic blood-brain barrier. *FEBS Journal*, 282(21), 4067–4079.

Khoshnam, S. E., Winlow, W., Farzaneh, M., Farbood, Y. and Moghaddam, H. F. (2017). Pathogenic mechanisms following ischemic stroke. *Neurological Sciences*, 38(7), 1167–1186.

Kilkenny, C., Browne, W. J., Cuthill, I. C., Emerson, M. and Altman, D. G. (2010). Improving bioscience research reporting: The arrive guidelines for reporting animal research. *PLoS Biology*, 8(6), 6–10.

Kim, J. H., Byun, H. M., Chung, E. C., Chung, H. Y. and Bae, O. N. (2013). Loss of integrity: Impairment of the blood-brain barrier in heavy metal-associated ischemic stroke. *Toxicological Research*, 29(3), 157–164.

Kim, J. Y., Kawabori, M. and Yenari, M. A. (2014). Innate inflammatory responses in stroke: mechanisms and potential therapeutic targets. *Current medicinal chemistry*, 21(18), 2076–97.

Kim, J. Y., Park, J., Chang, J. Y., Kim, S.-H. and Lee, J. E. (2016). Inflammation after Ischemic Stroke: The Role of Leukocytes and Glial Cells. *Experimental Neurobiology*, 25(5), 241.

Kim, Jongshin, Lim, D., Koh, G. Y., Kim, Jongshin, Kim, Y. H., Kim, Jaeryung, Park, D. Y., Bae, H., Lee, D. and Kim, K. H. (2017). YAP / TAZ regulates sprouting angiogenesis and vascular barrier maturation Find the latest version : YAP / TAZ regulates sprouting angiogenesis and vascular barrier maturation, 127(9), 3441–3461.

Kim, Y. K., Na, K. S., Myint, A. M. and Leonard, B. E. (2016). The role of pro-inflammatory cytokines in neuroinflammation, neurogenesis and the neuroendocrine system in major depression. *Progress in Neuro-Psychopharmacology and Biological Psychiatry*, 64 277–284.

Koh, S. H. and Park, H. H. (2017). Neurogenesis in Stroke Recovery. *Translational Stroke Research*, 8(1), 3–13.

Koizumi, J., Yoshida, Y., Nakazawa, T. and Ooneda, G. (1986). Experimental studies of ischemic brain edema. *Nosotchu*, 8(1), 1–8.

Konsman, J. P., Vigues, S., Mackerlova, L., Bristow, A. and Blomqvist, A. (2004). Rat brain vascular distribution of interleukin-1 type-1 receptor immunoreactivity: relationship to patterns of inducible cyclooxygenase expression by peripheral inflammatory stimuli. *The Journal of comparative neurology*, 472(1), 113–29.

Kristianto, J., Johnson, M. G., Zastrow, R. K., Radcliff, A. B. and Blank, R. D. (2017). Spontaneous recombinase activity of Cre–ERT2 in vivo. *Transgenic Research*, 26(3), 411–417.

Krupinski, J., Kaluza, J., Kumar, P., Kumar, S. and Wang, J. (1994). Role of angiogenesis in patients with cerebral ischemic stroke. *Stroke*, 25(9), 1794–1798.

Kwok, J. C. F., Dick, G., Wang, D. and Fawcett, J. W. (2011). Extracellular matrix and perineuronal nets in CNS repair. *Developmental Neurobiology*, 71(11), 1073–1089.

Lakhan, S. E., Kirchgessner, A. and Hofer, M. (2009). Inflammatory mechanisms in ischemic stroke: Therapeutic approaches. *Journal of Translational Medicine*, 7 1–11.

Lau, L. W., Cua, R., Keough, M. B., Haylock-Jacobs, S. and Yong, V. W. (2013). Pathophysiology of the brain extracellular matrix: A new target for remyelination. *Nature Reviews Neuroscience*, 14(10), 722–729.

Li, L., Liu, F., Welser-Alves, J. V, McCullough, L. D. and Milner, R. (2012). Upregulation of fibronectin and the α5β1 and αvβ3 integrins on blood vessels within the cerebral ischemic penumbra. *Experimental neurology*, 233(1), 283–91.

Liao, S., Luo, C., Cao, B., Hu, H., Wang, S., Yue, H., Chen, L. and Zhou, Z. (2017). Endothelial Progenitor Cells for Ischemic Stroke: Update on Basic Research and Application. *Stem Cells International*, 2017.

Libby, P. (2009). Inframmation in Atherosclerosis: From Pathology To Practice. *J Am Coll Cardiol.*, 53(23), 2129–2138.

Libby, P., Ridker, P. M. and Maseri, A. (2002). Inflammation and atherosclerosis. *Circulation*, 105(9), 1135–1143.

Liesz, A., Suri-Payer, E., Veltkamp, C., Doerr, H., Sommer, C., Rivest, S., Giese, T. and Veltkamp, R. (2009). Regulatory T cells are key cerebroprotective immunomodulators in acute experimental stroke. *Nature Medicine*, 15(2), 192–199.

Ligasová, A., Konečný, P., Frydrych, I. and Koberna, K. (2017). Looking for ugly ducklings: The role of the stability of BrdU-antibody complex and the improved method of the detection of DNA replication. *PLoS ONE*, 12(3), 1–18.

Lin, T.-N., Sun, S.-W., Cheung, W.-M., Li, F. and Chang, C. (2002). Dynamic changes in cerebral blood flow and angiogenesis after transient focal cerebral ischemia in rats. Evaluation with serial magnetic resonance imaging. *Stroke*, 33(12), 2985–91.

Liu, F., Lagares, D., Choi, K. M., Stopfer, L., Marinković, A., Vrbanac, V., Probst, C. K., Hiemer, S. E., Sisson, T. H., Horowitz, J. C., Rosas, I. O., Fredenburgh, L. E., Feghali-Bostwick, C., Varelas, X., Tager, A. M. and Tschumperlin, D. J. (2015). Mechanosignaling through YAP and TAZ drives fibroblast activation and fibrosis. *American Journal of Physiology - Lung Cellular and Molecular Physiology*, 308(4), L344–L357.

Liu, T., Zhang, L., Joo, D. and Sun, S. C. (2017). NF-κB signaling in inflammation. *Signal Transduction and Targeted Therapy*, 2(April),.

Liu, X., Nemeth, D. P., McKim, D. B., Zhu, L., DiSabato, D. J., Berdysz, O., Gorantla, G., Oliver, B., Witcher, K. G., Wang, Y., Negray, C. E., Vegesna, R. S., Sheridan, J. F., Godbout, J. P., Robson, M. J., Blakely, R. D., Popovich, P. G., Bilbo, S. D. and Quan, N. (2019). Cell-Type-Specific Interleukin 1 Receptor 1 Signaling in the Brain Regulates Distinct Neuroimmune Activities. *Immunity*, 0(0), 1–17.

Liu, X. S., Chopp, M., Zhang, R. L., Hozeska-Solgot, A., Gregg, S. C., Buller, B., Lu, M. and Zhang, Z. G. (2009). Angiopoietin 2 mediates the differentiation and migration of neural progenitor cells in the subventricular zone after stroke. *Journal of Biological*

Chemistry, 284(34), 22680–22689.

Liu, X. S., Zhang, Z. G., Zhang, R. L., Gregg, S., Morris, D. C., Wang, Y. and Chopp, M. (2007). Stroke induces gene profile changes associated with neurogenesis and angiogenesis in adult subventricular zone progenitor cells. *Journal of Cerebral Blood Flow and Metabolism*, 27(3), 564–574.

Longa, E. Z., Weinstein, P. R., Carlson, S. and Cummins, R. (1989). Reversible middle cerebral artery occlusion without craniectomy in rats. *Stroke*, 20(1), 84–91.

Lopez-Castejon, G. and Brough, D. (2011). Understanding the mechanism of IL-1β secretion. *Cytokine and Growth Factor Reviews*, 22(4), 189–195.

Lu, P., Takai, K., Weaver, V. M. and Werb, Z. (2011). Extracellular matrix degradation and remodeling in development and disease. *Cold Spring Harb Perspect Biol*, 3(12), 1–24.

Luheshi, N. M., Kovács, K. J., Lopez-Castejon, G., Brough, D. and Denes, A. (2011). Interleukin-1α expression precedes IL-1β after ischemic brain injury and is localised to areas of focal neuronal loss and penumbral tissues. *Journal of neuroinflammation*, 8(1), 186.

Luissint, A. C., Artus, C., Glacial, F., Ganeshamoorthy, K. and Couraud, P. O. (2012). Tight junctions at the blood brain barrier: Physiological architecture and disease-associated dysregulation. *Fluids and Barriers of the CNS*, 9(1), 1–12.

Lv, Y., Kim, K., Sheng, Y., Cho, J., Qian, Z., Zhao, Y.-Y., Hu, Gang, Pan, D., Malik, A. B. and Hu, Guochang (2018). YAP Controls Endothelial Activation and Vascular Inflammation Through TRAF6Novelty and Significance. *Circulation Research*, 123(1), 43–56.

MacKenzie, A., Wilson, H. L., Kiss-Toth, E., Dower, S. K., North, R. A. and Surprenant, A. (2001). Rapid secretion of interleukin-1β by microvesicle shedding. *Immunity*, 15(5), 825–835.

Maysami, S., Wong, R., Pradillo, J. M., Denes, A., Dhungana, H., Malm, T., Koistinaho, J., Orset, C., Rahman, M., Rubio, M., Schwaninger, M., Vivien, D., Bath, P. M., Rothwell, N. J. and Allan, S. M. (2016). A cross-laboratory preclinical study on the effectiveness of interleukin-1 receptor antagonist in stroke. *Journal of Cerebral Blood Flow & Metabolism*, 36(3), 596–605.

McMeekin, P., White, P., James, M. A., Price, C. I., Flynn, D. and Ford, G. A. (2017). Estimating the number of UK stroke patients eligible for endovascular thrombectomy. *European Stroke Journal*, 2(4), 319–326.

Menezes, M. J., McClenahan, F. K., Leiton, C. V., Aranmolate, A., Shan, X. and Colognato, H. (2014). The extracellular matrix protein laminin α2 regulates the maturation and function of the blood–brain barrier. *Journal of Neuroscience*, 34(46), 15260–15280.

Meng, Z., Moroishi, T. and Guan, K. L. (2016). Mechanisms of Hippo pathway regulation. *Genes and Development*, 30(1), 1–17.

Merali, Z., Huang, K., Mikulis, D., Silver, F. and Kassner, A. (2017). Evolution of blood-brain-barrier permeability after acute ischemic stroke. *PLoS ONE*, 12(2), 1–11.

Merson, T. D. and Bourne, J. A. (2014). Endogenous neurogenesis following ischaemic brain injury: Insights for therapeutic strategies. *International Journal of Biochemistry and Cell Biology*, 56 4–19.

Mi, H., Haeberle, H. and Barres, B. A. (2001). Induction of astrocyte differentiation by endothelial cells. *Journal of Neuroscience*, 21(5), 1538–1547.

Miner, J. H., Cunningham, J. and Sanes, J. R. (1998). Roles for laminin in embryogenesis: Exencephaly, syndactyly, and placentopathy in mice lacking the laminin α5 chain. *Journal of Cell Biology*, 143(6), 1713–1723.

Miner, J. H., Patton, B. L., Lentz, S. I., Gilbert, D. J., Snider, W. D., Jenkins, N. A., Copeland, N. G. and Sanes, J. R. (1997). The Laminin α Chains: Expression, Developmental Transitions, and Chromosomal Locations of α1-5, Identification of Heterotrimeric Laminins 8–11, and Cloning of a Novel α3 Isoform. *Journal of Cell Biology*, 137(3), 685–701.

Miranti, C., Miranti, C. K. and Brugge, J. S. (2015). perspective on integrin signal transduction Sensing the environment : a historical perspective on integrin signal transduction, 4(May 2002),.

Moore, C. J. and Winder, S. J. (2010). Dystroglycan versatility in cell adhesion: A tale of multiple motifs. *Cell Communication and Signaling*, 8 1–12.

Mouw, J. K., Ou, G. and Weaver, V. M. (2014). Extracellular matrix assembly: A multiscale deconstruction. *Nature Reviews Molecular Cell Biology*, 15(12), 771–785.

Munji, R. N., Soung, A. L., Weiner, G. A., Sohet, F., Semple, B. D., Trivedi, A., Gimlin, K., Kotoda, M., Korai, M., Aydin, S., Batugal, A., Cabangcala, A. C., Schupp, P. G., Oldham, M. C., Hashimoto, T., Noble-Haeusslein, L. J. and Daneman, R. (2019). Profiling the mouse brain endothelial transcriptome in health and disease models reveals a core blood–brain barrier dysfunction module. *Nature Neuroscience*, 22(11), 1892–1902.

Murray, K. N., Parry-Jones, A. R. and Allan, S. M. (2015). Interleukin-1 and acute brain injury. *Frontiers in Cellular Neuroscience*, 9(February), 1–17.

Musuka, T. D., Wilton, S. B., Traboulsi, M. and Hill, M. D. (2015). Diagnosis and management of acute ischemic stroke: speed is critical. *CMAJ : Canadian Medical Association journal = journal de l'Association medicale canadienne*, 187(12), 887–93.

Nguyen, N. M., Kelley, D. G., Schlueter, J. A., Meyer, M. J., Senior, R. M. and Miner, J. H. (2005). Epithelial laminin α5 is necessary for distal epithelial cell maturation, VEGF production, and alveolization in the developing murine lung. *Developmental Biology*, 282(1), 111–125.

Ni, Y., Teng, T., Li, R., Simonyi, A., Sun, G. Y. and Lee, J. C. (2017). TNFα alters occludin and cerebral endothelial permeability: Role of p38MAPK. *PLoS ONE*, 12(2), 1–20.

Nirwane, A., Johnson, J., Nguyen, B., Miner, J. H. and Yao, Y. (2019). Mural cell-derived laminin-α5 plays a detrimental role in ischemic stroke. *Acta neuropathologica communications*, 7(1), 23.

Oeckinghaus, A. and Ghosh, S. (2009). The NF-kappaB family of transcription factors and its regulation. *Cold Spring Harbor perspectives in biology*, 1(4), 1–14.

Park, J. A. and Kwon, Y. G. (2018). Hippo-YAP/TAZ signaling in angiogenesis. *BMB Reports*, 51(3), 157–162.

Percie du Sert, N., Alfieri, A., Allan, S. M., Carswell, H. V. O., Deuchar, G. A., Farr, T. D., Flecknell, P., Gallagher, L., Gibson, C. L., Haley, M. J., Macleod, M. R., McColl, B. W., McCabe, C., Morancho, A., Moon, L. D. F., O'Neill, M. J., Pérez de Puig, I., Planas, A., Ragan, C. I., Rosell, A., Roy, L. A., Ryder, K. O., Simats, A., Sena, E. S., Sutherland, B. A., Tricklebank, M. D., Trueman, R. C., Whitfield, L., Wong, R. and Macrae, I. M. (2017). The IMPROVE Guidelines (Ischaemia Models: Procedural Refinements Of in Vivo Experiments). *Journal of Cerebral Blood Flow and Metabolism*, 37(11), 3488–3517.

Perez-de-Puig, I., Miró-Mur, F., Ferrer-Ferrer, M., Gelpi, E., Pedragosa, J., Justicia, C., Urra, X., Chamorro, A. and Planas, A. M. (2015). Neutrophil recruitment to the brain in mouse and human ischemic stroke. *Acta Neuropathologica*, 129(2), 239–257.

Piccolo, S., Dupont, S. and Cordenonsi, M. (2014). The Biology of YAP/TAZ: Hippo Signaling and Beyond. *Physiological Reviews*, 94(4), 1287–1312.

Pinteaux, E., Parker, L. C., Rothwell, N. J. and Luheshi, G. N. (2002). Expression of interleukin-1 receptors and their role in interleukin-1 actions in murine microglial cells.

Journal of Neurochemistry, 83(4), 754–763.

Plantman, S., Patarroyo, M., Fried, K., Domogatskaya, A., Tryggvason, K., Hammarberg, H. and Cullheim, S. (2008). Integrin-laminin interactions controlling neurite outgrowth from adult DRG neurons in vitro. *Molecular and Cellular Neuroscience*, 39(1), 50–62.

Potjewyd, G., Moxon, S., Wang, T., Domingos, M. and Hooper, N. M. (2018). Tissue Engineering 3D Neurovascular Units: A Biomaterials and Bioprinting Perspective. *Trends in Biotechnology*, 36(4), 457–472.

Radisavljevic, Z., Avraham, H. and Avraham, S. (2000). Vascular endothelial growth factor up-regulates ICAM-1 expression via the phosphatidylinositol 3 OH-kinase/AKT/nitric oxide pathway and modulates migration of brain microvascular endothelial cells. *Journal of Biological Chemistry*, 275(27), 20770–20774.

Raichle, M. E. and Gusnard, D. A. (2002). Appraising the brain's energy budget. *Proceedings of the National Academy of Sciences of the United States of America*, 99(16), 10237–10239.

Rajkovic, I., Wong, R., Lemarchand, E., Rivers-Auty, J., Rajkovic, O., Garlanda, C., Allan, S. M. and Pinteaux, E. (2018). Pentraxin 3 promotes long-term cerebral blood flow recovery, angiogenesis, and neuronal survival after stroke. *Journal of Molecular Medicine*, 96(12), 1319–1332.

Rauch, U. (2007). Brain matrix: Structure, turnover and necessity. *Biochemical Society Transactions*, 35(4), 656–660.

Relton, J. K. and Rothwell, N. J. (1992). Interleukin-1 receptor antagonist inhibits ischaemic and excitotoxic neuronal damage in the rat. *Brain Research Bulletin*, 29(2), 243–246.

Ridder, D. A., Lang, M. F., Salinin, S., Röderer, J. P., Struss, M., Christiane, M. G. and Schwaninger, M. (2011). TAK1 in brain endothelial cells mediates fever and lethargy. *Journal of Experimental Medicine*, 208(13), 2615–2623.

Rodriguez-Grande, B., Swana, M., Nguyen, L., Englezou, P., Maysami, S., Allan, S. M., Rothwell, N. J., Garlanda, C., Denes, A. and Pinteaux, E. (2014). The acute-phase protein PTX3 is an essential mediator of glial scar formation and resolution of brain edema after ischemic injury. *Journal of Cerebral Blood Flow and Metabolism*, 34(3), 480–488.

Rodriguez-Grande, B., Varghese, L., Molina-Holgado, F., Rajkovic, O., Garlanda, C., Denes, A. and Pinteaux, E. (2015). Pentraxin 3 mediates neurogenesis and angiogenesis after cerebral ischaemia. *Journal of Neuroinflammation*, 12(1), 1–11.

Rolls, A., Shechter, R. and Schwartz, M. (2009). The bright side of the glial scar in CNS repair. *Nature Reviews Neuroscience*, 10(3), 235–241.

Rosenberg, G. A., Estrada, E. Y. and Dencoff, J. E. (1998). Matrix metalloproteinases and TIMPs are associated with blood-brain barrier opening after reperfusion in rat brain. *Stroke*, 29(10), 2189–95.

Rustenhoven, J., Jansson, D., Smyth, L. C. and Dragunow, M. (2017). Brain Pericytes As Mediators of Neuroinflammation. *Trends in Pharmacological Sciences*, 38(3), 291–304.

Saini, M. G. and Bix, G. J. (2012). Oxygen-glucose deprivation (OGD) and interleukin-1 (IL-1) differentially modulate cathepsin B/L mediated generation of neuroprotective perlecan LG3 by neurons. *Brain research*, 1438(2), 65–74.

Saini, M. G., Pinteaux, E., Lee, B. and Bix, G. J. (2011). Oxygen-glucose deprivation and interleukin-1α trigger the release of perlecan LG3 by cells of neurovascular unit. *Journal of Neurochemistry*, 119(4), 760–771.

Salic, A. and Mitchison, T. J. (2008). A chemical method for fast and sensitive detection of DNA synthesis in vivo. *Proceedings of the National Academy of Sciences of the United States of America*, 105(7), 2415–20.

Salmeron, K., Aihara, T., Redondo-Castro, E., Pinteaux, E. and Bix, G. (2016). IL-1alpha induces angiogenesis in brain endothelial cells in vitro: Implications for brain angiogenesis after acute injury. *Journal of Neurochemistry*, 136(3), 573–580.

Sandoval, K. E. and Witt, K. A. (2008). Blood-brain barrier tight junction permeability and ischemic stroke. *Neurobiology of Disease*, 32(2), 200–219.

Schroeter, M. L., Mertsch, K., Giese, H., Müller, S., Sporbert, A., Hickel, B. and Blasig, I. E. (1999). Astrocytes enhance radical defence in capillary endothelial cells constituting the blood-brain barrier. *FEBS Letters*, 449(2–3), 241–244.

Seevinck, P. R., Deddens, L. H. and Dijkhuizen, R. M. (2010). Magnetic resonance imaging of brain angiogenesis after stroke. *Angiogenesis*, 13(2), 101–111.

Seto, S.-W., Chang, D., Jenkins, A., Bensoussan, A. and Kiat, H. (2016). Angiogenesis in Ischemic Stroke and Angiogenic Effects of Chinese Herbal Medicine. *Journal of Clinical Medicine*, 5(6), 56.

Sharma, V. K. (2016). *Cerebrovascular Disease*. Second Edi. *International Encyclopedia of Public Health*. Second Edi.

Shi, Y., Zhang, L., Pu, H., Mao, L., Hu, X., Jiang, X., Xu, N., Stetler, R. A., Zhang, F., Liu, X., Leak, R. K., Keep, R. F., Ji, X. and Chen, J. (2016). Rapid endothelial cytoskeletal reorganization enables early blood–brain barrier disruption and long-term ischaemic reperfusion brain injury. *Nature Communications*, 7, January, 10523.

Singh, N., Hopkins, S. J., Hulme, S., Galea, J. P., Hoadley, M., Vail, A., Hutchinson, P. J., Grainger, S., Rothwell, N. J., King, A. T. and Tyrrell, P. J. (2014). The effect of intravenous interleukin-1 receptor antagonist on inflammatory mediators in cerebrospinal fluid after subarachnoid haemorrhage: A phase II randomised controlled trial. *Journal of Neuroinflammation*, 11 2–9.

Sixt, M., Engelhardt, B., Pausch, F., Hallmann, R., Wendler, O. and Sorokin, L. M. (2001). Endothelial cell laminin isoforms, laminins 8 and 10, play decisive roles in T cell recruitment across the blood-brain barrier in experimental autoimmune encephalomyelitis. *The Journal of cell biology*, 153(5), 933–46.

Sizemore, N., Leung, S. and Stark, G. R. (1999). Activation of Phosphatidylinositol 3-Kinase in Response to Interleukin-1 Leads to Phosphorylation and Activation of the NF-κB p65/RelA Subunit. *Molecular and Cellular Biology*, 19(7), 4798–4805.

Slevin, M., Kumar, P., Gaffney, J., Kumar, S. and Krupinski, J. (2006). Can angiogenesis be exploited to improve stroke outcome? Mechanisms and therapeutic potential. *Clinical Science*, 111(3), 171–183.

Smith, C. J., Hulme, S., Vail, A., Heal, C., Parry-Jones, A. R., Scarth, S., Hopkins, K., Hoadley, M., Allan, S. M., Rothwell, N. J., Hopkins, S. J. and Tyrrell, P. J. (2018). SCIL-STROKE (subcutaneous interleukin-1 receptor antagonist in ischemic stroke): A randomized controlled phase 2 trial. *Stroke*, 49(5), 1210–1216.

Sobowale, O. A., Parry-Jones, A. R., Smith, C. J., Tyrrell, P. J., Rothwell, N. J. and Allan, S. M. (2016). Interleukin-1 in Stroke: From Bench to Bedside. *Stroke*, 47(8), 2160–2167.

Sobrino, T., Hurtado, O., Moro, M. Á., Rodríguez-Yáñez, M., Castellanos, M., Brea, D., Moldes, O., Blanco, M., Arenillas, J. F., Leira, R., Dávalos, A., Lizasoain, I. and Castillo, J. (2007). The increase of circulating endothelial progenitor cells after acute ischemic stroke is associated with good outcome. *Stroke*, 38(10), 2759–2764.

Song, J., Zhang, X., Buscher, K., Wang, Y., Wang, H., Di Russo, J., Li, L., Lütke-Enking, S., Zarbock, A., Stadtmann, A., Striewski, P., Wirth, B., Kuzmanov, I., Wiendl, H., Schulte, D., Vestweber, D. and Sorokin, L. (2017). Endothelial Basement Membrane Laminin 511 Contributes to Endothelial Junctional Tightness and Thereby Inhibits Leukocyte Transmigration. *Cell Reports*, 18(5), 1256–1269.

Strbian, D., Durukan, A., Pitkonen, M., Marinkovic, I., Tatlisumak, E., Pedrono, E., Abo-

Ramadan, U. and Tatlisumak, T. (2008). The blood-brain barrier is continuously open for several weeks following transient focal cerebral ischemia. *Neuroscience*, 153(1), 175–181.

Stroke Association (2018). *State of the nation: Stroke statistics.* Stroke Association. [Online] [Accessed on 30th July 2020] https://www.stroke.org.uk/sites/default/files/state_of_the_nation_2018.pdf.

Summers, L., Kangwantas, K., Nguyen, L., Kielty, C. and Pinteaux, E. (2010). Adhesion to the extracellular matrix is required for interleukin-1 beta actions leading to reactive phenotype in rat astrocytes. *Molecular and Cellular Neuroscience*, 44(3), 272–281.

Summers, L., Kangwantas, K., Rodriguez-Grande, B., Denes, A., Penny, J., Kielty, C. and Pinteaux, E. (2013). Activation of brain endothelial cells by interleukin-1 is regulated by the extracellular matrix after acute brain injury. *Molecular and Cellular Neuroscience*, 57 93–103.

Szalay, G., Martinecz, B., Lénárt, N., Környei, Z., Orsolits, B., Judák, L., Császár, E., Fekete, R., West, B. L., Katona, G., Rózsa, B. and Dénes, Á. (2016). Microglia protect against brain injury and their selective elimination dysregulates neuronal network activity after stroke. *Nature Communications*, 7(May),.

Tagaya, M., Haring, H. P., Stuiver, I., Wagner, S., Abumiya, T., Lucero, J., Lee, P., Copeland, B. R., Seiffert, D. and Del Zoppo, G. J. (2001). Rapid loss of microvascular integrin expression during focal brain ischemia reflects neuron injury. *Journal of Cerebral Blood Flow and Metabolism*, 21(7), 835–846.

Takada, Y., Ye, X. and Simon, S. (2007). The integrins. *Genome Biology*, 8(5), 215.

Taylor, R. A. and Sansing, L. H. (2013). Microglial responses after ischemic stroke and intracerebral hemorrhage. *Clinical and Developmental Immunology*, 2013(Figure 1),.

Thomsen, M. S., Birkelund, S., Burkhart, A., Stensballe, A. and Moos, T. (2017). Synthesis and deposition of basement membrane proteins by primary brain capillary endothelial cells in a murine model of the blood–brain barrier. *Journal of Neurochemistry*, 140(5), 741–754.

Thornton, P., W. McColl, B., Cooper, L., J. Rothwell, N. and M. Allan, S. (2010). Interleukin-1 Drives Cerebrovascular Inflammation via MAP Kinase-Independent Pathways. *Current Neurovascular Research*, 7(4), 330–340.

Thyboll, J., Kortesmaa, J., Cao, R., Soininen, R., Wang, L., Iivanainen, A., Sorokin, L., Risling, M., Cao, Y. and Tryggvason, K. (2002). Deletion of the Laminin α4 Chain Leads to Impaired Microvessel Maturation. *Molecular and Cellular Biology*, 22(4), 1194–1202.

Ucuzian, A. A., Gassman, A. A., East, A. T. and Greisler, H. P. (2011). Molecular mediators of angiogenesis. *Journal of burn care & research : official publication of the American Burn Association*, 31(1), 158–75.

Valny, M., Honsa, P., Kirdajova, D., Kamenik, Z. and Anderova, M. (2016). Tamoxifen in the Mouse Brain: Implications for Fate-Mapping Studies Using the Tamoxifen-Inducible Cre-loxP System. *Frontiers in cellular neuroscience*, 10, 243.

Vidale, S., Consoli, A., Arnaboldi, M. and Consoli, D. (2017). Postischemic Inflammation in Acute Stroke. *Journal of clinical neurology (Seoul, Korea)*, 13(1), 1–9.

Wade, G. N. and Heller, H. W. (1993). Tamoxifen mimics the effects of estradiol on food intake, body weight, and body composition in rats. *The American journal of physiology*, 264(6 Pt 2), R1219-23.

Wagner, S., Tagaya, M., Koziol, J. A., Quaranta, V. and del Zoppo, G. J. (1997). Rapid Disruption of an Astrocyte Interaction With the Extracellular Matrix Mediated by Integrin α 6 β 4 During Focal Cerebral Ischemia/Reperfusion. *Stroke*, 28(4), 858–865.

Wang, K.-C., Yeh, Y.-T., Nguyen, P., Limqueco, E., Lopez, J., Thorossian, S., Guan, K.-L., Li, Y.-S. J. and Chien, S. (2016). Flow-dependent YAP/TAZ activities regulate

endothelial phenotypes and atherosclerosis. *Proceedings of the National Academy of Sciences*, 113(41), 11525–11530.

Wang, L., Luo, J.-Y., Li, B., Tian, X. Y., Chen, L.-J., Huang, Y., Liu, J., Deng, D., Lau, C. W., Wan, S., Ai, Di., Mak, K.-L. K., Tong, K. K., Kwan, K. M., Wang, N., Chiu, J.-J., Zhu, Y. and Huang, Y. (2016). Integrin-YAP/TAZ-JNK cascade mediates atheroprotective effect of unidirectional shear flow. *Nature*, 540(7634), 579–582.

Wang, Q., Tang, X. N. and Yenari, M. A. (2007). The inflammatory response in stroke. *Journal of Neuroimmunology*, 184(1–2), 53–68.

Wang, S., Voisin, M.-B., Larbi, K. Y., Dangerfield, J., Scheiermann, C., Tran, M., Maxwell, P. H., Sorokin, L. and Nourshargh, S. (2006). Venular basement membranes contain specific matrix protein low expression regions that act as exit points for emigrating neutrophils. *The Journal of Experimental Medicine*, 203(6), 1519–1532.

Wang, S., Zhou, L., Ling, L., Meng, X., Chu, F., Zhang, S. and Zhou, F. (2020). The Crosstalk Between Hippo-YAP Pathway and Innate Immunity. *Frontiers in Immunology*, 11(February), 1–14.

Wang, X., Freire Valls, A., Schermann, G., Shen, Y., Moya, I. M., Castro, L., Urban, S., Solecki, G. M., Winkler, F., Riedemann, L., Jain, R. K., Mazzone, M., Schmidt, T., Fischer, T., Halder, G. and Ruiz de Almodóvar, C. (2017). YAP/TAZ Orchestrate VEGF Signaling during Developmental Angiogenesis. *Developmental Cell*, 42(5), 462-478.e7.

Warren, J. S. A., Xiao, Y. and Lamar, J. M. (2018). YAP/TAZ activation as a target for treating metastatic cancer. *Cancers*, 10(4),.

Weber, A., Wasiliew, P. and Kracht, M. (2010). Interleukin-1 (IL-1) Pathway, 3(105), 1–7.

Weksler, B., Romero, I. A. and Couraud, P. O. (2013). The hCMEC/D3 cell line as a model of the human blood brain barrier. *Fluids and Barriers of the CNS*, 10(1), 1.

Wiltrout, C., Lang, B., Yan, Y., Dempsey, R. J. and Vemuganti, R. (2007). Repairing brain after stroke: A review on post-ischemic neurogenesis. *Neurochemistry International*, 50(7–8), 1028–1041.

Winkler, E. A., Bell, R. D. and Zlokovic, B. V (2011). Central nervous system pericytes in health and disease. *Nature neuroscience*, 14(11), 1398–1405.

Wong, R., Lénárt, N., Hill, L., Toms, L., Coutts, G., Martinecz, B., Császár, E., Nyiri, G., Papaemmanouil, A., Waisman, A., Müller, W., Schwaninger, M., Rothwell, N., Francis, S., Pinteaux, E., Denés, A. and Allan, S. M. (2019). Interleukin-1 mediates ischaemic brain injury via distinct actions on endothelial cells and cholinergic neurons. *Brain, Behavior, and Immunity*, 76(July 2018), 126–138.

Woodruff, T. M., Thundyil, J., Tang, S. C., Sobey, C. G., Taylor, S. M. and Arumugam, T. V. (2011). Pathophysiology, treatment, and animal and cellular models of human ischemic stroke. *Molecular Neurodegeneration*, 6(1), 11.

Wu, C., Ivars, F., Anderson, P., Hallmann, R., Vestweber, D., Nilsson, P., Robenek, H., Tryggvason, K., Song, J., Korpos, E., Loser, K., Beissert, S., Georges-Labouesse, E. and Sorokin, L. M. (2009). Endothelial basement membrane laminin α5 selectively inhibits T lymphocyte extravasation into the brain. *Nature Medicine*, 15(5), 519–527.

Wu, X. and Reddy, D. S. (2012). Integrins as receptor targets for neurological disorders. *Pharmacology and Therapeutics*, 134(1), 68–81.

Xu, L., Nirwane, A. and Yao, Y. (2019). Basement membrane and blood-brain barrier. *Stroke and Vascular Neurology*, 4(2), 78–82.

Xu, T., Wang, W., Zhang, S., Stewart, R. A. and Yu, W. (1995). Identifying tumor suppressors in genetic mosaics: the Drosophila lats gene encodes a putative protein kinase. *Development (Cambridge, England)*, 121(4), 1053–63.

Yang, T., Roder, K. E. and Abbruscato, T. J. (2007). Evaluation of bEnd5 cell line as an in vitro model for the blood-brain barrier under normal and hypoxic/aglycemic conditions. *Journal of Pharmaceutical Sciences*, 96(12), 3196–3213.

Yao, Y. (2019). Basement membrane and stroke. *Journal of Cerebral Blood Flow and Metabolism*, 39(1), 3–19.

Yenari, M. A., Sun, G. H., Kunis, D. M., Onley, D. and Vexler, V. (2001). L-selectin inhibition does not reduce injury in a rabbit model of transient focal cerebral ischemia. *Neurological Research*, 23(1), 72–78.

Yepes, M., Sandkvist, M., Wong, M. K. K., Coleman, T. A., Smith, E., Cohan, S. L. and Lawrence, D. A. (2000). Neuroserpin reduces cerebral infarct volume and protects neurons from ischemia-induced apoptosis. *Blood*, 96(2), 569–576.

You, B., Yang, Y. L., Xu, Z., Dai, Y., Liu, S., Mao, J. H., Tetsu, O., Li, H., Jablons, D. M. and You, L. (2015). Inhibition of ERK1/2 down-regulates the Hippo/YAP signaling pathway in human NSCLC cells. *Oncotarget*, 6(6), 4357–4368.

Yun, S., Budatha, M., Dahlman, J. E., Coon, B. G., Cameron, R. T., Langer, R., Anderson, D. G., Baillie, G. and Schwartz, M. A. (2016). Interaction between integrin α 5 and PDE4D regulates endothelial inflammatory signalling. *Nature Cell Biology*, 18(10), 1043–1053.

Yurchenco, P. D. (2011). Basement membranes: Cell scaffoldings and signaling platforms. *Cold Spring Harbor Perspectives in Biology*, 3(2), 1–27.

Zhang, D., Yang, S., Toledo, E. M., Gyllborg, D., Saltó, C., Carlos Villaescusa, J. and Arenas, E. (2017). Niche-derived laminin-511 promotes midbrain dopaminergic neuron survival and differentiation through YAP. *Science Signaling*, 10(493), eaal4165.

Zhang, Q., Han, X., Chen, J., Xie, X., Xu, J., Zhao, Y., Shen, J., Hu, L., Xu, P., Song, H., Zhang, L., Zhao, B., Wang, Y. and Xia, Z. (2018). *Yes-associated protein (YAP) and transcriptional coactivator with PDZ-binding motif (TAZ) mediate cell density–dependent proinflammatory responses*. *Journal of Biological Chemistry*.

Zhao, B., Li, L. and Guan, K. L. (2010). Hippo signaling at a glance. *Journal of Cell Science*, 123(23), 4001–4006.

Zhao, B., Li, L., Tumaneng, K., Wang, C. Y. and Guan, K. L. (2010). A coordinated phosphorylation by Lats and CK1 regulates YAP stability through SCFβ-TRCP. *Genes and Development*, 24(1), 72–85.

Zhao, B., Wei, X., Li, W., Udan, R. S., Yang, Q., Kim, J., Xie, J., Ikenoue, T., Yu, J., Li, L., Zheng, P., Ye, K., Chinnaiyan, A., Halder, G., Lai, Z. C. and Guan, K. L. (2007). Inactivation of YAP oncoprotein by the Hippo pathway is involved in cell contact inhibition and tissue growth control. *Genes and Development*, 21(21), 2747–2761.

Zhao, B., Ye, X., Yu, Jindan, Li, L., Li, W., Li, S., Yu, Jianjun, Lin, J. D., Wang, C. Y., Chinnaiyan, A. M., Lai, Z. C. and Guan, K. L. (2008). TEAD mediates YAP-dependent gene induction and growth control. *Genes and Development*, 22(14), 1962–1971.

Appendix 1

Table of reagents/equipment and antibodies

Table A1.1 – Summary of reagents/equipment

Reagent	Company	Catalogue number
0.22 µm pore size filter	Starlab	E4780-1226
0.25 % trypsin/ 1 mM EDTA solution	Sigma	T4049-100ML
5-Bromo-2′-deoxyuridine (BrdU)	Sigma	B5002
70 µm cell strainer	Corning	CLS431751
96-pin IncuCyte WoundMaker Tool	Essen BioScience	4563
96-well Cell Migration Software Application Module	Essen BioScience	4400
96-well Cell Migration Software Application Module	Essen BioScience	4400
Acetic acid	Sigma	A6283
ACK lysis buffer	Thermo Fisher Scientific	A1049201
BCA Protein Assay Kit	Pierce Biotechnology	23225
bEnd.5 cells	Public Health of England	
Bovine Serum Albumin (BSA)	Sigma	A9647
CaseViewer	3DHISTECH Ltd	
Collagen IV	VWR	734-0099
Collagenase/dispase	Sigma	10269638001
Cresyl violet	Sigma	1052350025
Crystal violet	Gurr Certistain	343122N
Dextran	Affymetrix, Thermo Fisher Scientific	15865218

DNA ladder (1 kb)	New England Biolabs	N3232L
DNase I	Thermo Fisher Scientific	18047019
dNTP Mix 100mM Final Conc	Bioline	BIO-39028
DPX mounting medium	Sigma	6522
Dulbecco's Modified Eagle's Medium (DMEM)	Sigma	D6429
Dulbecco's Modified Eagle's Medium/Ham's Nutrient Mixture F12	Sigma	51445C
ECL Prime Western Blotting Detection Reagent	GE Healthcare	GERPN2232
EndoGRO-MV Complete Culture Media	Merck	SCME004
Endothelial cell growth supplement (ECGS)	VWR	734-2391
Extract-N-Amp™ Tissue PCR Kit	Sigma	XNAT2-1KT
Fetal Bovine Serum (FBS)	Thermo Fisher Scientific	10500064
Gelatin	BDH	24350.262
Glutamine	Sigma	G7513
Glutaraldehyde	Sigma	G6257
GraphPad Prism	GraphPad Software Inc	
Hanks' balanced salt solution (HBSS) with sodium bicarbonate / without calcium	Sigma	H9394

chloride and magnesium sulphate		
Heparin sodium salt	Sigma	H3149-50KU
High Glucose DMEM	Sigma	D6429
Human cerebral microvascular endothelial cell line, hCMEC/D3	Merck	SCC066
Human ERK-1/2 ELISA	R&D Systems	DYC1018B-2
Human ICAM-1 ELISA	R&D Systems	DY720
Human IL-8 ELISA	R&D Systems	DY208
Human phospho-p38a ELISA	R&D Systems	DYC869B-2
Human recombinant LM-10	BioLamina	BIOLAMININ 511 LN (LN511)
Human VCAM-1 ELISA	R&D Systems	DY809
IL-1RA	Kineret, SOBI	
Image J	ImageJ (NIH)	
ImageLock plate (96-well)	Essen BioScience	4379
Low endotoxin BSA	Sigma	A1470
Matrigel	Corning	354230
MoorFLPI software	Moor Instruments Ltd	
Mouse chemokine KC/CXCL1 ELISA	R&D Systems	DY453
Mouse E-selectin ELISA	R&D Systems	DY575
Mouse ICAM-1 ELISA	R&D Systems	DY796
Mouse IL-6 ELISA	R&D Systems	DY406
Mouse MCP-1 ELISA	R&D Systems	DY479
Mouse P-selectin ELISA	R&D Systems	DY737

Mouse VCAM-1 ELISA	R&D Systems	DY643
Mouse VEGF ELISA	R&D Systems	DY493
Nuclease free water	Gibco	10977035
One Taq Hot Start DNA Polymerase/5x One Taq standard reaction buffer	New England Biolabs	M0481S
Optimal Cutting Temperature (OCT) compound	Thermo Fisher Scientific	12678646
Penicillin Streptomycin	Sigma	P0781
Percoll	Sigma	P4937
Phosphatase inhibitors (PhosSTOP)	Sigma	4906845001
Phosphate-buffered saline (PBS)	Sigma	D8537
Plasma derived serum (PDS)	First Link Ltd	60-00-810
Polyvinylidene difluoride (PVDF)	Bio-rad	1620177
Power SYBR Green PCR Master Mix	Thermo Fisher Scientific	4368702
ProLong Diamond anti-fade Mountant	Thermo Fisher Scientific	P36970
Protease Inhibitor Cocktail Set I	Calbiochem	539131
Protease inhibitor Tosyl-L-lysine chloromethyl ketone hydrochloride (TLCK)	Sigma	90182-100MG
Purelink RNA minikit	Thermo Fisher Scientific	12183018A
PureLink™ DNase Set	Thermo Fisher Scientific	12185010

Rat tail collagen type I	Merck	08-115
Recombinant human fibroblast growth factor-basic	Merck	GF003
Recombinant human IL-1β	R&D Systems	201-LB
Recombinant mouse IL-1β	R&D Systems	401-ML
Roswell Park Memorial Institute (RPMI) media	Sigma	R0883
Sodium dodecyl sulfate (SDS)	Sigma Aldrich	62862
SuperScript™ III Reverse Transcriptase	Thermo Fisher Scientific	18080044
SYBR™ Safe DNA Gel Stain	Thermo Fisher Scientific	S33102
Tamoxifen	Sigma	T5648-5G
Transwell inserts (6.5 mm with 3.0 μm pore polycarbonate membrane)	Corning	3415
Triton X	Sigma	T8787
Trypsin	Sigma	T4174-100ML
Tween 20	Sigma	P9416

Table A1.2 – Summary of antibodies

Antibody	Company	Catalogue number	Dilution
BrdU	Abcam	ab1893	1:200
donkey anti-goat Alexa Fluor 594	Thermo Fisher Scientific	A-11058	1:400
donkey anti-rabbit Alexa Fluor 594	Thermo Fisher Scientific	R37119	1:400
donkey anti-sheep Alexa Fluor 594	Thermo Fisher Scientific	A-11016	1:400

HRP β-actin	Abcam	ab49900	1:50000
IκBα	Cell Signalling	9242	1:1000
Laminin α4	R&D Systems	AF3837	1:400
Laminin α5	Miner et al. 1997		1:800
Phospho-p65 (Ser536)	Cell Signalling	3033	1:1000
p-YAP127	Cell Signalling	13008	1:1000
p-YAP397	Cell Signalling	13619	1:1000
Rabbit anti-IgG (rabbit polyclonal)	Agilent	P0448	1:1000
YAP	Cell Signalling	14074	1:1000